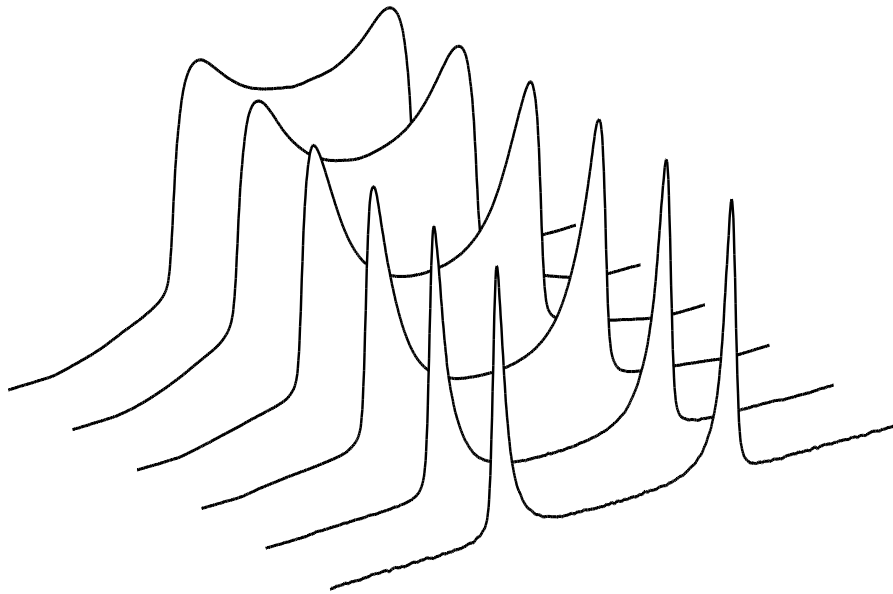


# Secondary relaxation processes in neat and binary glass formers studied by $^2\text{H}$ NMR spectroscopy



Von der Universität Bayreuth  
zur Erlangung des Grades eines  
Doktors der Naturwissenschaften (Dr. rer. nat.)  
genehmigte Abhandlung

von

Björn Micko

geboren am 15. August 1980 in Ostfildern-Ruit

1. Gutachter: Prof. Dr. E. Rößler  
2. Gutachter: Prof. Dr. M. Vogel

Tag der Einreichung: 24.02.2012  
Tag des Kolloquiums: 20.06.2012

---

The cover page shows  $^2\text{H}$  NMR solid echo spectra of cyanocyclohexane recorded in the plastically crystalline phase for different inter pulse delays (146.8 K,  $t_p=10\ \mu\text{s}$  to  $300\ \mu\text{s}$  back to front). The  $\beta$ -process imposes prominent fast motion limit line shape effects in this temperature range, which allow for a direct determination of the degree of restriction.

# Contents

<b>1</b>	<b>Introduction</b>	<b>1</b>
<b>2</b>	<b>The glass transition phenomenon</b>	<b>5</b>
2.1	Supercooled liquids and glasses . . . . .	5
2.2	The $\alpha$ -process . . . . .	8
2.3	The $\beta$ -process . . . . .	9
2.3.1	Open questions . . . . .	11
<b>3</b>	<b><math>^2\text{H}</math> NMR spectroscopy</b>	<b>13</b>
3.1	The nuclear spin and its interactions . . . . .	13
3.2	Hamiltonians . . . . .	14
3.2.1	Density matrix representation . . . . .	16
3.2.2	The rotating frame . . . . .	17
3.2.3	Radio frequency pulses . . . . .	17
3.2.4	Spherical tensor operators . . . . .	18
3.3	Relaxation phenomena . . . . .	18
3.4	$^2\text{H}$ NMR experiments in the solid state . . . . .	19
3.4.1	Solid echo . . . . .	20
3.4.2	Spin-lattice and spin-spin relaxation measurements . . . . .	22
3.4.3	2D NMR . . . . .	23
3.4.4	Stimulated echo . . . . .	24
3.4.5	2D NMR in the frequency domain . . . . .	28
3.5	Development of a low temperature double resonance probe . . . . .	31
<b>4</b>	<b>Random walk simulations</b>	<b>35</b>
4.1	Introduction . . . . .	35
4.2	Isotropic motion . . . . .	36
4.2.1	2D NMR in time domain . . . . .	37
4.2.2	Solid echo line shape . . . . .	41
4.2.3	Heterogeneous dynamics . . . . .	43
4.3	Anisotropic reorientation . . . . .	46
4.3.1	Random jump type motion on a cone . . . . .	46
4.3.2	Random jump type motion within a cone . . . . .	49
4.3.3	Multi step motion within a cone . . . . .	52
4.3.4	Distributions of geometries and correlation times . . . . .	56
4.4	Summary and conclusions . . . . .	57
<b>I</b>	<b>Plastic Crystals</b>	<b>59</b>
<b>5</b>	<b>Introduction</b>	<b>61</b>

<b>6</b>	<b>Cyanocyclohexane</b>	<b>65</b>
6.1	Introduction . . . . .	65
6.1.1	Chemical and physical properties . . . . .	66
6.1.2	Dielectric loss spectra . . . . .	68
6.2	Structure elucidation . . . . .	70
6.3	Experimental results – overview . . . . .	72
6.3.1	Experimental details . . . . .	72
6.3.2	Spin-lattice relaxation . . . . .	73
6.3.3	Solid echo spectra . . . . .	75
6.3.4	Solid echo spectra: low temperature regime . . . . .	78
6.3.5	Solid echo spectra: fast motion limit effects . . . . .	80
6.3.6	Stimulated echoes $T < T_g$ . . . . .	83
6.3.7	2D exchange spectra of the $\alpha$ -process . . . . .	85
6.3.8	Stimulated echoes $T > T_g$ . . . . .	87
6.3.9	Preliminary conclusions . . . . .	91
6.4	Experimental results – refinement . . . . .	92
6.4.1	Modelling spin-lattice relaxation . . . . .	92
6.4.2	Modelling solid echo spectra . . . . .	95
6.4.3	The $t_p$ -dependence of solid echo spectra $T > T_g$ . . . . .	105
6.4.4	Dynamics of the $\alpha$ -process – reassessment . . . . .	107
6.5	Summary and conclusions . . . . .	112
<b>II</b>	<b>Binary Glass Forming Systems</b>	<b>115</b>
<b>7</b>	<b>Introduction</b>	<b>117</b>
7.1	Digest . . . . .	117
7.2	Spectroscopic amendments . . . . .	121
<b>8</b>	<b>Toluene in PCB</b>	<b>123</b>
8.1	Introduction . . . . .	123
8.2	Dielectric Spectroscopy . . . . .	124
8.3	Experimental details . . . . .	127
8.4	Thermal analysis . . . . .	128
8.5	NMR results – an overview . . . . .	130
8.5.1	Spin lattice relaxation . . . . .	130
8.5.2	Solid echo spectra – high temperature regime . . . . .	135
8.5.3	2D exchange spectra . . . . .	139
8.5.4	Stimulated echoes – high temperature regime . . . . .	141
8.5.5	Solid echo line shape – low temperature regime . . . . .	147
8.5.6	Stimulated echoes – low temperature regime . . . . .	152
8.5.7	Spin lattice relaxation – revisited . . . . .	155
8.6	Plausibility check . . . . .	160
8.6.1	Modelling the toluene dynamics in mixtures with PCB . . . . .	161
8.6.2	Models for two dynamically distinct toluene sub-ensembles . . . . .	165
8.6.3	Discussion . . . . .	171

---

<b>9</b>	<b>Universal behaviour of toluene in binary mixtures</b>	<b>173</b>
9.1	Motivation . . . . .	173
9.2	Toluene in picoline . . . . .	173
9.2.1	Thermal analysis . . . . .	174
9.2.2	Dielectric measurements . . . . .	175
9.2.3	NMR results . . . . .	177
9.3	Toluene in polystyrene . . . . .	181
9.3.1	NMR results . . . . .	184
9.4	A model for the concentration dependence . . . . .	185
9.4.1	Application . . . . .	186
<b>10</b>	<b>Discussion and outlook</b>	<b>189</b>
<b>III</b>	<b>Summary, Appendix &amp; Bibliography</b>	<b>191</b>
<b>11</b>	<b>Summary</b>	<b>193</b>
<b>12</b>	<b>Summary - German translation</b>	<b>195</b>
<b>A</b>	<b>Additional results: cyanocyclohexane</b>	<b>199</b>
A.1	Dielectric spectroscopy . . . . .	199
A.2	Spin-lattice relaxation . . . . .	200
A.3	Spin-spin relaxation times . . . . .	202
A.4	Correlation of time scale and geometry for the $\beta$ -process . . . . .	202
<b>B</b>	<b>Additional results: binary glass forming systems</b>	<b>205</b>
B.1	Dielectric spectroscopy . . . . .	205
B.2	Methyl group dynamics . . . . .	207
B.3	Spin-spin relaxation times . . . . .	208
B.4	$T_1$ weighted stimulated echo experiments . . . . .	208
<b>C</b>	<b>Details on the random walk simulations</b>	<b>211</b>
C.1	Creation of trajectories . . . . .	211
C.2	Calculation of the NMR signal . . . . .	212
C.3	Phenomenological model functions . . . . .	213
C.3.1	Distribution functions for the $\alpha$ -process . . . . .	213
C.3.2	Distribution functions for the $\beta$ -process . . . . .	214
	<b>Bibliography</b>	<b>217</b>
	<b>List of figures</b>	<b>229</b>



# Introduction

---

At temperatures below the melting point of a liquid,  $T < T_m$ , the crystal represents the thermodynamically stable phase. For sufficiently large cooling rates, however, the formation of a crystalline phase can be avoided in practically all systems: the molecules do not achieve spatial order and a supercooled liquid is obtained. At the glass transition temperature  $T_g \ll T_m$  the characteristic time of structural relaxation in the supercooled liquid finally becomes longer than the time scale of a typical experiment – the system falls out of ergodicity. Hence the glassy state distinguishes itself from the crystalline one by a lack of translational symmetry; the structure of the liquid is virtually maintained.

The glass transition problem is exceptional in the sense that it features a long standing research history, but remains unsolved to the present day. In recent years the activity in the field is accelerated by the recognition of the fundamental nature of the problem on the one hand, and the importance of supercooled liquids and glasses in everyday life on the other hand. From traditional soda-lime-silica glasses, used in windows and other applications for centuries, to polymer-plasticizer systems, i.e. plastics, which revolutionized consumer goods in the last decades, amorphous substances play a major role in modern life. Yet there exists no commonly accepted theory that describes all features regarded as intrinsic to the phenomenon in the full temperature range from the simple liquid to the glassy state.

The outstanding features of the glass transition phenomenon – the viscosity changes by many orders of magnitude in a narrow temperature range – have drawn the attention of many experimentalists and various techniques have been developed to examine the properties of glass forming substances during the last century. Due to the pronounced thermodynamic effects, the changes regarding microscopic dynamics in conjunction with the glass transition have sometimes taken a back seat. The dynamics of the  $\alpha$ -process, which causes all correlations within a liquid to disappear and hence governs the structural relaxation, is well described by a diffusive motion in the liquid state,  $T \gg T_m$ , but becomes more complex in the supercooled liquid and particularly of cooperative nature: glass transition arises from many body effects. In addition faster secondary processes emerge at  $T > T_g$ , which display strikingly universal features in vastly different glass forming substances. The main focus of this work is placed on one of these processes: the Johari-Goldstein  $\beta$ -process. Johari and Goldstein discovered that also molecules without internal degrees of freedom show a secondary relaxation that exhibits thermally activated behaviour. Due to this – in contrast to the  $\alpha$ -process – low temperature dependence, the  $\beta$ -process dominates the relaxation behaviour in the glassy state. The authors attributed this process to “islands of mobility”, i.e. to a fraction of molecules that maintains enhanced mobility even below  $T_g$ . In recent years it was however demonstrated that all molecules

contribute to the  $\beta$ -process, which consequently represents a restricted local motion. The degree of restriction is rather pronounced at temperatures below  $T_g$ , but becomes significantly reduced at higher temperatures before ultimately the time scales of  $\alpha$ - and  $\beta$ -process merge in most glass forming substances. Consequently it is of great interest to study the  $\beta$ -process at temperatures above  $T_g$ , since the effects are typically rather subtle below the glass transition temperature. For most substances the applicable temperature range is however quite narrow due to a merging with the  $\alpha$ -process.

In addition to supercooled liquids, a glass transition can also be observed in plastically crystalline phases. Plastic crystals exhibit translational symmetry and orientational disorder: the molecules reorient around their point of gravity on the respective position in the lattice. The orientational degrees of freedom in such a system can be supercooled and subsequently undergo a glass transition that exhibits some or all characteristics of the glass transition observed in structural glass formers, including the arise of secondary relaxations. Consequently plastic crystals are often regarded as “model systems” for the glass transition due to the reduced complexity of molecular dynamics.

Apart from neat glass formers also binary systems, i.e. mixtures of two substances with at least one being a “good” glass former, are of industrial as well as theoretical interest. Binary mixtures serve as a model for the widely used polymer-plasticiser systems. Furthermore simulations and mode-coupling theory calculations for mixtures composed of small and large hard-spheres yield a glass transition of the smaller spheres within the rigid matrix of the larger ones. In mixtures of molecular liquids the dynamics of the respective species are however still a matter of debate. The arise of a single  $T_g$  for example often served as a criterion for miscibility, recent studies however reported the emergence of two glass transitions even in fully miscible systems, demonstrating a decoupling of time scales between the components. Yet it remains unclear if this decoupling holds for all sub-ensembles or if a fraction of molecules participates in the dynamics of the other component – i.e. a bimodal relaxation pattern arises. Due to the pronounced dynamic heterogeneities inherent to binary mixtures, i.e. the distributions of correlation times become very broad compared to the neat systems, it may often not be feasible to discriminate between the two scenarios in a typical experiment.

The present work attempts to provide further insight on the nature of the glass transition with special attention on the Johari-Goldstein  $\beta$ -process. The focus hereby lies on nuclear magnetic resonance (NMR) studies, as the technique provides the ability to elucidate the detailed mechanism of molecular reorientation. The employed  $^2\text{H}$  NMR technique furthermore has the advantages of selectivity, i.e. the site or molecule of interest can be marked via selective deuteration, and simplicity in data analysis, as the predominant quadrupolar interaction is of effective single-particle type. The selectivity of the method is of significance especially with regard to studies of binary systems, as the components can be monitored individually by  $^2\text{H}$  NMR.

---

## Scope and structure of the present work

After the basic features of the glass transition phenomenon and the employed  $^2\text{H}$  NMR technique are introduced in chapters 2 and 3, chapter 4 is devoted to random walk simulations of  $^2\text{H}$  NMR experiments for selected modes of reorientation. Due to the complex nature of dynamics in supercooled liquids and glasses this becomes necessary, as the  $^2\text{H}$  NMR results can often not be interpreted in straightforward manner and have to be discussed in the framework of random walk simulations to obtain a deeper understanding of molecular motion. This especially holds for the  $\beta$ -process in general and the  $\alpha$ -process in binary mixtures, as the inherent pronounced dynamic heterogeneities conflict with the available  $^2\text{H}$  NMR time window and render a detailed simulation approach a necessity.

In part I of the experimental section we address the dynamics of cyanocyclohexane in the plastically crystalline phase. Cyanocyclohexane exhibits a pronounced  $\beta$ -process that can be studied in a relatively broad temperature regime above  $T_g$  (as it does not merge with the  $\alpha$ -process) and yields distinct effects in the  $^2\text{H}$  NMR observables, previously not reported for glass forming systems. This allows us to extend present hypothesis on the microscopic nature of the  $\beta$ -process and gain further insight on the dynamics of the  $\alpha$ -process, as the processes are well separated within the  $^2\text{H}$  NMR time window, which is typically not the case.

In part II we selectively address the dynamics of toluene in mixtures with a polychlorinated biphenyl (PCB54), which exhibits a higher glass transition temperature, i.e. toluene serves as a plasticizer. Toluene is a well studied glass former, consequently a  $^2\text{H}$  NMR assessment of the concentration dependent change in dynamics is facilitated as comprehensive literature data regarding the neat system is at hand. In particular we address the question of possible bimodal relaxation behaviour and attempt to clarify the role of the Johari-Goldstein  $\beta$ -process for the complex dynamics in binary mixtures. If the  $\beta$ -process represents an intrinsic phenomenon of the glass transition and serves as precursor for the structural relaxation – as often speculated – a distinct concentration dependence is anticipated as the structural relaxation of toluene is slowed in the mixtures, even more so if dynamically different toluene sub-ensembles arise. Although refuted in the case of neat glass formers, where the contribution of all molecules to the  $\beta$ -process has been confirmed, a reintroduction of the “islands of mobility” concept may not be argued for binary systems.



# The glass transition phenomenon

## Contents

<b>2.1 Supercooled liquids and glasses</b> . . . . .	<b>5</b>
<b>2.2 The <math>\alpha</math>-process</b> . . . . .	<b>8</b>
<b>2.3 The <math>\beta</math>-process</b> . . . . .	<b>9</b>
2.3.1 Open questions . . . . .	11

The present chapter serves to provide a basic understanding of the glass transition phenomenon, including a brief discussion of recent advances regarding the understanding of molecular dynamics in supercooled liquids and glasses. Due to the vast research interest in disordered systems in the past decades, numerous books and review articles cover the field (for example [Angell 2000, Donth 2001, Ediger 2000, Ngai 2000, Blochowicz 2006, Ngai 2011] and references therein, for a review of NMR studies see [Böhmer 2001, Vogel 2005]). For this reason the remarks here will be limited to the basic principles; furthermore open questions will be pointed out that are addressed in the remainder of this work.

## 2.1 Supercooled liquids and glasses

Upon cooling, the viscosity of a liquid, i.e. its resistance under stress, increases. For many liquids crystallization at the melting temperature  $T_m$  can be avoided via sufficiently large cooling rates – in such a case, upon further cooling, finally viscosity values on the order of  $\eta = 10^{12}$ Pa·s, i.e. of a solid body, are approached. At this temperature, called the glass transition temperature  $T_g$ , the system falls out of equilibrium and the macroscopic sample becomes rigid on experimental time scales. Along with the viscosity the time scale  $\tau$  of molecular reorientation changes more than 14 orders of magnitude from the picosecond regime in the simple liquid

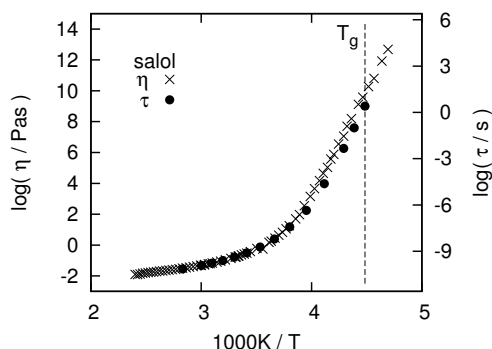


**Figure 2.1:** Viscosity of the glass former salol (phenyl salicylate) [Cuikermann 1973]. In addition the rotational correlation times obtained from dielectric spectroscopy are plotted (full symbols, right y-axis) [Kudlik 1997b].

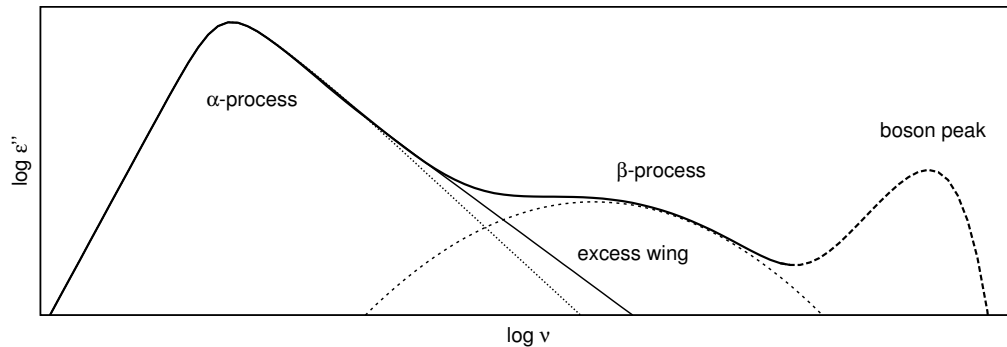


**Figure 2.2:** Schematic sketch of the dielectric loss in a supercooled liquid, figure adapted from Kudlik [Kudlik 1997b].

to hundreds of seconds around  $T_g$ , cf. figure 2.1. Glass transition does however not represent a first order phase transition: the drastic changes in  $\eta$  and  $\tau$  are continuous and no distinct alteration of the material structure appears at  $T_g$ , hence the phenomenon is of purely kinetic nature.

Supercooled liquids exhibit dynamics on virtually all time scales: from picoseconds to seconds – which poses a great challenge to the experimental technique. An overview on glassy dynamics is conveniently achieved by means of dielectric spectroscopy, as the technique covers a relatively broad frequency range (up to  $1 \times 10^{-6}$  Hz – 1 THz, for details on the method see for example [Böttcher 1978a, Böttcher 1978b]).

Figure 2.2 displays a sketch of the typical dielectric loss of a supercooled liquid: at low frequencies the so-called  $\alpha$ -process dominates the dielectric spectrum, the corresponding loss peak is typically asymmetrically broadened. In the GHz to THz regime on the other end of the frequency window the *boson peak* arises due to vibrational excitations in disordered systems<sup>1</sup>. The “gap” arising between the boson peak and the  $\alpha$ -process in the vicinity of  $T_g$  is in many substances “filled” by secondary processes: the  $\beta$ -process and the excess wing. The latter is seen as a change of the high frequency slope of the  $\alpha$ -peak to a power law with a different exponent  $\gamma$ , whereas the  $\beta$ -process manifests itself in a broad, symmetric peak at frequencies higher than of the  $\alpha$ -peak. As the occurrence of such secondary processes in the dielectric spectrum differs among glass forming substances, a phenomenological classification was introduced by Kudlik et al. [Kudlik 1999]: so-called *type-A* glass formers do not exhibit a distinct  $\beta$ -process in the dielectric spectrum, whereas for *type-B* such a peak becomes discernible.

Dielectric spectra of the type-A system glycerol are displayed in figure 2.3 (a): the pronounced excess wing and the strong temperature dependence of the peak maximum is observable. Furthermore it is seen that the shape of the  $\alpha$ -process does not change in first approximation (*frequency-temperature-superposition* principle, FTS), albeit the relative contribution of the excess wing slightly varies at the selected temperatures. The temperature dependence of the  $\alpha$ -process can be quantified via

<sup>1</sup>This frequency range is not accessible by means of NMR and conventional broadband dielectric spectroscopy. The boson peak is typically studied by light scattering methods and will not be further addressed in this work.

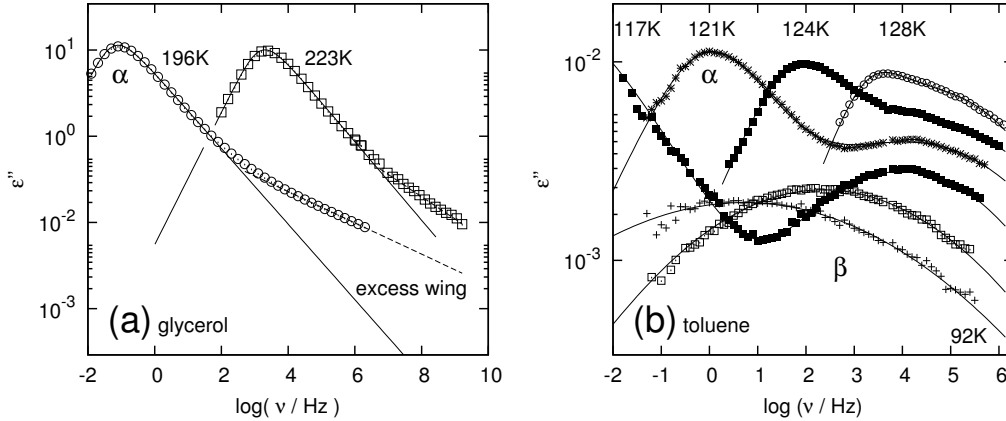


**Figure 2.3 (a):** Dielectric spectra of glycerol [Kudlik 1997b] above  $T_g=189$  K. An excess wing appears at the high frequency flank of the  $\alpha$ -process. **(b):** Dielectric spectra of toluene [Kudlik 1997b],  $T_g=117$  K. In contrast to the spectra of glycerol a pronounced  $\beta$ -peak is observed.

the maximum position of the peak  $\tau_\alpha^m = 1/(2\pi\nu_\alpha^m)$  and does not follow temperature activated behaviour, cf. figure 2.4 (a). In the supercooled liquid it can be described by the Vogel-Fulcher-Tammann (VFT) equation [Vogel 1921]:

$$\langle \tau_\alpha \rangle = \tau_0 \exp\left(\frac{D}{T - T_\infty}\right), \quad (2.1)$$

plotted as dashed line in figure 2.4 (a). The temperature  $T_\infty$  ( $0 < T_\infty < T_g$ ) marks a diverging time scale for the  $\alpha$ -process in this description, which is experimentally however not accessible. The deviation from an Arrhenius temperature dependence is often discussed in terms of fragility, via the fragility or steepness index  $m$  [Angell 1988]:

$$m = \left. \frac{d(\log \tau_\alpha)}{d(T_g/T)} \right|_{T=T_g}. \quad (2.2)$$

Whereby substances with low  $m$ , i.e. small deviations from an Arrhenius behaviour, are referred to as *strong* and such with high  $m$  as *fragile* glass formers.

The dielectric loss of the type-B glass former toluene is displayed in figure 2.3 (b): in addition to the discussed features of the  $\alpha$ -process a broad and symmetric peak at higher frequencies is observed: the  $\beta$ -process. Due to its weaker temperature dependence the  $\beta$ -peak separates from the  $\alpha$ -process above  $T_g$  and dominates the dielectric spectrum for  $T < T_g$ . In contrast to the  $\alpha$ -process the  $\beta$ -process exhibits thermally activated behaviour and follows an Arrhenius temperature dependence (solid line in figure 2.4 (b)):

$$\tau_\beta = \tau_0 \exp\left(\frac{E_a}{RT}\right). \quad (2.3)$$

As seen for toluene in figure 2.3 (b), the emergence of an excess wing is often very subtle or not observed at all in type-B systems, whereas for type-A glass formers the feature is typically present.

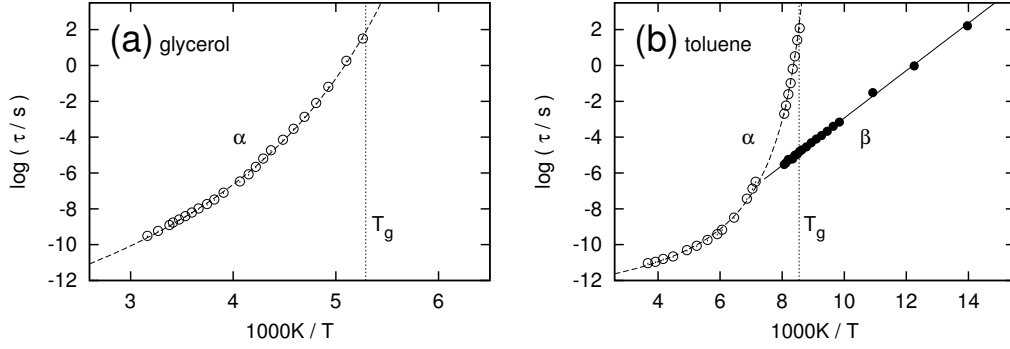


**Figure 2.4 (a):** Time constants of the  $\alpha$ -process in glycerol from dielectric spectroscopy [Kudlik 1997b]. **(b):** Time constants of the  $\alpha$ -process (open symbols,  $\tau > 10^{-6}$ s: dielectric [Kudlik 1997b],  $\tau < 10^{-6}$ s: NMR [Rössler 1984]) and  $\beta$ -process (full symbols, dielectric [Kudlik 1997b]) in toluene with corresponding VFT and Arrhenius fits.

## 2.2 The $\alpha$ -process

The  $\alpha$ -process or structural relaxation in the simple and supercooled liquid and governs the glass transition, i.e. it determines the long time behaviour of any correlation function. Alongside with the deviation from an Arrhenius temperature dependence for the  $\alpha$ -process (equation 2.1) arise a number of universal characteristics for the respective motional process: the motion is rendered cooperative, the correlation functions become stretched, i.e. non-exponential, and correlation is lost via a sequence of complex (jump) processes.

The VFT temperature dependence is often explained in the scope of a cooperative volume. Below a certain temperature molecules are no longer able to reorient individually, they are *caged* by neighbouring molecules. The respective cooperative volume is on the order of nanometers [Tracht 1988].

In the simple liquid the correlation function is fairly exponential, whereas in the supercooled regime it becomes stretched, as observed in figure 2.3 via an asymmetric broadening of the  $\alpha$ -peak in the dielectric spectra (phenomenological functions to model the characteristic shape of the dielectric loss are introduced in section C.3). The correlation functions measured in  $^2\text{H}$  NMR are typically well described by a stretched-exponential or Kohlrausch function in this regime [Kohlrausch 1854, Williams 1970]:

$$f(t) = \exp \left[ - \left( \frac{t}{\tau_\alpha} \right)^{\beta_K} \right], \quad (2.4)$$

with  $0 < \beta_K \leq 1$  and the mean correlation time  $\langle \tau_\alpha \rangle$ :

$$\langle \tau_\alpha \rangle = \frac{\tau_\alpha}{\beta_K} \Gamma \left( \frac{1}{\beta_K} \right). \quad (2.5)$$

This non-exponentiality of the correlation functions can be discussed within two limiting scenarios: homogeneous dynamics, i.e. each molecule exhibits intrinsically non-exponential correlation loss, or a heterogeneous scenario based on a distribution

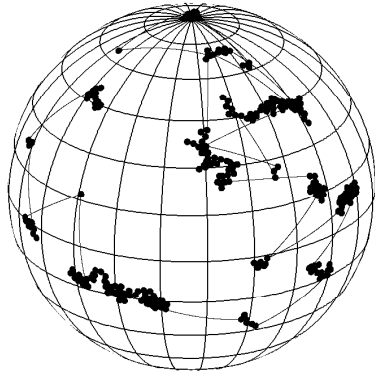


**Figure 2.5:** Sketch of the rotational motion of the  $\alpha$ -process: a bi-modal jump scenario is presented, which is dominated by small angular jumps (on the order of  $2^\circ$ ). In addition a 5% fraction of  $30^\circ$  jumps is assumed. Figure adapted from [Böhmer 2001].

of correlation times  $G(\log \tau_\alpha)$  with an exponential correlation function of each sub-ensemble. For glasses typically broad distributions of correlation times are found [Schmidt-Rohr 1991, Heuer 1996, Böhmer 1996]. Yet exchange within  $G(\log \tau_\alpha)$  appears on the time scale of  $\tau_\alpha$ , hence none of the discussed limiting cases strictly describes glassy dynamics. As dynamic sub-ensembles within  $G(\log \tau_\alpha)$  can however be selectively probed in the experiment [Böhmer 1998a, Böhmer 2006], the notation *dynamic heterogeneities* is commonly used when referring to glassy dynamics.

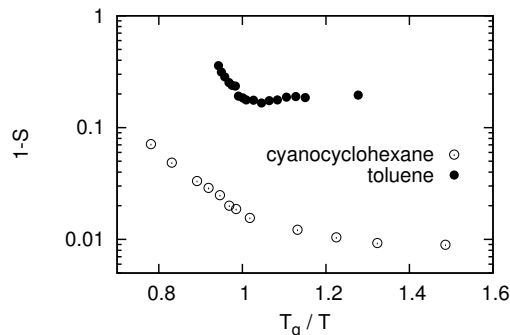
2D NMR experiments to study the microscopic dynamics of the  $\alpha$ -process at temperatures close to but above  $T_g$  unanimously depict a complex motional process, significantly different from the diffusive motion observed at higher temperatures [Hinze 1998, Jörg 2000, Baldus 2005]. The motion is commonly described in terms of a model which is dominated by small angular reorientations, with a subtle but distinct fraction of large angular jumps, as sketched in figure 2.5. The latter fraction is typically reported to exhibit a strong temperature dependence – a finding which we will reassess in section 6.4.4.

## 2.3 The $\beta$ -process

The arise of a secondary peak in the dielectric spectrum is anticipated for polymers with side-groups and molecules with internal degrees of freedom, as a small reorientation of the chain or molecule may be followed by a relocation of the side-group [McCrum 1967] or trigger a conformational change. It was however demonstrated by Johari and Goldstein that also rigid molecules exhibit such a secondary relaxation [Johari 1970, Johari 1973, Johari 1976], consequently it was argued by the authors that the  $\beta$ -process represents an intrinsic property of the glassy state. In honor of this discovery the process is often referred to as *Johari-Goldstein (JG)  $\beta$ -process* to distinguish it from e.g. the  $\beta$ -process predicted by mode-coupling theory, as they describe different phenomena.

The basic features of the  $\beta$ -process are: it dominates the dielectric spectrum for  $T < T_g$  and manifests in a broad, symmetric peak which is well described by a log-Gaussian

**Figure 2.6:** Relative relaxation strength  $1-S = \Delta\epsilon / \Delta\epsilon_\beta$  of the  $\beta$ -process in cyanocyclohexane [Tschirwitz 2002a] and toluene [Benkhof 1999]. Whereas the absolute strengths are different, the qualitative temperature dependence with respect to  $T_g$  is comparable.



distribution [Kudlik 1997a, Kudlik 1998]:

$$G(\log \tau_\beta) = \frac{1}{2\pi\sigma^2} \exp \left[ -\frac{(\log \tau_\beta - \log \tau_\beta^m)^2}{2\sigma^2} \right], \quad (2.6)$$

with a temperature dependent width  $\sigma$  [Kudlik 1998]:

$$\bar{\sigma}(T) = \frac{\sigma}{\ln 10} \cdot \left( \frac{1}{T} - \frac{1}{T_\delta} \right). \quad (2.7)$$

The temperature dependence of the peak maximum exhibits thermally activated behaviour and the rule  $E_a \simeq 24 \cdot T_g$  holds for many substances [Kudlik 1999, Blochowicz 2004, Ngai 2004a]. The relaxation strength of the  $\beta$ -process in dielectric spectroscopy is typically quantified via the fraction  $1-S = \Delta\epsilon_\beta / \Delta\epsilon$  of the total relaxation strength:  $1-S$  is small and virtually constant for temperatures  $T < T_g$ , but rapidly grows above  $T_g$  until around typically  $\tau_\beta(T) \approx 10^{-6}$  s [Hansen 1997] the time scales of  $\alpha$ - and  $\beta$ -process merge and only a single peak is observed in the dielectric spectra at higher temperatures. Whereas the temperature dependence of  $1-S$  is rather universal, the absolute strength varies among different systems, cf. figure 2.6. Johari and Goldstein introduced the “islands of mobility” concept [Johari 1976] to explain the arise of a  $\beta$ -peak in the dielectric spectrum: it was speculated that certain groups of molecules remain an enhanced mobility with respect to their surroundings even in the glassy state. Williams and Watts on the other hand postulated that all molecules contribute to the  $\beta$ -process, which yields a small correlation loss for all sub-ensembles before any remaining correlation is destroyed at much longer times by the  $\alpha$ -process [Williams 1971].

By means of dielectric spectroscopy, solvation [Wagner 1998] and NMR [Vogel 2001a, Vogel 2001b, Vogel 2002] techniques it was demonstrated that the latter assumption holds, also in case of molecules without internal degrees of freedom, i.e. all molecules contribute to the Johari-Goldstein  $\beta$ -process – the “islands of mobility” concept was refuted. On the basis of the latter NMR experiments (an overview is presented in [Vogel 2005]) it was furthermore demonstrated that the  $\beta$ -process is a restricted, i.e. anisotropic, multi-step motion. For toluene a model was proposed wherein the motional process is restricted to the circumference of a cone with half opening angle

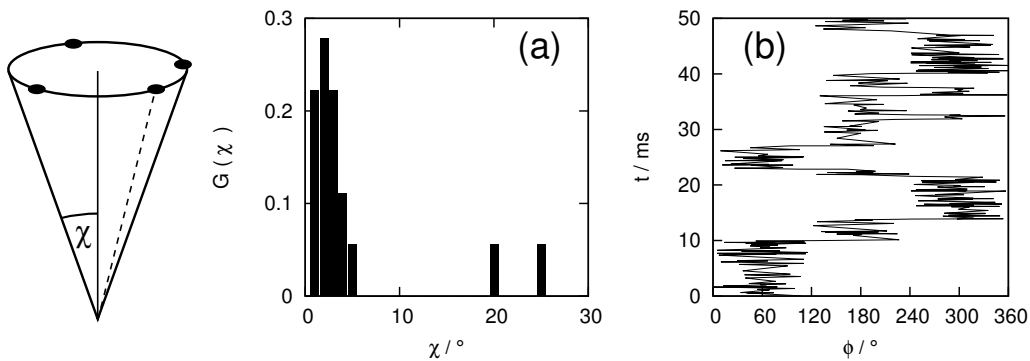


**Figure 2.7 left:** Proposed model of a reorientation on the circumference of a cone for the  $\beta$ -process. **(a):** Distribution of opening angles from an adaptation of the model to  $^2\text{H}$  NMR results of toluene [Vogel 2000a]. **(b):** Sketch of the proposed multi step motion for the  $\beta$ -process,  $\phi$  denotes the orientation on the circumference [Vogel 2000a].

$\chi$ , cf. figure 2.7. By means of a distribution  $G(\chi)$ , which is centred around  $4^\circ$  but incorporates also a small fraction of larger angles (figure 2.7 (a)), and a complex multi-step reorientation by which the circumference is explored (cf. figure 2.7 (b)), all  $^2\text{H}$  NMR observables for  $T < T_g$  in toluene were successfully reproduced. The model has furthermore been applied to different glass formers where comparable results in terms of  $G(\chi)$  were obtained [Vogel 2005].

### 2.3.1 Open questions

Whereas the described model has proven successful in reproducing the  $^2\text{H}$  NMR results obtained in several systems, the proposed scenario certainly is ambiguous and purely phenomenological. A straightforward connection to the energy landscape of the glass, which could serve to explain the universal features of the  $\beta$ -process, is lacking. Numerous questions regarding the nature of the  $\beta$ -process remain and are currently a matter of debate.

First of all the description of the  $\beta$ -process as an “intrinsic property of the glassy state” according to Johari and Goldstein apparently conflicts with the afore introduced classification of type-A/B glass formers. Whereas the excess wing in type-A systems was argued by some to represent an inseparable feature of the  $\alpha$ -process [Dixon 1990, Leheny 1997], other authors suggest that the excess wing is nothing but the high frequency flank of a  $\beta$ -process hidden underneath the  $\alpha$ -peak [Hensel-Bielowka 2002, Ngai 2004b, Schneider 2000]. Blochowicz et al. [Blochowicz 2004] demonstrated that the excess wing in 2-picoline is gradually transformed into a  $\beta$ -peak upon a slowing down of the  $\alpha$ -process in binary mixtures with tri-styrene, an effect which was also reported for other type-A systems [Shahin Thayyilab 2008]. Furthermore the excess wing in glycerol was demonstrated to proceed via small angular displacements [Gainaru 2008], i.e. the large angular reorientations, which account for the better part of correlation loss due to the  $\alpha$ -process, are not observed in the respective frequency range. Yet certain glass formers exhibit both, an excess wing and a resolved  $\beta$ -peak,

in their dielectric spectra, challenging the interpretation of the first in terms of a submerged representation of the latter.

For glass formers with a distinct  $\beta$ -peak in the dielectric spectrum the interdependence of the latter and the  $\alpha$ -process is currently also a matter of debate: as mentioned before, the rule  $E_a \simeq 24 \cdot T_g$  holds for many substances. 2D  $^2\text{H}$  NMR experiments demonstrated that a positive correlation between  $\tau_\alpha$  and  $\tau_\beta$  within the respective distributions exists [Böhmer 2006], i.e. molecules with a momentarily fast  $\beta$ -process also exhibit a relatively fast  $\alpha$ -process and vice versa. Furthermore the entropy and volume dependencies of the processes (i.e. under pressure and temperature variation) suggest a strong correlation [Prevosto 2009], which is anticipated in the *coupling model* introduced by K.L. Ngai [Ngai 1979].

As the relaxation strength of the  $\beta$ -process strongly grows above  $T_g$  and since all molecules participate already at  $T < T_g$ , i.e. the effect can not be rationalised by an increasing number of contributing sub-ensembles, it was argued that the  $\beta$ -process governs relaxation at temperatures above the merging of  $\alpha$ - and  $\beta$ -process and the former becomes extinct [Garwe 1996]. The random first-order transition (RFOT) theory [Lubchenko 2007] of glasses also predicts that the secondary process becomes the dominant mode of structural relaxation at high temperatures [Stevenson 2010], yet no agreement has been reached regarding the dominance of either process above the merging temperature. The fast and non-merging  $\beta$ -process in cyanocyclohexane yields the possibility to monitor the  $\beta$ -process at relatively high temperatures by means of  $^2\text{H}$  NMR in this work and hence quantify the relaxation strength, hence the substance represents a hopeful candidate regarding the elucidation of the high temperature relaxation behaviour.

The  $\beta$ -process was assumed to be of non-cooperative nature by Johari and Goldstein [Johari 1976], a perception which was recently challenged by theory [Stevenson 2010]. If the process indeed exhibits a certain degree of cooperativeness, a characteristic concentration dependence is expected to arise in binary mixtures of glass forming substances as the local environment of a molecule is gradually altered. The study of toluene in binary mixtures, presented in part II of this work allows us – amongst other things – to investigate a possible cooperativeness.

# $^2\text{H}$ NMR spectroscopy

## Contents

<b>3.1</b>	<b>The nuclear spin and its interactions</b>	<b>13</b>
<b>3.2</b>	<b>Hamiltonians</b>	<b>14</b>
3.2.1	Density matrix representation	16
3.2.2	The rotating frame	17
3.2.3	Radio frequency pulses	17
3.2.4	Spherical tensor operators	18
<b>3.3</b>	<b>Relaxation phenomena</b>	<b>18</b>
<b>3.4</b>	<b><math>^2\text{H}</math> NMR experiments in the solid state</b>	<b>19</b>
3.4.1	Solid echo	20
3.4.2	Spin-lattice and spin-spin relaxation measurements	22
3.4.3	2D NMR	23
3.4.4	Stimulated echo	24
3.4.5	2D NMR in the frequency domain	28
<b>3.5</b>	<b>Development of a low temperature double resonance probe</b>	<b>31</b>

In the following we will briefly review the principles and methods of  $^2\text{H}$  NMR spectroscopy as employed in the experimental part of this work. Unless noted otherwise, the according references for this overview are to be found in standard NMR literature [Abraham 1973, Mehring 1983, Slichter 1990], the outline of this chapter in particular follows the presentation given by Schmidt-Rohr and Spiess [Schmidt-Rohr 1994].

## 3.1 The nuclear spin and its interactions

Nuclei with a spin  $I \neq 0$  exhibit interactions with external magnetic fields and internal magnetic and electric fields. In NMR the external fields consist of a static magnetic field  $\vec{B}_0$  (w.l.o.g. aligned along the  $z$ -axis) and an alternating magnetic field  $\vec{B}_1$  with frequencies typically in the MHz regime. The internal fields are governed by the local electronic structure in the sample and allow for a determination of order and dynamics.

Nuclei with a non-vanishing spin possess a magnetic dipole moment

$$\vec{\mu} = \gamma \vec{I}, \quad (3.1)$$

with the characteristic gyromagnetic ratio  $\gamma$ . In zero field the eigenvalues of the spin  $I$  are degenerated, if an external field  $\vec{B}_0$  is applied, the levels split up (Zeeman splitting) and the magnetic moment precesses with the frequency

$$\omega_0 = -\gamma B_0. \quad (3.2)$$

The characteristic Larmor frequency  $\omega_0$  hence depends on the type of nuclei and different nuclei can be probed selectively in a resonance experiment.

In thermal equilibrium the magnetization is aligned parallel to the  $\vec{B}_0$  field according to Boltzmann distribution. In this work we only consider Fourier transform (FT-) NMR experiments, in which the spin system is modified via short radio frequency pulses. If such a radio frequency pulse is applied to the probe coil under resonance condition  $\omega_{RF} = \omega_0$ , a static field  $\vec{B}_1$  in the frame of the magnetization is created and magnetization is deflected from the  $z$ -direction to the  $x, y$ -plane for a pulse of suitable strength and length, a so-called  $90^\circ$ -pulse. In the  $x, y$ -plane the preceding magnetization yields an alternating magnetic flux which induces a voltage in the probe coil – the *free induction decay* (FID), which represents the NMR signal.

Due to the influence of local fields the resonance frequency of nuclei  $i$  differs from  $\omega_0$ : the distribution of charge carriers, the dipole-dipole interaction of the nuclei etc. yield  $\omega \neq \omega_0$ : the NMR spectrum  $\omega - \omega_0$  is obtained. After the equilibrium magnetization is perturbed by an RF-pulse, the spin system relaxes via a coupling to the so-called lattice, i.e. via statistic fluctuations of the local fields that reflect the dynamics of the sample.

In the following we will present a theoretical treatment of the conducted experiments, the extensiveness of which will be kept to a minimum. For a more detailed discussion we refer again to standard NMR literature cited above.

## 3.2 Hamiltonians

Due to the strength of the external magnetic field  $B_0$  (7.05 T for the experiments conducted in this work), the Zeeman interaction is dominant in NMR. The corresponding Hamiltonian reads<sup>1</sup>:

$$\hat{H}_Z = -\gamma \hbar B_0 \hat{I}_z \quad (3.3)$$

In the following we will use the Hamiltonians in terms of frequency units, i.e.  $\hat{H}^\omega = \hat{H}/\hbar$ . As this represents the common notation in NMR literature, we will drop the index  $\omega$  and equation 3.3 reads:

$$\hat{H}_Z = -\gamma B_0 \hat{I}_z = \omega_0 \hat{I}_z, \quad (3.4)$$

with the Larmor frequency  $\omega_0$ . In FT-NMR the coupling to the alternating  $\vec{B}_1$  field acts only during the short duration of an RF pulse (typically on the order of 2 to 3  $\mu\text{s}$  for a  $90^\circ$  pulse), and is in case of an  $x$ -pulse e.g. given via:

$$\hat{H}_{RF,x} = -\gamma B_1 \hat{I}_x. \quad (3.5)$$

<sup>1</sup>A separate notation for vector operators is not used in this work.

As the deuterium nuclei considered in this work exhibit spin  $I = 1$ , they possess a quadrupole moment  $Q$  which interacts with the electric field gradient (EFG) at the site of the nucleus, which results from the charge distribution in the respective chemical bond(s). The EFG tensor  $V$  is defined via the second spatial derivatives of the electric potential  $\Phi$ :

$$V_{\alpha\beta}^j = \frac{\partial^2 \Phi}{\partial r_\alpha \partial r_\beta} \quad ; \quad \alpha, \beta \in x, y, z \quad (3.6)$$

For a single spin this interaction is described via the corresponding quadrupolar Hamiltonian  $\hat{H}_Q$ :

$$\hat{H}_Q = \frac{eQ}{2I(2I-1)\hbar} \hat{I}V\hat{I}, \quad (3.7)$$

with the elementary charge  $e$ . As the Zeeman interaction dominates for the  $\vec{B}_0$  fields commonly used in NMR, the internal interactions can be treated in first order perturbation theory. Therefore only the secular part of  $\hat{H}_Q$  has to be considered, i.e. the part that commutes with  $\hat{I}_z$  and hence  $\hat{H}_Z$ . This so-called truncated part of the quadrupolar Hamiltonian reads:

$$\hat{H}_Q = \frac{eQ}{2I(2I-1)\hbar} V_{zz} \frac{1}{2} (3\hat{I}_z\hat{I}_z - \hat{I}\hat{I}). \quad (3.8)$$

The remainder of treatment is facilitated by a transition from the laboratory frame (LF) to the principal axis system (PAS) of the EFG tensor:

$$V_{zz}^{LF} = \frac{1}{2} [3\cos^2\theta - 1 - \eta\sin^2\theta\cos(2\phi)] V_{zz}^{PAS}, \quad (3.9)$$

with the polar angles  $\theta, \phi$  of the external  $\vec{B}_0$  field in the PAS of the tensor. As the tensor has diagonal form in the PAS, it is defined via two principal values:  $V_{zz}^{PAS}$  and the asymmetry parameter  $\eta$ :

$$\eta = \frac{V_{yy}^{PAS} - V_{xx}^{PAS}}{V_{zz}^{PAS}}. \quad (3.10)$$

With  $V_{zz}^{PAS} = e \cdot q$  equation 3.8 reads:

$$\hat{H}_Q = \frac{eQeq}{2I(2I-1)\hbar} \frac{1}{4} [3\cos^2\theta - 1 - \eta\sin^2\theta\cos(2\phi)] (3\hat{I}_z\hat{I}_z - \hat{I}\hat{I}). \quad (3.11)$$

For  $I=1$  and  $\Delta m \pm 1$  the corresponding transitions are in  $^2\text{H}$  NMR (cf. figure 3.1) observed at the frequency:

$$\begin{aligned} \omega(\theta, \phi) &= \frac{E_0 \pm E_Q}{\hbar} = \omega_0 \pm \omega_Q(\theta, \phi) \\ &= \omega_0 \pm \frac{\delta}{2} [3\cos^2\theta - 1 - \eta\sin^2\theta\cos(2\phi)], \end{aligned} \quad (3.12)$$

with the anisotropy parameter  $\delta$ :

$$\delta = \frac{3eQeq}{4\hbar}. \quad (3.13)$$

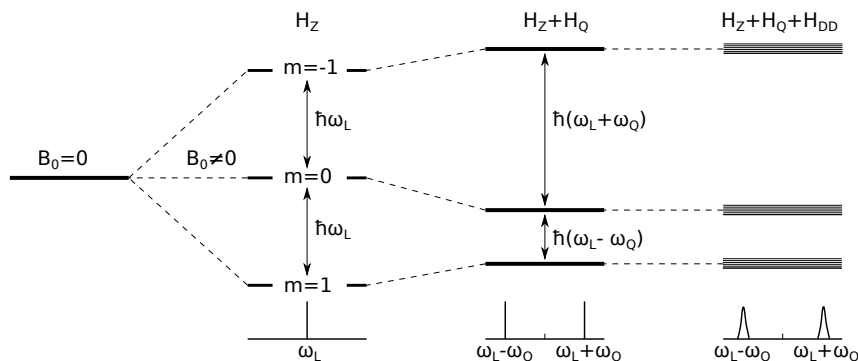


**Figure 3.1:** Energy level diagram of a spin  $I=1$ . Under the influence of a magnetic field and the quadrupolar coupling the otherwise degenerated energy levels split up. The additional (relatively weak) dipolar coupling yields in the ensemble average a broadening of the observed lines.

For all deuterated compounds in this work the aliphatic C- $^2\text{H}$  bonds in first approximation have an axially symmetric charge density, hence the EFG tensor is also axially symmetric in good approximation. In this case the asymmetry parameter  $\eta$  vanishes and the quadrupolar frequency does not depend on the polar angle  $\phi$ :

$$\omega_Q = \frac{\delta}{2} [3 \cos^2 \theta - 1]. \quad (3.14)$$

As for  $\eta = 0$  the principal value  $V_{zz}^{PAS}$  of the EFG tensor is parallel to the direction of the C- $^2\text{H}$  bond,  $\omega_Q$  observed in the experiment directly yields the angle  $\theta$  between  $\vec{B}_0$  and the respective C- $^2\text{H}$  bond.

### 3.2.1 Density matrix representation

As the spin systems under consideration are usually not fully polarized, a simple treatment via the Schrödinger equation is often not possible. Instead a convenient description in terms of statistical quantum mechanics via the density matrix representation is employed. The density operator  $\hat{\rho}$  describes the state of the spin system (including any incoherent superposition of spin states) and the Hamiltonians represent the internal and external interactions. Analogous to the Schrödinger equation, the operators  $\hat{\rho}$  and the total Hamiltonian  $\hat{H}$  of the spin system are connected via the von Neumann equation:

$$\frac{d}{dt} \hat{\rho}(t) = -i [\hat{H}(t), \hat{\rho}(t)] \quad (3.15)$$

In this formalism the physical observables are obtained from the trace of the density operator:

$$\langle A \rangle = \text{Tr}(\hat{\rho}A) \quad (3.16)$$

For a time-independent Hamiltonian  $\hat{H}$ , a formal solution of the von Neumann equation is given by:

$$\hat{\rho}(t) = e^{-i\hat{H}t} \hat{\rho}(0) e^{i\hat{H}t}, \quad (3.17)$$

with the propagator

$$\hat{U}(t) = e^{-i\hat{H}t}. \quad (3.18)$$

In thermal equilibrium the description in terms of the density operator  $\hat{\rho}$  is analogous to the classical Boltzmann distribution:

$$\begin{aligned} \hat{\rho}_{eq} &= \frac{1}{Z} e^{-\hat{H}/kT} \\ Z &= \text{Tr} \left( e^{-\hat{H}/kT} \right) \end{aligned} \quad (3.19)$$

As for temperatures above 1 K and common  $\vec{B}_0$  field strengths  $|\hbar\gamma B_0/kT| \ll 1$  holds, an expansion of the exponential operator in equation 3.19 can be truncated after the linear term. This so called high temperature approximation yields:

$$\hat{\rho}_{eq} \propto \left( \hat{1} + \frac{\hbar\gamma B_0}{kT} \hat{I}_z \right). \quad (3.20)$$

Within this framework the evolution of the density matrix under the influence of  $\hat{H}$  can in principal be calculated, for the consideration of RF-pulses it is however convenient to employ a description in the rotating frame.

### 3.2.2 The rotating frame

For the Hamiltonian  $\hat{H}_Z$  of the Zeeman interaction the time evolution according to equation 3.17 reads:

$$\hat{\rho}(t) = e^{-i\omega_0 t \hat{I}_z} \hat{\rho} e^{i\omega_0 t \hat{I}_z}, \quad (3.21)$$

i.e. any magnetization  $\hat{I}_\alpha$  is rotated about the  $z$ -axis with an angle  $\omega_0 t$ . Via the transformation to a rotating frame with  $\omega_r = \omega_0$ , this precession is eliminated:

$$\hat{\rho}_r(t) = e^{-i\omega_r t \hat{I}_z} \hat{\rho}(t) e^{i\omega_r t \hat{I}_z} = e^{-i(\omega_r - \omega_0) t \hat{I}_z} \hat{\rho} e^{i(\omega_r - \omega_0) t \hat{I}_z}. \quad (3.22)$$

If we now consider the Hamiltonian  $\hat{H} = \hat{H}_Z + \hat{H}_Q$  of the Zeeman and the quadrupolar interaction for example in the rotating frame, the von Neumann equation reads:

$$\frac{d}{dt} \hat{\rho}(t)_r = -i \left[ \hat{H}_{Q,r}(t), \hat{\rho}(t)_r \right], \quad (3.23)$$

i.e.  $\hat{H}_Z$  does no longer appear. As the experimental NMR frequency is also obtained in terms of the rotating frame, the remainder of this section will be presented in this notation and the index  $r$  will be dropped.

### 3.2.3 Radio frequency pulses

Of the alternating  $\vec{B}_1$  field acting during the duration of radio frequency pulses, only the components perpendicular to the  $B_0$  field are of interest:

$$B_1^{LF}(t) = 2B_1 \cos(\omega_{RF}t + \phi). \quad (3.24)$$

This produces two rotating fields: one with  $+\omega_{RF}$  and one with  $-\omega_{RF}$ . For an RF pulse in resonance,  $\omega_0 = \omega_{RF}$ , the field rotating with  $-\omega_{RF}$  can be neglected in first

approximation. Furthermore the alternating  $\vec{B}_1$  field is transformed to a static one in the rotating frame under this condition ( $\omega_r = \omega_0 = \omega_{RF}$ ).

In most experiments  $90^\circ$  pulses are employed, i.e. the magnetization is turned by  $90^\circ$  with respect to a certain axis:

$$\frac{\pi}{2} = \gamma B_1 t_P. \quad (3.25)$$

If we adopt the 'left handed' convention (as common in NMR literature), the propagator of an  $+x$  pulse reads:

$$\hat{P}_x(t) = e^{i\hat{H}_{P,x}t} = e^{i\gamma B_1 t \hat{I}_x}, \quad (3.26)$$

i.e.  $+z$  magnetization is rotated to the  $+y$  axis.

### 3.2.4 Spherical tensor operators

To circumvent the explicit solution of the von Neumann equation, the symmetry of the system can be exploited in the expansion of the Hamiltonians in terms of spherical tensor operators according to the Wigner-Eckart theorem:

$$\hat{H}_\lambda = c_\lambda \sum_{l=0}^2 \sum_{m=-l}^l (-1)^m \hat{T}_{l,m}^\lambda \hat{R}_{l,-m}^\lambda, \quad (3.27)$$

with the irreducible spin operators  $\hat{T}_{l,m}^\lambda$  and the spatial part  $\hat{R}_{l,-m}^\lambda$ . The evolution of these operators under the influence of RF-pulses and the quadrupolar coupling is tabulated [Schmidt-Rohr 1994] and can conveniently be employed in the description of the pulse sequences in the remainder of this chapter – without explicitly solving the von Neumann equation.

## 3.3 Relaxation phenomena

The introduced density matrix formalism does not account for relaxation phenomena, which drive the system to thermal equilibrium. Relaxation is mediated via weak couplings of the spin to the lattice (spin-lattice relaxation  $T_1$ ), which provides means of energy transfer and restores magnetization parallel to  $\vec{B}_0$ , and to other spins (spin-spin relaxation  $T_2$ ), which leads to a correlation loss of the transversal magnetization, i.e. no energy transfer is involved.

Both components can be described as coupling to a fluctuating local field introduced by e.g. molecular motion in terms of perturbation theory. The spectral density  $J(\omega)$  connects the correlation function of the molecular motion to the  $^2\text{H}$  NMR relaxation processes:

$$J(\omega) = \frac{1}{2} \int_{-\infty}^{\infty} F(t) e^{i\omega t} dt. \quad (3.28)$$

For an isotropic motion and an axial symmetric EFG tensor ( $\eta = 0$ ) the spin-lattice relaxation  $T_1$  is then given via [Abragam 1973]:

$$\frac{1}{T_1} = \frac{2}{15} \delta^2 [J(\omega_0) + 4J(2\omega_0)]. \quad (3.29)$$

The transversal spin-spin relaxation  $T_2$  reads under these conditions:

$$\frac{1}{T_2} = \frac{1}{15} \delta^2 [3J(0) + 5J(\omega_0) + 2J(2\omega_0)]. \quad (3.30)$$

For a simple dynamic process where  $F_2$  is exponential (i.e. for a spectral density of Debye type) equation 3.29 (and eq. 3.30 accordingly) can be transformed to the so-called *BPP* equation [Bloembergen 1948]:

$$\frac{1}{T_1} = \frac{2}{15} \delta^2 \left[ \frac{2\tau}{1 + (\omega_0\tau)^2} + \frac{8\tau}{1 + (2\omega_0\tau)^2} \right]. \quad (3.31)$$

In supercooled liquids and glasses the motion is typically characterized by a distribution of correlation times  $G(\log \tau)$ . In the presence of such dynamic heterogeneities equation 3.31 is no longer applicable, instead the average rate  $\langle 1/T_1 \rangle$  has to be expressed in terms of the distribution after Resing et al. [Resing 1965]:

$$\left\langle \frac{1}{T_1} \right\rangle = \int_{-\infty}^{\infty} \frac{1}{T_1(\tau)} G(\log \tau) d \log \tau, \quad (3.32)$$

where  $T_1(\tau)$  denotes equation 3.31. In this case the corresponding magnetization curve

$$\Phi(t) = \frac{M_{z,\infty} - M_z(t)}{M_{z,\infty}} \quad (3.33)$$

is non-exponential and  $\langle 1/T_1 \rangle$  is obtained from the initial decay:

$$\left\langle \frac{1}{T_1} \right\rangle = \lim_{t \rightarrow 0} \frac{\partial \Phi(t)}{\partial t}. \quad (3.34)$$

In the experimental part of this work also an alternative approach will be employed to describe non-exponential magnetization curves. Hereby  $\Phi(t)$  is fitted via a Kohlrausch function:

$$\Phi(t) = M_{z,\infty} \exp \left( - \left( \frac{t}{T_1} \right)^{\beta_K} \right), \quad (3.35)$$

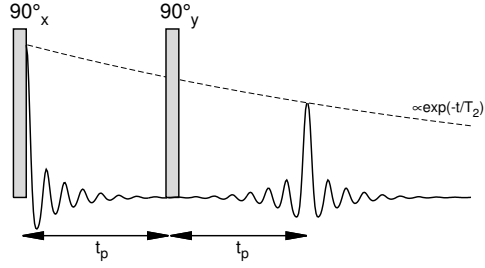
where the mean spin-lattice relaxation time is then obtained via:

$$\langle T_1 \rangle = \frac{T_1}{\beta_K} \Gamma \left( \frac{1}{\beta_K} \right). \quad (3.36)$$

### 3.4 $^2\text{H}$ NMR experiments in the solid state

In the following we present the main pulse sequences used throughout this work. The effects of the radio frequency pulses on the density matrix are thereby given in the formalism of the spherical tensor operators introduced in section 3.2.4. As before, the discussion is restricted to the peculiar features of  $^2\text{H}$  NMR experiments on supercooled liquids and in the solid, respectively glassy state.

**Figure 3.2:** Solid echo pulse sequence: the NMR signal is refocused at time  $2t_p$  after the first pulse. During the sequence the signal is damped via spin-spin relaxation processes.



### 3.4.1 Solid echo

As demonstrated in equation 3.26, a  $90^\circ +x$  pulse rotates any  $+z$  magnetization into the  $+y$  direction. In the laboratory frame the magnetization then precesses with  $\omega = \omega_0 + \omega_Q$ , which yields an alternating magnetic flux and hence an induced voltage in the coil of the NMR probe. For  $^2\text{H}$  NMR experiments in the solid state it is however often not possible to record the corresponding signal: due to the disordered nature of the samples the  $^2\text{H}$  NMR spectrum is typically broad (as all possible orientations  $\theta, \phi$  are found) and consequently the single spins de-phase very quickly and cancel via destructive interference. This fast decaying signal represents a problem since the receiver exhibits a dead time  $t_d$  directly after a pulse has been applied: the high power RF pulse creates a ringing tail in the probe coil and the pre-amplifier has to recover from a (potential) overload. Consequently echo techniques have to be employed to record the (undistorted) solid state NMR spectrum.

The widely used solid echo sequence [Powles 1963] consist of two  $90^\circ$  pulses with a  $\pi/2$  phase shift, separated by the time  $t_p$ :  $(\frac{\pi}{2})_x - t_p - (\frac{\pi}{2})_y - t'$ . The density matrix at time  $t'$  after the second pulse reads:

$$\hat{\rho}(t') = \left\langle \hat{I}_x \cos(\omega_Q(t' - t_p)) + i(\hat{T}_{21} + \hat{T}_{2-1}) \sin(\omega_Q(t' - t_p)) \right\rangle, \quad (3.37)$$

where the angle brackets denote the ensemble average over all spins. At  $t' = t_p$  again a pure  $\hat{I}_x$  state is obtained – a spin echo has been created. The solid echo sequence is sketched in figure 3.2: as the magnetization decays via the spin-spin relaxation  $T_2$  during the time of the pulse sequence and the successive detection period, the inter pulse delay  $t_p$  has to be chosen according to  $t_d < t_p < T_2$  (for the majority of solid echo experiments in this work  $t_p$  was set to  $20 \mu\text{s}$ ).

If a  $-y$  pulse is used instead of  $+y$  for the second pulse, again a pure  $\hat{I}_x$  state is obtained at  $t' = t_p$ . This behaviour is exploited to overcome small imperfections in the length (or amplitude) and phase of the RF pulses, due to which unwanted  $\hat{T}_{\alpha\beta}$  states remain at  $t' = t_p$ . As in a typical experiment a pulse sequence is executed several times with the results being accumulated to enhance the signal-to-noise ratio, a cycling in the phases of the first and second pulse efficiently suppresses the  $\hat{T}_{\alpha\beta}$  states, as their sign dependence on the phases is different from  $\hat{I}_\alpha$ . The full phase cycling of the solid echo experiment consists of eight cycles with different phases for the pulses and the receiver [Schaefer 1995].

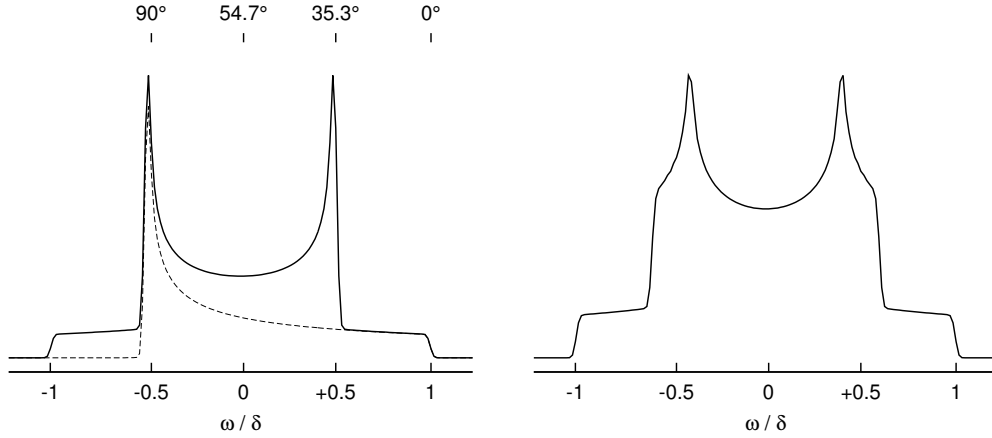


**Figure 3.3:** Numerically calculated Pake spectra for  $\eta = 0$  (left) and  $\eta = 0.2$  (right). Beneath the spectrum for  $\eta = 0$  the spectrum for a single transition is given as dashed line along with comprising orientations  $\theta$  of  $V_{zz}$  relative to  $\vec{B}_0$  (top).

### Solid echo spectrum

The spectrum is obtained from the signal after  $t' = t_p$  (which oscillates due to the evolution of the magnetization under the influence of the quadrupolar coupling) by means of Fourier transformation. For disordered systems with sufficiently slow motion (i.e. no reorientation of a C- $^2\text{H}$  bond is expected during the duration of the pulse sequence), a statistical distribution of C- $^2\text{H}$  bond orientations with respect to  $\vec{B}_0$  is probed. Samples which yield such a statistic distribution of the angle  $\theta$  are usually referred to as powders. For an EFG tensors with vanishing asymmetry parameter  $\eta$ , the spectrum is then obtained via the differential conservation of the integral:

$$S(\omega_Q(\theta)) |d\omega_Q| = P(\theta) |d\theta|. \quad (3.38)$$

As the probability to find a C- $^2\text{H}$  bond under the angle  $\theta$  with respect to the  $z$ -axis, is for  $\eta = 0$  solely defined by the surface element,

$$P(\theta) \propto \sin(\theta), \quad (3.39)$$

the spectral intensity follows directly from equation 3.14:

$$S_0(\omega_Q) = \begin{cases} \frac{1}{\sqrt{6\delta(\omega_Q + \frac{1}{2})}}, & -\frac{\delta}{2} \leq \omega_Q \leq \delta \\ 0, & \text{rest.} \end{cases} \quad (3.40)$$

For the two allowed transitions of a spin  $I = 1$  system, the full spectrum reads  $S(\omega_Q) = 1/2(S_0(\omega_Q) + S_0(-\omega_Q))$  and is often referred to as Pake spectrum in literature [Pake 1948]. Due to dipole-dipole coupling and the transversal relaxation  $T_2$  the individual lines of the spectrum are broadened (convolution with a Lorentzian), hence the singularities in equation 3.40 vanish in the experiment (cf. figure 3.3).

So far we have only discussed the case of static, statistically distributed C- $^2\text{H}$  bonds. If motion however becomes sufficiently fast ( $\tau \approx 1/\delta$ ), reorientation takes place

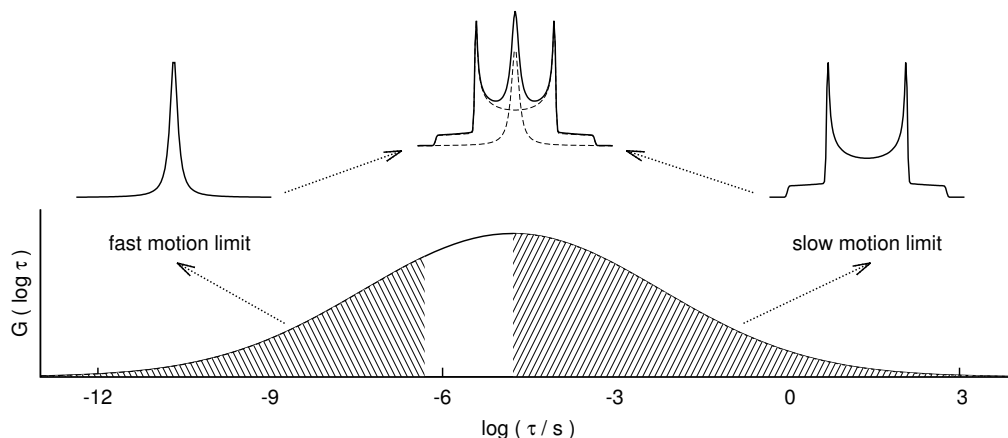


**Figure 3.4:** Two phase spectra resulting from a broad distribution of correlation times: the spectrum can be described via a weighted superposition of the spectra in the slow and fast motion limit case.

during the time  $2t_p$  and the subsequent detection period, i.e.  $\omega_Q$  changes during the pulse sequence, the echo creation becomes incomplete. The amplitude of the echo is reduced and the spectrum is subject to characteristic changes, depending on the details of the motional process. The spectra for a number of simple jump processes are discussed in chapter 4 by means of random walk simulations.

If dynamics becomes even faster ( $\tau \ll 1/\delta$ ) and is of isotropic nature (i.e.  $P(\theta) \propto \sin(\theta)$ ), then the quadrupolar coupling is averaged out before and after the second pulse and consequently an echo with the same amplitude as in the static case is formed. The corresponding spectrum is a Lorentzian with  $\omega_Q = 0$ .

If a broad, heterogeneous distribution of correlation times  $G(\log \tau)$  is present, which yields molecules in either limiting case ( $\tau \gg 1/\delta$  and  $\tau \ll 1/\delta$ ), then the remainder of molecules with  $\tau \approx 1/\delta$  can be neglected in first approximation due to their reduced contribution to the solid echo amplitude. The resulting spectrum is a weighted superposition of a Pake spectrum and a Lorentzian line:

$$S(\omega_Q) = S_{\tau \rightarrow 0}(\omega_Q) \int_{-\infty}^{\log 1/\delta} G(\log \tau) d \log \tau + S_{\tau \rightarrow \infty}(\omega_Q) \int_{\log 1/\delta}^{\infty} G(\log \tau) d \log \tau, \quad (3.41)$$

and often referred to as “two phase” spectrum in literature (cf. figure 3.4).

### 3.4.2 Spin-lattice and spin-spin relaxation measurements

To assure that each pulse sequence starts with the same initial conditions, typically a number of  $90^\circ$  pulses with various phases and spacing  $T_2 \ll t_p \ll T_1$  are executed in front of each pulse train. After each subsequent pulse  $z$  magnetization is transferred to the  $x, y$  plane and de-phases with  $T_2$ . As  $t_p \ll T_1$ , however no  $z$  magnetization is recovered between the pulses, i.e. the longitudinal magnetization is completely destroyed after this *saturation* sequence.

During the waiting time  $t_0$  between the saturation and the e.g. solid echo sequence, longitudinal magnetization is restored with  $T_1$  – hence an assessment of the  $t_0$ -dependence of the solid echo amplitude yields the magnetization curve  $\Phi(t)$ . This so-called saturation recovery experiment is employed in the slow motion limit, i.e. at temperatures where a Pake pattern is observed in the solid echo experiment. At higher temperatures, when the fast molecular dynamics average over the quadrupolar coupling, the inversion recovery sequence is typically used: hereby the first pulse in the solid echo sequence is replaced by a  $180^\circ$ -pulse, i.e. a  $-\hat{I}_z$  state is created. The following  $90^\circ$ -pulse again creates detectable transversal magnetization and the  $t_0$ -dependent amplitude ranges from  $-M_{z,\infty}$  to  $M_{z,\infty}$ .

In the solid state the amplitude of the FID decays much faster than  $T_2$  due to the rapid de-phasing of spins with different frequencies  $\omega_Q$ . As the solid echo sequences reverses this effect, the effective spin-spin relaxation time  $T_2^{\text{eff}}$  in the solid state is accessible via the  $t_p$ -dependence of the solid echo amplitude.  $T_2^{\text{eff}}$  contains contributions from  $T_2$ , i.e. from molecular dynamics, and from dipolar broadening. All spin-spin relaxation times present within this work depict  $T_2^{\text{eff}}$ .

### 3.4.3 2D NMR

The solid echo line shape allows to monitor dynamics on the time scale of  $\mu\text{s}$ , slower dynamic processes can be tracked via two-dimensional NMR methods. In a 2D  $^2\text{H}$  NMR experiment the orientation of a C- $^2\text{H}$  bond ( $\omega_Q(\theta_i)$ ) at two successive points in time is correlated. The end of the available time window is hereby given by  $T_1$  (typically on the order of ms to seconds), furthermore the technique allows to gain insight on the motional process under consideration.

The pulse sequence of a 2D experiment consists of at least three pulses:  $(\frac{\pi}{2})_x - t_e - (\frac{\pi}{2})_x - t_m - (\frac{\pi}{2})_x - t'$ , with the evolution time  $t_e$  and the mixing time  $t_m$ . After the first  $x$  pulse  $y$  magnetization is obtained that oscillates with  $\cos(\omega_{Q1}t_e)$ , i.e. evolves under the quadrupolar coupling analogous to the situation in the solid echo after the first pulse. The second  $x$  pulse transfers the magnetization in the  $-z$  direction, where the magnetization decays during  $t_m$  via the longitudinal relaxation  $T_1$ , which is typically orders of magnitude longer than  $T_2$  – the magnetization has been “stored”. After the third pulse again detectable transversal magnetization is obtained. As can be shown by means of the density matrix evolution in terms of spherical tensor operators [Schmidt-Rohr 1994], the obtained signal in the rotating frame is then proportional to:

$$\cos(\omega_{Q1}t_e) \cos(\omega_{Q2}t'), \quad (3.42)$$

where  $\omega_{Q1}$  denotes the frequency during evolution and  $\omega_{Q2}$  during the detection period. According to the spin state prepared during the mixing time  $t_m$  this pulse train is often referred to as *Zeeman* sequence. By means of different phases and a different length of the second pulse, the *Spin Alignment* state can be obtained during  $t_m$ , which yields a signal proportional to:

$$\sin(\omega_{Q1}t_e) \sin(\omega_{Q2}t'). \quad (3.43)$$

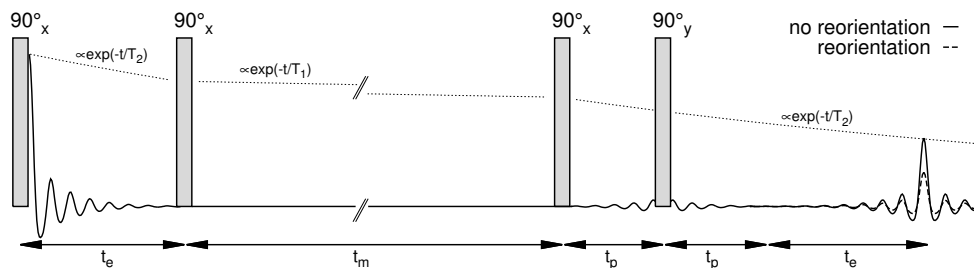


**Figure 3.5:** Stimulated echo four pulse sequence of the Zeeman experiment. The pulse delays are not represented to scale and the receiver phase is chosen arbitrarily. For the Spin Alignment experiment the second and third pulse are replaced by an  $(\frac{\pi}{4})_y$  pulse.

### 3.4.4 Stimulated echo

At first we will discuss the 2D NMR experiment in time domain, the so-called *stimulated echo*. In this sequence only the amplitude of the echo at  $t' = t_e$  is recorded for different mixing times  $t_m$ .

Typically the pulse sequences for the Zeeman and Spin Alignment experiment are expanded by a fourth  $90^\circ$  echo pulse at the end, to overcome dead time effects of the receiver as in case of the solid echo. The full sequences then read:

$$\begin{aligned} \text{Zeeman: } & \left(\frac{\pi}{2}\right)_x - t_1 - \left(\frac{\pi}{2}\right)_x - t_m - \left(\frac{\pi}{2}\right)_x - t_p - \left(\frac{\pi}{2}\right)_y - t' \\ \text{Spin Alignment: } & \left(\frac{\pi}{2}\right)_x - t_1 - \left(\frac{\pi}{4}\right)_y - t_m - \left(\frac{\pi}{4}\right)_y - t_p - \left(\frac{\pi}{2}\right)_y - t'. \end{aligned} \quad (3.44)$$

The echo amplitude for different  $t_m$  and a fixed evolution time  $t_e$  yields two one-particle two-time correlation functions (for  $t' = t_e + t_p$ ):

$$\begin{aligned} F^{ss}(t_e, t'; t_m) &= \frac{3}{4} \langle \sin(\omega_{Q1} t_e) \sin(\omega_{Q2} t') \rangle \\ F^{cc}(t_e, t'; t_m) &= - \langle \cos(\omega_{Q1} t_e) \cos(\omega_{Q2} t') \rangle \end{aligned} \quad (3.45)$$

where the angle brackets again denote the ensemble average and the index *ss/cc* stands sine-sine / cosine-cosine correlation, i.e. Zeeman and Spin-Alignment sequence. As sketched in figure 3.5, transversal and longitudinal relaxation yield further decay of  $F^{ss/cc}$  during  $t_e, t_p$  and  $t_m$ , which an analysis of the observables in the experiment has to account for.

Zeeman and Spin Alignment pulse sequence hence correlate the cosine and sine of the phases during evolution and detection time, allowing to monitor any reorientation during the mixing time  $t_m$ . The probability to find a frequency  $\omega_{Q2}$  during detection when the respective frequency was  $\omega_{Q1}$  at  $t = 0$  is expressed via  $P(\omega_{Q1}, \omega_{Q1}; t_m)$ , which can be separated into an a-priori and a conditional probability:

$$P(\omega_{Q1}, \omega_{Q2}; t_m) = P_0(\omega_{Q1}) P(\omega_{Q2}; t_m | \omega_{Q1}). \quad (3.46)$$

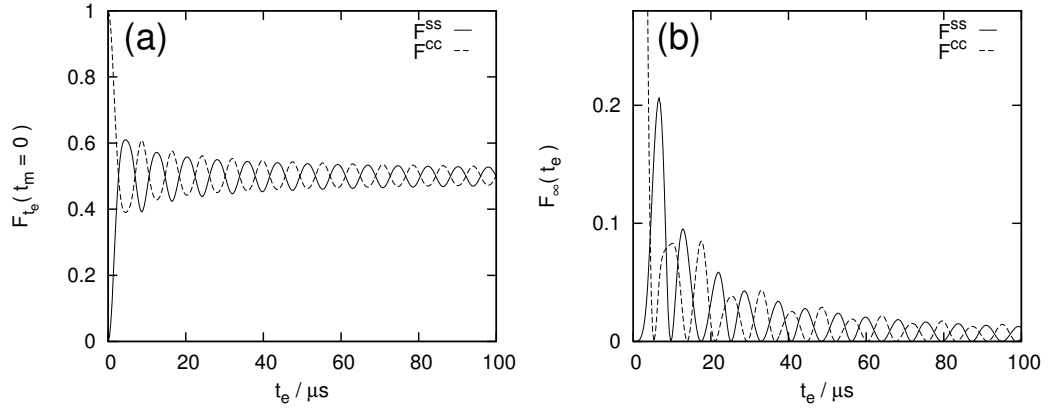


**Figure 3.6 (a):** Initial correlation of the stimulated echo experiment for Spin Alignment and Zeeman phase cycling ( $\delta=129$  kHz). **(b):** Remaining correlation  $F_\infty$  of the stimulated echo experiment for an isotropic motion.

Insertion into equation 3.45 yields in the case of  $F^{cc}$ :

$$F^{cc}(t_e, t'; t_m) = \int_{-\infty}^{\infty} \int_{-\infty}^{\infty} \cos(\omega_{Q1} t_e) \cos(\omega_{Q2} t') P_0(\omega_{Q1}) P(\omega_{Q2}; t_m | \omega_{Q1}) d\omega_{Q1} d\omega_{Q2}, \quad (3.47)$$

which in position space reads:

$$F^{cc}(t_e, t'; t_m) = \int_0^\pi \int_0^\pi \cos(\omega(\theta_1) t_e) \cos(\omega(\theta_2) t') P_0(\theta_1) P(\theta_2; t_m | \theta_1) d\theta_1 d\theta_2. \quad (3.48)$$

$F^{ss}$  is obtained analogous by replacing the cosine in equation 3.48 with the sine.

### Initial and remaining correlation

For  $t_m \rightarrow 0$  no reorientation arises during the mixing time and hence the amplitudes of  $F^{cc}$  and  $F^{ss}$  yield no information on the dynamics of the system.  $P(\omega_{Q1}, \omega_{Q2}; t_m)$  is reduced to  $\delta(\omega_{Q2} - \omega_{Q1})$  and equation 3.48 reads:

$$F^{cc}(t_e, t' = t_e; t_m \rightarrow 0) = \frac{1}{2} + \frac{1}{2} \int_0^{\pi/2} \cos(2\omega(\theta_1) t_e) \sin(\theta_1) d\theta_1$$

$$F^{ss}(t_e, t' = t_e; t_m \rightarrow 0) = \frac{1}{2} - \frac{1}{2} \int_0^{\pi/2} \cos(2\omega(\theta_1) t_e) \sin(\theta_1) d\theta_1. \quad (3.49)$$

Although no information on the dynamics is obtained, the initial correlation of the stimulated echo (figure 3.6 (a)) is of interest for mainly two reasons: as the employed evolution time  $t_e$  differs from the effective evolution time due to finite

pulse lengths in the experiment, a comparison with equation 3.49 allows to obtain the latter quantity. Furthermore the oscillations in  $F(t_e, t' = t_e; t_m \rightarrow 0)$  can be used to accurately determine the coupling constant  $\delta$ .

For sufficiently long mixing times  $t_m$  on the other hand, each C- $^2\text{H}$  bond probes all orientations accessible to the respective motional process. For full isotropic reorientation the conditional probability  $P(\omega_{Q1}, \omega_{Q2}; t_m)$  is equal to the a-priori probability  $P_0(\omega_{Q1})$ , and in this limit equation 3.48 reads (figure 3.6 (b)):

$$\begin{aligned} F^{cc}(t_e, t' = t_e; t_m \rightarrow \infty) &= \frac{1}{4} \left[ \int_0^{\pi/2} \cos(2\omega(\theta_1)t_e) \sin(\theta_1) d\theta_1 \right]^2 \\ F^{ss}(t_e, t' = t_e; t_m \rightarrow \infty) &= \frac{1}{4} \left[ \int_0^{\pi/2} \sin(2\omega(\theta_1)t_e) \sin(\theta_1) d\theta_1 \right]^2. \end{aligned} \quad (3.50)$$

In the remainder we will use the symbol  $F_\infty$  for  $F(t_e, t' = t_e; t_m \rightarrow \infty)$ .  $F_\infty$  consequently yields information on the geometry of the molecular motion, i.e. the number of accessible sites  $n$  for a C- $^2\text{H}$  bond. If the process exhibits cubic point symmetry (as does the isotropic motion discussed above) always  $F_\infty^{ss}(t_e \rightarrow 0) = 0$  is obtained [Fujara 1986]. For longest evolution times on the other hand the number of accessible sites is reflected:

$$F_\infty^{ss}(t_e \rightarrow \infty) = \frac{1}{n}, \quad (3.51)$$

i.e.  $F_\infty$  reflects the fraction of accessible sites that do not yield correlation loss: the initial correlation<sup>2</sup>.

### Model free correlation function

For sufficiently short evolution times  $t_e \ll 1/\delta$  an expansion of the sine in  $F^{ss}$  can be truncated after the linear term:

$$\begin{aligned} F^{ss}(t_e \rightarrow 0, t' = t_e; t_m) &= \frac{3}{4} \langle \sin(\omega_{Q1}t_e) \sin(\omega_{Q2}t_e) \rangle \\ &\propto \langle \omega_{Q1}\omega_{Q2} \rangle t_e^2 \\ &\propto \langle P_2(\cos\theta_1) P_2(\cos\theta_2) \rangle t_e^2 \\ &\propto F_2(t_m). \end{aligned} \quad (3.52)$$

In this limit  $F^{ss}$  correlates the frequencies, and hence via the second Legendre polynomial the orientations, during evolution and detection. The obtained correlation function is proportional to the one-particle two-time correlation function  $F_2$ , which can be compared to results from other methods in a model free approach.

In the experiment, the amplitude of the stimulated echo is typically fitted via a

<sup>2</sup>If the point group of the model contains the inversion operation,  $F_\infty^{ss}(t_e \rightarrow \infty) = \frac{2}{n}$  holds.

two-step decay function:

$$F_{t_e}^i(t_m) = A_0 \left[ (1 - F_{\infty, t_e}^i) \exp\left(-\left(\frac{t_m}{\tau_{t_e}}\right)^{\beta_{K, t_e}}\right) + F_{\infty, t_e}^i \right] \exp\left(-\left(\frac{t_m}{T_{1/1Q}}\right)^{\beta_{K, T_{1/1Q}}}\right), \quad (3.53)$$

where  $i$  stands for  $cc$  or  $ss$ . The first Kohlrausch function models the decay from  $A_0$  to  $F_{\infty, t_e}^i$  due to correlation loss via molecular motion. The second one describes the signal decay due to longitudinal relaxation during  $t_m$ :  $T_1$  in case of  $F^{cc}$  and  $T_{1Q}$  for  $F^{ss}$ .

The employed Kohlrausch function in many cases is an appropriate description of the correlation functions observed in disordered systems, the mean relaxation time is given via:

$$\langle \tau_{t_e} \rangle = \frac{\tau_{t_e}}{\beta_{K, t_e}} \Gamma\left(\frac{1}{\beta_{K, t_e}}\right). \quad (3.54)$$

### The reorientation angle distribution

Whereas  $F^{ss}$  yields the correlation function  $F_2$  in the limit  $t_e \rightarrow 0$ , the stimulated echo technique becomes increasingly sensitive on the elementary step of the motional process for prolonged evolution times. Hence the  $t_e$ -dependence of the stimulated echo allows to determine the geometry of motion, i.e. to discriminate between a random-jump like motion and rotational diffusion for example. A detailed assessment of the  $t_e$ -dependence is most expedient in the framework of random walk simulations, nevertheless we will present a brief introduction to the theoretical treatment of limiting cases. For corresponding random walk simulations and examples see chapter 4.

When addressing more complex modes of reorientation equation 3.48 can be separated into two parts:

$$F^{cc}(t_e, t' = t_e; t_m) = \int_0^\pi K^{cc}(t_e, \beta) R(\beta; t_m) d\beta, \quad (3.55)$$

where the integral kernel  $K^{cc}$  represents a geometrical quantity that is independent of any reorientation:

$$K^{cc}(t_e, \beta) = \int_0^\pi \int_0^\pi \cos(\omega(\theta_1) t_e) \cos(\omega(\theta_2) t_e) P_0(\theta_1) P(\theta_1; \theta_2 | \beta) d\theta_1 d\theta_2. \quad (3.56)$$

For disordered systems  $K^{cc}$  is determined by the statistical distribution of C- $^2\text{H}$  bonds with the a-priori probability  $P_0(\theta) \propto \sin \theta$  and the conditional probability  $P(\theta_1; \theta_2 | \beta)$  to find a pair of angles  $\theta_1, \theta_2$  with the intermediate angle  $\beta$ , i.e.  $K^{cc}$  simply reflects the geometry of the powder.

The reorientation angle distribution  $R(\beta; t_m)$  on the other hand contains information on the dynamical process:  $R(\beta; t_m)$  yields the probability that any C- $^2\text{H}$  bond with initial orientation  $\theta_1$  at  $t = 0$  has reoriented by the angle  $\beta$  at  $t = t_m$ . Due to the symmetry in  $^2\text{H}$  NMR the integration in equation 3.55 can be limited to  $0 - \frac{\pi}{2}$  as

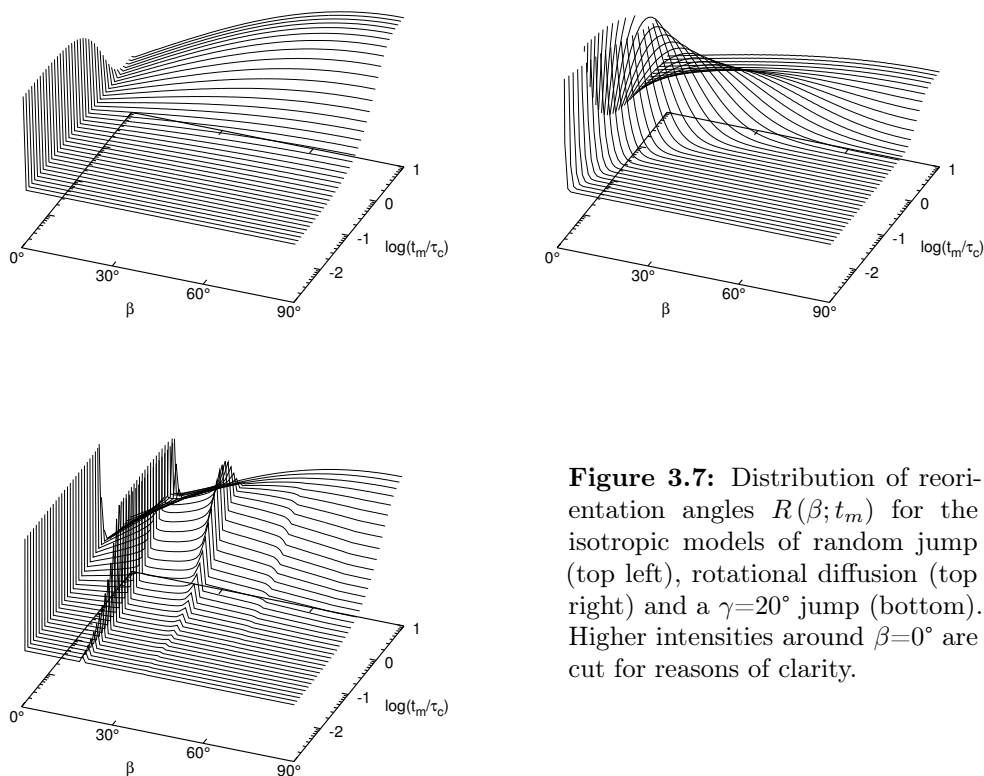


**Figure 3.7:** Distribution of reorientation angles  $R(\beta; t_m)$  for the isotropic models of random jump (top left), rotational diffusion (top right) and a  $\gamma=20^\circ$  jump (bottom). Higher intensities around  $\beta=0^\circ$  are cut for reasons of clarity.

$$\omega_Q(\theta) = \omega_Q(\pi - \theta).$$

$R(\beta; t_m)$  is obtained in straightforward manner for simple models of reorientation (cf. figure 3.7) and hence the  $t_e$ -dependence of the stimulated echo is conveniently accessible via equation 3.55.

### 3.4.5 2D NMR in the frequency domain

Instead of analysing only the amplitude at  $t' = t_e + t_p$  in the pulse sequences of the stimulated echo, it is also feasible to Fourier transform the resulting FID and obtain a 2D spectrum. The 2D spectrum yields direct information on the frequencies  $\omega_{Q1}$  and  $\omega_{Q2}$  before and after the mixing time  $t_m$ . Consequently the spectral intensity maps if and how the individual molecules have reoriented during  $t_m$ .

As an FID corresponding to  $t_e = 0$  is required for the 2D Fourier transform, the four pulse sequence of the stimulated echo is typically extended by an echo pulse between

the first and second pulse:

$$\begin{aligned} \text{ZE: } & \left(\frac{\pi}{2}\right)_x - t_{p1} - \left(\frac{\pi}{2}\right)_y - t_{p1} + t_e - \left(\frac{\pi}{2}\right)_x - t_m - \left(\frac{\pi}{2}\right)_x - t_{p2} - \left(\frac{\pi}{2}\right)_y - t' \\ \text{SA: } & \left(\frac{\pi}{2}\right)_x - t_{p1} - \left(\frac{\pi}{2}\right)_y - t_{p1} + t_e - \left(\frac{\pi}{4}\right)_y - t_m - \left(\frac{\pi}{4}\right)_y - t_{p2} - \left(\frac{\pi}{2}\right)_y - t'. \end{aligned} \quad (3.57)$$

To obtain a 2D spectrum, the mixing time  $t_m$  is held constant and the evolution time  $t_e$  is varied typically with the same stepping as employed in the detection period  $t'$ , hence equidistant points are sampled in either dimension (in NMR this sampling period is often referred to as “dwell time”). A two-dimensional Fourier transform of the signal does – in contrast to the solid echo sequence – not yield a purely absorptive spectrum, hence the so-called States method is employed: after the first Fourier transform the imaginary part in the Zeeman and the real part in the Spin-Alignment sequence is set to zero. After the Fourier transform in the second dimension the obtained spectra are purely absorptive: the Zeeman part is symmetric with respect to  $\omega_1 = \omega_2 = 0$  and the Alignment part antisymmetric. The sum of both parts reduces the ambiguity and the 2D  $^2\text{H}$  NMR spectrum is obtained.

To obtain the same amplitude from both sequences, typically the length of the second and third pulse is set to  $54.7^\circ$ : the unwanted spin states created by this deviation are eliminated via appropriate phase cycling. This procedure furthermore brings the merit that both sequences are equal with respect to the times  $t_p$  and  $t_e$ , as the effective pulse distance depends on the finite pulse lengths.

### Limiting case spectra

The 2D  $^2\text{H}$  NMR spectrum yields the probability to find the frequency  $\omega_2$  after  $t_m$  if it was  $\omega_1$  at  $t = 0$ . Consequently the spectral intensity is again given as product of a conditional and an a-priori probability:

$$P(\omega_1, \omega_2; t_m) = P(\omega_2; t_m | \omega_1) P_0(\omega_1). \quad (3.58)$$

If no reorientation takes place during  $t_m$  the conditional probability  $P(\omega_2; t_m | \omega_1)$  equals the delta function  $\delta(\omega_2 - \omega_1)$  and hence the 1D (Pake) spectrum is observed along the main diagonal, cf. figure 3.9 (a). If the molecules on the other hand reorient isotropically during  $t_m$ , i.e. the orientation after the mixing time is independent of the initial orientation, equation 3.58 reads:

$$P(\omega_1, \omega_2; t_m) = P_0(\omega_1) P_0(\omega_2), \quad (3.59)$$

and the corresponding spectrum covers the full accessible frequency range, cf. figure 3.9 (b). In-between these limiting cases the evolution of the 2D spectrum under the influence of dynamics can again be expressed in terms of the reorientation angle distribution  $R(\beta; t_m)$ :

$$S(\omega_1, \omega_2; t_m) = \int_0^{\pi/2} R(\beta; t_m) S(\omega_1, \omega_2 | \beta) d\beta, \quad (3.60)$$

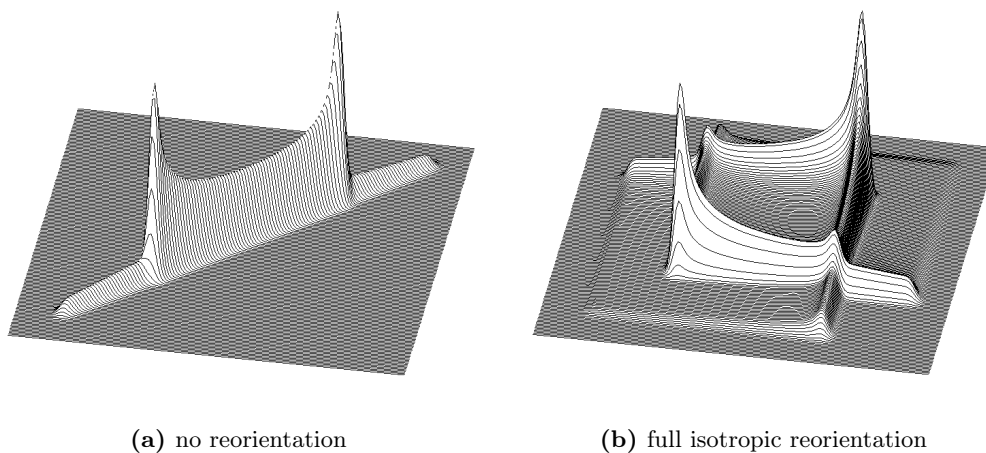


**Figure 3.8:** Simulated 2D  $^2\text{H}$  NMR spectra for the limiting cases of a static sample and for full isotropic reorientation during  $t_m$ .

where  $S(\omega_1, \omega_2 | \beta)$  is again a purely geometrical term and  $R(\beta; t_m)$  the same as in case of the stimulated echo, i.e. contains the dynamics of the system.

### Reorientation during evolution and detection

As in the case of the solid echo discussed above, also in 2D experiments the effects of molecular motion become more complex and ambiguous if reorientation takes place during evolution and detection time. The resulting 2D line shapes can typically only be addressed by means of random walk simulations in this limit.

If a 2D spectrum is however recorded in a system that is characterized by a distribution of correlation times which extends to  $\tau \ll 1/\delta$  and  $\tau \gg 1/\delta$ , i.e. for which a two phase spectrum is observed in the solid echo experiment (cf. section 3.4.1), exchange within this distribution  $G(\log \tau)$  during  $t_m$  can be monitored.

For molecules which are fast during the evolution period (i.e. contribute to a Lorentzian line) and slow during detection (i.e. contribute to a Pake spectrum) or vice versa, characteristic cross peaks arise in the spectrum (figure 3.9 (a)). The spectral intensity is given via ( $S_L$  represents a Lorentzian):

$$S_x(\omega_1, \omega_2) = \frac{1}{4} [(P_0(\omega_1) + P_0(-\omega_1)) S_L(\omega_2) + S_L(\omega_1) (P_0(\omega_2) + P_0(-\omega_2))]. \quad (3.61)$$

A typical spectrum recorded under these conditions yields (depending on the mixing time) a static fraction of molecules contributing to a Pake pattern along the main diagonal, a fraction of molecules which are fast during evolution and detection which yields a central Lorentzian line, exchange or cross-peaks between those fractions according to equation 3.61 and a characteristic reorientation pattern resulting from molecules which are static during  $t_e$  and  $t'$ , but reorient during  $t_m$ . An example for such a spectral pattern is sketched in figure 3.9 (b).

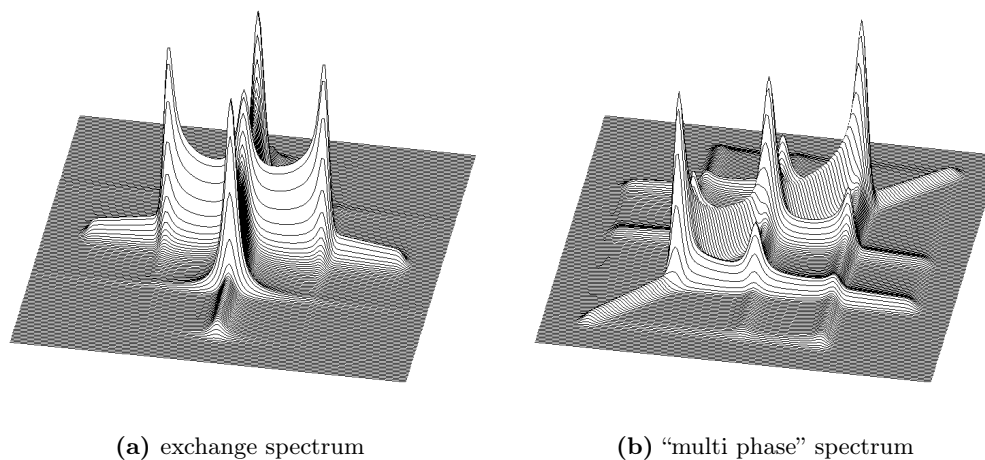


**Figure 3.9:** Simulated 2D  $^2\text{H}$  NMR spectra for exchange processes via relatively fast and slow reorienting molecules.

### 3.5 Development of a low temperature double resonance probe

In the course of this work a low-temperature  $^{31}\text{P}/^1\text{H}$  double resonance probe was designed and built in collaboration with Bruker BioSpin GmbH<sup>3</sup>. Due to the lack of commercially available double resonance probes for the temperature regime  $T \geq 4\text{ K}$ , a new probe was designed on the basis of the HP.LTSTAT single resonance probe from Bruker BioSpin GmbH and a probe built by I. Roggatz in our lab [Roggatz 2000]. The probe was manufactured in part by Bruker and the University of Bayreuth. The purpose of this probe was to extend the available setup in our laboratory with respect to  $^{31}\text{P}$  NMR studies of glass forming substances and supercooled liquids at low and lowest temperatures, while maintaining the possibility of proton decoupling in the experiments. The previously available (wide bore) double resonance probes are cooled via a stream of cold nitrogen gas, which is only feasible down to approximately 160 K and provides less thermal stability than a typical cryostat setup. The design of the probe was adapted to an available CF 1200 cryostat from Oxford Instruments, which fits inside the shim systems of typical wide bore NMR magnets (i.e. in a 89 mm bore) and offers an inner diameter of 49 mm. The employed NMR magnet provides a field strength of 9.4 T, i.e. the resonance frequency of  $^1\text{H}$  nuclei equals 400 MHz and 161.9 MHz in case of  $^{31}\text{P}$ .

For the purpose of recording  $^{31}\text{P}$  solid state spectra at low temperatures, the probe has to fulfil certain criteria which are in part contradictory [Roggatz 2000]:

- The resonance circuits should generally exhibit a low temperature dependence. Frequency tuning and impedance matching on both channels must be adjustable from outside the cryostat.

<sup>3</sup>The exciting and fruitful collaboration with Dr. E. Naumann of Bruker BioSpin is greatly acknowledged.

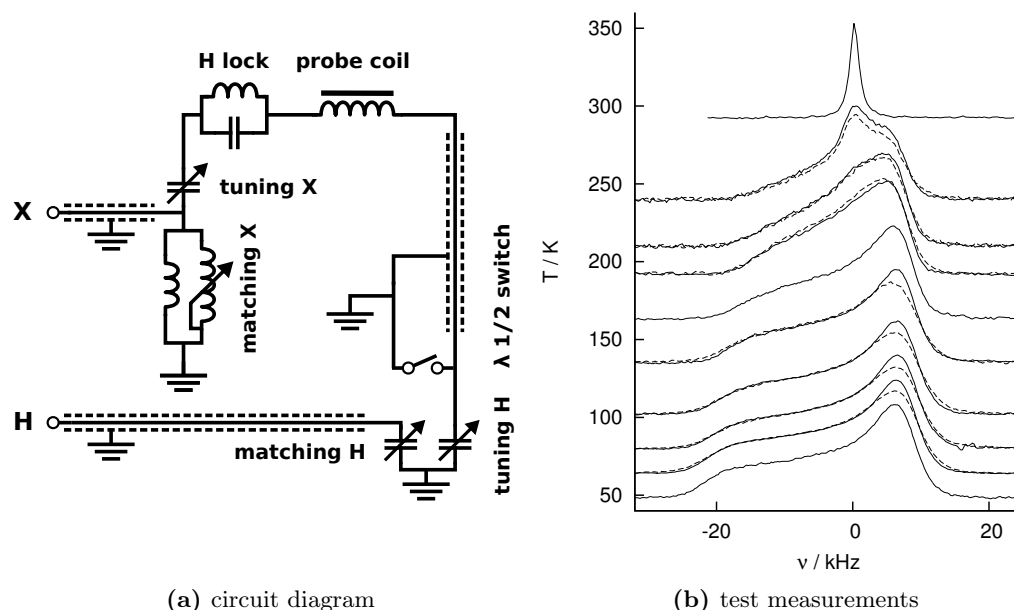


**Figure 3.10** Left: Circuit diagram of the  $^{31}\text{P}/^1\text{H}$  double resonance probe developed within this work. The dotted parallel lines mark coaxial cables. Right: Test measurements of the described setup with a sample of 19% (by weight) trimethyl phosphate in polystyrene. Hahn-echo pulse sequence, 16 scans, with  $^1\text{H}$ -decoupling: solid line, without: dashed line. The intersection with the y-axis marks the temperature.

- The quality factor of the resonant circuit must be sufficiently low to record broad solid state spectra (typically about 60 kHz) without distortion.
- The quality factor must be sufficiently high to assure adequate  $90^\circ$  pulse lengths (below  $3\ \mu\text{s}$ ) and signal-to-noise ratio during recording.
- The resonant circuit must withstand pulsed RF power on the order of 1 kW and continuous excitation with hundreds of Watts without RF flash-overs in the regions of high field strength.

The basic design of the probe is as such that all components of the resonant circuits are located inside of the cryostat. This yields higher reliability and a better signal-to-noise ratio, especially at low temperatures. Hence all electric components are incorporated into a frame made of three glass fibre reinforced plastic rods, that were copper plated and soldered to cylindrical brass plates to support the components, cf. figure 3.11. This design provides low heat conductance and a low thermal expansion coefficient, which is crucial for the application at lowest temperatures.

The circuit diagram is sketched in figure 3.10 (a): the  $^1\text{H}$  part of the resonant circuit consists of two adjustable capacitors, one for frequency tuning and the other for impedance matching to  $50\ \Omega$ . Both capacitors are adjustable from outside the cryostat by means of axles made from glass fibre reinforced plastics and a vacuum-tight duct at the bottom of the probe (cf. figure 3.11). During adjustment the upper

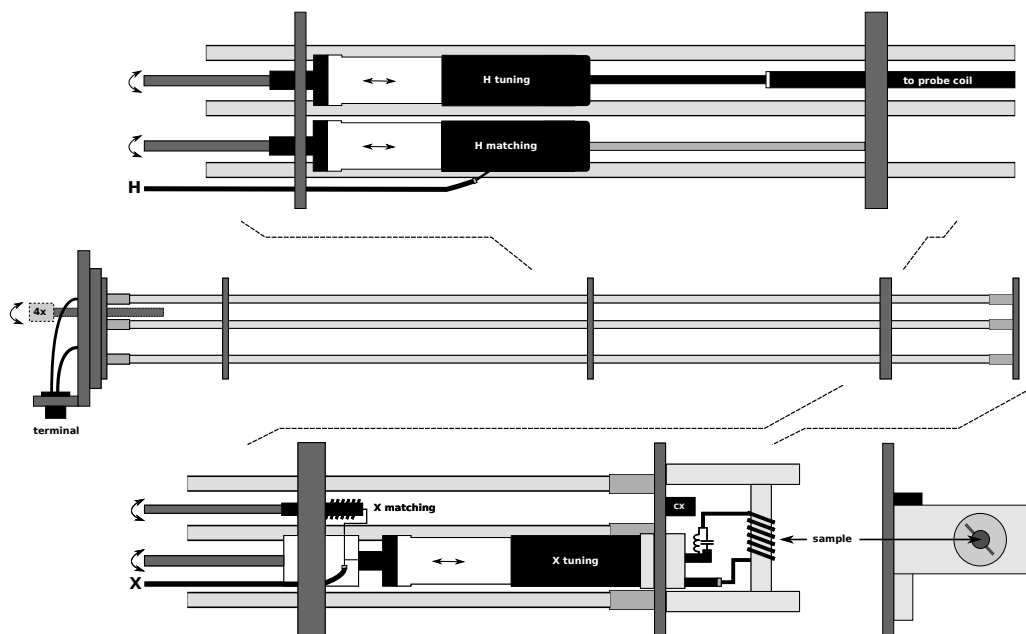


**Figure 3.11:** Sketch of the basic design of the  $^{31}\text{P}/^1\text{H}$  double resonance probe developed within this work. For details of the wiring see figure 3.10 (a).

part of the capacitor body remains fixed, which is essential as both capacitors are coupled inductively via the alignment of this part. The rigid  $\lambda/2$  wire connecting the  $^1\text{H}$  tuning capacitor to the probe coil provides a  $\lambda/4$  switch, which allows for  $^{13}\text{C}$  operation on the X-channel ( $\omega_0=100.58$  MHz). The solenoid probe coil made of a copper/silver flat wire is supported by PTFE framework which contains the 5 mm NMR tube.

The X-channel ( $^{31}\text{P}/^{13}\text{C}$ ) consists of an adjustable capacitor for frequency tuning and an inductance for impedance matching, which is adjustable by means of a spindle to bypass the appropriate amount of turns. The connection to the probe coil includes a low-pass filter which efficiently shields this path of the circuit from the proton frequency. The temperature in the area of the NMR sample is monitored by a Cernox<sup>TM</sup> resistance temperature sensor from Lake Shore Cryotronics Inc. The sensor is read out via a four-wire measurements, which allows for wiring with low heat conductance. By means of the employed sensor the temperature can be monitored accurately<sup>4</sup> in the region 1.4 K to 325 K, due to the four-wire readout however the sensor has to be disconnected during NMR measurements, as it introduces spikes in the NMR signal.

Test measurements with the described probe down to approximately 20 K showed stable and convenient operation of the setup. RF flash-overs of the proton channel in helium atmosphere could be efficiently reduced by a slight modification of the PTFE dielectric employed in the tuning and matching capacitors.

As the present work focuses on  $^2\text{H}$  NMR, the probe was however not employed in

<sup>4</sup>We however detected a slight temperature offset between the sample and the location of the sensor, which is currently still under evaluation.

the remainder of this thesis – for further results obtained with the described setup see [Bock 2011, Hoff 2010, Pötzschner 2011].

# Random walk simulations

## Contents

<b>4.1 Introduction</b> . . . . .	<b>35</b>
<b>4.2 Isotropic motion</b> . . . . .	<b>36</b>
4.2.1 2D NMR in time domain . . . . .	37
4.2.2 Solid echo line shape . . . . .	41
4.2.3 Heterogeneous dynamics . . . . .	43
<b>4.3 Anisotropic reorientation</b> . . . . .	<b>46</b>
4.3.1 Random jump type motion on a cone . . . . .	46
4.3.2 Random jump type motion within a cone . . . . .	49
4.3.3 Multi step motion within a cone . . . . .	52
4.3.4 Distributions of geometries and correlation times . . . . .	56
<b>4.4 Summary and conclusions</b> . . . . .	<b>57</b>

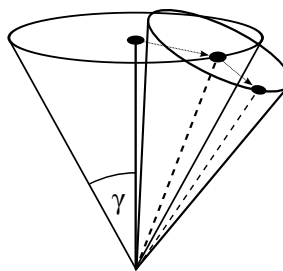
The raison d'être of the present chapter is to discuss a number of limiting cases for (molecular) motion typically associated with disordered systems from a principal point of view on the one hand, and to analyse their respective imprint on  $^2\text{H}$  NMR observables on the other. We will therefore expand the discussion of the last chapter in this regard with special attention towards the the solid echo line shape and the stimulated echo decay.

The models presented in the following are not to be regarded as realistic or physically plausible for the systems studied in this work – rather they present an arbitrary subset of scenarios, which distinguish themselves by their simplicity (from a mathematical point of view) and serve to raise awareness for the analysis of experimental results presented in the following chapters. The reader familiar with  $^2\text{H}$  NMR experiments regarding dynamics in supercooled liquids and glasses may skip ahead to the experimental section in chapter 5 and eventually return to certain sections of the present chapter when referred to.

## 4.1 Introduction

The angular resolution of solid state  $^2\text{H}$  NMR is a great vantage of the method, but on the other hand accounts for the challenge of correct data interpretation – with various, often ambiguous and subtle effects. 2D NMR methods were often employed to study simple motional processes with fixed geometries like  $\pi$ -flips, methyl group rotations etc., whereas isotropic dynamics were typically modelled via simple modes of reorientation like rotational diffusion [Pschorn 1991], as the evolution of  $R(\beta; t_m)$  within these models can be readily calculated and an adaptation to the experimental

**Figure 4.1:** Sketch of an isotropic random jump type motion. After each jump about an angle  $\gamma_i$  a random position on the circumference of a cone with opening angle  $2\gamma_i$  is occupied.



results if often possible via the introduction of a distribution  $G(\log \tau)$ . A comprehensive description of two dimensional NMR methods and simple modes of reorientation can be found in the book of Schmidt-Rohr and Spiess [Schmidt-Rohr 1994].

In contrast to the simple models presented in chapter 3, a straightforward calculation of the NMR observables via  $R(\beta; t_m)$  may become infeasible for more complex modes of reorientation. Particularly this procedure does not account for reorientation during the evolution and detection time of a typical 2D experiment; for the broad distributions  $G(\log \tau)$  typically found in (binary) glass formers, such effects can however no longer be neglected. Hence the  $^2\text{H}$  NMR observables will be calculated by means of a continuous time random walk [Hinze 1998], which represents a class of Monte Carlo simulations. The outline of the conducted simulations is as follows: given that the NMR frequency  $\omega$  is known at all times, the results of the  $^2\text{H}$  NMR pulse sequences presented in section 3.4 can be calculated. Consequently the trajectories  $\Omega_i(t)$  of a large number of molecules (typically  $10^5$  to  $10^7$ ) were recorded for sufficiently long time. From the time dependent NMR frequency  $\omega$  of each molecule under consideration, the evolution in the respective pulse sequence was calculated and the results were added to obtain the ensemble averaged quantities.

Reorientation is considered in the Ivanov model [Ivanov 1964], i.e. the molecules jump instantaneously between two subsequent orientations. The waiting time  $t_w$  between two jumps is drawn from an exponential distribution:

$$P(t_w) = \frac{1}{\tau_j} \exp\left(-\frac{t_w}{\tau_j}\right), \quad (4.1)$$

with the jump time  $\tau_j$ . As hence no correlation between two subsequent waiting times exists, the present random walk simulations represent stationary Markov processes. Simulations in this manner have been successfully applied in  $^2\text{H}$  NMR studies of disordered systems [Hinze 1998, Geil 1993, Böhmer 1998b, Fujara 1986, Wefing 1988, Vogel 2005], an overview is presented in [Böhmer 2001]. The following brief survey follows the approach presented in [Geil 1993, Micko 2007, Vogel 2000a].

## 4.2 Isotropic motion

In the first part of this chapter we will consider models for isotropic reorientation: in  $^2\text{H}$  NMR the term isotropic denotes a process, for which all possible orientations of the field gradient tensor with respect to the external magnetic field are approached

at  $t \rightarrow \infty$ , i.e. the reorientation of the vector covers the whole unit sphere.

One limiting case of isotropic rotational motion is given by a random jump type motion, which also represents the simplest model with regard to the theoretical treatment, as the correlation is completely lost after each individual step. Hence the distribution of reorientation angles  $R(\beta; t_m)$  (cf. equation 3.55) is described by a weighted sum of the initial (i.e. a  $\delta$ -function) and final ( $\propto \sin \beta$ ) state [Schmidt-Rohr 1994]:

$$R(\beta; t_m) = w(t_m) \delta(\beta) + (1 - w(t_m)) \sin \beta. \quad (4.2)$$

With the general weighting factor  $w(t_m)$ :

$$w(t_m) = \int d\tau g(\tau) e^{-t_m/\tau}, \quad (4.3)$$

whereby  $g(\tau)$  reflects a (possible) distribution of correlation times. The resulting distribution of reorientation angles  $R(\beta; t_m)$  is displayed in figure 3.7 for different fractions of  $t_m/\tau_c$ . As the loss of correlation is complete after a single jump, the correlation times extracted from the stimulated echo exhibit no dependence on the evolution time  $t_e$  and the correlation functions are well described by a single exponential decay in the case  $g(\tau) = \delta(\tau)$ . This scenario will be employed to test the random walk simulation code written as part of this work.

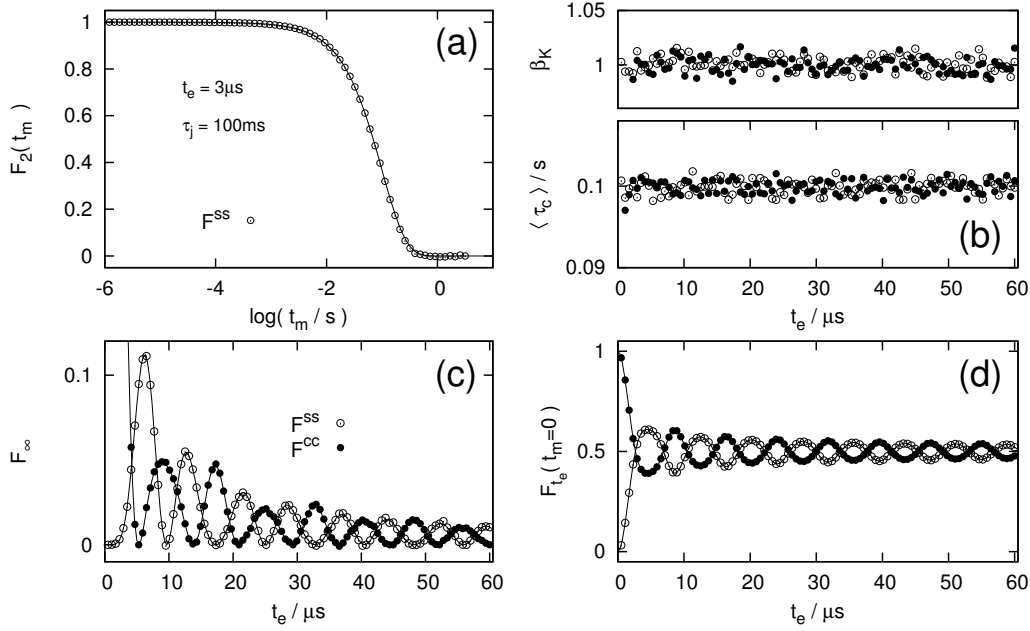
### 4.2.1 2D NMR in time domain

Figure 4.2 presents the results of a random walk simulation for a random jump type motion with a fixed jump time  $\tau_j=100$  ms. As for the experiments in this work a four-pulse sequence with an echo delay of  $t_p=15$   $\mu$ s at the end was employed. The quadrupolar coupling constant was set to  $\delta=129.6$  kHz, as experimentally found for cyanocyclohexane in section 6.4.4 since the number is of typical magnitude for the EFG tensors in the studied substances (i.e. for C-<sup>2</sup>H bonds in organic liquids). The simulation was conducted for 100 evolution times ranging from 0.5  $\mu$ s to 60  $\mu$ s and the stimulated echo decay for each evolution time was fitted via

$$F_{t_e}^{cc/ss}(t_m) = A_0 \left[ \left( 1 - F_{\infty}^{cc/ss}(t_e) \right) \exp \left( (-\tau/t_m)^\beta \right) + F_{\infty}^{cc/ss}(t_e) \right]. \quad (4.4)$$

In part (a) of the figure the correlation function  $F_2$  is plotted, which was obtained – as in case of the experiments – from the sine-sine correlation for  $t_e=3$   $\mu$ s via a subtraction of  $F_{\infty}$  and normalization.  $F_2$  is in good agreement with an exponential decay for  $\tau = \tau_j$  represented by the full line. Furthermore no deviation from the numerically calculate values (full lines) can be observed in the initial and remaining amplitude for sine-sine and cosine-cosine functions determined from a fit via eq. 4.4 and presented in parts (c) and (d) of the figure. As expected for a random jump type motion,  $\langle \tau \rangle$  exhibits no  $t_e$ -dependence and the correlation loss is well described by an exponential, as  $\beta \approx 1$  holds for all evolution times. For the calculated number of trajectories ( $\approx 1 \cdot 10^5$ )<sup>1</sup> the resulting parameters for all evolution times are

<sup>1</sup>Due to the *zcv* algorithm [Cheng 1973] employed in defining the initial orientations on the unit sphere the actual number of trajectories has to be a Fibonacci number, i.e. 121393 in this case. For details cf. section C.



**Figure 4.2 (a):** Random walk simulation of the sine-sine correlation function for a random jump type motion with  $\tau_j=100$  ms,  $t_e=3$   $\mu$ s. The solid line represents an exponential decay with  $\tau_c = \tau_j$ . **(b):** Parameters  $\tau, \beta$  from free stretched exponential fits to  $F_{t_e}^{ss}$  and  $F_{t_e}^{cc}$  for different evolution times  $t_e$ . The standard deviation is 0.007 in case of  $\beta$  and 0.87 ms for  $\tau$  ( $F_{t_e}^{ss}$ ). **(c):** Residual amplitude  $F_\infty$  of the stimulated echo. **(d):** Initial correlation for  $t_m \rightarrow 0$ .

$\langle\langle\tau\rangle_{t_e}\rangle = (99.9 \pm 0.8)$ ms and  $\langle\beta_{t_e}\rangle = (1.001 \pm 0.007)$  and hence in good agreement with the theoretical values. The given error margins represent a typically magnitude for the remainder of data presented in this section.

### $\gamma$ -jump type motions

Having demonstrated that the employed random walk simulation routine yields reasonable and consistent results, we will now address more elaborate modes of motion, in which the correlation is lost via a multi-step process. The simplest of which is a reorientation via a fixed jump angle  $\gamma$ . As the number of elementary steps needed for the complete loss of oriental correlation of a single molecule is dependent on the angle  $\gamma$ , the time scales of  $\tau_c$  and  $\tau_j$  diverge for  $\gamma \rightarrow 0$ , i.e. when the limit of isotropic rotational diffusion is approached. The ratio between  $\tau_c$  and  $\tau_j$  for the present model is given via [Anderson 1972]:

$$\frac{\tau_j}{\tau_c} = \frac{3}{2} \sin^2 \gamma \quad (4.5)$$

and often referred to as the *Anderson limit*. Due to the fact that correlation loss occurs via a  $\gamma$  dependent number of well defined individual steps, the stimulated

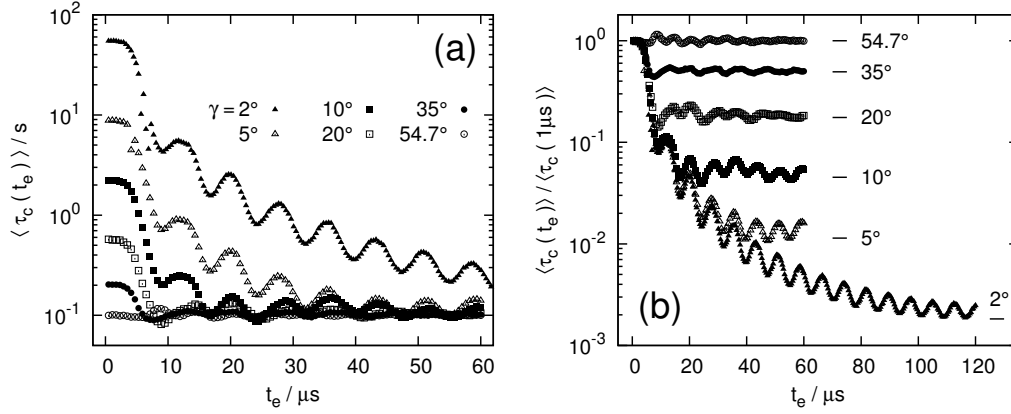


**Figure 4.3 (a):** Average correlation times  $\langle \tau_{t_e} \rangle$  from stretched exponential fits to  $F_{t_e}^{\text{ss}}$  for different jump angles  $\gamma$ . In all cases the limit  $\tau_{t_e} \rightarrow \tau_j = 100 \text{ ms}$  is approached for  $t_e \rightarrow \infty$ . **(b):** Same data sets normalized with respect to  $\langle \tau_{t_e} \rangle$  for  $t_e \rightarrow 0$ . The plateaus marked on the right represent the respective Anderson limits (cf. equation 4.5) for each jump angle.

echo experiment is rendered  $t_e$ -dependent – the evolution time acts as a geometrical filter: for longer evolution times more phase is acquired during  $t_e$  and hence a smaller change in  $\omega$  is required for equation 3.45 to decay to a certain value.

Figure 4.3 (a) presents  $\langle \tau_{t_e} \rangle$  from stretched exponential fits via equation 4.4 to simulated stimulated echo decays for different evolution times  $t_e$  and jump angles  $\gamma$  with a fixed jump time of  $\tau_j = 100 \text{ ms}$ . Whereas the extracted correlation times for short  $t_e$  change by almost three orders of magnitude from  $\gamma = 54.7^\circ$  to  $\gamma = 2^\circ$ , as more and more individual jumps are required for  $F_{t_e}^{\text{ss}}$  to decay, the limit  $\langle \tau_{t_e} \rangle \approx \tau_j$  is approached in all cases for  $t_e \rightarrow \infty$ . Since the jump time  $\tau_j$  is experimentally not accessible in straightforward manner, as typically distributions of time scale and geometry are present,  $\langle \tau_{t_e} \rangle$  is usually normalized with respect to the limit  $t_e \rightarrow 0$ , as displayed in figure 4.3 (b). For each jump angle  $\gamma$  the respective Anderson limit is in good agreement with the plateau value of  $\langle \tau_{t_e} \rangle$  observed for longest evolution times. The characteristic oscillations observed in  $\langle \tau_{t_e} \rangle$  are also reflected in the stretching parameter  $\beta_K$  displayed in figure 4.4 (a). Whereas  $F_{t_e}^{\text{ss}}$  is exponential for shortest evolution times and all jump angles (as expected for the employed model), the values begin to oscillate for longer times  $t_e$  – the stronger, the smaller the angle  $\gamma$ .  $F_{t_e}^{\text{ss}}$  and  $F_{t_e}^{\text{cc}}$  (not shown) appear considerably stretched for small jump angles at certain evolution times  $t_e$ . This behaviour results from a deviation of the calculated curves from a stretched exponential behaviour, as seen in the mean square error of a fit via eq. 4.4 (additional points in figure 4.4 (a)). The error exhibits a  $t_e$ -dependence proportional to  $F_\infty$ : for evolution times at which  $F_\infty$  vanishes, the  $F_{t_e}^{\text{ss}}$  and  $F_{t_e}^{\text{cc}}$  decays are well described by an exponential with  $\beta_K$  close to one and a minimum in the error of the fit. At evolution times where  $F_\infty$  traverses a local maximum on the other hand, a minimum in  $\beta_K$  and a local maximum in the fitting error are found, both of which become more pronounced for longer evolution times  $t_e$ .

The deviations from a Kohlrausch decay at the  $t_e$ -values where  $F_\infty$  exhibits a local maximum are demonstrated in figure 4.4 (b): whereas for  $\gamma = 54.7^\circ$   $F_{t_e}^{\text{ss}}$  is well

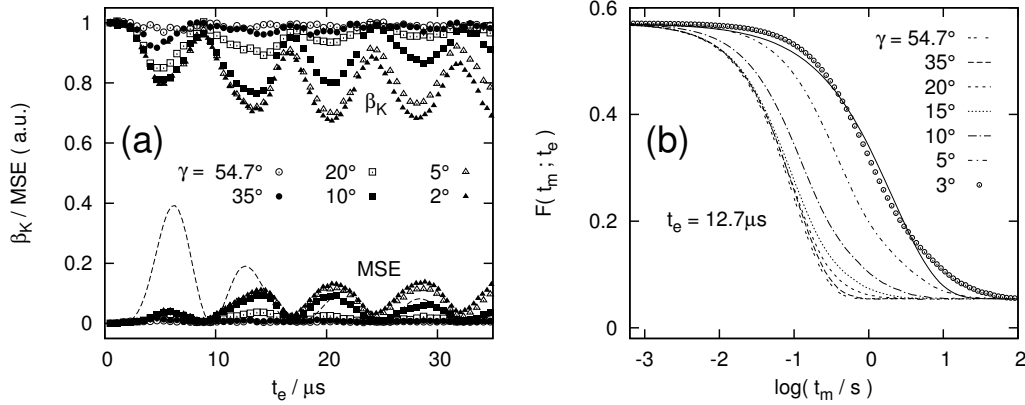


**Figure 4.4 (a):** Corresponding stretching parameters  $\beta_K$  to the time constants from  $F_{t_e}^{\text{ss}}$  presented in figure 4.3. In the same figure the mean square errors of the stretched exponential fits are presented (corresponding symbols, arbitrary units). The dashed line represents  $F_\infty$  (arbitrary units). **(b):**  $F_{t_e}^{\text{ss}}$  for different  $\gamma$ -jump motions to demonstrate the deviations from a Kohlrausch fit (full line) for  $F_\infty \neq 0$ .

described by an exponential, a bimodal behaviour is observed in the decay for smaller jump angles. Hence a fit via a stretched exponential function yields  $\beta_K < 1$ , but fails to model the  $F_{t_e}^{\text{ss}}$  decay at long and short mixing times  $t_m$ .

This peculiarity is extenuated if a distribution of correlation times is present, i.e. the correlation functions are inherently stretched – as being the case for the heterogeneous scenario found in supercooled liquids and glasses.

### Fast motion limit effects

So far we discussed simulations of the stimulated echo decay for sufficiently long jump times  $\tau_j$ , i.e. no reorientation was expected during the evolution time  $t_e$  and the echo delays  $t_p$  of the pulse sequence. Due to the (broad) distributions of correlation times  $G(\log \tau)$  typically found in supercooled liquids, it is often not possible to assure that  $\tau_j \gg t_e, t_p$  holds for all sub ensembles.

If the jump time  $\tau_j$  becomes sufficiently short and reorientation takes place on the  $\mu\text{s}$  time scale, the initial amplitude  $F_{t_e}(t_m \rightarrow 0)$  in the sine-sine and cosine-cosine correlation decays due to a phase change during  $t_e$  or  $t_p$ . Figure 4.5 displays the reduction factor

$$R_f(\tau_j) = \frac{F_{t_e}(t_m = 0, \tau_j)}{F_{t_e}(t_m = 0, \tau_j \rightarrow \infty)}, \quad (4.6)$$

for different evolution times and values of  $\tau_j$ . The initial amplitude of  $F_{t_e}^{\text{ss}}$  vanishes around  $\tau_j = 10^{-5} \text{s}$  for  $t_e = 3 \mu\text{s}$  and an echo delay of  $t_p = 15 \mu\text{s}$ , i.e. a correlation function can no longer be obtained for reorientation on this time scale. For longer evolution times the decay in  $R_f$  is shifted towards greater values of  $\tau_j$ . For  $F_{t_e}^{\text{cc}}$  the effect is the same – for  $\tau_j < 10^{-6} \text{s}$  the reduction factor  $R_f$  however rises again and the initial amplitude becomes even larger than for  $\tau_j \rightarrow \infty$ . For  $\tau_j \ll 10^{-6} \text{s}$  a complete loss of correlation is obtained already during  $t_e$ , i.e. after the evolution time an average

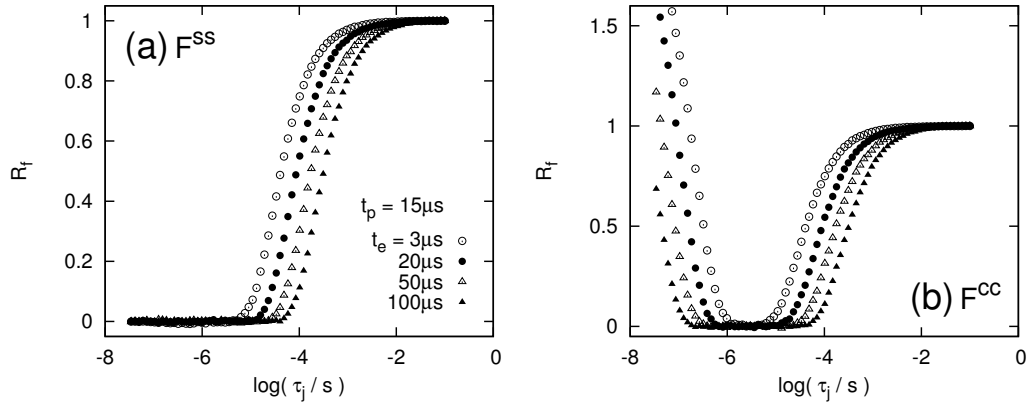


**Figure 4.5 (a):** Simulated reduction factor  $R_f$  of  $F_{t_e}^{ss}$  for a random jump type motion and different evolution times  $t_e$ . **(b):** Same representation for  $F_{t_e}^{cc}$ .

phase, independent of the initial orientation, is accumulated for all molecules, which subsequently is refocused in the  $F_{t_e}^{cc}$  pulse sequence. Consequently a constant value for all mixing times  $t_m$  is obtained, i.e. no further information on the dynamics of the system is accessible in this limit.

These results remind us that special care has to be taken when employing the  $t_e$ -dependence of the stimulated echo in systems with a broad distribution  $G(\log \tau)$ : in a heterogeneous scenario the relatively fast molecules are easily under-estimated in the experiment. Depending on the motional process observed this may lead to a systematic error in the extracted jump geometries due to the  $t_e$ -dependence of  $R_f$ .

### 4.2.2 Solid echo line shape

In the following we discuss the most prominent effects in the solid echo line shape, imposed by the motional models introduced in the last section. Figure 4.6 displays spectra for a random jump and distinct  $\gamma$ -jump type motions at different correlation times  $\tau_c$ .  $\tau_c$  in the latter models is determined via equation 4.5, i.e.  $\tau_j$  differs by almost three orders of magnitude between the spectra for random jump and the “2°+40°”<sup>2</sup> model, as exemplarily denoted for the shortest and longest time  $\tau_c$  in figure 4.6. In comparison with the rigid limit spectra ( $\tau_j \rightarrow \infty$ ), represented by the dashed lines in the same figure, it is obvious that first line shape changes appear at longer times  $\tau_c$  and are more pronounced in the case of small angular jumps, whereas for  $\tau_c \approx 5 \cdot 10^{-7}$ s all models again yield a liquid line of comparable width.

This behaviour is also reflected in the reduction factor  $R_{SE}$  of the solid echo spectra in figure 4.7 (a): the arise of the liquid line for  $\tau_c < 10^{-6}$ s is universal for all discussed models, whereas the intensity of the solid state spectrum starts to decrease at considerable longer times  $\tau_c$  for the models incorporating small angular jumps. Consequently the minimum in  $R_{SE}$  is significantly broader for the latter models.

Apart from the span in  $\tau_c$  for which line shape effects are observed, also the qualitative

<sup>2</sup>In this scenario 5% of 40° jumps are added to a 2° jump model, i.e. on average every twentieth jump of a molecule is about  $\gamma=40^\circ$ .

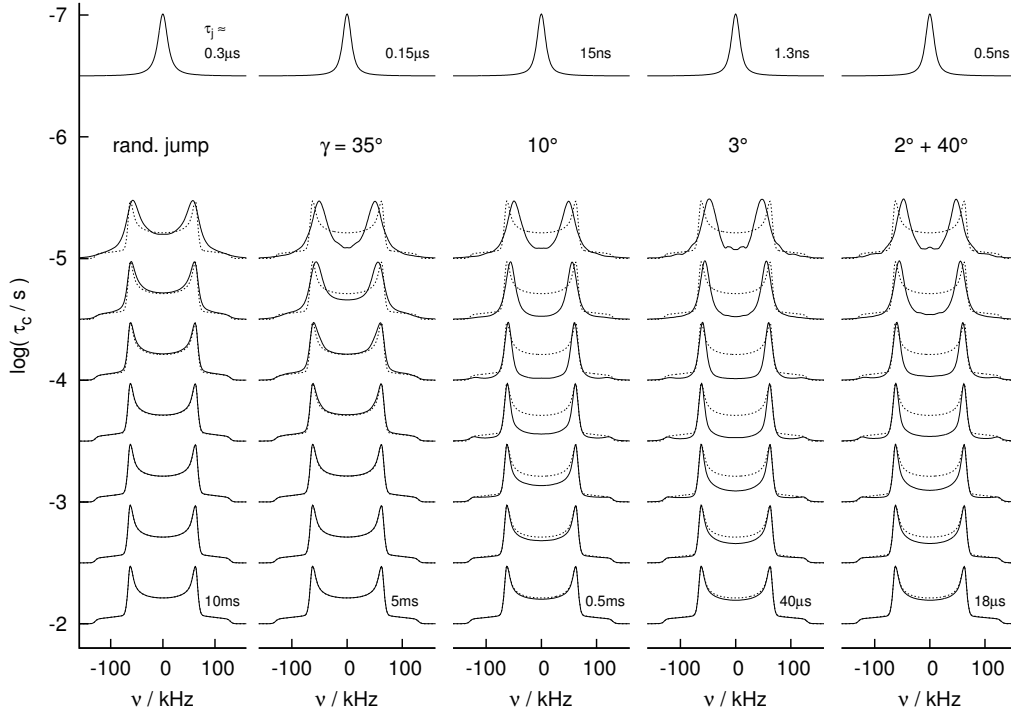


**Figure 4.6:** Random walk simulations of the solid echo line shape according to different models of motion in the intermediate motional regime,  $\tau \approx 1/\delta$ . The position of the baseline with respect to the y-axis denotes the respective correlation time  $\tau_c$ , in all cases the inter pulse delay was set to  $20 \mu\text{s}$ . Rightmost spectra comprise from a model where 5% of  $40^\circ$ -jumps are added to a  $2^\circ$   $\gamma$ -jump motion. The dotted spectrum represents the limiting Pake pattern and is included in all models for reasons of comparison.

nature of those changes is different amongst the employed models: for all  $\gamma$ -jump scenarios the intensity in the centre of the spectra decreases, whereas in the random jump type model a slight increase is observed.

### Line shape parameters

As the calculated spectra for short  $\tau_c$  significantly differ from a rigid limit Pake spectrum, we will introduce phenomenological line shape parameters to quantify the change in spectral intensity in the style of S. Lusceac [Lusceac 2005a]. The latter change in central intensity is monitored via the quantity  $R(t_p)$  that measures the relative intensity around zero frequency, cf. figure 4.7 (b). The angular sensitivity of the solid echo spectrum is largest around  $\omega = 0$ , i.e. a small angular displacement imposes the most prominent effect here. Corresponding  $R(t_p)$  values to the spectra presented in figure 4.6 are plotted in figure 4.8 (a): motions with  $\gamma \leq 10^\circ$  exhibit a prominent minimum in  $R(t_p)$  around  $\tau_c \approx 7 \cdot 10^{-5} \text{s}$ , whereas models proceeding via large angular jumps yield constant  $R(t_p)$  in this region. The behaviour of  $R(t_p)$  in the model comprised of a mixture of  $2^\circ$  and  $40^\circ$  jumps is dominated by the small angular displacements.

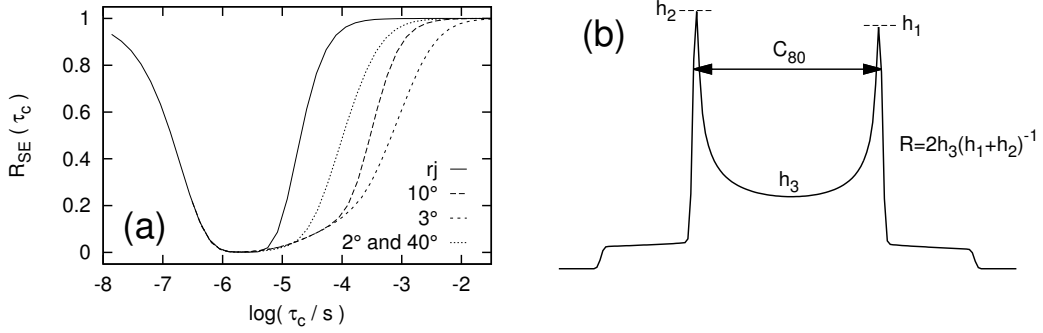


**Figure 4.7 (a):** Reduction factor  $R_{SE}$  of the solid echo spectra presented in figure 4.6 ( $t_p=20\mu\text{s}$ ). **(b):** Definition of the line shape parameters  $R(t_p)$  and  $C_x$ :  $R(t_p)$  measures the relative intensity at zero frequency. Due to slight distortions sometimes arising in experimental spectra, the average height of the singularities is used.  $C_x$  measures the apparent spectral width at height  $x$ , e.g. at 80% for  $C_{80}$ .

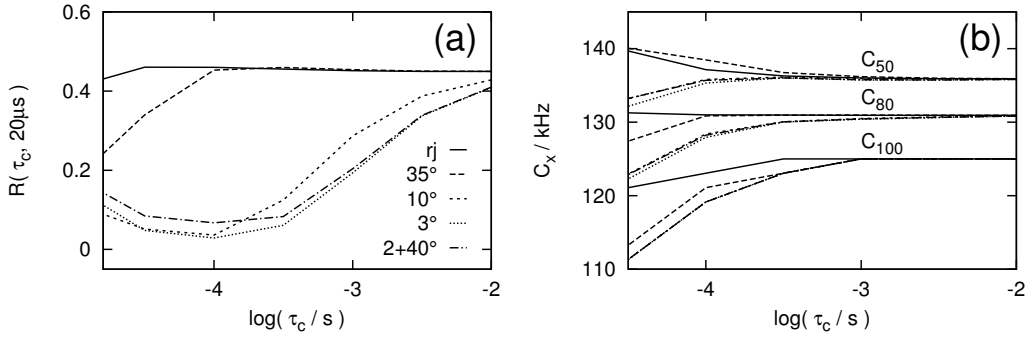


**Figure 4.8 (a):** Relative intensity at zero frequency  $R(t_p)$  of the solid echo spectra presented in figure 4.6. **(b):** Apparent spectral width  $C_x$  of the simulated solid echo spectra presented in figure 4.6.

The line shape effects are however not limited to the centre of the spectra. Therefore we introduce the apparent spectral width  $C_x$ , which measures the width of the spectra at relative height  $x$ , i.e. at 80% in case of  $C_{80}$  (cf. figure 4.7 (b)).  $C_x$  of the simulated spectra is presented in figure 4.8 (b): the reduction in  $C_x$  of the  $\gamma=10^\circ, 3^\circ$  and the  $2^\circ+40^\circ$  models is rather universal. The spectra calculated for the random and the  $\gamma=35^\circ$  jump model on the other hand maintain their width  $C_{80}$  down to shorter correlation times  $\tau_c$  and exhibit an increase of  $C_{50}$  for  $\tau_c < 1 \cdot 10^{-3}\text{s}$ . A broadening of the spectra in the lower half is hence a fingerprint of a motion dominated by large angular jumps.

### 4.2.3 Heterogeneous dynamics

So far we have only considered motional processes for a single correlation time  $\tau_c$ , i.e. the effects of a possible distribution  $G(\log \tau)$  have been neglected. With regard to the study of binary glass formers in part II of this work, we will briefly review

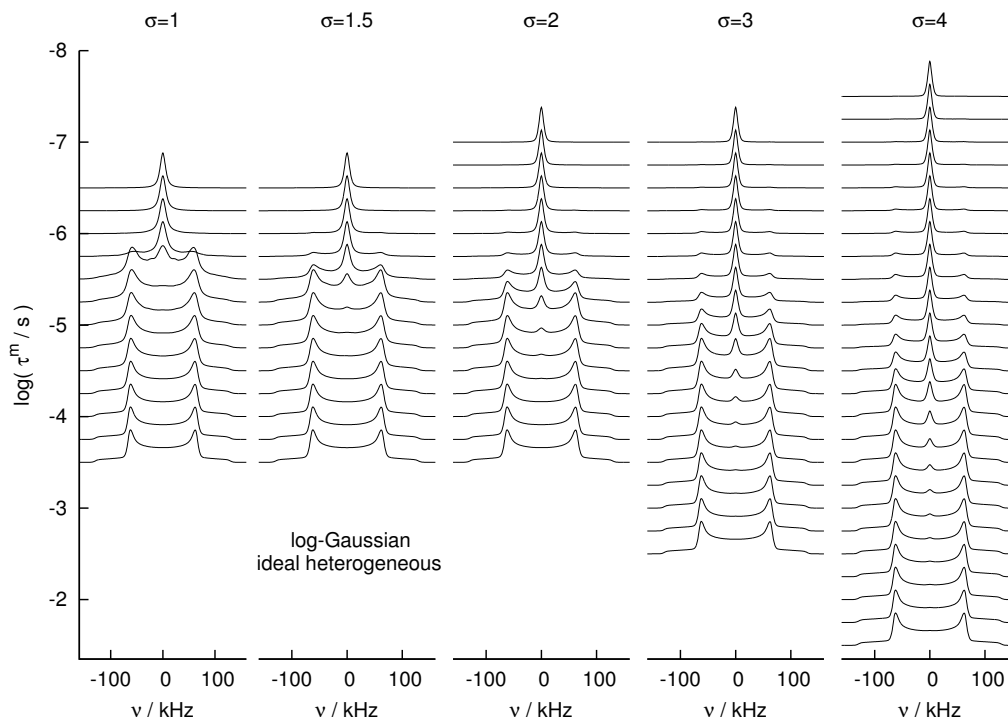


**Figure 4.9:** Random walk simulations of the solid echo line shape according to a random jump type motion with an underlying (ideal heterogeneous) log-Gaussian distribution of correlation times. The position of the baseline with respect to the y-axis denotes  $\tau^m$  (the median of the distribution) for each spectrum. Simulations for various widths  $\sigma$  are displayed, in all cases the inter pulse delay  $t_p$  was set to 20  $\mu$ s.

the effects of a broad distribution  $G(\log \tau)$ , as typically present in these systems, on the solid echo line shape. Therefore we assume a random jump type motion with an underlying ideal heterogeneous log-Gaussian distribution of correlation times, i.e. no exchange within the distribution is considered. With regard to the reduction factor presented for the case of a single correlation time in figure 4.7 (a), it becomes obvious that a superposition of a liquid line and a solid state spectrum is expected if the distribution spans more than a decade in  $\tau_c$ . This behaviour is demonstrated in figure 4.9: for a log-Gaussian distribution with  $\sigma = 1$  such two phase spectra are observed in a very narrow range for  $\tau^m$ . In case of  $\sigma = 4$  pronounced two phase spectra are observed for about 4.5 decades in  $\tau^m$ .

We determined the relative weight  $W$  of the liquid line in the individual spectra via a fit with a superposition of a Lorentzian and a rigid-limit Pake pattern, the resulting  $W(\tau)$  is plotted in figure 4.10 (b). As this weighting factor is often exploited in the analysis of experimental data, we will compare the results of our simulation with a theoretical prediction in terms of  $G(\log \tau)$ . Conventionally the liquid line is attributed to molecules with a correlation time faster than the inverse of the coupling

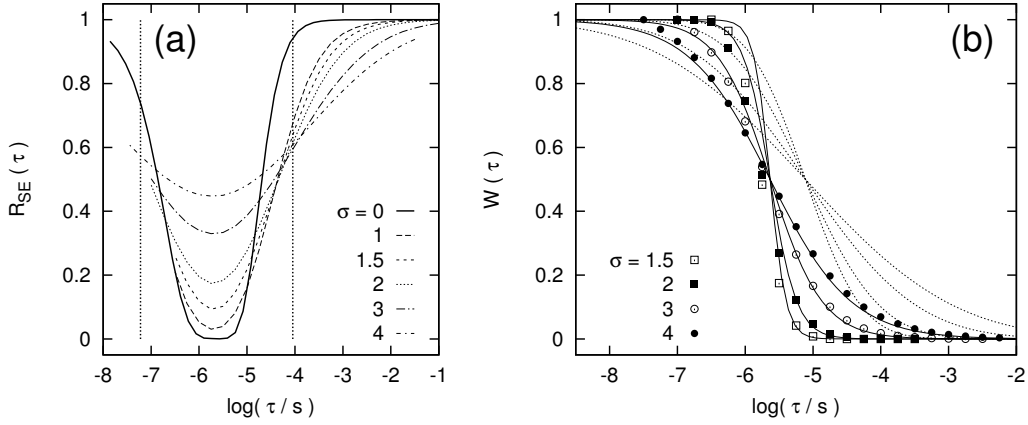


**Figure 4.10 (a):** Reduction factor  $R_{SE}$  of the solid echo spectra presented in figure 4.9 ( $t_p=20\ \mu\text{s}$ ). **(b):** Weighting factor of the Lorentzian line from a simple “two phase” fit to the spectra in figure 4.9. The lines represent the weighting calculated via equation 4.7 (dotted line) and 4.8 (full line).

constant  $\tau_c < 1/\delta$ :

$$W(\tau_m) = \int_{-\infty}^{\log 1/\delta} G(\log \tau) d\log \tau, \quad (4.7)$$

which is represented by the dotted line in figure 4.10 (b). With regard to the simulation results the predicted weighting factor from equation 4.7 is shifted towards longer times  $\tau^m$  and significantly over-estimates the regime in which two phase spectra are observed.

The deviations arise because the reduction factor  $R_{SE}$  is neglected in eq. 4.7: if we account for the fraction of molecules not observed in the experiment due to  $R_{SE} \approx 0$ , significantly better agreement can be achieved. In figure 4.10 (a) it is seen that molecules with a correlation time on the order of  $\tau=0.5\text{-}13.5\ \mu\text{s}$  in first approximation do not contribute to the solid echo intensity (if relatively faster or slower fractions with  $R_{SE} \approx 1$  are present). Consequently equation 4.7 is modified to account for this fraction:

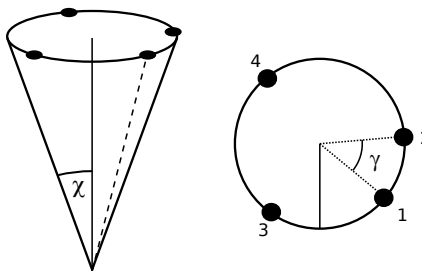
$$W(\tau_m) = \frac{1}{N} \int_{-\infty}^{\log 0.5\ \mu\text{s}} G(\log \tau) d\log \tau \quad (4.8)$$

with the normalization factor

$$N = \int_{\log 13.5\ \mu\text{s}}^{\infty} G(\log \tau) d\log \tau + \int_{-\infty}^{\log 0.5\ \mu\text{s}} G(\log \tau) d\log \tau. \quad (4.9)$$

The results are given by the solid lines in figure 4.10 (b), which are in agreement with  $W(\tau)$  obtained from the simulated spectra. We will exploit this result in the analysis of the two phase spectra in mixtures of toluene and PCB54 in part II of this work.

**Figure 4.11:** Sketch of a random jump type motion on the circumference of a cone with half opening angle  $\chi$ . The (initial) direction of the C-<sup>2</sup>H bond is marked by the dashed line. After each jump a random position on the circumference of the base circle is occupied.



### 4.3 Anisotropic reorientation

The remainder of this chapter is devoted to studies of anisotropic dynamics and their imprint on <sup>2</sup>H NMR experiments, which will serve as foundation for a more advanced discussion of the  $\beta$ -process in the experimental parts of this work.

Although <sup>2</sup>H NMR studies of the  $\beta$ -process, for example in ethanol, were reported to be sensitive on the placement of the “active” bond (i.e. via selective deuteration) [Schneider 2001], the majority of glass forming systems exhibit a remarkably universal manifestation of the  $\beta$ -process in <sup>2</sup>H NMR – despite vast differences in molecular size and shape [Micko 2007]. Therefore it does not appear justified to derive jump geometries from molecular symmetry arguments, hence we begin the discussion with the most general forms of restriction, i.e. for the rotational motion probed by <sup>2</sup>H NMR the confinement of the C-<sup>2</sup>H vector to a certain area on the unit sphere, in the most simplest case the circumference of a cone.

The impact of the latter cone models on one- and two-dimensional <sup>2</sup>H NMR experiments has been intensively discussed by M. Vogel [Vogel 2000b, Vogel 2000a, Vogel 2005] and S. Lusceac [Lusceac 2005a] in the framework of random walk simulations, which have been successfully applied to the experimental results of numerous systems. Nevertheless it is necessary to refine and broaden the analysis with respect to the fast and non-merging  $\beta$ -process found in cyanocyclohexane and the binary mixtures of toluene presented in this work. For the sake of clarity we reproduced some of the previously reported results<sup>3</sup>, hence the following sections cater to provide a comprehensive overview.

#### 4.3.1 Random jump type motion on a cone

To demonstrate the basic effects common to all the models based on a conical restriction, we begin this section with the simplest thereof: a random jump type motion on the circumference of a cone with a fixed jump time  $\tau_j$ . Subsequently we will focus on more complicated (in terms of geometry and computational effort) but more general and hence plausible models for the  $\beta$ -process in supercooled liquids and glasses. The model proposed in this section is sketched in figure 4.11: after each individual jump a random position on the circumference of a cone with half opening angle  $\chi$  is occupied, hence (the  $\chi$  dependent fraction of) correlation is completely lost after each step (the assumptions made in all calculations are the same as in the

<sup>3</sup>The simulation routine developed within this work was shown to provide consistent results with previously published data.

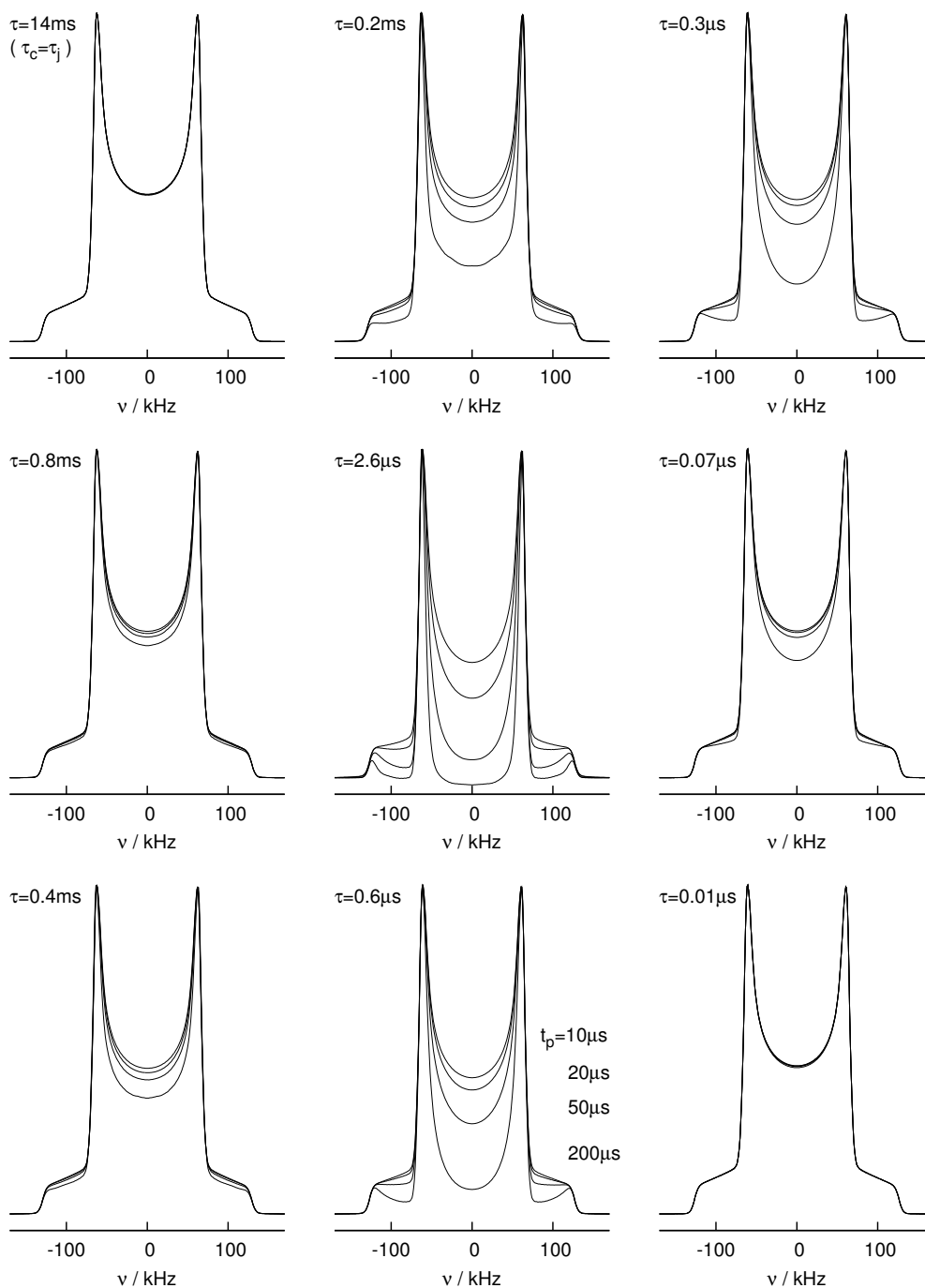


**Figure 4.12:** Simulated solid echo spectra for a random jump motion on the circumference of a cone with half opening angle  $\chi=7^\circ$ . For each correlation (i.e. jump-) time the spectra corresponding to  $t_p=10, 20, 50$  and  $200\ \mu\text{s}$  (top to bottom) are plotted. The calculated spectra have been convoluted with a Gaussian and damped with respect to pulse excitation effects to resemble the experimental spectra in part I and II, this routine was kept constant throughout this work.  $3 \cdot 10^6$  trajectories were simulated in the present case.

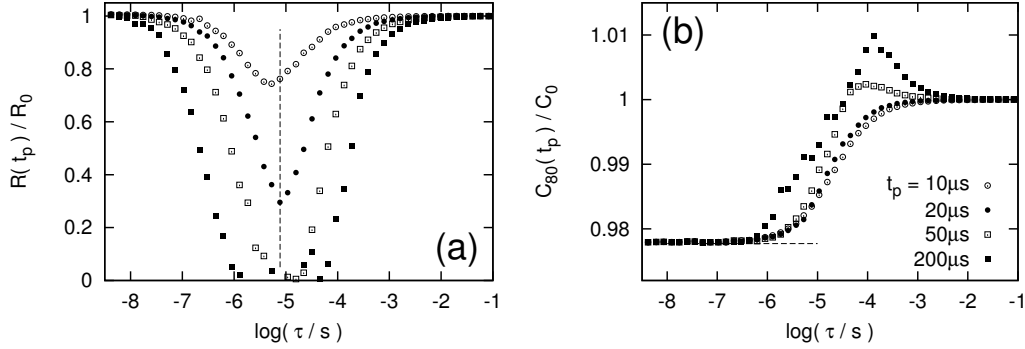


**Figure 4.13 (a):** Normalized intensity around zero frequency  $R(t_p)/R_0$  of the spectra displayed in figure 4.12 ( $\chi=7^\circ$ , including additional data) for  $t_p=10\text{--}200\ \mu\text{s}$  (key see figure (b)). The dashed line marks  $\tau = 1/\delta$ . **(b):** Corresponding normalized apparent spectral width  $C_{80}$ . The dashed line marks the fast motion limit plateau predicted by equation 4.10.

previous sections, i.e. Ivanov model, Markov process and  $\delta=129.6\ \text{kHz}^4$ ). In virtue of this property the correlation functions are exponential and  $\tau_j = \tau_c$  holds, which significantly reduces simulation effort with respect to the more complex scenarios propagating via small angular displacements. As the resulting correlation functions  $F_{1/2}$  are hence trivial apart from  $F_\infty$  (which may not be the case in the experimental stimulated echo due to time window effects), the considerations will be limited to the solid echo line shape in the present case, which is displayed in figure 4.12 for selected  $\tau_j$  and a cone of half opening angle  $\chi=7^\circ$  at different inter pulse delays  $t_p$ . The line shape changes predicted in chapter 3 are rather articulate: for jump correlation times on the order of  $10^{-6}\text{s}$  the intensity in the central part of the spectrum decreases, an effect which can be intensified by prolonging the inter pulse delay  $t_p$ . The spectra for  $\tau_j=0.01\ \mu\text{s}$  and different inter pulse delays  $t_p$  are again indistinguishable and resemble the slow motion limit case observed for  $\tau_j \geq 14\ \text{ms}$  – albeit with a slightly reduced apparent coupling constant  $\bar{\delta}$ . For all models in which the reorientation is restricted to the circumference of a cone (i.e. independent of the elementary jump) the reduced apparent coupling is given via:

$$\bar{\delta} = \delta \frac{1}{2} [3 \cos^2(\chi) - 1]. \quad (4.10)$$

As the changes in apparent width are hardly observed in this representation, the line shape parameters  $R(t_p)$  and  $C_{80}$  are displayed in figure 4.13 for the sake of a more quantitative discussion. The apparent spectral width  $C_x$  is used as the coupling constant  $\bar{\delta}$  is often not directly accessible – as being the case experimentally, where distributions in  $\tau$  and  $\chi$  and hence distorted line shapes are found, which do not resemble a Pake pattern. The spectral intensity around zero frequency  $R(t_p)$  vs.  $\log(\tau)$  displays a (symmetrical) minimum around  $\tau_j=1/\delta \approx 8\ \mu\text{s}$  which is about 3.5 ( $t_p=10\ \mu\text{s}$ ) to 5.5 ( $t_p=200\ \mu\text{s}$ ) decades wide. The position of the minimum itself exhibits little  $t_p$ -dependence, with the minimum condition  $\tau_j=1/\delta$  being best fulfilled for  $t_p=20\ \mu\text{s}$ . As with further reduction of the jump time the motion enters the

<sup>4</sup>Data treatment is sketched in the caption to figure 4.12.

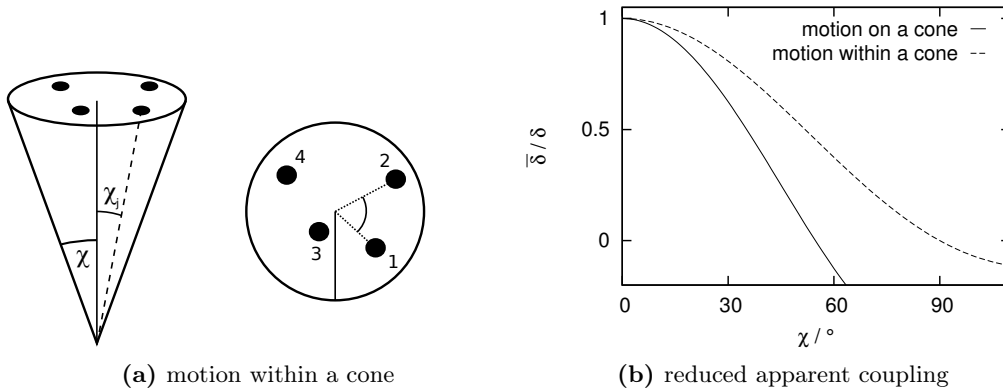


**Figure 4.14 (a):** Sketch of a random jump type motion within a cone of half opening angle  $\chi$ . The (initial) direction of the C-<sup>2</sup>H bond is marked by the dashed line. After each jump a random position within (or on) the base circle is occupied. **(b):** Normalized reduced apparent spectral widths according to equations 4.10 and 4.11.

fast motion limit regime and consequently the  $R(t_p)$  effects vanish, the apparent spectral width drops about 2%, approaching the theoretical value given via equation 4.10 at  $\tau_j \approx 0.1/\delta$  for all simulated inter pulse delays  $t_p$ . Whereas  $C_{80}$  decreases monotonically for short  $t_p$  (10  $\mu$ s and 20  $\mu$ s), a local maximum is traversed for  $t_p \geq 50 \mu$ s. This effect is also visible in the spectra displayed in figure 4.12, as the slope of the inner singularities becomes steeper for the spectra with lowest intensity around  $\nu=0$  Hz.

### 4.3.2 Random jump type motion within a cone

Albeit the results already mimic the experimental low temperature findings in systems with a  $\beta$ -process quite well, the “motion on a cone” model however appears rather artificial: a fast motion of on the circumference of a cone would demand for a certain molecular (or in case of plastic crystals probably lattice) symmetry which accounts for such dynamics. Naively one would rather expect to find some sort of diffusive motion, limited by constraints imposed by the local energy landscape in the heterogeneous glass. A behaviour which is better mimicked by the model of a motion within a cone, which will also be considered as of random jump type in a first step. If a C-<sup>2</sup>H bond freely moves on the unit sphere within a cone of half opening angle  $\chi$ , a similar relation for  $\bar{\delta}$  as in case of equation 4.10 is found [Batchelder 1983]:

$$\bar{\delta} = \delta \frac{1}{2} \cos(\chi) [1 + \cos(\chi)]. \quad (4.11)$$

The resulting apparent coupling  $\bar{\delta}/\delta$  is plotted in figure 4.14 (b): as, on average, the reorientation angle of a single C-<sup>2</sup>H bond is smaller than in the case of a motion on the circumference of a cone with the same opening angle  $\chi$ , the effects are more subtle in the present case – the qualitative behaviour is however the same in both models for  $\chi < 54.7^\circ$ .

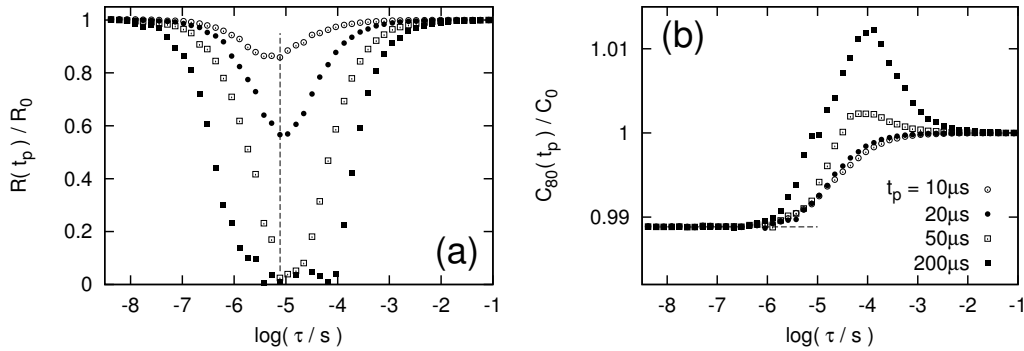


**Figure 4.15 (a):** Normalized intensity around zero frequency of simulated spectra for a motion within a cone ( $\chi=7^\circ$ ,  $t_p=10\text{-}200\ \mu\text{s}$ , key see figure (b)). The dashed line marks  $\tau = 1/\delta$ . **(b):** Corresponding normalized apparent spectral width  $C_{80}$ . The dashed line marks the fast motion limit plateau given via equation 4.11.

This trend is reflected in all extracted quantities (cf. figure 4.15 for  $R(t_p)$ , where the same opening angle  $\chi=7^\circ$  as in figure 4.13 was chosen): the minimum in the  $t_p=20\ \mu\text{s}$  trace appears again at  $\tau_j \approx 1/\delta$ , the minimum value is however significantly higher within this approach (approx. 0.55 opposed to about 0.3 for a motion “on the cone”). The reduction in  $C_{80}$  is in good agreement with the theoretical prediction of eq. 4.11 and about half the magnitude as in the previous case. Again a maximum in  $C_{80}$  is traversed for longest  $t_p$  values, this particularity being however more pronounced in the present scenario than for the “motion on a cone” model: at  $t_p=200\ \mu\text{s}$  the apparent spectral width around  $\tau_j=10^{-4}\ \text{s}$  has grown roughly 1% and therefore exceeds the effect found in the previous model, albeit the overall changes in  $C_{80}$  (i.e. from the static to the fast motion limit case) are smaller in the present case.

Even though the centre of the  $^2\text{H}$  NMR solid state spectrum is most sensitive to the small angular displacements considered here, it was already seen in figure 4.12 that the changes are not limited to this frequency range: the outer ridges of the spectrum are also clearly affected for intermediate jump times – which explains the peculiarity arising in  $C_{80}$  in this region. To monitor the overall loss in intensity, the reduction factor  $R_{SE}$  is displayed in figure 4.17: the curves resemble the dependence of  $R(t_p)$  on  $\tau_j$ : the position and width of the minimum is almost identical to the one arising in  $R(t_p)$  and the difference between the employed models is also qualitatively similar. This however follows naturally as both quantities are closely related and in the present case probe mainly the same spectral changes.

Apart from the subtle differences between the two models discussed so far, which furthermore only become relevant when extracting quantitative information from the experimental solid echo line shape, there arises a clear qualitative difference for vanishing restriction, i.e. growing opening angle  $\chi$  between the models. Although the models were chosen to mimic a highly restricted motion (like the  $\beta$ -process below  $T_g$ ), it is worth discussing what predictions can be made for the case of vanishing restriction, as it is known (e.g. from dielectric spectroscopy) that the amplitude of the  $\beta$ -process universally grows above the glass transition temperature, albeit the observation in the line shape is in most systems hampered by the onset

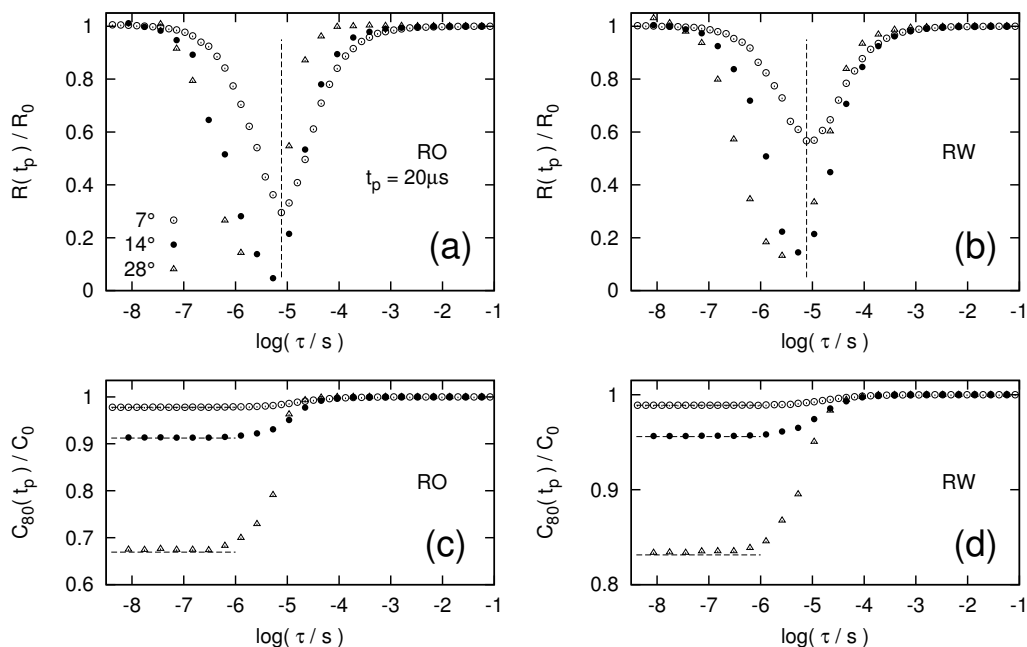


**Figure 4.16 (a):**  $R(t_p)$  values simulated in the “random jump type motion on a cone” model for different opening angles  $\chi$ ,  $t_p = 20 \mu\text{s}$  in all cases. **(b):**  $R(t_p)$  values for a simulation of the “random jump type motion within a cone”, otherwise the same parameters as in (a) were used. **(c):** Corresponding apparent spectral widths  $C_{80}$  for the data displayed in (a), same symbols denote same cone angles. **(d):** Corresponding  $C_{80}$  values for figure (b).

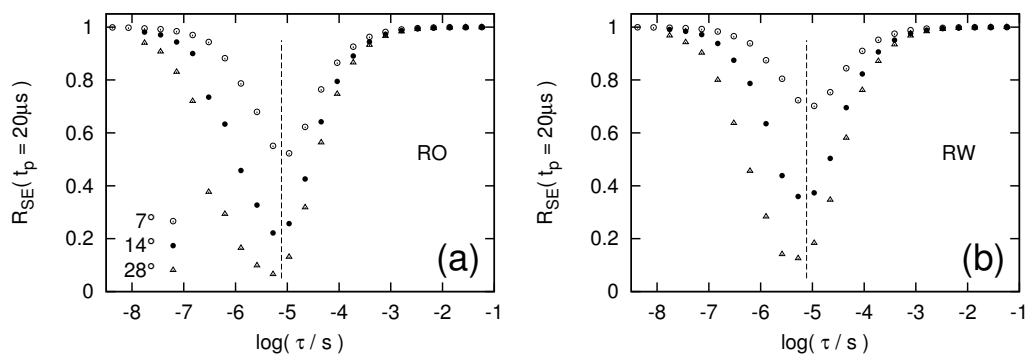


**Figure 4.17 (a):** Reduction factor for the “random jump type motion on a cone” model for different opening angles  $\chi$  and  $t_p = 20 \mu\text{s}$ . **(b):** Reduction factor for the “random jump type motion within a cone” model for different  $\chi$ , otherwise same parameters as in (a).

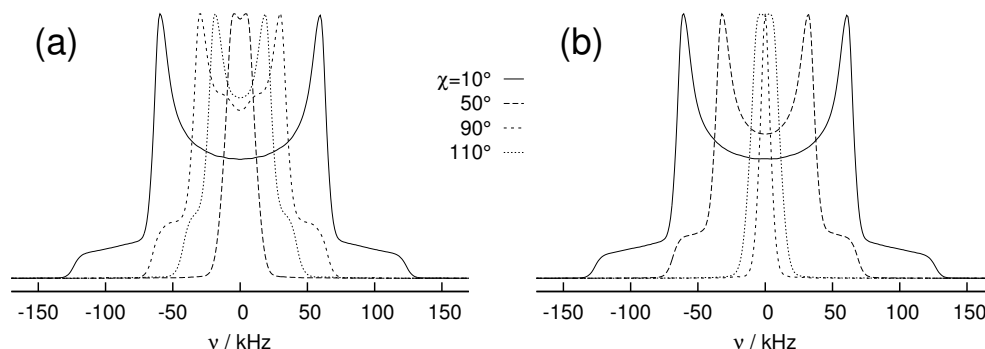


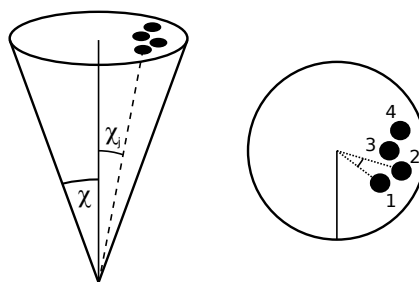
**Figure 4.18 (a):** Simulated spectra ( $t_p = 20 \mu\text{s}$ ) for a motion on the circumference of a cone for very large opening angles  $\chi$  and  $\tau = 10^{-8}$  s (i.e. in the fast motion limit regime) in all cases. **(b):** Representation for the motion within a cone model.

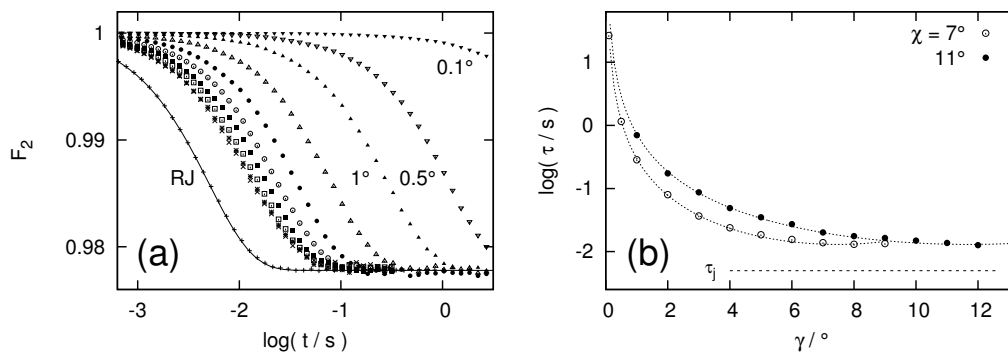
of the  $\alpha$ -process. In cyanocyclohexane however the processes do not merge and consequently the  $\beta$ -process can be monitored via  $^2\text{H}$  NMR at high temperatures, where it is expected to exhibit an enhanced relaxation strength.

Figure 4.18 displays simulated spectra for the case of very large angles  $\chi$  and a jump time in the fast motion limit regime ( $\tau = 10^{-8}$  s,  $t_p = 20 \mu\text{s}$ ): for both models the apparent spectral width of the spectra is drastically reduced for  $\chi = 50^\circ$  and for  $90^\circ$  the solid state spectrum has virtually collapsed to a central line in both cases – for even larger opening angles the “motion on a cone” model however again yields a solid state spectrum (albeit with changed sign) whereas the width in the more general case of a motion within the cone oscillates around zero for larger angles until an isotropic scenario is approached. If the geometrical restriction (at least for a sub ensemble of molecules) of the  $\beta$ -process indeed diminishes to such extent at temperatures significantly above  $T_g$ , and given that the  $\alpha$ -process is still sufficiently slow in this regime, the  $\beta$ -process would contribute to a central feature in the  $^2\text{H}$  NMR spectra in case of a motion within a cone – whereas for a motion on the circumference the spectra would simply broaden again in  $^2\text{H}$  NMR and for spin 1/2 nuclei the spectra (dominated by chemical shift anisotropy like in  $^{31}\text{P}$  NMR e.g.) would change their sign, which to our knowledge has not been observed so far in combination with the  $\beta$ -process.

### 4.3.3 Multi step motion within a cone

**Figure 4.19:** Sketch of a multi step motion within a cone of half opening angle  $\chi$ . The (initial) direction of the C- $^2\text{H}$  bond is marked by the dashed line. For each individual jump the bond reorients about a well defined angle  $\gamma$  in a random direction.





**Figure 4.20 (a):** Simulated correlation functions  $F_2$  for a multi step motion within a cone of  $\chi=7^\circ$  for different step sizes  $\gamma$ . **(b):** Corresponding time constants from a fit to  $F_2$  for two different cone angles  $\chi$ . The dashed line marks the jump time  $\tau_j$  in both geometries, the dotted lines represent a fit with a modified Anderson relation, cf. equation 4.12.

Whereas the peculiar fast motion limit effects discussed in the last paragraph are independent of the elementary step in the considered model and only depend on the fraction of the unit sphere accessible after infinite jumps, the 1D and 2D  $^2\text{H}$  NMR methods for prolonged  $t_p/t_e$  become increasingly sensitive on the elementary step for larger inter pulse delays and evolution times as the time scales of  $\tau_c$  and  $\tau_j$  diverge for smaller angles  $\gamma$ . It becomes therefore necessary to consider models of reorientation more elaborate than a simple random jump process also in the case of anisotropic dynamics.

In this section multi step models will be considered, that arise of a reorientation via a fixed jump angle  $\gamma$  between two subsequent orientations of a C- $^2\text{H}$  bond on the unit sphere, cf. figure 4.19. Within this approach, as in the case of non-random isotropic dynamics, the condition  $\tau_j=\tau_c$  is no longer fulfilled: for an isotropic reorientation the two quantities are related via equation 4.5 and hence strongly dependent on the jump angle  $\gamma$ . In the case of anisotropic dynamics the relation is a-priori unknown, as it is furthermore dependent on the degree of restriction which in the present models is quantified by the angle  $\chi$ . The situation becomes even more unfavourable as a simple  $\gamma$ -jump model is insufficient to provide a consistent extension to the processes discussed so far, since the boundary conditions are non-trivial in the present case. A straightforward scenario, where the direction of a jump upon angle  $\gamma$  is randomly chosen until the new position also resides within the cone, probes all points in space within the restriction after infinite jumps, but yields a probability of presence different from the random jump case (i.e. not  $\propto \sin \chi_i$ ) and dependent on  $\gamma$ . As this imposes rather unfavourable peculiarities ( $F_\infty$  would be dependent on  $\gamma$  for example), we chose a different approach for the boundary conditions that maintains the probability of presence: each time a jump upon an angle  $\gamma$  in a random direction would cross the base circle of the cone, a jump upon a smaller angle  $\gamma'$ , (randomly) chosen from the interval  $]0, \gamma]$  in a different direction  $\phi'$ , is executed (or if the new position still resides outside the cone a new pair  $\gamma', \phi'$  is chosen). Apart from providing the desired properties (probability of presence  $\propto \sin \chi_i$ ), this model furthermore appears naively more adequate for a disordered system than, say a reflection on the circumference of

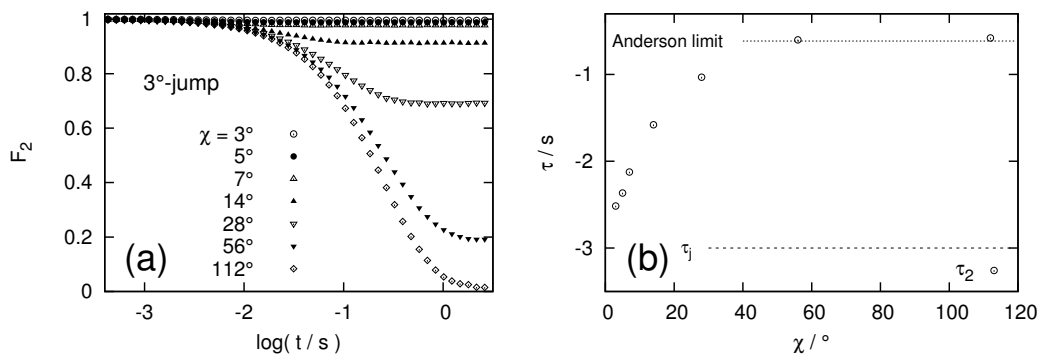


**Figure 4.21 (a):** Simulated correlation functions  $F_2$  for a  $3^\circ$ -jump within cones of different opening angles  $\chi$ . **(b):** Corresponding time constants  $\tau_c$ , the horizontal lines mark the used jump time  $\tau_j$  and the associated Anderson limit found for an isotropic process proceeding via  $\gamma=3^\circ$ .

the cone.

Figure 4.20 displays correlation functions  $F_2$  simulated<sup>5</sup> for the described multi-step motion of different step sizes  $\gamma$  within a cone of  $\chi=7^\circ$  for a fixed jump time of  $\tau_j=50$  ms: whereas in all cases the correlation decays exponentially to a  $\gamma$ -independent plateau value, a divergence in time scale about several orders of magnitudes becomes evident. Furthermore the correlation function does not approach the random jump limit for large reorientation angles  $\gamma$  due to the fraction of smaller jump angles introduced by the afore discussed boundary conditions.

The correlation times  $\tau_c$  extracted from an exponential fit exhibit a modified Anderson behaviour, which can be phenomenologically modelled via

$$\frac{\tau_j}{\tau_c} = a \frac{3}{2} \sin^2 \left( \frac{\gamma}{c \cdot \chi} \right), \quad (4.12)$$

represented by the dotted lines in figure 4.20 (b). Equation 4.12 is versatile enough to reproduce simulated data for  $\chi = 7^\circ$  and  $11^\circ$  with one set of parameters  $c, a$ <sup>6</sup>. Figure 4.21 illustrates the dependence of  $\tau_c$  on  $\chi$  via the exemplary calculated correlation functions of a  $3^\circ$ -jump within different restricting geometries: whereas  $F_2$  exhibits the same initial decay in all cases, i.e. at times when a typical trajectory has not reached the circumference of the cone, the number of individual reorientations needed to probe all accessible sites is on the other hand dependent on the degree of restriction. Hence the onset of the plateau – and consequently  $\tau_c$  – depend on the angle  $\chi$ . This is illustrated by the correlation times displayed in figure (b), which range for the selected  $3^\circ$ -jump between  $\tau_j$  for vanishing cones angles, i.e. strongly restricted dynamics, and the corresponding Anderson limit for very large  $\chi$ , i.e. vanishing restriction<sup>7</sup>.

<sup>5</sup>Here, as in the remainder of the section unless noted otherwise, the correlation function of the second Legendre polynomial was directly calculated, opposed to  $F_{t_e}^{ss}$  in the previous sections which originates from a simulation of the four-pulse sequence.

<sup>6</sup>We found the proportionality factors  $c = 0.0018$  and  $a = 3.9$ .

<sup>7</sup>Due to the employed boundary conditions the Anderson limit for an isotropic  $3^\circ$ -jump does not strictly apply here.

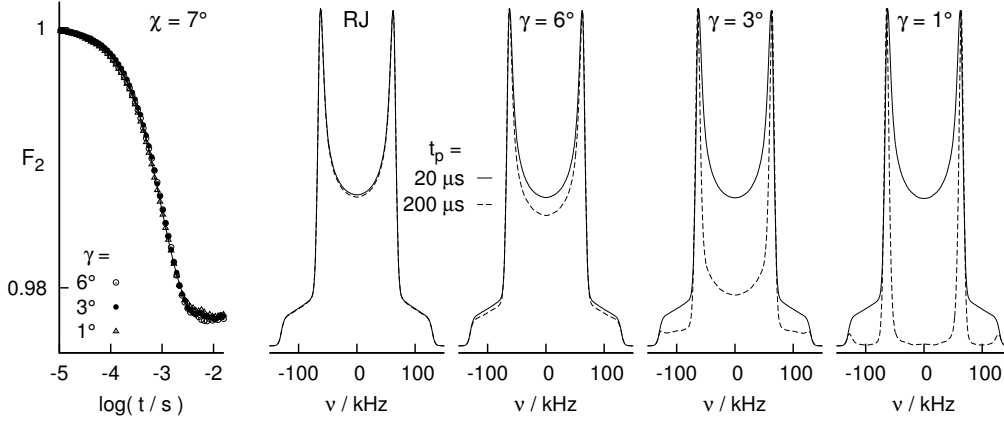


**Figure 4.22:** Normalized intensity around zero frequency for simulated spectra of a motion within a cone.

The important attribute of the present model, i.e. a divergence of  $\tau_j$  and  $\tau_c$ , is visualized in figure 4.22: here the jump times for different multi step motions within the same confining geometry where chosen according to equation 4.12, hence the correlation functions are indistinguishable within the error. This also approximately holds for the spectra corresponding to  $t_p = 20 \mu\text{s}$ , whereas for longer inter pulse delays – when the technique becomes more sensitive to the elementary step – the spectra are widely different. This is also well seen in the  $R(t_p)$  and  $C_{80}$  line shape parameters presented in figure 4.22: whereas both quantities are virtually the same for  $\gamma = 6^\circ, 3^\circ$  and  $1^\circ$  in case of  $t_p = 20 \mu\text{s}$ , the values for  $t_p = 200 \mu\text{s}$  are very sensitive on the jump angle for  $\tau_c \geq 10^{-4}\text{s}$  – the  $R(t_p)$  minimum extends towards longer correlation times for smaller jump angles. Hence the changes in width and position of the minimum in  $R(t_p)$  are a clear fingerprint of the elementary jump process in the framework of the

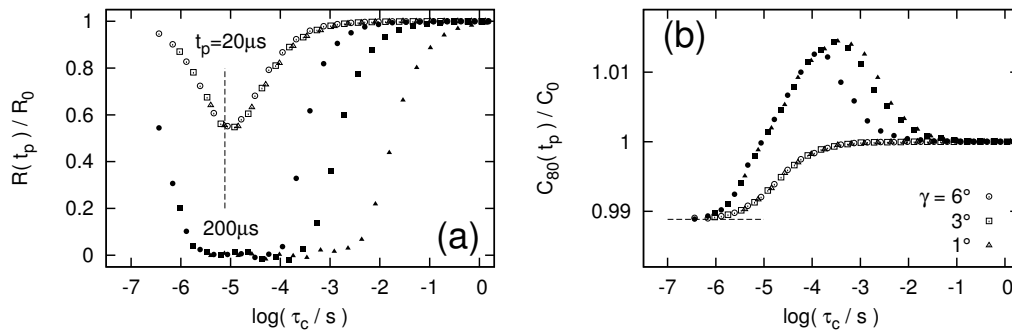
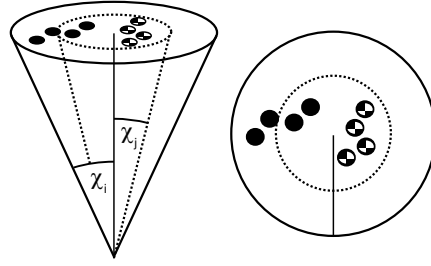


**Figure 4.23 (a):** Normalized intensity around zero frequency of simulated spectra for a multi step motion within a cone with different jump angles  $\gamma$  ( $\chi = 7^\circ$ ,  $t_p = 10\text{-}200 \mu\text{s}$ , key see figure (b)). The dashed line marks  $\tau = 1/\delta$ . **(b):** Corresponding normalized apparent spectral width  $C_{80}$ . The dashed line marks the fast motion limit plateau predicted by equation 4.11.

**Figure 4.24:** Sketch of a multi step motion within a distribution of cone opening angles  $\chi_i$ . The (initial) direction of the C-<sup>2</sup>H bond is marked by the dashed line. After each jump a random position within the circumference of the respective base circle for  $\chi_i$  is approached.



current model. Furthermore it is seen in figure (b) that the local maximum arising in  $C_{80}$  becomes more distinct for smaller jump angles  $\gamma$ .

#### 4.3.4 Distributions of geometries and correlation times

Before summarizing the findings of the last sections, we present an outlook towards more realistic scenarios that have to be considered when comparing simulation results with experimental data in the remainder of this work. As previously mentioned, one expects to find a distribution of confining geometries in a heterogeneous system such as a glass or supercooled liquid. Furthermore it is known that the  $\beta$ -process at temperatures below  $T_g$  exhibits a distribution of correlation times which is typically several decades wide.

To exemplary visualize the effect of a distribution  $G(\log \tau)$  on the solid echo line shape, a random jump type motion within a cone (again  $\chi = 7^\circ$ ) was simulated employing a log-Gaussian distribution of jump times for several widths  $\sigma$ , the results of which are displayed in figure 4.25. The minimum in  $R(t_p)$  still appears around  $\tau^m = 1/\delta$ , it however becomes more complicated to derive a certain geometry of jump or restriction from the results as width and height of the minimum are strongly dependent on  $G(\log \tau)$  in the present case. In contrast to the multi step motions

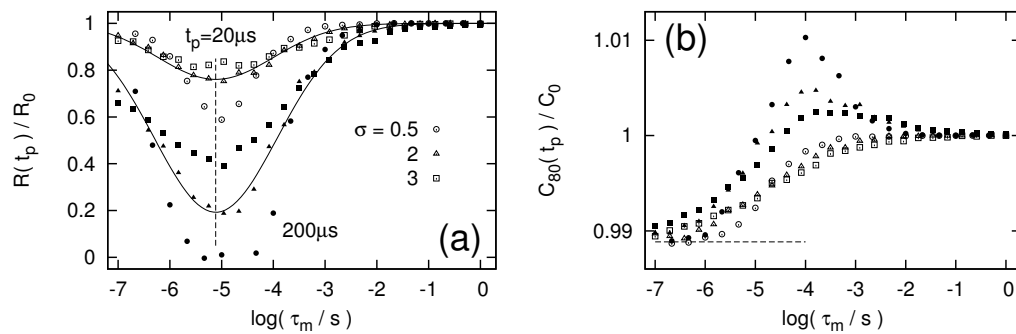


**Figure 4.25 (a):** Normalized intensity around zero frequency for simulated spectra of a random jump type motion within a cone ( $\chi=7^\circ$ , full symbols  $t_p=20\ \mu\text{s}$ , corresponding open symbols  $t_p=200\ \mu\text{s}$ ) in the presence of a distribution  $G(\log \tau)$ . The dashed line marks  $\tau = 1/\delta$ , the full lines serve as guide for the eye. **(b):** Corresponding normalized apparent spectral width  $C_{80}$ . The dashed line marks the fast motion limit plateau predicted by equation 4.11.

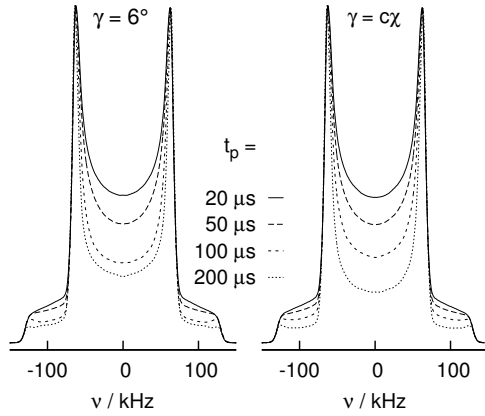


**Figure 4.26:** Simulated spectra for a multi step motion within a distribution of cone opening angles (Gaussian distribution  $\bar{\chi}=7^\circ$ ,  $\sigma_\chi=5^\circ$ ,  $\tau_c=100\ \mu\text{s}$ ). For the spectrum plotted on the left a constant jump angle  $\gamma=6^\circ$  was used, in the other case  $\gamma$  is proportional to  $\chi$ .

discussed in the last chapter, the minimum in  $R(t_p)$  for longer inter pulse delays is yet still symmetric with respect to  $1/\delta$ . The transition in  $C_{80}$  also broadens if a distribution of correlation times is present, furthermore the “overshoot” for longer  $t_p$  values is reduced with increasing width of  $G(\log \tau)$  as seen in figure 4.25 (b). If in addition a distribution of confining geometries is present and the jump mechanism is not of random jump type, the scenario becomes yet more complex as further assumptions with regard to the elementary jump have to be made. If a fixed jump angle  $\gamma$  is maintained throughout the distribution of cone opening angles, the relation 4.12 is no longer valid as different  $\tau_c$  result from a fixed  $\tau_j$  depending on  $\chi$  – hence the relation between the distributions on both time scales becomes non-trivial. This is exemplary visualized in figure 4.26.

## 4.4 Summary and conclusions

As pointed out in the introduction to this chapter, the proposed models are not to be regarded as strictly applicable or plausible with regard to the dynamics in supercooled liquids and glasses. Nevertheless the presented simulation results yield some interesting results for a number of limiting cases, which can readily be applied for a process of elimination when discussing experimental  $^2\text{H}$  NMR results in the remainder of this work. Hence we will recapitulate the most prominent features as a guideline for the experimental part.

Regarding the isotropic motion of the  $\alpha$ -process we have demonstrated that great care has to be taken when employing the  $t_e$ -dependence of the stimulated echo technique to determine the detailed motional process. In the presence of a distribution  $G(\log \tau_\alpha)$  the fast part of this distribution is efficiently suppressed for longer evolution times already around  $\tau_c < 10\ \text{ms}$ . This may lead to undue conclusions when analysing  $\tau(t_e)$  to determine the jump geometry. This especially holds for small angular jumps processes, as the effect becomes more pronounced when  $\tau_c$  and  $\tau_j$  are decoupled – even more so if a correlation between time scale and geometry of the process is present.

For the anisotropic motion of the  $\beta$ -process we found that the position of the  $R(t_p)$

minimum for  $t_p=20\ \mu\text{s}$  provides an independent measure of the correlation time and hence the ability to extract  $\tau_\beta$  from  $^2\text{H}$  NMR solid echo measurements. This holds independently of the elementary step considered and is also valid in the presence of a distribution of correlation times  $G(\log \tau_\beta)$ . For a motion proceeding via small angles  $\gamma$  the line shape changes for longer values of  $t_p$  become visible at relatively longer times  $\tau_c$ . The fast motion limit regime is however unaltered - hence a shift of the  $R(t_p)$  minimum with  $t_p$  represents an indicator for small angular displacements. The fast motion limit plateau value in  $C_{80}$  directly reflects the degree of restriction, i.e. the cone opening angle in the present models. For previously studied glass forming systems the observation of this plateau value was in all cases obstructed by first line shape changes due to the  $\alpha$ -process at  $T>T_g$ . The fast and non-merging  $\beta$ -process of cyanocyclohexane studied in part I is however a hopeful candidate to quantify the relaxation strength of the  $\beta$ -process above  $T_g$  directly by means of  $^2\text{H}$  NMR.

Part I

# Plastic Crystals



# Introduction

Apart from various works regarding the glass transition phenomenon in molecular glass formers, polymers and ionic liquids that have been published in recent years, the literature also contains numerous studies focusing on supercooled plastic crystals. These systems are of special interest, as the complexity of dynamics and therefore the effort needed in complex modelling to interpret typical bulk experiments is reduced, but yet they display some or all features regarded as intrinsic to the glass transition phenomenon.

Most plastically crystalline systems consist of molecules with almost globular shape [Sherwood 1979] and form a cubic lattice, the crystallization to which is characterized by a relatively low entropy of fusion [Timmermans 1961]. The molecules are hence centred on fixed lattice points, their orientation however maintains random to at least some degree. Consequently the systems exhibit translational order but orientational disorder, the degrees of freedom are reduced to three. Interestingly the orientational degrees of freedom can be supercooled in many of these substances and subsequently undergo a calorimetric glass transition which resembles the features known from structural glass formers: a non-exponential main ( $\alpha$ -) relaxation following a non-Arrhenius temperature dependence [Brand 2002, Tschirwitz 2002a] and for some systems in addition a thermally activated secondary relaxation: the Johari-Goldstein  $\beta$ -process [Singh 1982, Ramos 1996, Bonjour 1981]. Concerning the dynamics of the  $\alpha$ -process it is noteworthy that the crystalline packing in virtually all systems does not allow for a free rotation of a single molecule around its center of gravity: the tumbling motion is hindered via the constraints imposed by neighbouring molecules on the lattice [Sherwood 1979]. Hence any isotropic motion in plastically crystalline systems – if present – has to be of cooperative nature.

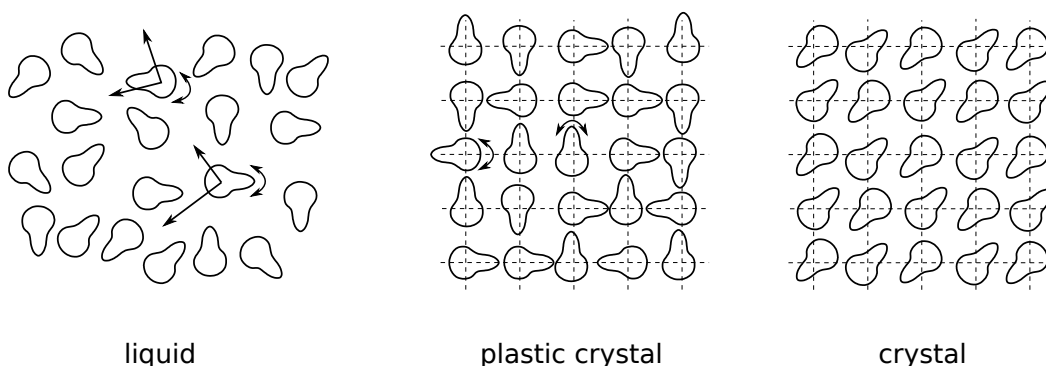


**Figure 5.1:** Sketch of the phases accessible to a plastic crystalline system below the boiling point, adapted from N. Petzold [Petzold 2008].

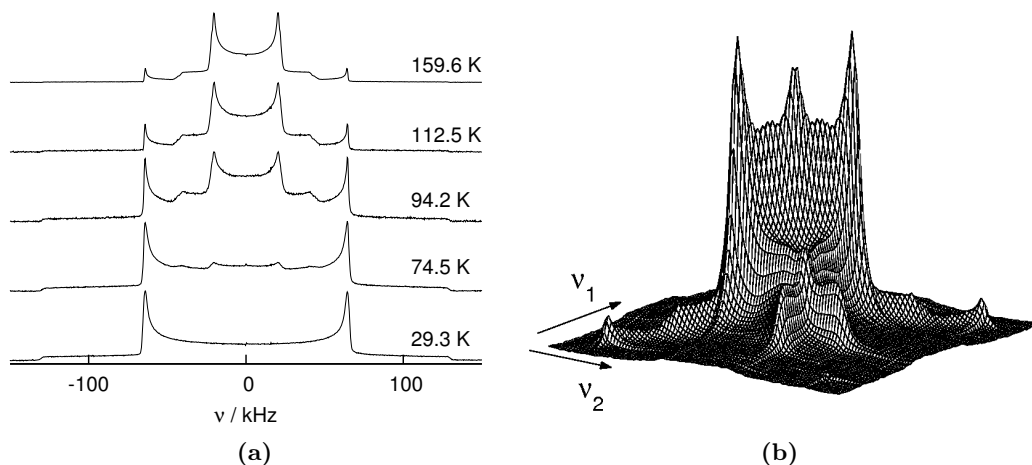


**Figure 5.2 (a):** Solid echo spectra of cyanoadamantane ( $t_p=20\ \mu\text{s}$ ): at lowest temperatures the rotation of the molecule around its  $C_3$  axis is slow with respect to the  $^2\text{H}$  NMR time scale, hence a broad solid state spectrum is observed. At higher temperatures a superposition of the latter line shape and a spectrum with reduced apparent coupling constant  $\bar{\delta}$  due to a fraction of fast rotating molecules is obtained [Roggatz 2000]. **(b):** 2D exchange spectrum of cyanoadamantane recorded in the supercooled plastic crystalline phase:  $T = 245\ \text{K}$ ,  $t_m=3\ \text{ms}$ . The  $90^\circ$ -ridges reflecting a jump process according to the cubic symmetry of the lattice are well seen [Lusceac 2005a].

Although promising for numerous reasons, NMR studies – especially employing two-dimensional techniques – are still quite rare [Böhmer 2001, Winterlich 2003]. As a prominent example we present selected results from the plastic crystalline phase of cyanoadamantane, that were previously obtained in our group [Roggatz 2000, Lusceac 2005a]. The cyanoadamantane molecule is of almost globular shape and exhibits a  $C_3$  symmetry axis around which the molecule rotates even at relatively low temperatures, as the motion requires negligible free volume. This behaviour is demonstrated via the solid echo spectra presented in figure 5.2 (a): at lowest temperatures the rotation of the molecule around its  $C_3$  axis is slow with respect to the  $^2\text{H}$  NMR time scale, hence a broad solid state spectrum is observed. At higher temperatures a superposition of the latter line shape and a spectrum with reduced apparent coupling constant  $\bar{\delta}$  due to a fraction of fast rotating molecules is obtained. The fact that those characteristic “two phase” spectra appear over a quite large temperature range indicates a broad distribution of correlation times for the rotation of cyanoadamantane, reflecting the heterogeneous structure of the glass.

With respect to the remainder of dynamics observed, the system represents an archetype concerning (lattice-) symmetry induced dynamics: the cubic symmetry of the lattice is directly reflected in the elementary jump of the  $\alpha$ -process: two dimensional  $^2\text{H}$  NMR experiments in time and frequency domain clearly exhibit the characteristics of a  $90^\circ$  jump. This is well seen in figure 5.2 (b), as the 2D exchange spectrum (which exhibits the described “two phase” spectrum along the main diagonal at the given temperature) shows characteristic ridges typical for a  $\gamma=90^\circ$  jump motion. This finding is supported by the stimulated echo measurements,

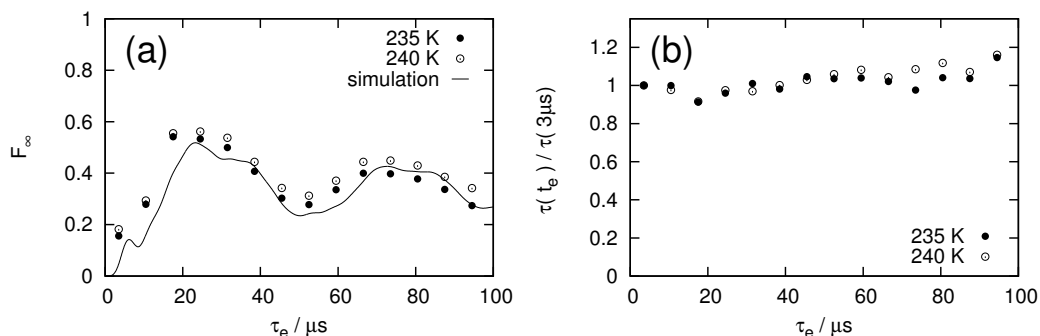


**Figure 5.3 (a):** Residual amplitude of the  $F_{t_e}^{\text{ss}}$  stimulated echo decay in cyanoadamantane at two temperatures [Lusceac 2005a]. **(b):** Corresponding normalized correlation times  $\tau_e$  [Lusceac 2005a].

as the extracted correlations times  $\tau(t_e)$  become slightly longer with  $t_e$  (cf. figure 5.3 (b)), as expected for large angular jumps ( $\gamma > 54.7^\circ$ ). Furthermore the residual amplitude  $F_\infty$  saturates around a value of  $\frac{1}{3}$  (figure 5.3 (a)), reflecting the cubic symmetry of the motion (cf. chapter 3).

Whereas similar dynamics reflecting the structure and symmetry of the lattice were observed in other plastically crystalline systems, this description does not hold up to the melting point. For various systems it was observed – by means of different techniques – that at relatively high temperatures  $T_g \ll T < T_m$  a crossover exists between the symmetry induced motion found in the deeply supercooled plastic crystal and isotropic rotational diffusion as observed in the liquid  $T > T_m$ . This behaviour was reported for example by Bée et al. from a incoherent quasielastic neutron scattering study on chloroadamantane [Bee 1983], which crystallizes in the same space group as cyanodamantane ( $Fm\bar{3}m$ ) but exhibits considerably faster dynamics due to the smaller substituent.

These results are supported by Affouard et al., who found a dynamical transition via proton spin-lattice relaxation and DSC measurements on the same system [Affouard 2000]. The transition temperature was reported in a region where the correlation times of the  $\alpha$ -process are on the order of  $10^{-12} - 10^{-9}$  s, i.e. inaccessible to multidimensional NMR methods as employed for cyanodamantane at relatively lower temperatures. Due to the fast dynamics this region is however suitable for molecular dynamics (MD) simulations (as opposed to the deeply supercooled and glassy regime) and here also a dynamic crossover was observed: MD simulations of the plastic crystals norbornene [Affouard 2003] and chloroadamantane [Affouard 2000] demonstrated that at low temperatures the system exhibit a restricted “cage rattling” motion within the constraints imposed by the neighbouring molecules (attributed to the  $\beta$ -process of mode-coupling theory by the authors) accompanied by a scarce large angular tumbling motion from one lattice direction to another (cf. figure 5.4 (b)). In consequence two-step correlation functions are observed in the low temperature regime; the fraction  $\tau_1/\tau_2$  – readily accessible in the simulations – is close to one. At higher temperatures the dynamics change in the sense that the symmetry constraints of the lattice diminish and the observed motion is comparable to the model of

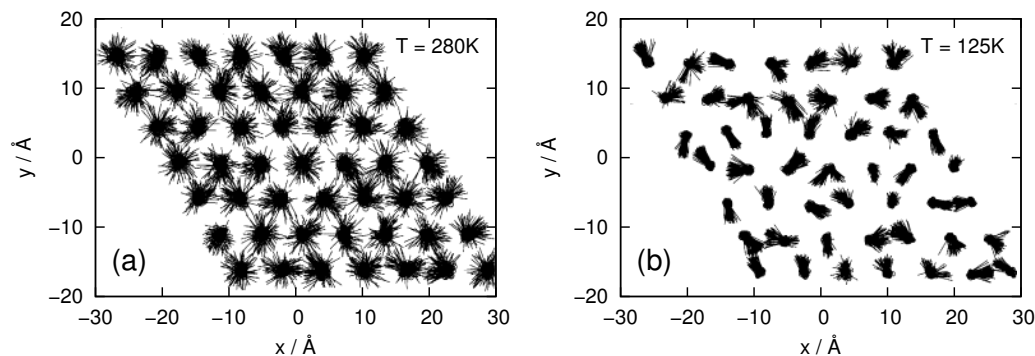


**Figure 5.4:** Molecular dynamics simulation of plastically crystalline norbornene: snapshots of the molecular orientations projected on the x,y-plane at different instants for two temperatures. Figure from [Affouard 2003].

isotropic rotational diffusion with  $\tau_1/\tau_2 \approx 3$  (cf. figure 5.4 (a)).

Cyanoadamantane, for which the prominent  $^2\text{H}$  NMR results were presented, is a type-A glass former as it displays no discernible  $\beta$ -process in dielectric spectroscopy. Apart from the previously outlined advantages of plastically crystalline systems with regard to studies of glassy dynamics, it appears therefore promising to compare the results of cyanoadamantane to a plastically crystalline system with a pronounced  $\beta$ -process. Even more so as the relaxation strength of the latter process is known to grow above  $T_g$  and presumably can be studied in a rather broad temperature range here due to the typically *strong* nature of the  $\alpha$ -process (i.e. low fragility  $m$ ) in plastic crystals – yet  $^2\text{H}$  NMR studies of the  $\beta$ -process in plastic crystals are sparse.

# Cyanocyclohexane - dynamics in a plastic crystal

## Contents

<b>6.1 Introduction</b>	<b>65</b>
6.1.1 Chemical and physical properties	66
6.1.2 Dielectric loss spectra	68
<b>6.2 Structure elucidation</b>	<b>70</b>
<b>6.3 Experimental results – overview</b>	<b>72</b>
6.3.1 Experimental details	72
6.3.2 Spin-lattice relaxation	73
6.3.3 Solid echo spectra	75
6.3.4 Solid echo spectra: low temperature regime	78
6.3.5 Solid echo spectra: fast motion limit effects	80
6.3.6 Stimulated echoes $T < T_g$	83
6.3.7 2D exchange spectra of the $\alpha$ -process	85
6.3.8 Stimulated echoes $T > T_g$	87
6.3.9 Preliminary conclusions	91
<b>6.4 Experimental results – refinement</b>	<b>92</b>
6.4.1 Modelling spin-lattice relaxation	92
6.4.2 Modelling solid echo spectra	95
6.4.3 The $t_p$ -dependence of solid echo spectra $T > T_g$	105
6.4.4 Dynamics of the $\alpha$ -process – reassessment	107
<b>6.5 Summary and conclusions</b>	<b>112</b>

## 6.1 Introduction

Following the general introduction regarding the dynamics in plastically crystalline phases in the last chapter, the remainder of this part will focus on the substance cyanocyclohexane, which exhibits a plastic crystalline phase that is in several aspects promising with regard to studies of the  $\alpha$ - and  $\beta$ -process. Before discussing the  $^2\text{H}$  NMR results obtained within this work, we will summarize prior DSC and dielectric studies to provide an overview regarding the phase diagram and the dynamical processes (yet known) in cyanocyclohexane to emphasize the promising character of  $^2\text{H}$  NMR measurements in the system. The results from dielectric spectroscopy will furthermore turn out be crucial for a more elaborate analysis of the  $^2\text{H}$  NMR data in a joint approach of the techniques.

### 6.1.1 Chemical and physical properties

The molecular structure of cyanocyclohexane (also known as cyclohexanecarbonitrile, cyclohexanecarboxylic acid nitrile or cyclohexyl cyanide,  $C_6H_{11}CN$ ) is sketched in figure 6.1. Cyanocyclohexane is not a rigid molecule, hence different conformations with respect to the orientation of the carbonitrile group relative to the cyclohexane ring can be observed: of particular interest are the equatorial (*e*-) and axial (*a*-) chair conformations (cf. figure 6.2) which have almost the same potential energy [Schneider 1978] and can inter convert crossing an energy barrier of  $\Delta E/k_B \approx 4500$  K [Corfield 1964], hence the abundance of the two conformers is almost equal in the liquid at room temperature [Raber 1977]<sup>1</sup>. The boat conformation exhibits a higher potential energy and therefore its abundance can be neglected at room temperature and below.

Calorimetric measurements [Gonthier-Vassal 1986, Tschirwitz 2002a] show two dis-

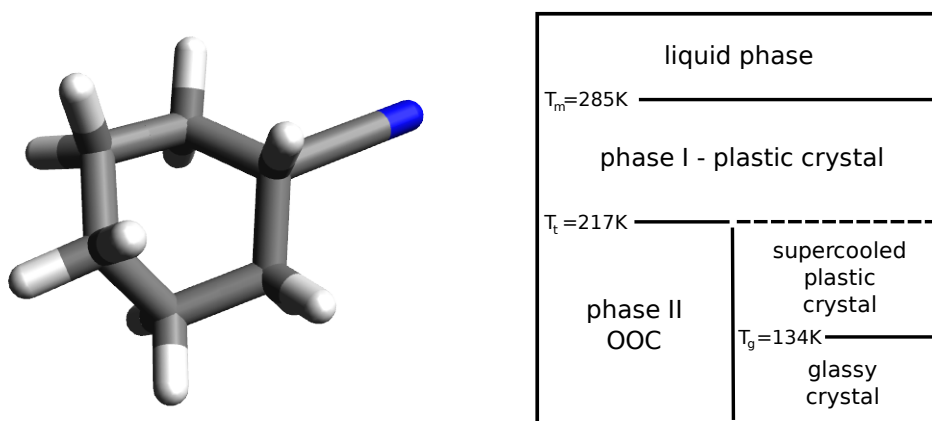


**Figure 6.1 Left:** Molecular structure of cyanocyclohexane. White represents hydrogen (in case of the  $^2H$  NMR sample deuterons), light grey edges are carbon atoms and marked in blue / dark grey is the triple-bonded nitrogen atom of the cyano group. **Right:** Phase-diagram of cyanocyclohexane.

tinct signals: an exothermic one at the melting temperature of  $T_m=285$  K with an entropy of fusion of  $\Delta S_m = \Delta H_m/T_m = (13 \pm 0.8)$  J/mol K and a prominent step like signal at the glass transition temperature  $T_g=(134 \pm 1)$  K. According to the low entropy of fusion Gonthier et al. speculated in 1986 that cyanocyclohexane forms a plastic crystalline phase (phase I) below 285 K according to Timmermans' law as  $\Delta S_m < 21$  J/mol K [Timmermans 1961] – X-ray scattering studies to confirm the supposed translational order in the respective phase were however lacking to this point.

At atmospheric pressure the plastic crystalline phase is stable above  $T_t = (217 \pm 3)$  K [Reuter 1993] and consists of a mixture of the axial and equatorial conformers. Below  $T_t$  the supercooled phase I persist alongside the orientationally ordered crystal (phase II), but is still sufficiently stable on experimental time scales. It has been reported that phase II can be obtained via sufficiently long annealing times at temperatures

<sup>1</sup>At 303 K the abundance of the *e*-conformer is reported to be  $(54.5 \pm 3.5)$  % in a  $CCl_4$  solution.

slightly below  $T_t$  or by applying elevated pressure [Woldbaek 1982]<sup>2</sup>. In this work we were not able to observe a transition to phase II of cyanocyclohexane, as also reported by Tschirwitz et al. in case of dielectric measurements [Tschirwitz 2002a]. The exceptional stability of phase I at temperatures below  $T_t$ , i.e. in the metastable regime, can be explained via the structural properties of the ordered crystalline phase: it is known that cyanocyclohexane crystallizes only in the axial conformer [Woldbaek 1982], hence requiring a substantial number of molecules to overcome the energy barrier of 4500 K for crystallites to form. Regarding thermal energy this would presume for long annealing times at temperatures below  $T_t$ , the transition yet being even more unfavourable as the equatorial conformer exhibits slightly lower potential energy.

Owing to these favourable circumstances, the supercooled plastically crystalline phase

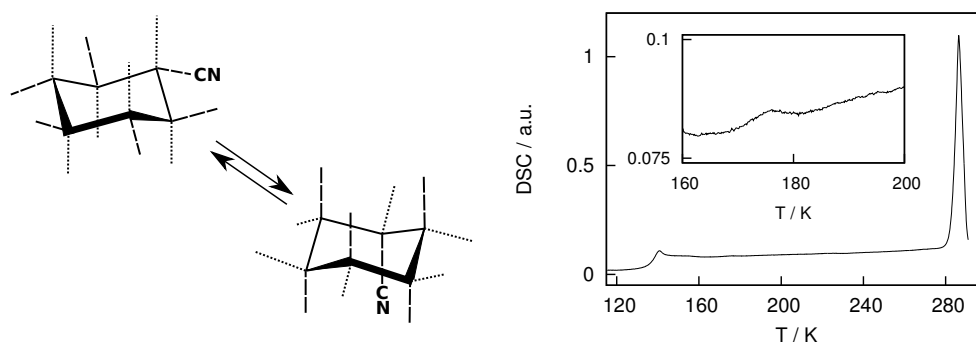


**Figure 6.2 Left:** The two chair conformations of cyanocyclohexane. **Right:** DSC curves of cyanocyclohexane [Tschirwitz 2002b]. The melting peak at  $T_m=285$  K and the prominent glass transition step at  $T_g=134$  K are observed, the inset shows the weak step-like signal around 170 K, attributed to the conformational change of cyanocyclohexane.

can easily be obtained and studied on long time scales. Upon further cooling the phase undergoes a calorimetric glass transition of the rotational degrees of freedom accompanied by a step in the DSC measurements at  $T_g=(134 \pm 1)$  K. Apart from afore mentioned features, the calorimetric measurements (cf. figure 6.2) evince two weaker, step-like features: one at 55 K and one at 170 K, the latter was attributed by Pinvidic et al. [Pinvidic 1988] to a dynamic process with an activation energy of ca.  $\Delta E/k_B=4300$  K that freezes and was identified by the authors with the free chair-chair transformation of cyanocyclohexane. These findings are supported by Raman scattering experiments from Woldbaek et al. [Woldbaek 1982]: in a sample quench-cooled to 90 K the equilibrium of *a*- and *e*-conformers of the room temperature liquid was maintained. Upon gradually heating no effect was observed until around 170 K the abundance of the *e*-conformer was slightly enhanced due to its lower potential energy and the fact that the chair-chair conversion becomes observable on experimental time scales.

Previous light scattering experiments in our group [Surovtsev 2003] gave hint to the existence of a second plastic crystalline phase or an incomplete transition to phase I as the  $\alpha$ -relaxation times  $\tau_\alpha$  exhibited a dependency on the cooling rate

<sup>2</sup>Woldbaek et al. reported a slow transition to phase II at  $10 - 15 \cdot 10^8$  Pa.

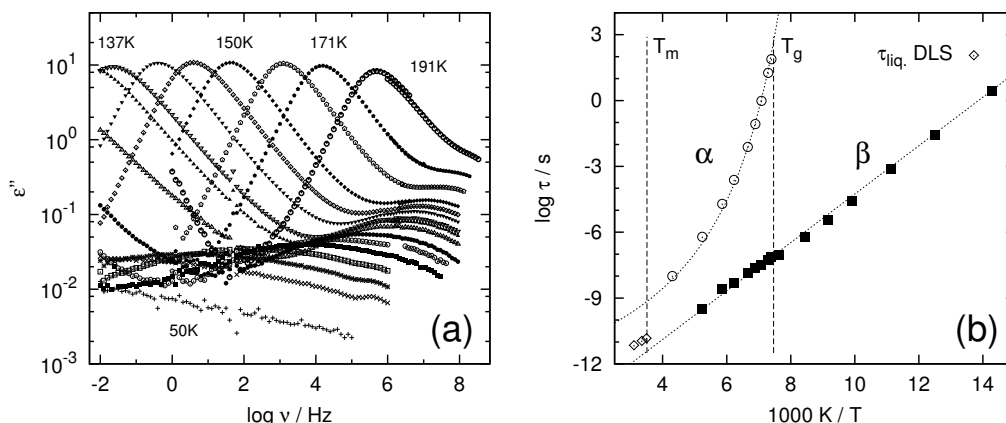


**Figure 6.3 (a):** Dielectric loss spectra of cyanocyclohexane [Tschirwitz 2002a]. **(b):** Corresponding time constants of the main ( $\alpha$ -) relaxation and the  $\beta$ -process [Tschirwitz 2002a] including time constants obtained in the liquid phase by means of depolarized light scattering [Surovtsev 2003].

in the temperature region between 250 K and 285 K. Below  $T=250$  K however no dependency of the dynamics on the cooling rate was found, hence there appears to exist only one stable phase (phase I) in this regime.

### 6.1.2 Dielectric loss spectra

Cyanocyclohexane was previously also studied by means of dielectric spectroscopy in our group [Tschirwitz 2002a]. Figure 6.3 (a) displays dielectric loss spectra which resemble the typical behaviour of a so-called type-B glass former [Kudlik 1999]: the  $\alpha$ -peak shifts towards lower frequencies with lowering the temperature and is well described by a Cole-Davidson function with a stretching parameter  $\beta_{CD}$  of 0.35-0.65, indicating a distribution of correlation times. In addition cyanocyclohexane exhibits a secondary relaxation that manifests in a broad, symmetric high-frequency contribution which dominates the dielectric spectrum at low temperatures. Figure 6.3 (b) displays the time constants of the two dynamic processes:  $\tau_\alpha$  shows a strong non-Arrhenius temperature dependence which can be modelled by a Vogel-Fulcher-Tammann function [Vogel 1921] (cf. equation 2.1) with  $\tau_0=2.1$  ps,  $D=1064$  K and  $T_\infty=100$  K, whereas the secondary relaxation exhibits an Arrhenius behaviour following equation 2.3 with a rather low activation enthalpy of  $\langle H_\beta \rangle / k_B = 2542$  K  $\approx 19 \cdot T_g$  and a pre-factor  $\tau_0$  of  $5 \cdot 10^{-16}$  s. It is noteworthy that no merging of the time constants  $\tau_\alpha$  and  $\tau_\beta$  is observed in the accessible frequency window, nor expected at even higher temperatures. Due to this non-merging characteristic of the  $\beta$ -process a small excess wing is observed in cyanocyclohexane, i.e. the high frequency flank of the  $\alpha$ -process changes its slope and a power law emerges in between  $\alpha$ - and  $\beta$ -process, cf. figure A.1 (b) in the appendix. Furthermore the separation of  $\tau_\alpha / \tau_\beta$  at high temperatures renders cyanocyclohexane a very interesting candidate for studies of the  $\beta$ -process above  $T_g$ . For the majority of molecular glass-forming systems it is unfavourable to study the  $\beta$ -process in this temperature regime since, due to the

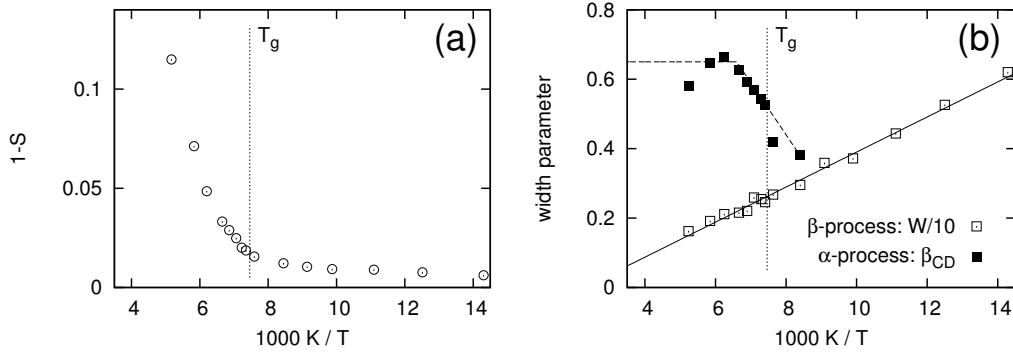


**Figure 6.4 (a):** Relaxation strength of the  $\beta$ -process from dielectric spectroscopy  $1 - S \approx \Delta\epsilon_\beta/\Delta\epsilon$  [Tschirwitz 2002a]. **(b):** Width parameter  $W$  of the  $\beta$ -process (divided by 10 for scaling reasons, the dashed line represents a fit via equation 2.7,  $T_\delta=440$  K,  $\sigma=1162$  K) and  $\beta_{CD}$  of the  $\alpha$ -process from dielectric spectroscopy (the dashed line represents an interpolation employed in section 6.4.1) [Tschirwitz 2002a].

merging of the processes, usually a straightforward and model-free assignment of experimental results to either one is no longer possible. This especially holds in  $^2\text{H}$  NMR, where due to the restricted time window all observables usually start to be affected by the  $\alpha$ -process a few Kelvin above  $T_g$ . This region however is of particular interest regarding secondary relaxations as the relaxation strength of the  $\beta$ -process, which is usually very weak and nearly constant at temperatures  $T < T_g$  (and therefore the NMR effects are rather subtle), exhibits a kink at the glass transition temperature and grows intensively with temperature – making it the only quantity that directly probes  $T_g$  (cf. figure 6.4). Therefore ( $^2\text{H}$  NMR) studies regarding the microscopic dynamics of secondary relaxations are for many glass-forming systems hindered by a combination of obstacles:

- at temperatures  $T < T_g$  the relaxation strength is small, hence one typically deals with subtle changes in all measured quantities
- the distribution of correlation times  $G(\log \tau_\beta)$  is typically several decades wide in this temperature regime, making it impossible to fully exploit the aptitude of multidimensional NMR due to the limited time window of the technique
- at temperatures above  $T_g$ , where the relaxation strength grows and the distribution  $G(\log \tau_\beta)$  narrows, it is often no longer possible to de-convolute the effects of  $\alpha$ - and  $\beta$ -process.

With regard to the aforementioned properties, cyanocyclohexane appears to be a promising candidate for studies on the microscopic dynamics in supercooled liquids, overcoming some of the mentioned obstacles. For the first time the possibility arises to study the  $\beta$ -process in the interesting region above  $T_g$ , where  $1-S$  grows significantly, in a considerably large temperature region without influence of the  $\alpha$ -process by means of  $^2\text{H}$  NMR. As the  $\beta$ -process exhibits for the better part correlation times in the fast motion limit regime ( $\tau_\beta \ll 1/\delta$ ) at  $T > T_g$  prominent effects on the solid echo line shape are expected due to the  $\beta$ -process, which so far have not been observed in

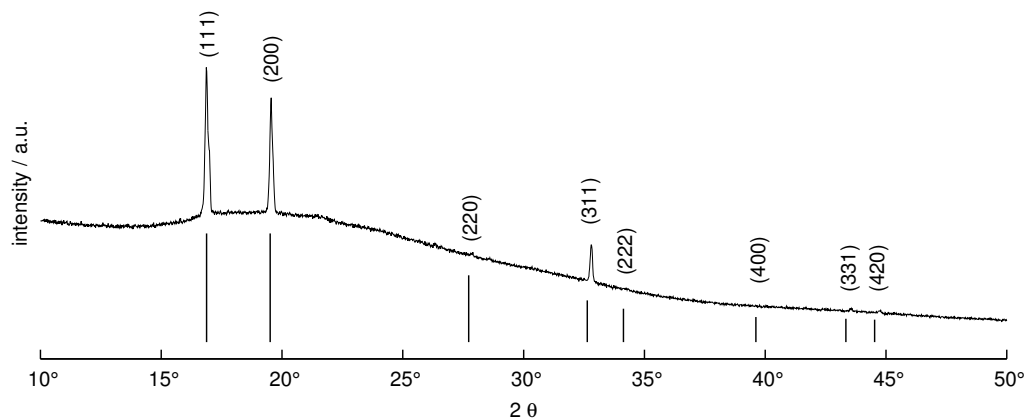


**Figure 6.5:** X-ray diffraction pattern of cyanocyclohexane recorded at 230 K ( $\lambda = 1.54178 \text{ \AA}$ ). The calculated reflexes for an *fcc* lattice with lattice constant  $a = 9.10 \text{ \AA}$  are labelled.

any other glass forming system and yield the possibility to quantify the relaxation strength and distribution of restricting geometries directly by means of  $^2\text{H}$  NMR.

## 6.2 Structure elucidation

The results obtained by dielectric spectroscopy presented in the last section are even in detail identical to those typically obtained for type-B structural glass-forming systems, i.e. the translational order in the plastic crystalline phase imposes no peculiarities whatsoever on the dielectric loss spectra. Hence, apart from the low entropy of fusion, there exists no further argument that cyanocyclohexane indeed forms a plastic crystalline phase, rendering structural studies a necessity. Furthermore it may be crucial to know the detailed structure of the plastic crystalline phase to unravel the microscopic dynamics of the  $\alpha$ -process, which may also in the present system be governed by symmetry of the lattice, as demonstrated for cyanoadamantane in the introduction to this part.

As previously mentioned, the structures of phase I (PC) and II (OOC) in cyanocyclohexane are unknown [Singh 2008], phase I is yet speculated to be either face-centred cubic (*fcc*) or simple cubic (*sc*) like found in many cognate compounds (e.g. *fcc*: cyclohexanol, neopentanol, neopentylglycol, cyanoadamantane; *sc*: cycloheptanol [Singh 2009, Amoureux 1983]).

To affirm these speculations structural studies<sup>3</sup> employing X-ray powder diffraction techniques were conducted. For this purpose the sample was prepared of fully protonated cyanocyclohexane from Sigma-Aldrich, used as received and sealed in a 0.5 mm glass capillary. The sample was studied in a Siemens D5000 X-ray powder diffractometer (copper  $K_{\alpha 1}$  X-ray source) and cooled via a direct stream of cold nitrogen gas controlled by an Oxford temperature controller.

<sup>3</sup>The measurements were conducted in the laboratory of Prof. Breu, Universität Bayreuth. The help of Dunja Hirsemann is greatly acknowledged.

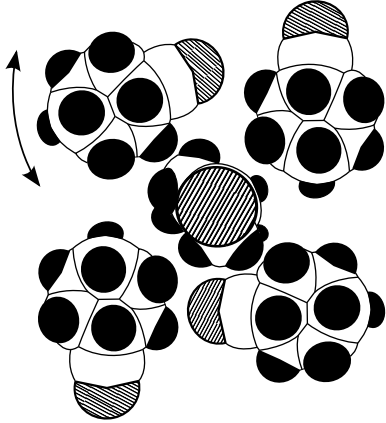


**Figure 6.6:** Sketch of cyanocyclohexane molecules (van der Waals spheres representation) placed in arbitrary orientation on the  $(100)$  plane of  $fcc$  unit cell with  $a = 9.10 \text{ \AA}$ . In this representation it becomes evident, that a free rotation of a molecule around its point of gravity is not possible in cyanocyclohexane. Hence isotropic dynamics has to be of cooperative nature.

The powder diffraction measurements were conducted at  $T=230 \text{ K} < 250 \text{ K}$ , therefore no dependence on the thermal history of the sample is expected with regard to the findings of Surovtsev et al. [Surovtsev 2003]. Figure 6.5 shows the obtained diffraction pattern without any corrections applied. Due to its composition cyanocyclohexane has a rather low scattering diameter, hence the signal is rather weak. The dominant features of diffraction patterns in a plastic crystal are however clearly observed: a broad, amorphous background in combination with sharp reflexes indicating a large degree of translational order. The low overall number of reflexes indicates a highly ordered structure, the three most dominant reflexes occur at angles  $2\theta$  of  $16.88^\circ$ ,  $19.55^\circ$  and  $32.80^\circ$ . In combination with the results from dielectric spectroscopy, which exhibit the dynamic fingerprint of a supercooled liquid (i.e. not a simple rotor phase), these results confirm the formation of a plastic crystalline phase below  $T_m$ . For the assumed cubic symmetry the quadratic form of the Bragg relation reads

$$h^2 + k^2 + l^2 = a^2 \frac{4 \sin^2 \theta}{\lambda^2} \quad (6.1)$$

with  $\lambda = 1.54178 \text{ \AA}$  for the copper  $K_\alpha$  source used. The best agreement is achieved for an  $fcc$  lattice (selection rule:  $h, k, l$  all odd or even). According to the above relation this assignment yields a lattice constant of  $a = 9.10 \text{ \AA}$  at  $230 \text{ K}$ . The x-ray diffraction density  $Z$ , i.e. the number of molecules per unit cell, is given by

$$Z = \frac{\rho a^3 N_L}{M} \quad (6.2)$$

with the density  $\rho$ , the molar mass  $M$  and the Avogadro constant  $N_L$ . With the molar mass  $M = 109.17 \text{ g/mol}$  of cyanocyclohexane and the density of the room temperature liquid  $\rho = 0.919 \text{ g/cm}^3$  this yields a value of  $Z = 3.82$ . Allowing for the error made in using the density of the liquid at  $20^\circ \text{C}$  this value is in reasonable agreement with the theoretical value of  $Z = 4$  molecules per unit cell for a  $fcc$  lattice.

The positions of the  $(111)$ ,  $(200)$  and  $(311)$  reflexes in figure 6.5 are in good agreement with the theoretical angles indicated by the marks underneath the spectrum. The  $(220)$ ,  $(331)$  and  $(420)$  reflexes are also resolved, although with much lower intensity and a slight shift towards larger angles  $2\theta$ . The  $(400)$  reflex on the other hand is missing, which renders the proposed assignment of an  $fcc$  structure somewhat

ambiguous and calls for further (refined) measurements. Finally we note that the sketch presented in figure 6.6 suggests that free rotation of a cyanocyclohexane molecule around its point of gravity is hindered by its neighbours: the positions of the carbonitrile groups are subject to symmetry constraints – i.e. any isotropic tumbling motion has to be a cooperative processes in the system, as being the case in virtually all plastic crystals [Sherwood 1979].

### 6.3 Experimental results – overview

For the sake of clarity the remainder of the experimental section will be divided into two parts: an overview concentrating all  $^2\text{H}$  NMR results followed by a more in-depth discussion of selected results in section 6.4. Whereas section 6.4 will deviate from a model-free approach by discussing the results in the scope of random walk simulations presented in chapter 4, the following overview will be of general validity. For the complex dynamics accompanying the glass transition phenomenon it is however crucial to combine the results of different techniques in the attempt to gain further insight into the microscopic motion of the different processes. Consequently, whenever expedient, we will employ the results obtained by dielectric spectroscopy – especially the correlations times and their respective distributions, which often will serve as basis for a conservative estimate in the attribution of observed effects to either of the processes. Prior to the presentation of the experimental results however details of the measurements will be summarized.

#### 6.3.1 Experimental details

The perdeuterated sample cyanocyclohexane- $\text{d}_{11}$  was synthesized by H. Zimmermann (Max Planck-Institut für Medizinische Forschung, Heidelberg) and used without further purification; the NMR sample was prepared by S. Lusceac.  $^2\text{H}$  NMR measurements were conducted at a magnetic field strength of 7.05 T, corresponding to a deuteron Larmor frequency of 46.07 MHz. Certain solid echo spectra, spin-spin and spin-lattice relaxation time measurements in the temperature regime between 77 K and  $T_g$  were already conducted by Sorin Lusceac [Lusceac 2005b] in our group, employing a home built low temperature probe placed in an Oxford static cryostat CF 1200, where temperature stability was better than 0.3 K. For latter experiments a Bruker CXP spectrometer equipped with a TecMAG data acquisition system was used. The remainder of experiments were executed employing the same magnet and probe (hence the same temperature sensor and calibration) which however in this case was mounted in a Cryovac static cryostat controlled by the same Oxford ITC 503 temperature controller as used for the CF 1200 cryostat. The setup achieved comparable temperature stability. The NMR spectrometer was replaced with a Bruker Avance DSX 300 console, the  $90^\circ$  pulse lengths in both setups were on the order of 2.5  $\mu\text{s}$  to 3.5  $\mu\text{s}$ .

Virtually all experiments performed by S. Lusceac were repeated or verified within this work – in the case of  $T_1, T_2$  by measuring at additional temperatures in all regions. Employed of the former results for the present study were only a certain number of  $T_1, T_2$  data points at temperatures below  $T_g$ , which are presented alongside

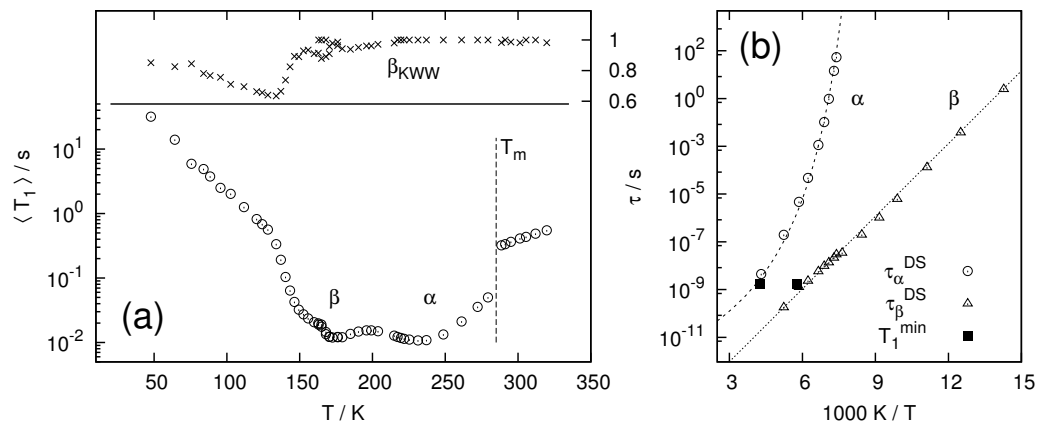


**Figure 6.7 (a):** Average spin-lattice relaxation times  $\langle T_1 \rangle$ , inset shows corresponding stretching parameter  $\beta_K$ . For a discussion of the small apparent step around 170 K see appendix A.2. **(b):** Time constants extracted from the  $\langle T_1 \rangle$  minima (full symbols) in comparison with results from dielectric spectroscopy (open symbols, [Tschirwitz 2002a]).

present results in figures 6.7, 6.8, 6.11 (b) and A.3, as well as the solid echo spectrum in figure 6.10 and a number of spectra  $T < T_g$  used for the analysis of line shape parameters in figures 6.11 and 6.13. The vast remainder of experimental results and all analysis are part of this work.

Whenever expedient the cyanocyclohexane results will be compared against those of other glass-forming substances to emphasise the peculiarities in the present system. Hereby mostly ethanol- $d_2$  and toluene- $d_5$ <sup>4</sup> measured by Schneider [Schneider 2001] and Vogel [Vogel 2000a] in our group<sup>5</sup> will be employed, as the latter represents a “typical” type-B molecular glass former with  $\langle H_\beta \rangle / k_B \approx 24 \cdot T_g$  and was intensively studied by means of  $^2\text{H}$  NMR. Ethanol- $d_2$  on the other hand exhibits – as cyanocyclohexane – a relatively fast  $\beta$ -process with  $\langle H_\beta \rangle / k_B \approx 14.6 \cdot T_g$  and  $^2\text{H}$  NMR results are also readily available.

For a first review of the dynamics in the plastic crystalline phase of cyanocyclohexane (including the supercooled and glassy plastically crystalline regime) the temperature dependence of the spin-lattice relaxation time will be discussed.

### 6.3.2 Spin-lattice relaxation

As spin-lattice relaxation measurements are a useful tool to study dynamics on the time scale of the inverse Larmor frequency [Sillecu 1992], i.e. on the order of nanoseconds for typical  $^2\text{H}$  NMR  $B_0$  field strengths, the resulting spin-lattice relaxation times of cyanocyclohexane presented in figure 6.7 provide a comprehensive overview of the dynamics in the system. The average relaxation time  $\langle T_1 \rangle$  is plotted as spin-lattice relaxation becomes non-exponential below about 200 K, i.e. a Kohlrausch

<sup>4</sup>Ethanol and toluene are always denoted with the degree of deuteration since different samples - $d_x$  were investigated. Cyanocyclohexane however was only studied in the perdeuterated case (- $d_{11}$ ).

<sup>5</sup>In both cases the Bruker CXP / TecMAG setup was employed, hence  $\omega_L$  and all other relevant parameters are the same as in the case of cyanocyclohexane.

fit to the magnetization curves yields  $\beta_K < 1$  in this regime, cf. figure 6.7. In this temperature regime the structural relaxation is no longer effective on the time scale of  $T_1$ , instead a faster process ( $\beta$ -process) dominates spin-lattice relaxation. Regarding the temperature dependence of  $\langle T_1 \rangle$  in cyanocyclohexane one immediately detects the arise of two distinct minima around 240 K and 170 K<sup>6</sup>. A minimum in  $T_1$  occurs if the corresponding dynamic process approaches correlation times on the order of  $\tau(T_{\min}) \approx 1/\omega_L$  and hence becomes most effective with regard to spin-lattice relaxation. In most structural glass formers  $\alpha$ - and  $\beta$ -process have merged before either of them has approached the nanosecond regime, resulting in a single minimum in  $\langle T_1 \rangle$  somewhat above  $T_g$ , depending on the fragility of the system. The kink (universally) appearing at  $T_g$  in deuteron spin lattice relaxation measurements has to be attributed to the growing relaxation strength of the  $\beta$ -process however. As  $\alpha$ - and  $\beta$ -process do not merge in cyanocyclohexane due to a relatively fast  $\beta$ -process and - as found in most plastic crystalline systems - a rather *strong*  $\alpha$ -process (fragility index  $m = 55.1$  [Tschirwitz 2002a]), the time constants are still well separated at temperatures where the minima are expected to arise. In a first approach it is therefore reasonable to connect the  $\langle T_1 \rangle$  minimum at lower temperatures to the  $\beta$ -process in cyanocyclohexane. Applying the condition  $\tau = 1/\omega_L$  for both minima yields time constants in good agreement with  $\tau_\alpha$  respectively  $\tau_\beta$  from dielectric spectroscopy, cf. figure 6.7 (b). Regarding the absolute values of  $\langle T_1 \rangle$  one notices that the spin-lattice relaxation times at the respective minima for  $\alpha$ - and  $\beta$ -process are very similar: naively one would expect a substantial lower rate for a restricted motion like the  $\beta$ -process with its relatively small relaxation strength (c.f. figure 6.4). We will however show in section 6.4.1, that this finding is in agreement with results from other techniques. To our knowledge this is the first time that a  $\langle T_1 \rangle$  minimum in  $^2\text{H}$  NMR is reported for the  $\beta$ -process.

To illustrate this peculiarity, figure 6.8 (a) displays the spin-lattice relaxation times of cyanocyclohexane in comparison with data of toluene and ethanol on a reduced temperature scale  $T_g/T$ . The spin-lattice relaxation times of toluene represent an archetype of a supercooled liquid: a kink at  $T_g$  followed by a single minimum at higher temperatures. In dielectric spectroscopy  $\alpha$ - and  $\beta$ -process of toluene can no longer be separated around  $\tau_{\alpha/\beta} \approx 10^{-7}$  s: due to the fragile nature of the  $\alpha$ -process and the rather large activation energy of the  $\beta$ -process the time scales merge and hence one finds a single minimum in  $T_1$ . Ethanol on the other hand exhibit a relatively fast  $\beta$ -process with a low activation energy of  $E_a/k_B \approx 15 \cdot T_g$  – yet the temperature dependence of  $T_1$  is comparable to the one in toluene: only one distinct minimum arises at  $T > T_g$  which corresponds to the  $\alpha$ -process<sup>7</sup>. Considering  $\tau_\beta$  of ethanol in figure 6.8 (c) it becomes obvious that the condition  $\tau_\beta \approx 1/\omega_L$  is already approached at temperatures below  $T_g$ : as previously mentioned, one may speculate that the small relaxation strength of the  $\beta$ -process in this region hampers the observation of clear effects in  $T_1$ , further discussions thereof will be postponed to section 6.4.1 where a more quantitative analysis is conducted.

From this comparison it becomes evident that a reduced temperature scale with

<sup>6</sup>For a discussion of the small apparent step in this temperature region see appendix A.2

<sup>7</sup>The minimum itself is not shown in figure 6.8 since data in the region of interest is not available in literature.

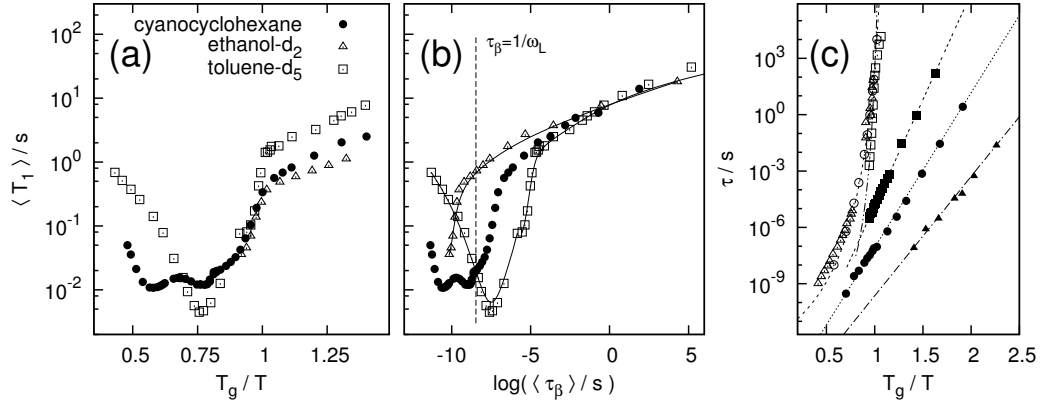


**Figure 6.8 (a):** Average spin-lattice relaxation times  $\langle T_1 \rangle$  of type-B glass forming systems plotted versus reduced temperature  $T_g/T$  (cyanocyclohexane:  $T_g=134$  K, toluene- $d_5$ :  $T_g=117$  K [Vogel 2000a, Rössler 1984], ethanol- $d_2$ :  $T_g=97$  K [Schneider 2001]). **(b):** Same data plotted versus an isodynamic temperature scale with respect to the  $\beta$ -process, the lines serve as guide for the eye. **(c):** Corresponding time constants extracted from dielectric spectroscopy [Tschirwitz 2002a, Kudlik 1997b, Benkhof 1999].

respect to the  $\alpha$ -process (i.e.  $T_g/T$ ) may not be indicated when comparing the evolution of  $^2\text{H}$  NMR measurements in different glass forming substances with regard to the  $\beta$ -process: large differences in fragility and relative activation enthalpies  $\langle H_\beta \rangle$  can promote hasty conclusions. Therefore a different reduced temperature scale will be aspired in the remainder of this work, when temperature dependent measurements of different glass formers are to be compared. The iso-dynamic scale with regard to the thermally activated nature of the  $\beta$ -process is a more expedient choice for those comparisons, as seen in figure 6.8 (b) where the spin-lattice relaxation times of the discussed systems are plotted with respect to  $\log(\tau_\beta)$  obtained from dielectric spectroscopy [Tschirwitz 2002a, Kudlik 1997b, Benkhof 1999]. In this representation it becomes obvious that the low temperature minimum in  $\langle T_1 \rangle$  of cyanocyclohexane forms around  $\tau_\beta \approx 1/\omega_L$  whereas the  $\beta$ -process is too fast / too slow with regard to the  $\alpha$ -process in ethanol / toluene. Apart from this trivial observation it is an interesting finding that the low temperature spin-lattice relaxation times of the three systems collapse on a single envelope when plotted in this representation – again pointing to the remarkable universality of the  $\beta$ -process (in  $^2\text{H}$  NMR), as it implies that width and relaxation strength of the secondary relaxation are comparable in all three systems with respect to  $\tau_\beta$ .

### 6.3.3 Solid echo spectra

Following the overview on glassy dynamics in cyanocyclohexane illustrated by  $T_1$ , which already demonstrated the advantageous situation in cyanocyclohexane for  $^2\text{H}$  NMR measurements, we will now focus on the discussion of the solid echo line shape, which is consequently expected to exhibit prominent features also. Figure 6.9 (a) presents an overview of the solid echo line shape ( $t_p = 20 \mu\text{s}$ ) from the

lowest measured temperature (34 K) to the line shape collapse around 172 K. In this representation it becomes evident that the temperature dependence of the solid echo spectrum in cyanocyclohexane can be forked in three different temperature regimes in an obvious manner:  $T < T_g$ ,  $T_g < T \lesssim 165$  K and above.

- $T < T_g = 134$  K: at lowest temperatures the line shape resembles the (rigid limit) Pake spectrum and changes with temperature are very subtle over an experimentally observable range of 100 K. The dominant line shape changes in this regime are limited to the centre of the spectrum and can be emphasized by prolonging the inter pulse delay  $t_p$  of the solid echo pulse sequence, as demonstrated in figure 6.9 (d).
- $T_g < T \lesssim 165$  K: at temperatures above  $T_g$  the line shape in cyanocyclohexane differs considerably from a rigid limit Pake spectrum. This peculiar line shape prevails over a large temperature interval of about 30 K and exhibits little but continuous temperature dependence from  $T_g$  to the line shape collapse. Comparable line shape effects have not yet been observed in supercooled liquids and potentially offer new insights on the mechanism of relaxation in this regime.
- $T \approx 165$ -175 K: in this temperature regime the broad solid state spectrum collapses to a liquid line due to the fast isotropic tumbling motion of the  $\alpha$ -process.

Figure 6.9 (c) exemplarily illustrates the line shape in the second – most interesting – temperature regime: not only is the line shape for short inter pulse delays highly distorted, the spectra also exhibit considerable  $t_p$  dependence at the given temperature. The line shape hence exhibits the fingerprint of a dynamic process and according to the results of chapter 4 can be attributed to a motion faster than about 0.5 ms. For a preliminary allocation the fraction

$$W(T) = \int_{-\infty}^{-3.3} G(\log \tau) d \log \tau \quad (6.3)$$

extracted from fits to the dielectric spectra (cf. appendix C for details) is plotted in figure (b) for  $\alpha$ - and  $\beta$ -process respectively. Within this purely heterogeneous (i.e. exchange processes are neglected), phenomenological approach  $W(T)$  serves only as an conservative estimate, but illustrates that the  $\alpha$ -process is only expected to exhibit first, subtle effects on the line shape at temperatures above ca. 155 K, whereas the  $\beta$ -process is virtually in the fast motion limit above  $T_g$ .

Before going into detail on the line shape effects in the region  $T_g < T \lesssim 165$  K we will focus on the high and low temperature regimes, as the dominant effects observed here are well known from a variety of other glass forming systems and can be analysed in a straightforward manner.

In the high temperature regime of the line shape collapse the correlation time of the  $\alpha$ -process approaches  $10^{-6}$  s, i.e. is on the order of the inverse coupling constant  $1/\delta$ . The fast isotropic dynamics attributed to the structural relaxation averages over all orientations of the electric field gradient tensor relative to the external magnetic

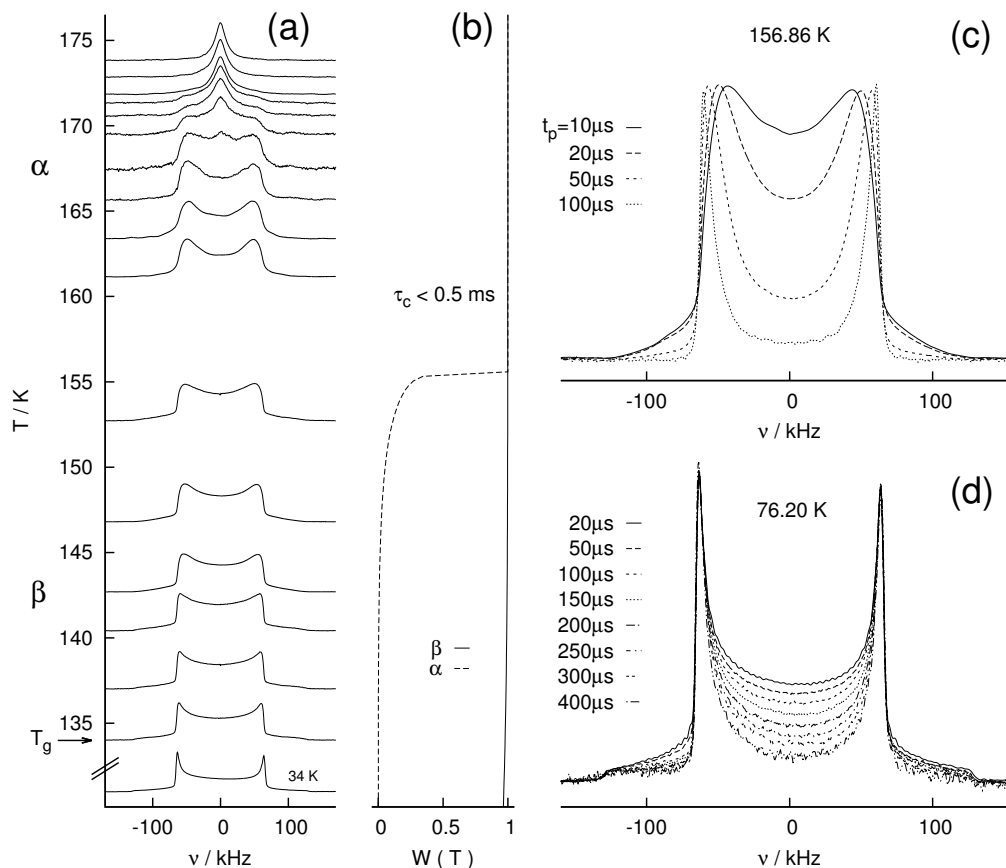


**Figure 6.9 (a):** Evolution of the line shape above  $T_g=134$  K. The intersection with the ordinate marks the temperature at which each spectrum was recorded. For comparison a spectrum at lowest temperatures (34 K) is plotted. **(b):**  $W(T)$  from equation 6.3, i.e. fraction of  $\tau_\alpha$  and  $\tau_\beta$  faster than 0.5 ms. The temperature scale of figure (a) is maintained. **(c):**  $t_p$  dependence of the line shape in the high temperature regime. **(d):**  $t_p$  dependence at lowest temperatures.

field and the solid state spectrum collapses to a central line at around 172 K<sup>8</sup>. The line shape of cyanocyclohexane in the vicinity of the collapse however exhibits a peculiarity: at temperatures where the solid state spectrum is still well established, it coexists with a central feature at intermediate temperatures ( $T=168$ -171 K, cf. figure 6.9 (a)). For systems with a broad distribution of correlation times this is usually explained in the context of a “two phase” model: the broad dynamic heterogeneities lead to a scenario where the number of molecules exhibiting correlation times on the order of the inverse coupling constant are (due to the reduction factor being virtually zero) negligible in contrast to the relatively fast portion of the sample producing a liquid line and the slow fraction giving rise to a solid state spectrum, cf. figure 4.9. If no fast exchange mechanism is present, a simple superposition of the latter line shapes is observed. For cyanocyclohexane however this is not expected since the

<sup>8</sup>A VFT-fit to dielectric data [Tschirwitz 2002a] yields  $\tau_\alpha^{\text{DS}}(172 \text{ K}) \approx 4 \mu\text{s} \approx 1/\delta$ .

distribution  $G(\log \tau)$  for the  $\alpha$ -process is rather narrow and comparable to numerous other structural glass forming systems ( $\beta_{\text{CD}}=0.65$ , cf. section 6.1.2), which do not exhibit such behaviour at the line shape collapse. We will address this apparent “two phase” behaviour in the scope of discussion.

### 6.3.4 Solid echo spectra: low temperature regime

In the regime  $T < T_g$  any dynamics that is influencing the solid echo line shape has to be attributed to secondary relaxations, as the  $\alpha$ -process is virtually extinct in the glassy state. Typically the line shape changes at temperatures below  $T_g$  and short inter pulse delays  $t_p$  are very subtle and concentrate on the features of the spectrum around zero frequency, where the angular dependency is largest (cf. figure 6.10 (b) and chapter 3). Since the distribution  $G(\log \tau_\beta)$  extends already at these temperatures substantially towards times faster than the inverse of the quadrupolar coupling constant  $\delta$ , one may immediately declare that the corresponding dynamics must be of highly restricted nature, as the alterations to the limiting Pake spectrum are very subtle (cf. section 4.3). The systematic change of spectral intensity around zero frequency seen in figure 6.9 (d) is anticipated for a restricted multi-step motion as demonstrated in chapter 4. This tender effect can be amplified by prolonging the time  $t_p$  between the echo pulses and hence the time during which a phase shift (occurring after reorientation) is accumulated. As displayed in figure 6.10 the line shape changes with  $t_p$  in cyanocyclohexane resemble the behaviour reported for type-B structural glass formers, i.e. the intensity in the middle of the spectrum decreases for longer inter-pulse delays in a characteristic manner. The given spectra of different glass forming substances are recorded at similar reduced temperatures  $T_g/T$  and indeed the  $t_p$ -dependence in cyanocyclohexane, toluene and ethanol – which all exhibit a pronounced  $\beta$ -peak in dielectric spectroscopy – is very similar. Whereas for glycerol, which shows no distinct  $\beta$ -process in dielectric spectroscopy, consequently no systematic changes in the line shape with varying  $t_p$  are found. As in case of the random walk simulations presented in chapter 4, we will continue the discussion of the latter effect in terms of the  $R(t_p)$  parameter, which allows for a more direct comparison of the evolution with temperature as it maps the spectral changes around zero frequency to a single quantity (cf. section 4.2.2 for details).

As seen in figure 6.11 (a) the  $R(t_p)$  values for  $t_p \geq 50 \mu\text{s}$  traverse a pronounced and broad minimum around 115 K, whereas the values at  $T_g$  again roughly resemble the ones found at lowest temperatures. This mimics the behaviour found in the random walk simulations of chapter 4, where in case of restricted dynamics a minimum in  $R(t_p)$  was observed for  $\tau_c = 1/\delta$  independent of the details of the dynamical process. And indeed this holds for the minimum found in  $R(t_p = 50 \mu\text{s})$  of cyanocyclohexane, as the corresponding time constant is in agreement with  $\tau_\beta$  from dielectric spectroscopy, cf. figure 6.19. Within the random walk simulations the criterion  $\tau_c = 1/\delta$  was found to be fulfilled best in case of  $R(t_p = 20 \mu\text{s})$  – here however no minimum is observed in cyanocyclohexane: the trace traverses a maximum above  $T_g$  where the central intensity in the spectra is almost raised by a factor of two with respect to 34 K. As this effect is already pronounced well below  $T_g$ , the observation of a minimum is hampered. A raise in  $R(t_p)$  is generally found for a process proceeding via large

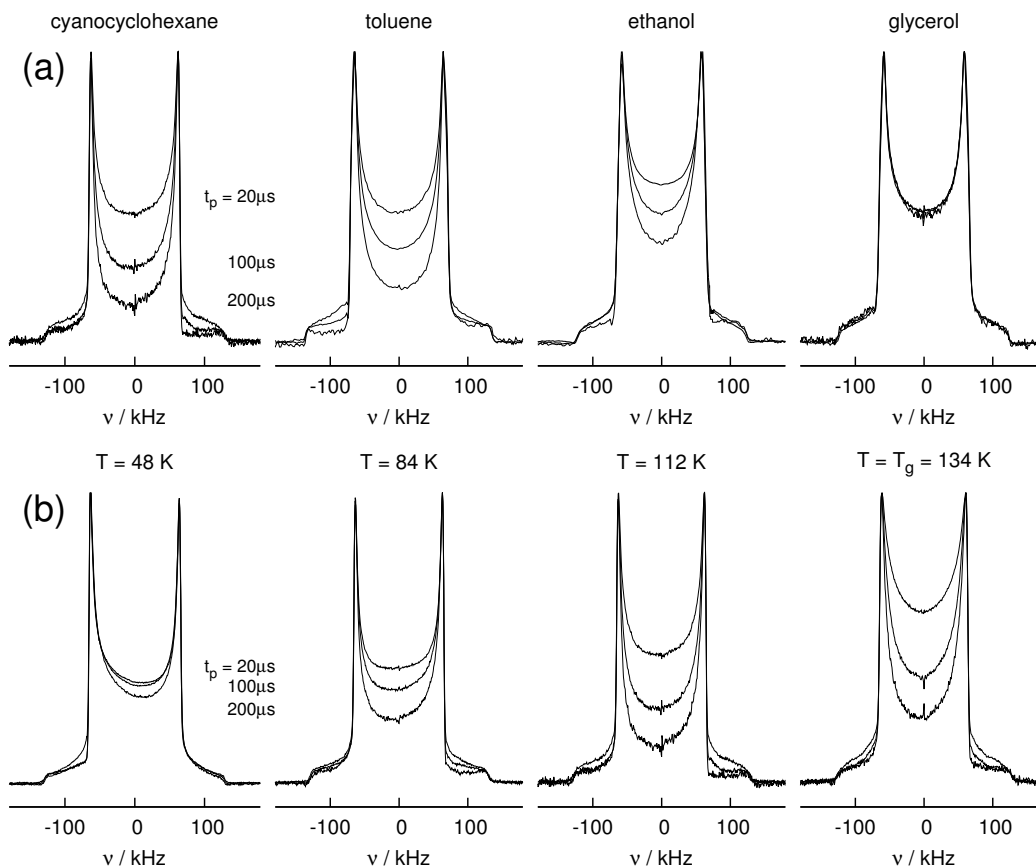


**Figure 6.10 (a):** Solid echo spectra of glass forming substances recorded at similar reduced temperatures  $T_g/T \approx 1.2$ . For each substance the spectra corresponding to solid echo inter pulse delays of  $t_p = 20 \mu\text{s}$ ,  $100 \mu\text{s}$  and  $200 \mu\text{s}$  are shown. Cyanocyclohexane:  $T = 112 \text{ K}$ ,  $T_g = 134 \text{ K}$ ; toluene- $\text{d}_5$ :  $T = 97 \text{ K}$ ,  $T_g = 117 \text{ K}$  [Vogel 2000a]; ethanol- $\text{d}_2$  (glassy phase):  $T = 73 \text{ K}$ ,  $T_g = 97 \text{ K}$  [Schneider 2001]; glycerol:  $T = 156 \text{ K}$ ,  $T_g = 189 \text{ K}$  [Vogel 2000a]. **(b):**  $t_p$ -dependence of the solid echo line shape in cyanocyclohexane for different temperatures  $T \leq T_g$ .

angle jumps, at the discussed temperatures below  $T_g$  the  $\alpha$ -process is however not observable at experimental time scales and the  $\beta$ -process is suspected to proceed via small angles. As  $G(\log\tau_\beta)$  extends to the fast motion limit regime already at  $T_g$  another explanation is however possible: as demonstrated by the random walk simulations in figure 4.18,  $R(t_p)$  also exhibits a distinct raise for a fast, restricted motion upon vanishing restriction, i.e. large opening angles in case of the cone models discussed in chapter 4. We will address this feature in the scope of section 6.4.2.

As the line shape changes below  $T_g$  are most dominantly reflected in the intensity around zero frequency, the  $R(t_p)$  values provide a measure closely related to the spin-spin relaxation time  $T_2$  in the solid state: in figure 6.11 (b) the quantities are plotted again vs.  $\log\tau_\beta$  for reasons of comparison with other glass forming systems (for additional  $T_2$  data see appendix A.3). It becomes imminently evident that  $R(t_p = 200 \mu\text{s})$  and  $\langle T_2 \rangle$  exhibit the same evolution with temperature, i.e. traverse a minimum around  $\tau_\beta = 1/\delta$  before strongly decreasing in the vicinity of  $T_g$ . As

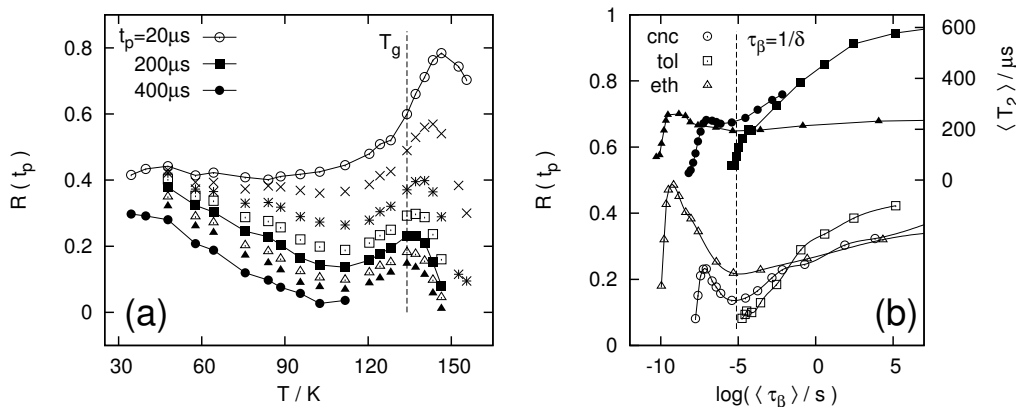


**Figure 6.11 (a):** Relative spectral intensity at zero frequency in cyanocyclohexane for different inter pulse delays  $t_p$  ( $t_p=20, 50, 100, 150, 200, 250, 300$  and  $400 \mu\text{s}$  top to bottom). **(b):**  $R(t_p=200 \mu\text{s})$  (open symbols) and  $\langle T_2 \rangle$  (corresponding full symbols) of cyanocyclohexane, toluene-d<sub>5</sub> [Vogel 2000a] and ethanol-d<sub>2</sub> [Schneider 2001] plotted versus  $\log \tau_\beta$ .

discussed before the experimental observation of this minima in cyanocyclohexane is possible due to the fast and non-merging nature of the  $\beta$ -process – as opposed to the vast majority of glass forming systems.

With regard to the deuteron spin-spin relaxation times and  $R(t_p=200 \mu\text{s})$  values of toluene-d<sub>5</sub> plotted in figure (b), the same arguments as in the discussion of  $T_1$  hold (cf. figure 6.8 (b)): the line shape collapse due to the  $\alpha$ -process appears at relatively lower temperatures (with regard to  $\tau_\beta$ ), hampering the observation of a minimum in either quantity. The behaviour at lower temperatures is however very similar to the one found in cyanocyclohexane, i.e. the onset of the minimum is discernible. In ethanol-d<sub>2</sub> also no stark effects in  $T_1$  were observed, which we tentatively attributed to the small relaxation strength below  $T_g$ , were the condition  $\tau_\beta=1/\omega_L$  is approached in this system. This argument does not hold for the present analysis as  $T_2$  and  $R(t_p)$  are more sensitive on the highly restricted dynamics found in this region and consequently the progression of both quantities closely mimics the one found in cyanocyclohexane, i.e. a distinct minimum is observed at  $\tau_\beta=1/\delta$ .

Before conducting a more quantitative analysis of the effects in section 6.4, we can already conclude at this point that the  $\beta$ -process in phase I of cyanocyclohexane displays all effects found in structural glass formers of type-B and hence the plastic crystalline phase appears to impose no peculiarities on the process.

### 6.3.5 Solid echo spectra: fast motion limit effects

So far the effects of the  $\beta$ -process in the slow motion limit at temperatures below  $T_g$  and the line-shape collapse due to the  $\alpha$ -process around  $T_g+40 \text{ K}$  were discussed. The fact that the line shape changes below  $T_g$  (at least for short  $t_p$ ) are hardly observable is linked to the small relaxation strength of the  $\beta$ -process ( $1-S$ ), i.e. high spatial restriction of the motional process under consideration – this is expected to change above  $T_g$  however as  $1-S$  grows significantly in this regime (cf. figure

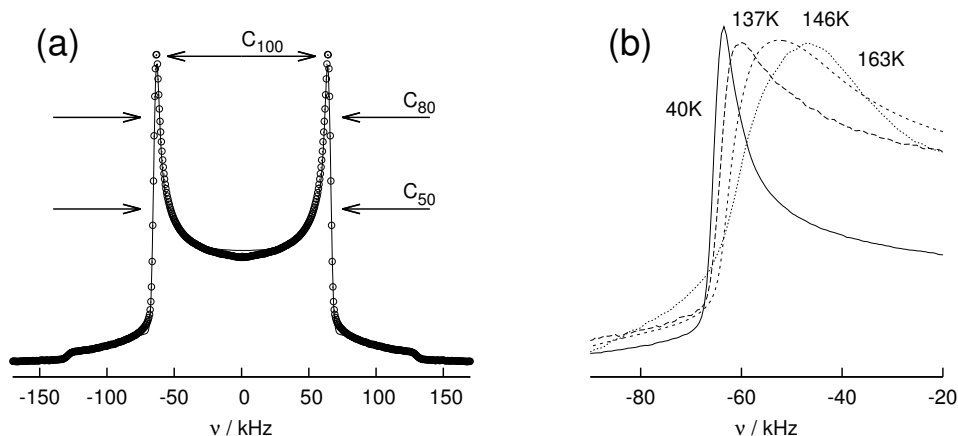


**Figure 6.12 (a):** Symmetrized experimental solid echo spectrum at 34.5 K ( $t_p=20 \mu\text{s}$ , open symbols) and numerical fit (solid line,  $\delta=129.6 \text{ kHz}$ , the numerical spectrum has been damped with respect to experimental pulse excitation effects). The arrows define the width parameters  $C_x$  for monitoring the evolution of the line-shape with temperature. **(b):** Detail around the inner singularity of solid echo spectra for  $t_p=20 \mu\text{s}$  at different temperatures.

6.4 (a)). Figure 6.12 (b) displays solid echo spectra for  $t_p=20 \mu\text{s}$  at four different temperatures: compared to the spectrum at lowest temperatures (40 K), which resembles the limiting Pake spectrum, the overall width of the spectrum at  $137 \text{ K} > T_g$  is slightly reduced, but yet more dominant is the deviation around the singularities: the spectrum tapers in the upper half and the singularities are *smear out*, which also holds for the outer singularities, which have transformed to a more or less structureless decay of intensity towards higher frequencies. The effects are even more pronounced in the spectra recorded at higher temperatures. The intensity deviations that arise around zero frequency (i.e. changes in  $R(t_p)$ ) are presumably due to slower dynamics ( $\tau_\alpha, \tau_\beta \gtrsim 1/\delta$ ) and will be neglected at first. While the tapering of the spectrum could also result from a non-vanishing asymmetry parameter  $\eta$  that changes with temperature, the remainder of spectral changes can not be explained within this scope. Furthermore we have no reason to expect  $\eta > 0$  for the aliphatic C-<sup>2</sup>H bonds in cyanocyclohexane. Yet we know that at  $T_g$  already more than half of the sub ensembles can be attributed a correlation time  $\tau_\beta$  in the fast motion limit regime,  $\tau_\beta \ll 1/\delta$ , i.e. prominent line shape effects are anticipated. Figure 6.12 (a) displays the (symmetrized<sup>9</sup>) spectrum at lowest temperatures (34.5 K) where the line shape is well described by a Pake spectrum, as demonstrated by the fit symbolized by the solid line. Also marked in this figure are the measures  $C_x$ , defined as the apparent spectral widths at  $x=50, 80$  and  $100\%$  of maximum intensity which will serve to quantify the spectral evolution with temperature as the spectra above  $T_g$  no longer can be described by a Pake pattern.

In figure 6.13 the quantities  $C_x$  are given for all recorded solid echo spectra. The right part shows an enlarged plot at low temperatures: in this representation it becomes immediately obvious that the spectrum for short inter pulse delays  $t_p$

<sup>9</sup>Due to minor problems with the resonant circuit of the the probe appearing at lowest temperatures, some of the spectra for  $T < 70 \text{ K}$  exhibit intensity deviations with respect to the singularities.

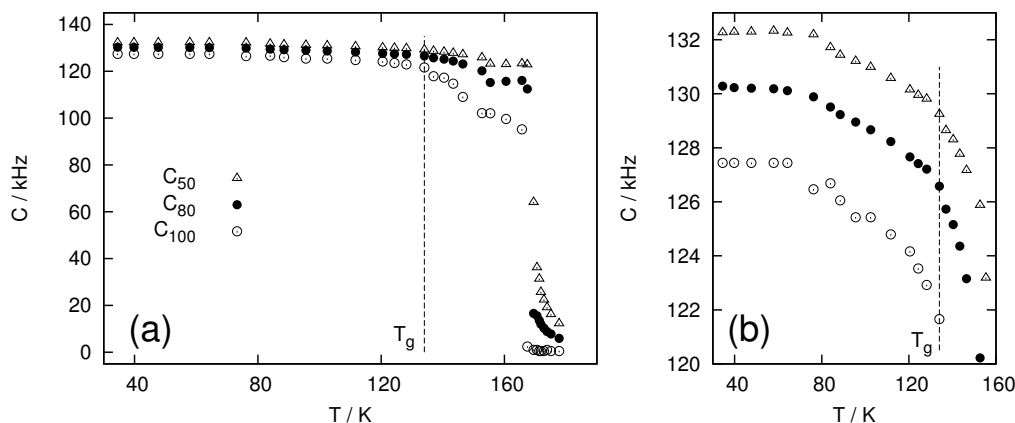


**Figure 6.13 (a):** Apparent spectral width of solid echo spectra for  $t_p=20\ \mu\text{s}$  at different relative intensities. **(b):** Enlarged plot of the low temperature regime  $T < T_g$ .

changes with temperature (aside from the  $R(t_p)$  value) also below  $T_g$ . Whereas the apparent spectral width  $C_{80}$  exhibits almost no temperature dependence at lowest temperatures, it starts to lessen around  $T=60\ \text{K}$  and decreases approximately linear until  $T_g$ . At the glass transition temperature the temperature dependence changes within a few Kelvin and contracts more pronounced towards higher temperatures until the solid state spectrum collapses. Apart from the overall narrowing of the spectra<sup>10</sup>, also systematic deviations in the widths taken at different relative intensities are observed. At low temperatures the three arbitrary  $C_x$  values display the same temperature dependence within the error margins, which means that the spectra retain their shape with respect to the singularities (Pake pattern). Starting at 70-80 K however, the values gradually diverge, leading to a reduction in the flank slope of the spectra. The effect is rather subtle for temperatures  $T < T_g$  but is clearly observed around  $T_g$  and grows continuously towards higher temperatures until at around 170 K the solid state spectrum collapses to a liquid line. This behaviour clearly is the fingerprint of molecular dynamics – and, as will be shown, related to the  $\beta$ -process in cyanocyclohexane.

The discussed changes in the line shape in the temperature region  $T_g < T < T_g + 40\ \text{K}$  can not be analysed further retaining a straightforward, model-free approach. Since the effect sets in well below  $T_g$  and becomes more pronounced at the glass transition temperature (where the relaxation strength of the  $\beta$ -process grows) it however is tempting to associate it with fast motion limit effects of the  $\beta$ -process growing in amplitude. Before a more in-depth analysis of the peculiarities in the high temperature solid echo line shape of cyanocyclohexane will be presented in section 6.4.2, the experimental overview will be completed with a discussion of results from two-dimensional  $^2\text{H}$  NMR methods.

<sup>10</sup>Which could also be related to a temperature dependence of the quadrupolar coupling constant  $\delta$  for  $T < T_g$ .

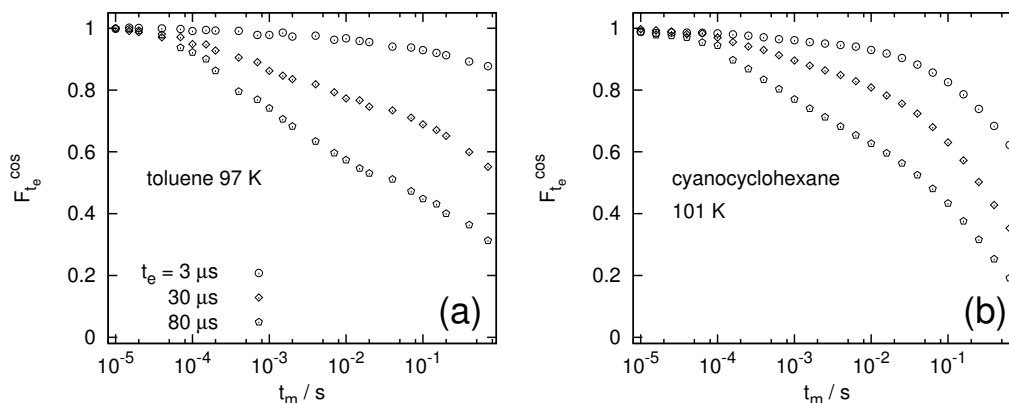


**Figure 6.14:** Stimulated echo decays of the cosine-cosine correlation in cyanocyclohexane (this work, (b)) and toluene ([Vogel 2000a], (a)) for different evolution times  $t_e$  at temperatures  $T < T_g$ . Same symbols denote same evolution times  $t_e$ .

### 6.3.6 Stimulated echoes $T < T_g$

Apart from measurements of  $T_1$ ,  $T_2$  and the solid echo line shape, the  $\beta$ -process was also previously studied by 2D  $^2\text{H}$  NMR methods below  $T_g$ . With the discussion of the latter we will consummate our overview on  $^2\text{H}$  NMR measurements related to the  $\beta$ -process, as the method directly maps the mechanism of the motion.

Due to the broad distribution of correlation times  $G(\log \tau_\beta)$ , the restricted nature of the underlying dynamics and the limited time window of the experiment, it is not possible to measure the full correlation loss due to the  $\beta$ -process below  $T_g$ . Nevertheless the stimulated echo decay in toluene- $d_5$  and polybutadiene at low temperatures was intensively studied by M. Vogel [Vogel 2000a] and successfully explained via a cone model for the  $\beta$ -process. Figure 6.14 displays the decay curves of the cosine-cosine correlation function  $F_{t_e}^{\text{cc}}$  for three different evolution times  $t_e$ <sup>11</sup> at one temperature: for an evolution time of  $3 \mu\text{s}$  toluene exhibits a very weak, almost not discernible, more or less structureless decay until about  $t_m = 100 \text{ ms}$  when another process decays the stimulated echo amplitude finally to zero. M. Vogel identified this slower process as spin diffusion, as it displays almost no temperature dependence and the extracted time constants are on the order of reported spin diffusion rates for deuterated substances. The initial decay for longer evolution times ( $30 \mu\text{s}$  and  $80 \mu\text{s}$ ) grows in amplitude, yet retains its overall shape – the fingerprint of a motion which agitates via small angular displacements. As the decay extends over several orders of magnitude in time and is almost not resolvable for short evolution times, it has to be attributed to a highly restricted process with a broad distribution of correlation times – the  $\beta$ -process.

The stimulated echo decays of cyanocyclohexane at comparable reduced temperature  $T_g/T$  are plotted in figure 6.14 (b). Here the qualitative picture is the same: a broad,

<sup>11</sup> $F^{\text{cc}}$  was recorded for reasons of the straightforward correction for spin-lattice relaxation decay during the mixing time  $t_m$ , as opposed to the  $T_{1Q}$  decay in the sine-sine correlation  $F^{\text{ss}}$ . All curves displayed in this section have already been corrected for  $T_1$  effects during  $t_m$ .

highly  $t_e$ -dependent, structureless decay which finally is cut off around 100 ms by spin diffusion<sup>12</sup>. In order to quantify the observed decay, the stimulated echo curves were fitted with a function decaying via two steps [Vogel 2000a]:

$$F_{t_e}^{cc}(t_m) = A_0 [(1 - C_{t_e}^{cc}) \Phi_{\beta, t_e}(t_m) + C_{t_e}^{cc}] \Phi_{SD, t_e}(t_m) \quad (6.4)$$

where  $\Phi_{\beta, t_e}(t_m)$  and  $\Phi_{SD, t_e}(t_m)$  denote stretched exponential functions. In toluene the stretching parameter  $\beta_{\beta, K}$  of the initial decay was found to be around 0.37 for all evolution times  $t_e$ , whereas  $\beta_{SD, K}$  for the spin diffusion part was around 0.5. Both numbers provided good interpolation also in case of cyanocyclohexane and were therefore kept constant in equation 6.4 to reduce the otherwise large number of free parameters.

Given that the relaxation strength of the  $\beta$ -process is nearly constant below  $T_g$ , the finite state amplitude  $C_{t_e}^{cc}$  (again in a purely heterogeneous, phenomenological scenario) only depends on the fraction of molecules exhibiting correlation times  $\tau_\beta$  within the time window defined by the experiment. The lower limit of which is set by experimental constraints and usually is on the order of 100  $\mu$ s (cf. chapter 4), the upper limit is in the case of toluene and cyanocyclohexane defined by the onset of spin diffusion and hence roughly 100 ms in both substances. The fraction of molecules contributing to the stimulated echo decay can thus be evaluated by integrating over the distribution  $G(\log \tau_\beta)$  provided by dielectric spectroscopy (cf. figure C.1) [Vogel 2000a]:

$$A(T) = \int_{\log 100 \mu s}^{\log 100 ms} d \log \tau_\beta G(\log \tau_\beta, T). \quad (6.5)$$

In the case of a constant relaxation strength the quantity  $A$  provides a measure proportional to  $C_{t_e}^{cc}$  with a proportionality factor  $p(t_e)$  depending only on the microscopic geometry, i.e. angular step size and isotropy of the motion. Figure 6.15 presents the  $C_{t_e}^{cc}$  values for 30  $\mu$ s and 80  $\mu$ s in toluene- $d_5$ , cyanocyclohexane and ethanol- $d_{1/2}$  obtained from a fit via equation 6.4, as well as  $p(t_e)(1 - A(T))$ , where the geometrical factor  $p(t_e)$  serves as a fit parameter. The qualitative temperature dependence is the same in all substances: the experimental  $C_{t_e}^{cc}$  as well as the calculated  $p(t_e)(1 - A(T))$  values traverse a maximum below  $T_g$  as the distribution  $G(\log \tau_\beta)$  is shifted through the experimental time window (in cyanocyclohexane and ethanol however this maximum is found at relatively lower temperatures with respect to  $T_g/T$  due to the fast  $\beta$ -process). Furthermore the absolute values are of similar magnitude and yet even more remarkable the fraction of the geometrical factors  $f_G = p(80 \mu s)/p(30 \mu s)$  for evolution times of 80  $\mu$ s and 30  $\mu$ s was found to be around 2.2 in all cases. When normalized and plotted vs.  $\log \tau_\beta$ , the finite state amplitudes  $1 - C_{t_e}^{cc}$  of all three substances exhibit very similar behaviour, almost collapsing on a common envelope<sup>13</sup> – i.e.  $^2\text{H}$  NMR detects in all three systems a

<sup>12</sup>The fact that this long time decay in perdeuterated cyanocyclohexane is somewhat faster than in toluene- $d_5$  may be explained via the density of deuterons / protons in the respective sample.

<sup>13</sup>A strictly universal behaviour is not expected as the width of the distribution  $G(\log \tau_\beta)$  slightly varies with respect to the reduced temperature in the different substances. This is however not observable due to the low signal to noise ratio (especially in the vicinity of  $T_g$ ).

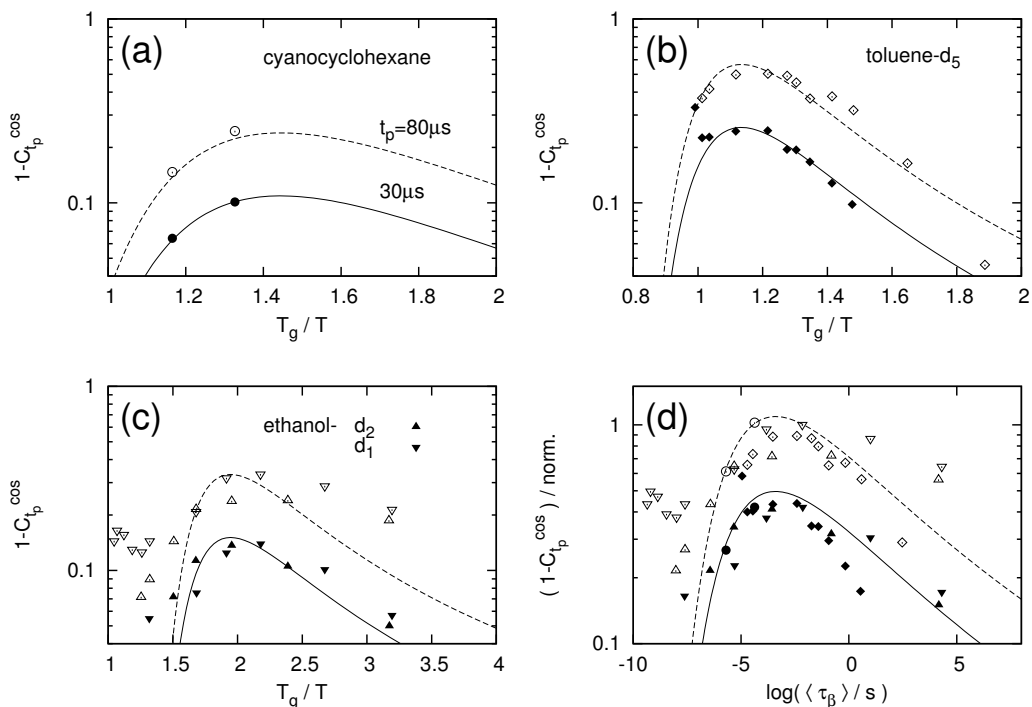


**Figure 6.15:** Amplitude of the  $F^{\text{cc}}$  decay in toluene- $\text{d}_5$  (b) [Vogel 2000a], ethanol- $\text{d}_{1/2}$  (c) [Schneider 2001] and cyanocyclohexane (a) versus reduced temperature  $T_g/T$  (cf. equation 6.4), the lines represent  $p(t_e)(1 - A(T))$  (cf. equation 6.5) calculated for each substance employing dielectric results. Figure (d) depicts all data on an isodynamic temperature scale regarding the  $\beta$ -process, in this case lines serve as guide for the eye only.

$\beta$ -process with comparable degree of restriction that progresses via akin elementary steps, the mechanism of the motion appears universal.

Thus summarizing all  $^2\text{H}$  NMR results obtained at  $T \leq T_g$  and therefore concerning the  $\beta$ -process, we can infer that the behaviour of cyanocyclohexane is even in detail identical to previously studied (structural) glass formers and hence no particularities whatsoever were found that reflect the high translational symmetry of the plastic crystalline phase. Consequently we can act on the assumption that the conclusions drawn from the prominent findings related to the  $\beta$ -process above  $T_g$  are of more general validity also.

### 6.3.7 2D exchange spectra of the $\alpha$ -process

Focusing again on temperatures well above  $T_g$  and hence the dynamics of the  $\alpha$ -process, we will begin the discussion of 2D  $^2\text{H}$  NMR results in this regime with the presentation of 2D exchange spectra. These are of considerable interest in the present system, as the method readily allows to identify motion reflecting the symmetry of the lattice, as demonstrated in the case of cyanoadamantane in the introduction to this part.

Figure 6.16 displays 2D exchange spectra recorded at 151 K and 156 K for different

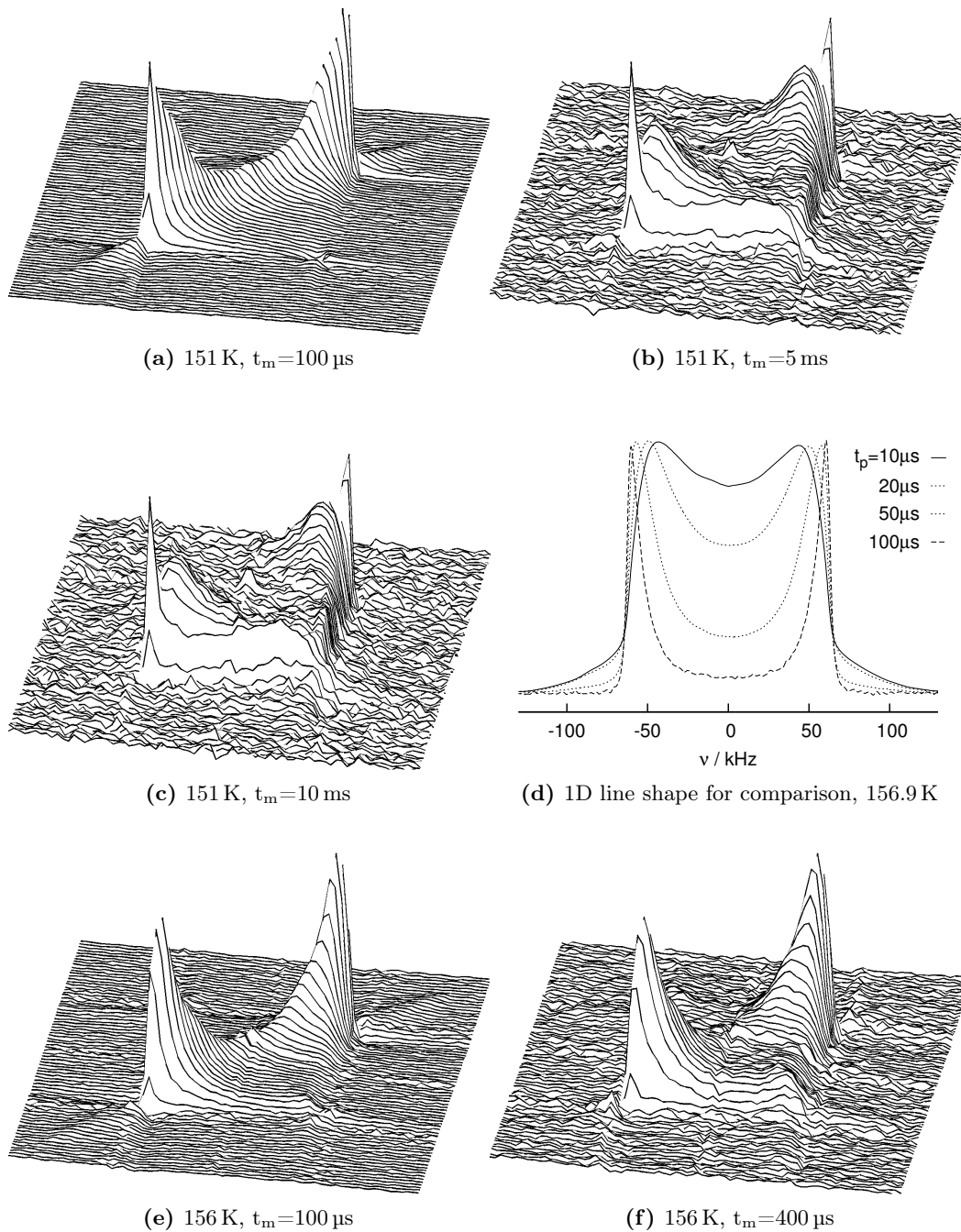


**Figure 6.16:** 2D exchange spectra of cyanocyclohexane recorded at 151 K (first and second row) and 156 K (lower row) for different mixing times  $t_m$ . For comparison the  $t_p$  dependence of the solid echo line shape in the same temperature regime is plotted, which resembles the artefacts observed along the main diagonal of the 2D spectra.

mixing times  $t_m$ . It is immediately obvious that the spectral intensity is in stark contrast to the one found in cyanoadamantane: the exchange intensity exhibits a structureless broadening of the diagonal that extends to the full spectral plane even at short mixing times – no traces of ridges resulting from discrete jump processes are observed. Apart from this lack of clear-cut signs for any motion reflecting the lattice symmetry, one further notices the distorted main diagonal of the 2D spectra, which does not resemble a Pake spectrum. With regard to the  $t_p$  dependence of the solid echo line shape in the same temperature region exemplary displayed in figure 6.16 (d) it becomes however evident that this feature is no peculiarity of the presented 2D exchange spectra, but yet already imposed on the 1D solid echo experiments. At temperatures where the present pulse sequence for 2D exchange spectroscopy can be applied to study the  $\alpha$ -process, i.e.  $T_2 \ll \tau_\alpha \ll T_1$ , the  $\beta$ -process is significantly faster than  $T_2$  and affects the solid echo spectrum, whereas it no longer contributes to exchange intensity in the 2D experiments for the same reason (cf. section 6.3.6:  $A(T)$ , eq. 6.5, is virtually zero above  $T_g$ ). As the 2D spectra are composed of several one dimensional experiments recorded for different  $t_e$ , one obtains a weighted sum of the  $t_p$ -dependent spectra seen in figure 6.16 (d).

Nevertheless the 2D spectra allow to draw an important conclusion: as the exchange intensity extends to the full spectral plane, no ridges or ellipses are found and the diagonal of the spectrum is already broadened for short mixing times, we can state that the  $\alpha$ -process in cyanocyclohexane is an isotropic process with a similar manifestation in the  $^2\text{H}$  NMR observables as in case of structural glass formers – and hence in strong contrast to the one observed in cyanoadamantane and reported for further plastically crystalline systems by means of other methods. Whereas a transition from a motion reflecting the lattice symmetry to a rotational diffusion scenario at high temperatures has been reported in plastically crystalline systems (cf. chapter 5), it is expected to occur at relatively higher temperatures with  $\tau_c$  in the nanosecond regime – i.e. about 100 K above the studied temperatures. Whether this transition is shifted towards lower temperatures in cyanocyclohexane due to the fast  $\beta$ -process will be discussed at the end of this chapter, when more information on the mechanism of the latter process is at hand.

### 6.3.8 Stimulated echoes $T > T_g$

If a dynamic process does not impose well resolved features on the 2D exchange spectra, as being the case for the  $\alpha$ -process in cyanocyclohexane, it is often more expedient to study the motion via multi-dimensional NMR methods in time domain, i.e. the evolution time dependence of the stimulated echo, which allows for an extraction of more quantitative information.

Figure 6.17 displays the stimulated echo (sine-sine correlation) decays in the applicable temperature regime (i.e.  $T_2 \ll \tau_\alpha \ll T_1$ ) between 147 K and 158 K and for evolution times  $t_e$  of typically 1.5–80  $\mu\text{s}$  at a maximum increment of 2.5  $\mu\text{s}$ . Already in this representation it becomes obvious that the  $t_e$  dependence changes noticeably within a narrow temperature interval (apart from obvious changes in  $T_2$  leading to a stronger reduction of the initial amplitude with  $t_e$  at higher temperatures): the  $F_{t_e}^{\text{SS}}$  decays for short and long evolution times differ more noticeably at lower temperatures,

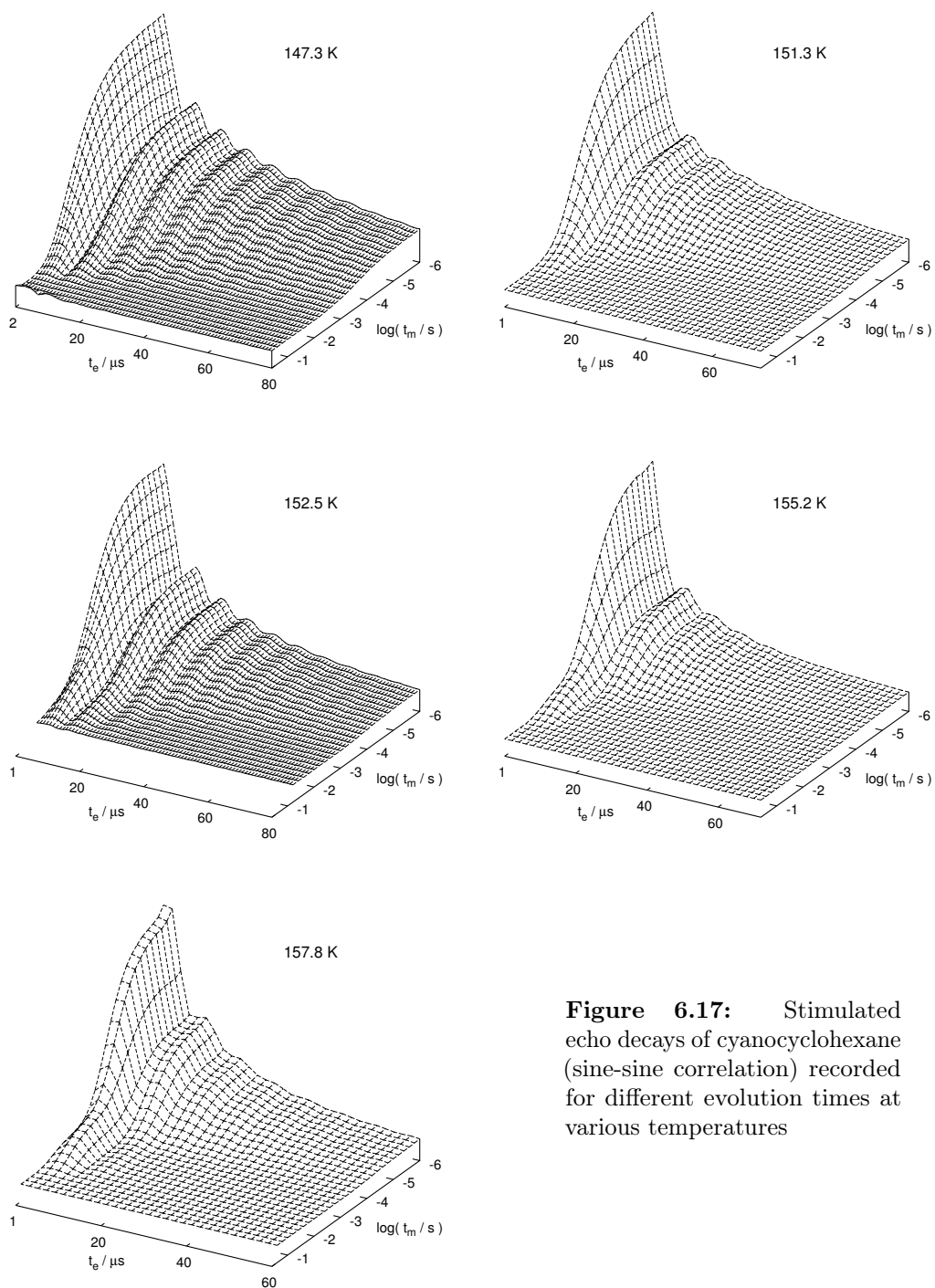


**Figure 6.17:** Stimulated echo decays of cyanocyclohexane (sine-sine correlation) recorded for different evolution times at various temperatures

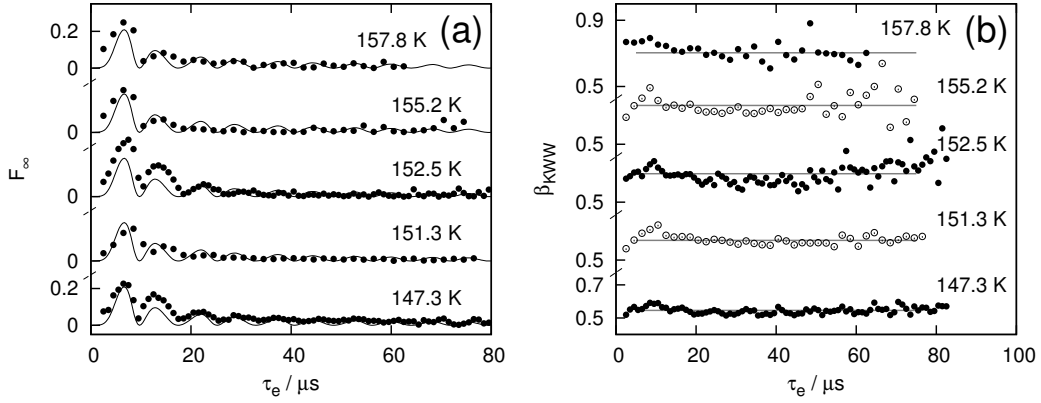


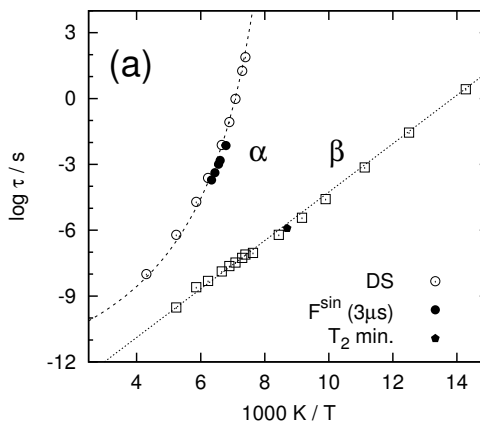
**Figure 6.18 (a):** Residual amplitude  $F_\infty$  obtained from fits via equation 6.6 to the experimental stimulated echo decays. For the sake of clarity the points for individual temperatures are shifted by 0.35 in the y-direction. The lines denote the prediction for an isotropic motion, cf. section 3.4.4. **(b):** Corresponding stretching parameter  $\beta_K$ . Again the y-axis is shifted for each temperature.

whereas the  $t_e$  dependence at 157.8 K is less significant. As demonstrated in chapter 4 the apparent change in  $\tau(t_e)$  is founded in the diverging time scales of  $\tau_c$  and  $\tau_j$  for a motion that progresses via small angular jumps and the fact that the stimulated echo experiment becomes increasingly sensitive on the elementary step with prolonged  $t_e$ . Hence the ratio  $\tau(t_e \rightarrow 0) / \tau(t_e \rightarrow \infty)$  is defined by the Anderson relation, cf. equation 4.5. If this ratio changes with temperature, consequently the dynamics observed within the time window of the experiment has to be temperature dependent – which for a distributed, heterogeneous processes not necessarily dictates an overall change of the process as it traverses the  $^2\text{H}$  NMR time window. For a detailed analysis the single curves have been fitted via a combination of two stretched exponential functions  $\Phi$ :

$$F_{t_e}^{ss}(t_m) = A_0 [(1 - F_\infty) \Phi_{t_e}(t_m) + F_\infty] \Phi_{T_{1Q}}(t_m), \quad (6.6)$$

where  $\Phi_{t_e}(t_m)$  models the decay from  $A_0$  to  $F_\infty$  due to dynamically induced correlation loss and  $\Phi_{T_{1Q}}(t_m)$  the decay via (the a-priori unknown)  $T_{1Q}$  at longer times. To reduce the number of free parameters and hence obtain more consistent results first a free fit to all  $F_{t_e}^{ss}$  curves at one temperature was conducted. Since  $T_{1Q}$  is however independent of  $t_e$ , the average of the obtained  $T_{1Q}$  and corresponding  $\beta_K$  values were subsequently used as fixed parameters for all evolution times in a second fitting procedure. The hereby obtained parameters  $F_\infty$ ,  $\beta_K$  and  $\langle \tau \rangle$  are displayed in figures 6.18 and 6.20 respectively. At the studied temperatures the distribution  $G(\log \tau_\alpha)$  traverses the experimental time window: from the solid echo and 2D line shapes presented in the last sections, which showed no traces of a motion reflecting the lattice symmetry, one would therefore expect to find isotropic dynamics at all temperatures - and indeed the residual amplitude  $F_\infty$  displayed in figure 6.18 is in good agreement with the numerically calculated values for an isotropic process (solid line,  $\delta=130$  kHz). At all investigated temperatures  $F_\infty$  converges towards zero for

**Figure 6.19:** Average correlation times of the  $\alpha$ -process extracted from  $F_{t_e}^{\text{SS}}$  for short evolution times  $t_e$  in comparison with dielectric time constants [Tschirwitz 2002a]. The  $^2\text{H}$  NMR results appear slightly shifted with respect to  $\tau_\alpha$  from dielectric spectroscopy.



evolution times  $t_e \rightarrow 0$  and  $t_e \rightarrow \infty$ , hence any lower symmetry can be clearly ruled out ( $n \rightarrow \infty$ ).

The stretching parameter  $\beta_K$  obtained from the fit via equation 6.6 is displayed in figure 6.18, the mean value for all observed evolution times increases from about 0.55 at lowest temperatures to approx. 0.7 at 157.8 K. The fact that the stretching parameter exhibits little dependence on  $t_e$  at all temperatures could be taken as a hint for the predominance of large angular displacements, but it is known that  $\beta_K(t_e)$  holds also a strong dependence on the width of the distribution  $G(\log \tau_\alpha)$  [Geil 1998], not allowing for any straightforward conclusions to be made. The  $\tau(t_e)$  values however have proven [Geil 1998] to be much less sensitive on any underlying distributions  $G(\log \tau)$  and therefore provide a more non-ambiguous “fingerprint” of the microscopic dynamics. As seen in figure 6.20 (b), the correlation time  $\langle \tau \rangle (t_e \rightarrow 0)$  changes by almost two orders of magnitude within the investigated temperature range of 10 K due to the non-Arrhenius behaviour of  $\tau_\alpha$  and is in good agreement with results from dielectric spectroscopy, cf. figure 6.19. More noteworthy though is the drastic change in  $\langle \tau \rangle (t_e)$  for longer evolution times: whereas  $\langle \tau \rangle (t_e = 2 \mu\text{s})$  and  $\langle \tau \rangle (t_e = 80 \mu\text{s})$  differ by more than an order of magnitude at 147.3 K, the difference at higher temperatures becomes much more subtle. This trend is better seen in the right plot of figure 6.20 where  $\langle \tau \rangle (t_e, T)$  is normalized with respect to  $\tau_\alpha(T) = \tau(t_e \rightarrow 0, T)$  for comparison<sup>14</sup>. In a first approach the experimental values are presented in comparison with simple random walk simulations for several discrete  $\gamma$ -jump motions, cf. chapter 4. This representation readily allows for some conclusions regarding the microscopic dynamics in the investigated temperature regime: at 147.3 K the plateau approached for long evolution times is approximately described by a  $10^\circ$  jump, whereas at 157.8 K a mean jump angle of roughly  $35^\circ$  (and therefore dynamics close to the random-jump type) is needed to model the experimental data. Hence either the mean jump angle increases dramatically within 10 K or the number of molecules undergoing large angular reorientations detectable by the experiment changes as  $G(\log \tau_\alpha)$  traverses the  $^2\text{H}$  NMR time window. This behaviour was also found for structural glass formers (e.g. ortho-terphenyl [Jörg 2000] or m-tricresylphosphate

<sup>14</sup> $\tau_\alpha$  from dielectric spectroscopy was chosen since  $\tau(t_e \rightarrow 0)$  is not accessible in a strictly model free approach from the experimental data.

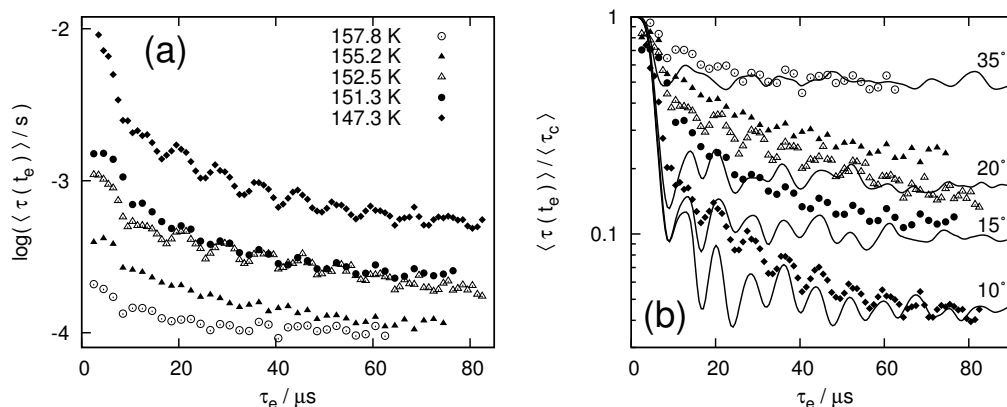


**Figure 6.20 (a):** Experimental  $\langle \tau \rangle$  values from a fit to  $F_{t_e}^{\text{ss}}$  of cyanocyclohexane at different temperatures and evolution times  $t_e$  in absolute representation. **(b):** Same results normalized to the corresponding correlation time  $\langle \tau_c \rangle$  obtained from dielectric spectroscopy [Tschirwitz 2002a].

[Baldus 2005]).

Although the behaviour towards long evolution times is described quite well by a fixed  $\gamma$ -jump type motion, it is evident that the model fails at shorter evolution times  $t_e$ : at all temperatures the experimental values are substantially larger than in the according simulations. This discrepancy is a result of keen simplifications in the model: only a fixed jump angle  $\gamma$  was chosen – this obviously contradicts the 2D exchange spectra presented in section 6.3.7 as a single  $\gamma=35^\circ$  jump e.g. would result in characteristic ellipses arising in the exchange intensity. If a distribution of jump geometries is introduced which substantially extends towards smaller angles – as previously employed for structural glass formers – the experimentally found behaviour is reproduced in more detail. A more in-depth analysis in this manner, that furthermore accounts for the limited time window of the experiment, is conducted in section 6.4.4.

### 6.3.9 Preliminary conclusions

Before we will refine the discussion of the presented results in the next section by applying random walk simulations and via a more quantitative approach incorporating  $G(\log \tau)$  obtained by dielectric spectroscopy, we briefly summarize the obtained findings at this point.

Regarding the  $\alpha$ -process we support the conclusions drawn from dielectric spectroscopy by Tschirwitz et al. [Tschirwitz 2002a] in the sense that also in  $^2\text{H}$  NMR the  $\alpha$ -process appears even in detail identical to the processes found in supercooled liquids and structural glasses: no signs of the translational symmetry of the plastic crystalline lattice were observed. The two dimensional experiments in time and frequency domain yield results closely related to those found in toluene e.g., hence the elementary jump processes are comparable. The same arguments hold for mea-

surements regarding the  $\beta$ -process: its manifestation in the  $^2\text{H}$  NMR observables of cyanocyclohexane exhibits all features known from structural glass formers – with the only difference being the favourable separation in time scales of  $\tau_\alpha/\tau_\beta$ , which gives rise to the appearance of new features like the (second) minimum found in  $T_1$ . The scope of next section will be a more detailed analysis of those features.

## 6.4 Experimental results – refinement

The presented peculiarities in the  $^2\text{H}$  NMR observables, arising from the well separated nature of  $\alpha$ - and  $\beta$ -process in cyanocyclohexane, are hopeful candidates with regard to further insight into the microscopic manifestation of the dynamics. This however brings the necessity of more elaborate data analysis.

The following part will address the most prominent findings in detail: first the spin-lattice relaxation and in particular the arise of two distinct minima in  $T_1$  will be discussed in a non-model free approach, thereafter the peculiar solid echo line shape above  $T_g$  and the apparent temperature dependence of the microscopic mechanism for the  $\alpha$ -process observed in the stimulated echo will be further analysed.

### 6.4.1 Modelling spin-lattice relaxation

In section 6.3.2 we attributed the minima in  $T_1$  to  $\alpha$ - and  $\beta$ -process via their respective temperature in comparison with correlation times from dielectric spectroscopy. To further exploit the prominent features in  $T_1$  with regard to the fast and non-merging  $\beta$ -process we will divert from this general, model-free approach by employing the spectral density as obtained from dielectric spectroscopy. This approach benefits from the fact that the spectral density – although only at a fixed frequency,  $\omega_L$  – is probed by NMR with great accuracy.

The ansatz is as follows: as long as the time scales of the two processes are well separated, the imaginary part of the normalized complex susceptibility  $\chi''(\omega)$  can be described within a Williams-Watts [Williams 1971] approach. We employed the sum of a Cole-Davidson function for the  $\alpha$ -process and a log-Gaussian distribution for the  $\beta$ -process, as used by Tschirwitz et al. [Tschirwitz 2002a] in the analysis of the dielectric spectra:

$$\chi''(\omega) = S\Im \left\{ \frac{1}{(1 + i\omega\tau_\alpha^{\text{CD}})^{\beta_{\text{CD}}}} \right\} + (1 - S) \frac{\sqrt{\pi}}{2W \ln 10} \exp \left[ -\frac{(\log \omega/2\pi - \log 1/2\pi\tau_\beta)^2}{W^2} \right], \quad (6.7)$$

the susceptibility  $\chi''(\omega)$  can subsequently be expressed in terms of spectral density via the fluctuation dissipation theorem [Böttcher 1978a],

$$\chi''(\omega) = \omega J^{(1)}(\omega). \quad (6.8)$$

Assuming for the moment that the individual contributions of  $\alpha$ - and  $\beta$ -process to the spectral density of the system are in first approximation independent of the rank

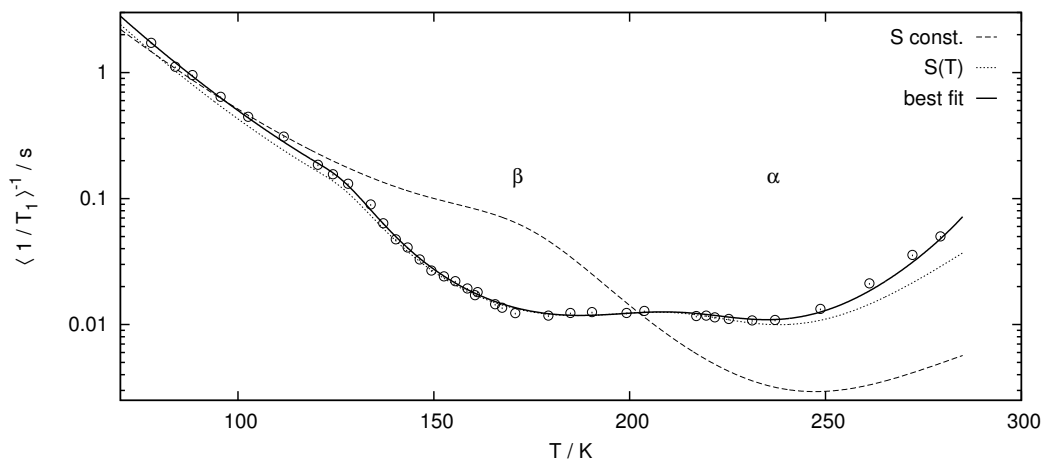


**Figure 6.21:** Experimental and calculated spin-lattice relaxation times. In contrast to  $\langle T_1 \rangle$  in figure 6.7 here the inverse of the average rate,  $\langle 1/T_1 \rangle$ , is plotted. The dotted line was calculated using parameters from dielectric spectroscopy and modelling  $1-S$ . The solid line results from the same calculations with a slight shift of  $\tau_{\alpha/\beta}$  towards shorter times, cf. figure 6.22 (b).

$l$ , hence  $J_{\alpha}^{(1)}(\omega, T) \approx J_{\alpha}^{(2)}(\omega, T)$  and  $J_{\beta}^{(1)}(\omega, T) \approx J_{\beta}^{(2)}(\omega, T)$  respectively hold<sup>15</sup>, we are now able to calculate the spectral density employing the time constants  $\tau_{\alpha}$ ,  $\tau_{\beta}$  and shape parameters  $W$ ,  $\beta_{CD}$  from dielectric spectroscopy<sup>16</sup>. The presumably  $l$ -dependent relaxation strength  $1 - S$  will serve as fit parameter and hence provides insight in the microscopic geometry of the process under consideration. Via equation 3.29 it is now possible to calculate  $T_1$  for a number of selected models concerning  $1-S$ .

Since the magnetization curves (and therefore  $\langle T_1 \rangle$ ) are affected by spin diffusion at low temperatures, the results of eq. 3.29 can only be compared to the the average spin-lattice relaxation rates  $\langle 1/T_1 \rangle$  (for details see chapter 3).  $\langle 1/T_1 \rangle$  is obtained from the initial slope of the magnetization curves<sup>17</sup> and is displayed in figure 6.21, as opposed to figure 6.7 where  $\langle T_1 \rangle$  was given. Furthermore we have to remind that  $T_1$  of a single spin depends on the orientation of the electric field gradient tensor relative to the external magnetic field and hence in the case of a restricted motion in solids (e.g. a two-site jump process or a rotation of the molecule like in the case of benzene) the general treatment for  $l=2$  does not strictly hold, instead  $\langle 1/T_1 \rangle$  has to be calculated from the powder average within the specific motional model considered. Following the general approach of Torchia and Szabo [Torchia 1982] it can be shown however that in the case of free diffusion on or within a cone of opening angle  $\chi$ ,

<sup>15</sup>Regarding the  $\alpha$ -process this approximation has proven to be valid in the case of glycerol [Blochowicz 1999a].

<sup>16</sup>The parameters  $\tau_{\alpha}, \tau_{\beta}$  and  $W$  were obtained directly from equations 2.1, 2.3 and 2.7 with the parameters given in section 6.1.2,  $\beta_{CD}$  was interpolated from dielectric results as shown in figure 6.4. The coupling constant obtained at low temperatures  $\delta_0=129.6$  kHz and the Larmor frequency  $\omega_L=46.07$  MHz were used in all calculations

<sup>17</sup>It is noteworthy to mention that by fitting the experimental curves in this manner the discontinuity in  $\langle T_1 \rangle$  around 170 K, caused by a peculiar behaviour of the stretching parameter  $\beta_K$  is eliminated.

the general treatment for  $l=2$  remains valid [Lipari 1982, Woessner 1962]. As these models are generally applied to the  $\beta$ -process throughout this work and are also proven to be applicable for cyanocyclohexane in the discussion of the solid echo line shape in the next section, we will – for the sake of simplicity – restrict ourselves to these scenarios for the present discussion of spin-lattice relaxation.

First  $\langle 1/T_1 \rangle$  was calculated for a temperature independent relaxation strength of the  $\beta$ -process ( $1-S$ ), chosen in a way to mimic the experimental rates observed below  $T_g$ . The result is given as dashed line in figure 6.21: whereas the qualitative progression below  $T_g$  and the position of the high temperature minimum for the  $\alpha$ -process are roughly captured within this approach, the absolute values above  $T_g$  differ by almost an order of magnitude and the low temperature behaviour exhibits a somewhat lower slope than found experimentally. The present calculation clearly demonstrates that a distinct minimum for the  $\beta$ -process in  $\langle 1/T_1 \rangle^{-1}$  can only be observed if the relaxation strength in the concerned temperature region is significantly enhanced with respect to the values typically found in the glassy regime below  $T_g$  – i.e. the results are in accordance with the experimental findings in ethanol, where no second minimum is observed.

Consequently  $1-S$  was modelled according to the behaviour observed in dielectric spectroscopy: subtle, linear temperature dependence below  $T_g$  where  $1-S$  exhibits a sharp bend which was modelled by a phenomenological function (comprised of a linear, an exponential and a quadratic term). The dotted line in figure 6.21 is calculated in this manner. Due to the enhanced relaxation strength of the  $\beta$ -process above  $T_g$ , modelled by the temperature dependence of  $1-S$  in this approach, a second minimum in  $\langle 1/T_1 \rangle^{-1}$  arises. The model provides excellent agreement with experimental data in the temperature region below about 160 K and exhibits the two desired minima for  $T_g < T < T_m$  with the same rates as found in the experiment, fails however to accurately reproduce the position of those minima. Regarding the subtle mismatch observed between correlation times of the  $\alpha$ -process determined via  $F_{te}^{ss}$  and dielectric spectroscopy, cf. figure 6.19, the parameters in equations 2.1 and 2.3 were slightly altered to obtain best agreement with respect to the experimental  $T_1$  values – the resulting model is represented by the solid line in figure 6.21, which reproduces  $\langle 1/T_1 \rangle^{-1}$  within the experimental error in the whole accessible temperature range  $T < T_m$ . The hereby employed correlation times are plotted in figure 6.22:  $\tau_\alpha$  is in good agreement with correlation times obtained in the stimulated echo experiment, i.e. exhibits the same amount of deviation from the dielectric results, whereas  $\tau_\beta$  only significantly deviates from the dielectric data at high temperatures. As the introduced changes in  $\tau_{\alpha/\beta}$  are of reasonable small magnitude, they will be accepted at this point.

Hence the sole free fitting parameter within this approach is  $1-S$ , plotted in figure 6.22 (a): the qualitative behaviour is very similar to the results obtained in dielectric spectroscopy. Quantitatively the obtained relaxation strengths differ however by more than a factor of three, i.e.  $1-S^{(2)} = 3 \cdot (1 - S^{(1)})$ , as expected for a highly restricted process progressing via small angular displacements, is not fulfilled (as demonstrated via the dotted line in figure 6.22 (a)). This discrepancy will be discussed at the end of this chapter, when further results from the line-shape analysis are at hand.

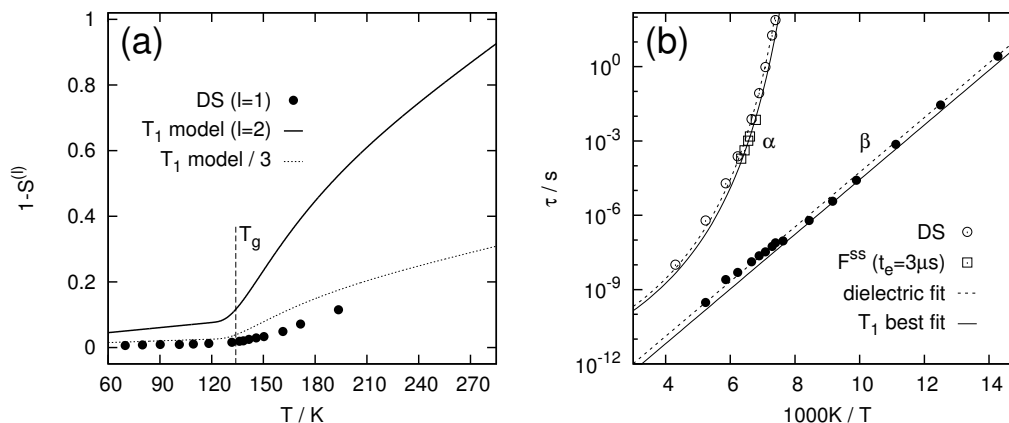


**Figure 6.22 (a):** Relaxation strength  $1 - S$  of the  $\beta$ -process used for calculating  $\langle 1/T_1 \rangle$  in figure 6.21 (solid line) in comparison with dielectric results. **(b):** Time constants of  $\alpha$ - and  $\beta$ -process used in the calculation of  $\langle 1/T_1 \rangle$ .

From our present efforts we can conclude that the spectral density  $J_{\alpha/\beta}^{(1)}(\omega, T)$  from dielectric spectroscopy is (with minor alterations) sufficient to fully describe the experimentally observed spin-lattice relaxation times at all temperatures, therefore accordance between techniques probing  $l=1$  and  $l=2$  was found. Furthermore the assumptions made by employing the Williams-Watts ansatz in the spectral density appear valid even at high temperatures. The evolution of the relaxation strength with temperature obtained from our model is compatible with the one found in dielectric spectroscopy, i.e. the – at first – peculiar fact that the  $\langle 1/T_1 \rangle$  minima of  $\alpha$ - and  $\beta$ -process exhibit comparable heights is deduced in a straightforward manner. Furthermore no plateau is observed in  $1-S$  even at higher temperatures. To model the experimental  $\langle 1/T_1 \rangle$  data a steady growth of the relaxation strength of the  $\beta$ -process is needed: at the temperature of the  $T_1$  minimum for the  $\alpha$ -process  $1-S^{(2)}$  is already about 0.7.

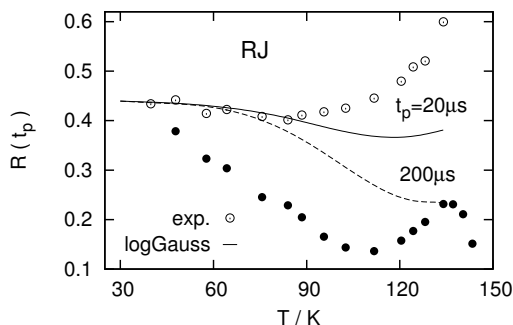
In summary we have shown that the strong effects observed in the  $^2H$  NMR spin-lattice relaxation times of cyanocyclohexane can be explained by the growing relaxation strength of the  $\beta$ -process above  $T_g$ , which is qualitatively in accordance with other techniques.

### 6.4.2 Modelling solid echo spectra

In the last section we have demonstrated that the simple model of a motion on or within a cone is versatile enough to reproduce the strong effects observed in  $T_1$  of cyanocyclohexane due to the fast  $\beta$ -process in the system. As previously pointed out, the peculiar solid echo line shape of cyanocyclohexane associated with the  $\beta$ -process in the temperature region  $T_g < T < 165$  K (cf. figure 6.9) is also very promising with regards to further insights on the mechanism of reorientation. Consequently the afore mentioned models will now be tested for compliance with the line shape effects observed in this regime.

Prior to this we will however briefly return to lower temperatures ( $T < T_g$ ) to validate

**Figure 6.23:** Random walk simulations for the  $\beta$ -process employing  $G(\log \tau_\beta)$  from dielectric spectroscopy. A random jump motion within a cone of  $\chi=11^\circ$  is assumed. The experimental behaviour at low temperatures is significantly different from the results within this simple model.



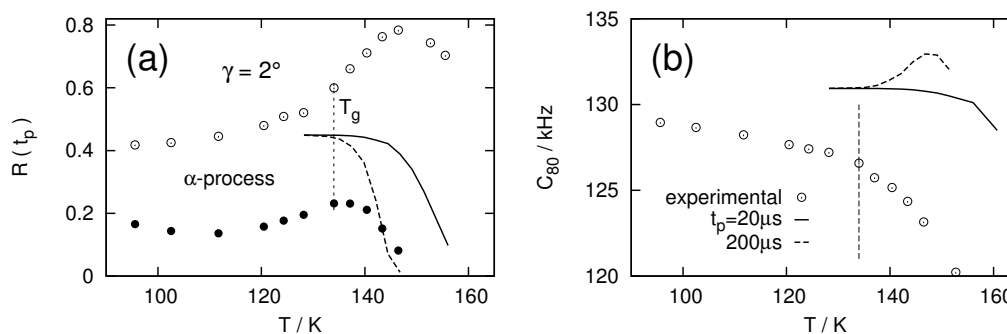
a number of assumptions for the present approach and furthermore estimate the effects of the  $\alpha$ -process on the solid echo line shape above  $T_g$  to define the applicable temperature range.

Figure 6.23 displays the line shape parameter  $R(t_p)$  obtained from random walk simulations in comparison with the experimental results discussed in section 6.3.4. For the calculations – again in a phenomenological, purely heterogeneous approach – the distribution of correlation times  $G(\log \tau_\beta)$  from dielectric spectroscopy<sup>18</sup> was used to obtain  $R(t_p)$  within the simplest scenario: a random jump motion within a cone of fixed (temperature independent) opening angle  $\chi=11^\circ$  (this roughly corresponds to the angle of  $7^\circ$  found in toluene within the “motion on a cone” model [Vogel 2000a]). The simulations exhibit a minimum in  $R(t_p=20\ \mu\text{s})$  around  $\tau_\beta=1/\delta$  not observed in the experiment due to the raise of  $R(t_p)$  around  $T_g$ . More dominant however is the discrepancy at lowest temperatures:  $R(t_p=20\ \mu\text{s})$  and  $R(t_p=200\ \mu\text{s})$  gradually diverge only around 80 K, whereas the experimental spectra exhibit line shape effects down to lowest temperatures,  $T=34\ \text{K}$ . As demonstrated in chapter 4, the  $R(t_p)$  effects at longest inter pulse delays are extended towards longer times  $\tau_c$  if the motion proceeds via small angles (albeit maintaining the “fast” side of the minimum, which is already approximately captured by the approach). Hence, as in the case of toluene [Vogel 2000a], a mechanism is observed that agitates via small angular displacements – this is however rather unfavourable for random walk simulations at temperatures above  $T_g$ , as due to the separation of time scales  $\tau_j \ll \tau_c$  very short jump times  $\tau_j$  have to be considered, resulting in large computational effort<sup>19</sup>. As the better part of  $G(\log \tau_\beta)$  is in the fast motion limit regime above  $T_g$  anyway, we will therefore divert from a random walk analysis and model the fast motion limit line shape in a simplified approach, as the elementary step of the motion does not affect the results in this limit.

As mentioned before, the influence of the  $\alpha$ -process at temperatures above  $T_g$  on the solid echo line shape will briefly be considered, before we proceed to develop and apply a suitable model for the  $\beta$ -process in this regime. Therefore  $G(\log \tau_\alpha)$

<sup>18</sup>Both distributions used in [Tschirwitz 2002a] were employed: a log-Gaussian and  $G_\beta$ . For the present case however no significant differences in the results are observed.

<sup>19</sup>At 160 K for example  $\tau_\beta$  is 2 ns, which according to equation 4.5 corresponds to a jump time of  $\tau_j \approx 4\ \text{ps}$  for a  $2^\circ$  jump. One C-<sup>2</sup>H bond would hence reorient, on average,  $10^8$  times during the pulse sequence for a solid echo spectrum of  $t_p=200\ \mu\text{s}$ . Typically  $10^5 - 10^6$  single trajectories have to be calculated to obtain a spectrum.



**Figure 6.24 (a):** Line shape parameter  $R(t_p)$  from random walk simulations (lines) of the  $\alpha$ -process employing  $G(\log \tau_\alpha)$  from dielectric spectroscopy. An isotropic motion proceeding via  $\gamma=2^\circ$  jumps is assumed. **(b):** Corresponding apparent spectral width  $C_{80}$ .

from dielectric spectroscopy was employed in random walk simulations of the solid echo line shape for an isotropic motion proceeding via small angles ( $\gamma=2^\circ$ , which roughly corresponds to the smallest jump angles extracted from the stimulated echo experiments in section 6.3.8).

The calculations do not aim to provide a realistic model, rather a conservative estimate is obtained as for more complex models, i.e. with fractions of larger angles  $\gamma$  or exchange within  $G(\log \tau_\alpha)$ , the line shape changes will be shifted towards higher temperatures. The results are displayed in figure 6.24 and allow to draw two important conclusions: any influence of the  $\alpha$ -process on the apparent spectral width ( $C_{80}$ , figure (b)) below about 155 K can be neglected. Even at 160 K the observed changes are rather subtle in case of  $t_p=20 \mu\text{s}$  and completely fail to reproduce the experimental results. The  $R(t_p)$  values are however strongly influenced within the model at temperatures slightly above  $T_g$  already, which explains the experimentally found reduction in this regime (as the  $\beta$ -process is already too fast to significantly influence the slow motion limit line shape here). Hence the large fractions of small reorientation angles observed in the stimulated echo experiments for the  $\alpha$ -process are in agreement with the  $R(t_p)$  changes of the solid echo line shape in the same temperature regime. The fast motion limit effects (i.e. changes in  $C_x$  for  $t_p=20 \mu\text{s}$ ) observed in the solid echo line shape at  $T \leq 165$  K on the other hand can be adequately modelled in a scenario which only accounts for the  $\beta$ -process.

Following the introductory remarks we will now focus on the region  $T_g < T < 165$  K and describe the line shape changes observed here within a model for the  $\beta$ -process. In consideration of our previous results, it is obvious that any applicable model has to incorporate an adjustable degree of restriction, i.e. the ability to account for the strong temperature dependence of  $1-S$  above  $T_g$ . Hence again the models discussed in chapter 4, i.e. a motion on or within a cone of (temperature dependent) semi angle  $\chi$  – which both haven proven to work well in case of the  $T_1$  analysis in the last section – are chosen for the present approach. In the anticipated model only the fast motion limit effects will be considered (since in the temperature range under discussion the better part of the distribution  $G(\log \tau_\beta)$  exhibits correlation times in the limit  $\tau_\beta \ll 1/\delta$ ), this however renders the situation quite favourable

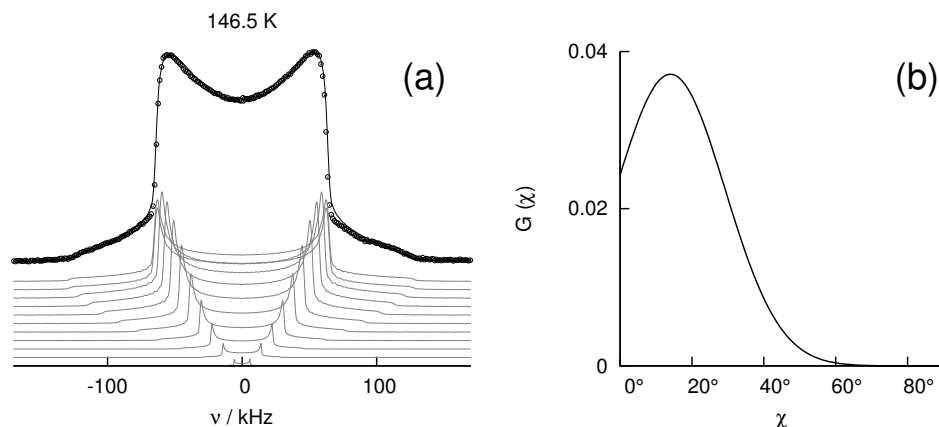


**Figure 6.25 (a):** Solid echo spectrum at 146.5 K (open symbols), simulation (solid line) according to equation 6.9 and comprising sub-spectra of different  $\bar{\delta}(\chi)$  (grey lines). A step size of  $5^\circ$  was chosen in  $\chi$  for the displayed sub-spectra, the simulated spectrum consists of sub-spectra with a step-size of  $1^\circ$  however. **(b):** Corresponding distribution of cone opening angles  $G(\chi)$  in the “motion on a cone” model.

as the details of the dynamic process, i.e. the elementary step of the motion, has no influence on the line shape any more. The proposed models differ therefore only by the distribution of angles  $\theta$  that are accessible after infinite jumps, hence it is impossible to differentiate between uniaxial rotational diffusion and a random jump motion on a cone for example. Consequently only two cases have to be considered, which both yield a Pake spectrum with reduced apparent coupling  $\bar{\delta}$  in this limit: the “motion on a cone” model, i.e. the fast motion around a  $C_n$  axis with  $n > 2$ , where  $\bar{\delta}$  is given by equation 4.10 and the more general case of a bond freely moving on the unit sphere within a cone (where  $\bar{\delta}$  is obtained from equation 4.11).

Regarding the peculiar line shape of cyanocyclohexane in the discussed temperature region (cf. figure 6.12 (b) or 6.25 e.g.) it is obvious that none of the models is sufficient to describe the experimentally observed spectra via a fixed opening angle  $\chi$ , as the spectra of cyanocyclohexane – apart from the overall narrowing – exhibit a significant broadening of the singularities which can only be reproduced via a distribution of cone angles  $G(\chi)$ . Since glassy dynamics is of heterogeneous nature, it seems straightforward not only to take into account a distribution of correlation times  $G(\log \tau_\beta)$ , but also to assume such a distribution of restricting geometries<sup>20</sup>, as found in the analysis of toluene below  $T_g$  [Vogel 2000a]. For the thermally activated  $\beta$ -process the log-Gaussian distribution  $G(\log \tau_\beta)$  is assumed to be connected to a Gaussian distribution of energy barriers  $g(E)$ . Indeed a Gaussian distribution of opening angles  $\chi$  proves to be versatile enough to reproduce the spectral intensity in cyanocyclohexane above  $T_g$ : the calculated spectrum represented by the solid line in figure 6.25 is obtained via a weighted sum of Pake spectra with different apparent

<sup>20</sup>Both assumptions are only justified as long as  $\tau_\beta \ll \tau_\alpha$ , i.e. the isotropic motion of the  $\alpha$ -process does not lead to exchange between the different sub ensembles of  $G(\log \tau_\beta)$  and  $G(\chi)$  within the experimental time window.

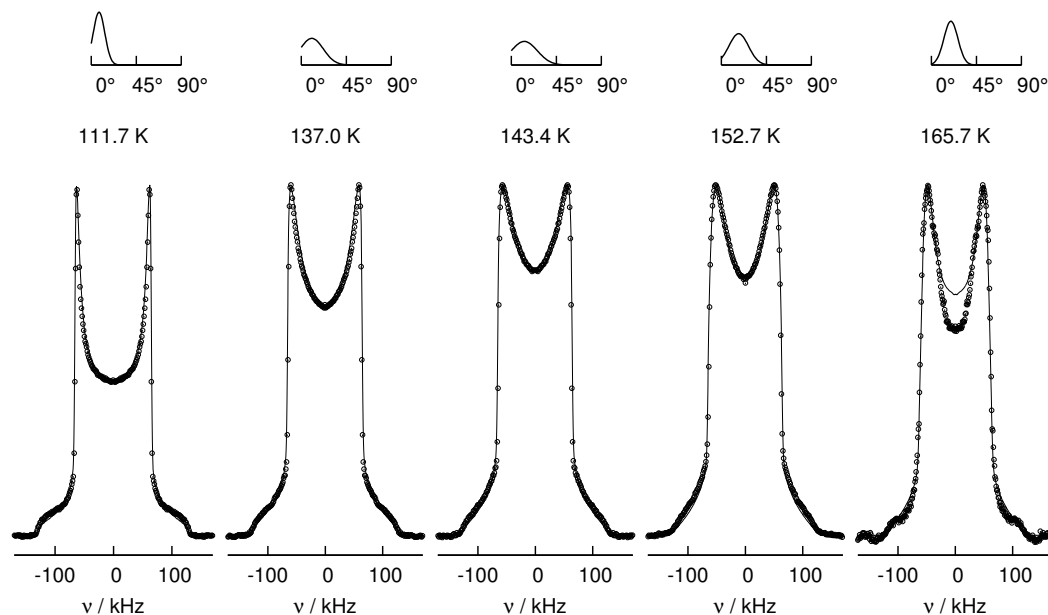


**Figure 6.26:** Solid echo spectra for short evolution times  $t_p=20\ \mu\text{s}$  (open symbols) at different temperatures with according simulations (solid line) within the “motion on a cone” model. All spectra have been symmetrized for reasons of clarity. Above each individual spectrum the corresponding distribution  $G(\chi)$  is plotted.

coupling constants  $\bar{\delta}(\chi)$ :

$$S'(\omega; T) = W(T) \sum_{\chi=0^\circ}^{90^\circ} G(\chi, T) S(\omega; \bar{\delta}(\chi)) + [1 - W(T)] S(\omega; \delta_0). \quad (6.9)$$

with a Gaussian distribution of opening angles  $G(\chi)$  and the weighting factor (determined from the log-Gaussian distribution of correlation times  $G(\log \tau_\beta)$  observed in dielectric spectroscopy [Tschirwitz 2002a]):

$$W(T) = \int_{\log 1/\delta}^{\infty} G(\log \tau_\beta, T) d \log \tau_\beta = 1 - \frac{1}{2} \operatorname{erfc} \left( -\frac{\log \delta - \log \frac{1}{\tau_\beta(T)}}{2W(T)} \right). \quad (6.10)$$

which maps the fraction  $\tau_\beta > 1/\delta$  to a rigid limit Pake spectrum  $S(\omega; \delta_0)$ <sup>21</sup>. Hence only molecules in the fast motion limit are considered as any other approach would imply so far unjustified correlations between time scale and geometry of the  $\beta$ -process. The “motion on a cone” model was used for the example given in figure 6.25, yet a single Gaussian distribution of opening angles  $\chi$  has proven to be flexible enough to reproduce the main features of the spectra within both models – by means of slightly different underlying distributions  $G(\chi)$  however. Hence it is not possible to exclude either geometry from further considerations at this point.

<sup>21</sup> $S(\omega; \delta_0)$  is represented by the (rigid limit) solid echo spectrum recorded at  $T=34\ \text{K}$ .

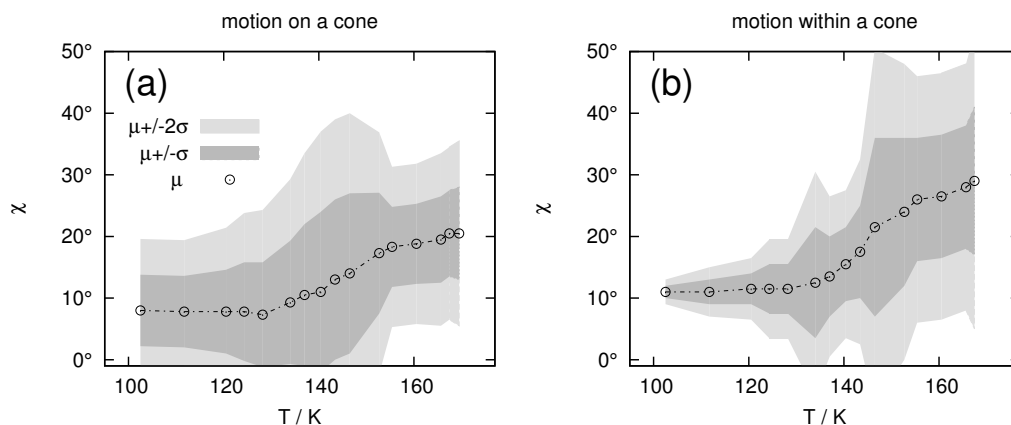


**Figure 6.27 (a):** Parameters for the Gaussian distribution of opening angles  $G(\chi)$  to model the fast motion limit effects on the experimental solid echo spectra for  $t_p=20\ \mu\text{s}$  within the motion on a cone model. **(b):** Fit parameters for the motion within a cone model.

Figure 6.26 demonstrates the quality of fit achieved at different temperatures<sup>22</sup>. The main fit criterion was in all cases a good reproduction of the line shape around the inner and outer singularities as the intensity around zero frequency may already be affected by the  $\alpha$ -process at highest temperatures, as demonstrated by the random walk simulations in figure 6.24. The resulting mean cone opening angle  $\chi_\mu$  and its corresponding standard deviation  $\sigma$  obtained for each individual spectrum ( $t_p=20\ \mu\text{s}$ ) at temperatures  $100\ \text{K} < T < 170\ \text{K}$  are displayed in figure 6.27.  $\chi_\mu$  provides a measure analogous to the relaxation strength  $1-S$  and displays qualitatively similar behaviour as found in dielectric spectroscopy and by means of the  $\langle 1/T_1 \rangle$  model: weak temperature dependence below  $T_g$  followed by a kink and a steep rise at  $T_g$ . In case of the “motion on a cone” model, the width of the distribution  $\sigma$  is almost constant over the whole temperature interval, except for a maximum around 130 K to 150 K. In the “motion in a cone” approach  $\sigma$  generally exhibits more scatter. For both models the angles extracted below  $T_g$  (about  $11^\circ$  for “motion in a cone” and roughly  $8^\circ$  for the “motion on a cone” model) are comparable to the numbers found by studying the slow motion limit effects below  $T_g$  in structural glass formers, where a mean angle  $7^\circ$  was reported for toluene [Vogel 2000a]. It seems therefore justified to further apply any of the models to the  $\beta$ -process below  $T_g$ . To discuss the applicability at higher temperatures, where so far no detailed  $^2\text{H}$  NMR line shape or 2D NMR studies regarding the  $\beta$ -process have been reported, the outcome of the models have to be quantitatively compared to previous results from other techniques – namely the relaxation strength  $1-S$  extracted from dielectric spectroscopy and from the  $T_1$  model in the previous paragraph.

Again, as the current approach only accounts for dynamics in the fast motion limit, the average distribution of reorientation angles with respect to the initial orientation  $g(\beta)$  (i.e. the area on the unit sphere accessible to the process, cf. section 3.4.4)

<sup>22</sup>Again the “motion on a cone” model was employed, the agreement achieved within the “motion in a cone” model is comparable.

is sufficient to calculate the generalized order parameter  $\mathcal{S}$  [Lipari 1982] and hence  $1 - S = 1 - \mathcal{S}^2$  of rank  $l$  [Blochowicz 1999a]<sup>23</sup>:

$$1 - \mathcal{S}^{(l)}(T) = 1 - \sum_{\chi=0^\circ}^{90^\circ} \int_0^{\pi/2} G(\chi; T) g(\beta; \chi) P_l(\cos \beta) d\beta \quad (6.11)$$

where  $P_l$  denotes the Legendre polynomial of rank  $l$  and the discrete sum over  $\chi$  is calculated in the same manner as for the spectra in equation 6.9, i.e. with a step size of  $1^\circ$ . One has to remind that the quantity  $S = \mathcal{S}^2$  denotes an ensemble average here, which is however consistent with our previous notation of the symbol (i.e. in case of dielectric spectroscopy and the  $T_1$  model), hence we will drop the brackets also in the present case. For the “motion in a cone” model the distribution  $G(\beta; \chi)$  at infinite times is given by the normalized weight of the surface element [Benkhof 1999]:

$$g(\beta; \chi) = \begin{cases} \frac{1}{1-\cos \chi} \sin \beta & \beta \leq \chi \\ 0 & \beta > \chi. \end{cases} \quad (6.12)$$

Insertion in equation 6.11 yields:

$$\begin{aligned} 1 - \mathcal{S}^{(1)} &= \sum_{\chi=0^\circ}^{90^\circ} \frac{1}{2} G(\chi; T) (1 - \cos \chi) \\ 1 - \mathcal{S}^{(2)} &= 1 - \sum_{\chi=0^\circ}^{90^\circ} G(\chi; T) \cos^2 \frac{\chi}{2} \cos \chi \end{aligned} \quad (6.13)$$

from which  $1 - \mathcal{S}$  and hence  $1 - S$  can be calculated analogously to the spectrum  $S'(\omega; T)$  itself, i.e. via a discrete sum over  $\chi$ . For the case of a motion on the circumference of a cone, the calculation is analogous with the reorientation angle distribution  $g(\beta; \chi)$  being equal to the case of uni-axial rotational diffusion – the extensive treatment of which is found in e.g. ref. [Schmidt-Rohr 1994].

The resulting relaxation strengths  $1 - \mathcal{S}^{(l)}$  for  $l = 1, 2$  within both models are plotted in figure 6.28. For both geometries  $\mathcal{S}^{(2)}$  reproduces the values found by means of the spin-lattice relaxation model ( $l=2$ ) rather well in the applicable temperature range, except for some deviations around 140 K in both cases. Hence we can conclude already at this point that the (afore preliminary) assignment of the peculiar solid echo line shape above  $T_g$  to the  $\beta$ -process is valid and that both employed models appear applicable, i.e. the presented  $^2\text{H}$  NMR analysis is self-consistent. With regard to the results of dielectric spectroscopy however a clear deviation is observed: as anticipated from the  $T_1$  analysis, the relaxation strength of the  $\beta$ -process appears enhanced in  $^2\text{H}$  NMR with respect to  $1 - S^{(1)} = \Delta\epsilon_\beta / \Delta\epsilon$ . This peculiarity will be addressed in the next subsection in comparison with results of structural glass formers at  $T < T_g$ .

For a final remark we will briefly discuss the arising deviations in  $1 - \mathcal{S}^{(2)}$  for both models: below  $T_g$   $1 - \mathcal{S}^{(1)}$  extracted from the “motion on a cone” model is considerably

<sup>23</sup>The name order parameter for  $\mathcal{S}$  does conventionally only apply to rank  $l=2$ .

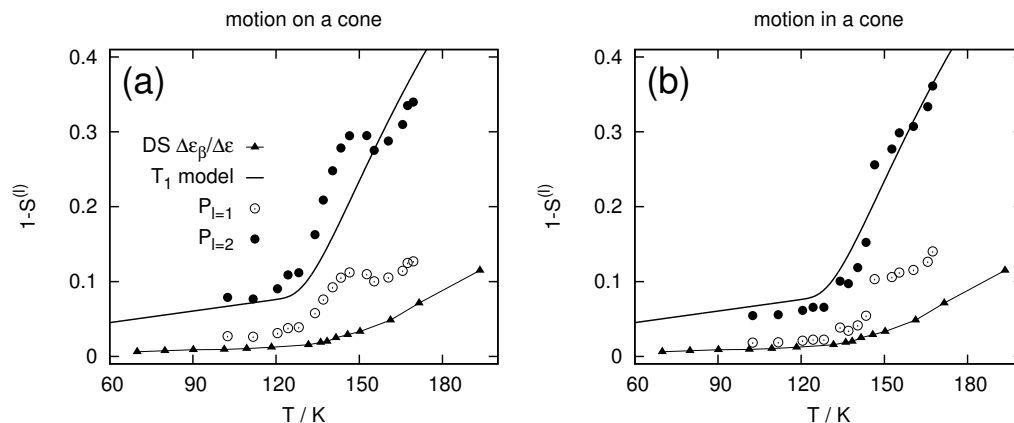


**Figure 6.28 (a):** Relaxation strengths  $1-S^{(l)}$  from the “motion on a cone” model and  $l = 1, 2$  in comparison with data from dielectric spectroscopy and results of the  $T_1$  model in section 6.4.1. **(b):** Same representation for the “motion in a cone” model.

larger than the values found by means of the  $T_1$  model, whereas the “motion within a cone” model yields values slightly lower than those found by other means. One possible explanation for this effect is a correlation between time scale and geometry of the  $\beta$ -process: in the present calculation of  $1-S$  the restricting geometry found for the fast motion limit part of  $G(\log \tau_\beta)$  is assumed to hold also for the slower molecules (not contributing to the fast motion limit effects), which must generally not be the case (cf. section A.4 for details). With growing temperature this effect becomes however negligible as  $W(T)$  approaches unity around 160 K. Furthermore the fast motion limit line shape effects are very subtle below  $T_g$ , and hence the assignment of  $G(\chi; T)$  becomes rather vague. For the given reasons we will not further discuss the present deviations at low temperatures, we will return to this regime however in the course of the next subsection.

The “hump” arising in  $S^{(2)}$  at intermediate temperatures around 140-150 K, which is found in both geometries, is connected to the behaviour of the width  $\sigma$  of the opening angle distribution  $G(\chi)$ . This effect is best seen in the “motion on a cone” model, where the peculiarity is more pronounced: at lowest and highest temperatures  $\sigma$  is more or less constant and of comparable magnitude. Slightly below  $T_g$ , where the amplitude of the  $\beta$ -process starts to grow, the distribution broadens but gradually retracts again to the low temperature value of  $\sigma \approx 7^\circ$  around 160 K. At this temperature the weighting factor  $W(T)$  approaches unity, hence all molecules are in the fast motion limit with regard to the solid state spectrum. As mentioned before, the criterion for good agreement within this approach is a reproduction of the line shape around the inner and outer singularities - recalling figure 6.26 it is obvious however that the center of the spectra are modelled equally well. To account for the intensity around zero frequency  $G(\chi)$  has to extend to substantially larger opening angles<sup>24</sup>. As the agreement in the outer parts is not significantly altered by a larger  $\sigma$ , the whole line shape is captured within the fit. Since the spectral intensity at zero

<sup>24</sup>Where  $\bar{\delta} \rightarrow 0$ .

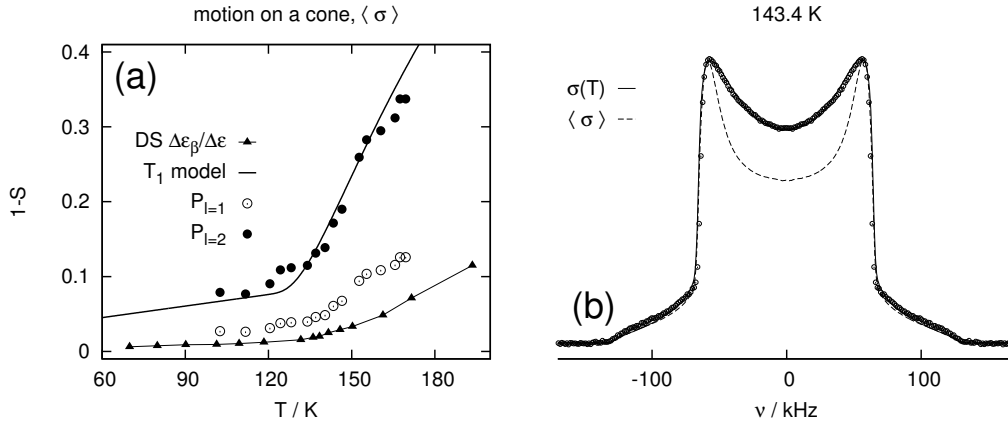


**Figure 6.29 (a):** Relaxation strength  $S^{(l)}$  for the "motion on a cone" model. In contrast to figure 6.28 a mean width  $\langle \sigma \rangle$  was used in the distribution  $G(\chi)$  at temperatures above  $T_g$ . **(b):** Comparison of the calculated spectra for the original fit (i.e.  $\sigma(T)$ , solid line) and employing  $\langle \sigma \rangle$  (dashed line) at a temperature where the deviation in  $\sigma$  is largest.

frequency in this temperature regime is both governed by the  $\alpha$ -process (cf. figure 6.24) and the  $\beta$ -process in the fast motion limit, the fitting procedure can not be altered without making undue assumptions. Yet assuming that  $\sigma$  is more or less temperature independent, a mean value  $\langle \sigma \rangle$  can be extracted from the spectra at  $T > 160$  K where  $W(T) \approx 1$  and subsequently be used for all temperatures above  $T_g$ . The right-hand part of figure 6.29 shows a comparison between the original fit and a calculated spectrum employing the mean width  $\langle \sigma \rangle$ : as previously speculated the agreement in the outer parts of the spectrum is mostly unaltered and still within the experimental error. The relaxation strength obtained after applying this correction provides good agreement over the whole temperature range. This leaves us however with the problem that the experimentally observed raise of  $R(t_p)$  above  $T_g$  is no longer fully captured within the approach. Whether or not better agreement – in terms of line shape and corresponding  $1-S$  – could be achieved by employing a non-Gaussian distribution  $G(\chi)$  has to be reviewed.

In figure 6.9 it was seen that around 167 K a central feature arises in the spectra of cyanocyclohexane, which somewhat resembles the "two phase" spectra observed in binary glass formers. This line shape can also be described in the present approach for  $\chi \rightarrow 90^\circ$ , i.e. vanishing restriction. This however yields values of  $1-S$  around 0.8 at 169 K, whereas  $1-S=0.38$  was found in the  $T_1$  model. Hence this prominent feature has to be mainly attributed to the  $\alpha$ -process – a significant contribution of the  $\beta$ -process can however not be waived.

#### Extension to temperatures $T < T_g$

So far the applied model has proven to work well at temperatures  $T_g \leq T < 165$  K and provided consistent results with our  $T_1$  analysis. As mentioned before, the fast motion limit effects on the solid echo line shape below  $T_g$  become yet so subtle, that a stable fit via  $G(\chi)$  is no longer possible. Therefore we will test the predictions of

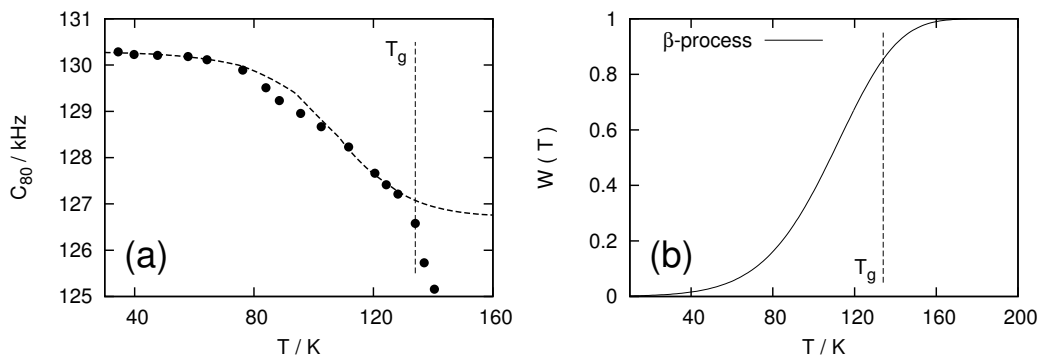


**Figure 6.30 (a):** Apparent spectral width of cyanocyclohexane  $C_{80}$  in comparison with predictions of a motion restricted to a cone (semiangle  $\chi=11^\circ$  for a motion within a cone and  $\chi \approx 8^\circ$  for reorientation on its circumference). **(b):**  $W(T)$  (eq. 6.10) for of the  $\beta$ -process as calculated with parameters from dielectric spectroscopy [Tschirwitz 2002a].

the model at lower temperatures by extrapolating  $G(\chi)$  obtained slightly below  $T_g$  and comparing the results to the experimental apparent spectral width  $C_{80}$ . For the sake of simplicity,  $G(\chi)$  was reduced to a delta function and hence the calculated spectrum at temperature  $T$  becomes

$$S'(\omega, T) = W(T) S(\omega; \bar{\delta}(\chi)) + (1 - W(T)) S(\omega; \delta_0). \quad (6.14)$$

Hereby  $\bar{\delta}$  was set to the mean value previously obtained at low temperatures: for the motion on a cone model the mean semi angle obtained below  $T_g$  is about  $8^\circ$ , for the motion within a cone case approximately  $11^\circ$  – both values correspond to roughly the same reduced coupling constant  $\bar{\delta}$ . Hence the following considerations hold again for either geometry. The resulting apparent spectral width is plotted as dashed line in figure 6.30 (a). As  $W(T)$  is almost zero at the temperature where  $\delta_0$  was arbitrarily defined (34.5 K), the low temperature plateau in  $C_{80}$  is inherently captured within the approach. Regarding the bold assumptions made within the model, the resulting  $C_{80}$  describes also the remainder of experimental data remarkably well: the overall progression with temperature is captured until at around  $T_g$  the weighting factor  $W(T)$  approaches unity and  $C_{80}$  saturates due to the employed fixed angle  $\chi$ , which is known to be no longer constant in this temperature regime.

In figure 6.31 the same calculations are employed for ethanol and toluene. The weighting factor  $W(T)$  was again calculated from the corresponding dielectric distributions of correlation times in the same way as for cyanocyclohexane. Since for both systems no apparent plateau in  $C_{80}$  at lowest temperatures is observed and therefore  $\delta_0$  can not be defined in straightforward manner, the curves are normalized in a rather arbitrary way to match the simulated values<sup>25</sup>. Whereby the strong decrease of  $C_{80}$  in the vicinity of  $T_g$  can be clearly attributed to the  $\beta$ -process in all three systems, the behaviour at lowest temperatures might still be dominated by a

<sup>25</sup>Whereas for toluene the resulting  $\delta_0$  value corresponds roughly to the experimental spectrum at lowest temperatures, in the case of ethanol the normalization neglects the lowest temperature. Since the experimental spectra of ethanol-d<sub>2</sub> at lowest temperatures are not available, the error margins can not be taken into consideration.

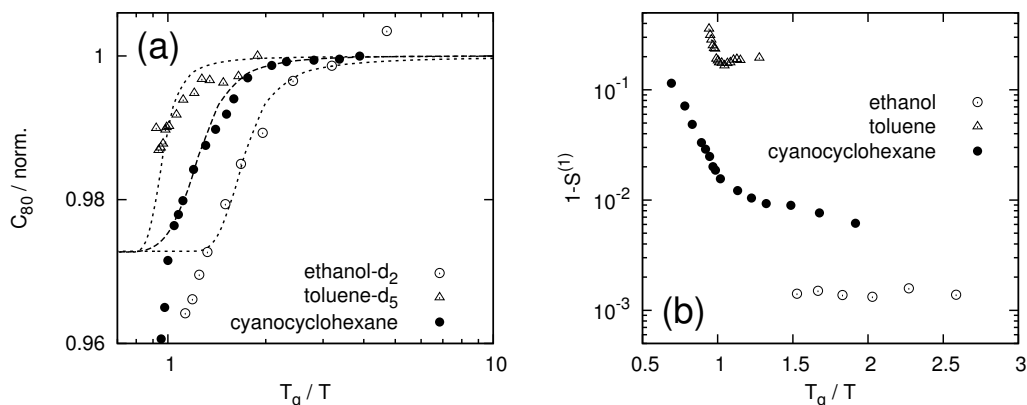


**Figure 6.31 (a):** Normalized apparent spectral width  $C_{80}$  of cyanocyclohexane, toluene-d<sub>5</sub> [Vogel 2000a] and ethanol-d<sub>2</sub> [Schneider 2001]. The lines are predictions for a motion within a cone model with fixed geometry employing  $W(T)$  (parameters from dielectric spectroscopy [Tschirwitz 2002a, Kudlik 1997b, Benkhof 1999]), details cf. figure 6.30. **(b):** Dielectric relaxation strength  $1 - S^{(1)} = \Delta\epsilon_\beta/\Delta\epsilon$  of the systems presented in figure (a) (adapted from the references given in (a)).

vibrational averaging of the coupling constant  $\delta$ , as demonstrated in part II of this work.

Again, the objective of this simple approach in modelling the apparent spectral width was not to gain absolute agreement with the experimental values but to demonstrate that all line shape changes around  $T_g$  can be explained in a straightforward manner by means of a simple geometry of motion for the  $\beta$ -process. Whereas this does not fix a certain geometry non-ambiguously, it validates a surprisingly universal  $\beta$ -process as origin of the observed effects in the rather varied group of presented glass forming systems. This universal manifestation is not reflected in the dielectric results, as demonstrated in figure 6.31 (b): the dielectric relaxation strength of the  $\beta$ -process varies by two orders of magnitude between the presented systems (below  $T_g$ ). This finding is incompatible with our present <sup>2</sup>H NMR results, as the scenario depicted by dielectric spectroscopy would yield vastly different changes in  $C_{80}$  among the different glass formers. Hence we do not observe a clear-cut relation between the relaxation strength in <sup>2</sup>H NMR and dielectric spectroscopy, which explains the deviations found in the case of our present analysis for cyanocyclohexane.

### 6.4.3 The $t_p$ -dependence of solid echo spectra $T > T_g$

The  $t_p$ -dependence of the  $R$  value below  $T_g$ , and hence the slow motion limit effect of the  $\beta$ -process, has already been discussed for all temperatures (cf. figure 6.11), but the solid echo line shape in cyanocyclohexane exhibits another peculiarity with regard to the inter-pulse delay  $t_p$ : figure 6.32 shows a detail around the inner singularity of spectra recorded at different temperatures above  $T_g$ . For each temperature several spectra at different  $t_p$  values are plotted: it becomes immediately obvious that the apparent spectral width  $C_x$  changes significantly with  $t_p$  in this interval.

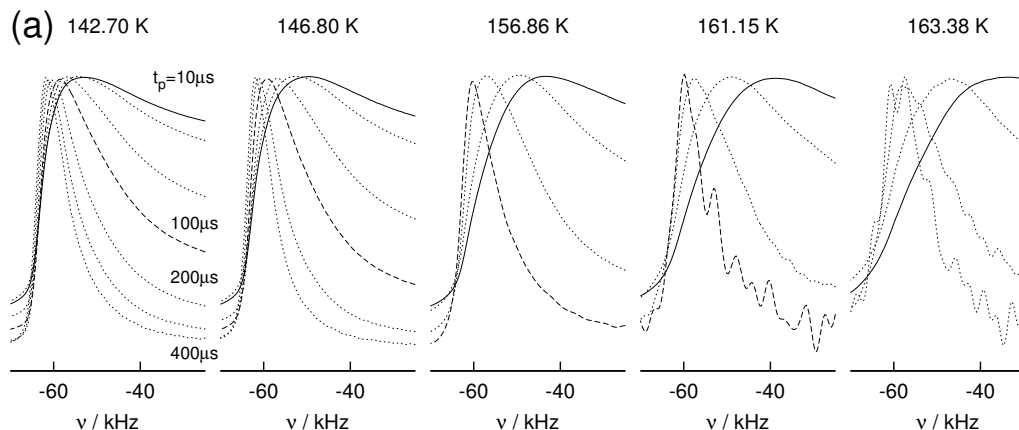
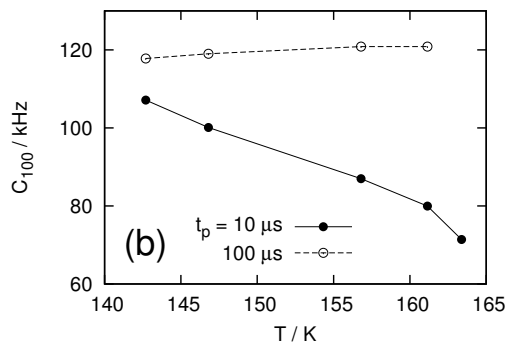


**Figure 6.32 (a):** Solid echo spectra for different echo delays  $t_p$  at temperatures  $T > T_g$ . A blow-up of the inner lower singularity is shown to demonstrate the  $t_p$ -dependence of the apparent coupling constant (solid line:  $t_p=10\ \mu\text{s}$ , dashed line:  $100\ \mu\text{s}$ ). **(b):** Corresponding  $C_{100}$ -values.



Prolonging the inter-pulse delay  $t_p$  recovers partially the spectrum observed at lower temperatures: the apparent width  $C_x$  grows with  $t_p$  and the outer flank (gradually) regains the rigid limit slope. In the same figure the  $C_{100}$  values at  $t_p=10$  and  $100\ \mu\text{s}$  are plotted: whereas the value taken at  $10\ \mu\text{s}$  decreases steadily towards higher temperatures (due to the dynamics of the  $\beta$ -process discussed in the last section), the values at  $100\ \mu\text{s}$  are almost constant.

As the results in chapter 4 have pointed out, such an effect can be attributed to a process with correlation times in the ms to  $\mu\text{s}$  regime, hence the secondary relaxation in cyanocyclohexane is already substantially too fast at the discussed temperatures. If the  $\alpha$ -relaxation however proceeds via small angular jumps, as assumed in the simulations displayed in figure 6.24, the described effects are also observed in this case (represented by the “overshoot” in  $C_{80}$  observed for  $t_p=200\ \mu\text{s}$ ) – and in contrast to the  $\beta$ -process the correlation times of the  $\alpha$ -process account for the afore mentioned criterion in this regime, i.e. are on the order of  $10^{-4} - 10^{-7}$  s.

If the observed behaviour is related to the dynamics of the  $\alpha$ -process – which exhibited no other peculiarities in the present study – one could speculate that the effect is inherent to the structural relaxation, not observed in other glass forming systems due to the lack of fast motion limit line shape effects of the  $\beta$ -process above  $T_g$ : if the width of the solid echo spectrum for  $t_p=20\ \mu\text{s}$  is not substantially reduced above  $T_g$ , the effect becomes very subtle and is easily overlooked.

Indeed we found a similar line shape in meta-fluoroaniline, a structural glass former

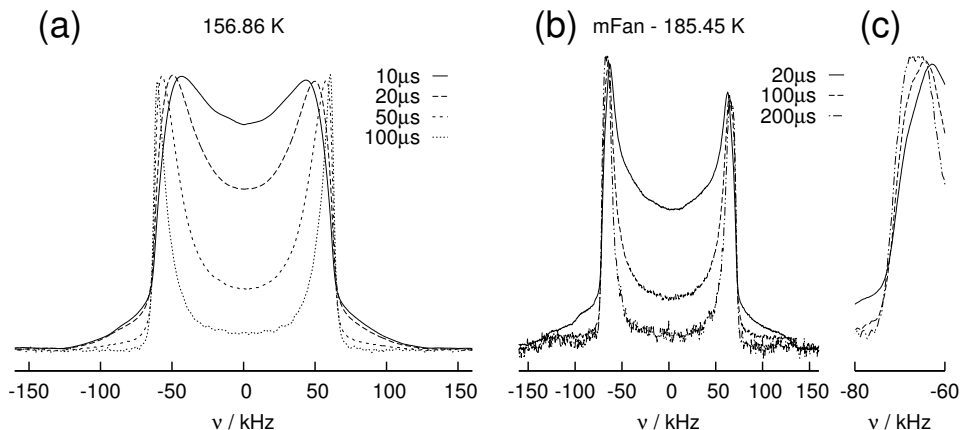


**Figure 6.33 (a):** Solid echo spectrum of cyanocyclohexane at 143 K for different interpulse delays  $t_p$ . **(b):** Solid echo spectra of meta-fluoroaniline (m-FAN) at 182 K  $> T_g$  for different  $t_p$  values. **(c):** Blow-up of the lower singularity to illustrate the analogy in  $t_p$ -dependence.

previously studied by S. Lusceac [Lusceac 2005a]. Meta-fluoroaniline also exhibits a fast  $\beta$ -process with  $G(\log \tau_\beta)$  partially extending to the fast motion limit before merging with the  $\alpha$ -process. In contrast to cyanocyclohexane the  $\alpha$ -process is more fragile, the relaxation strength of the  $\beta$ -process (as measured by dielectric spectroscopy) substantially smaller and furthermore the observation of the discussed line shape changes is somewhat obstructed by the  $\eta \neq 0$  spectrum of fluoroaniline. Nevertheless analogous  $t_p$ -dependence of the line shape at the singularities can be found at temperatures above  $T_g$  (cf. figure 6.33), which was previously overlooked. In other systems like toluene e.g., such an effect is not observed due to the lack of pronounced line shape effects of the  $\beta$ -process (i.e. the spectrum still resembles a Pake pattern at high temperatures where the  $\alpha$ -process becomes effective on the time scale of  $1/\delta$ ). We will reassess this point in part II of this work, where binary mixtures of toluene are presented.

#### 6.4.4 Dynamics of the $\alpha$ -process – reassessment

After we have successfully modelled the  $\beta$ -process in cyanocyclohexane throughout the whole accessible temperature range in the previous sections, one last dynamic imprint on the  $^2\text{H}$  NMR observables remained speculative and therefore will be subject to a refined discussion: the  $t_e$ -dependence of the stimulated echo measurements and hence the microscopic dynamics of the  $\alpha$ -process. In section 6.3.8 it was shown that the normalized  $\langle \tau(t_e) \rangle$  values are approximately described by a combination of small and large angular reorientations, with a strongly temperature dependent weighting of the latter fractions. As such a drastic change in the mechanism of reorientation within a narrow temperature range of about 10 K appears rather peculiar, we will discuss other possible reasons for the observed behaviour.

In section 6.3.6 we have demonstrated (in case of the  $\beta$ -process) that the time window of the stimulated echo experiment is a key value in understanding the results of the technique, consequently we will test its influence on our measurements regarding the

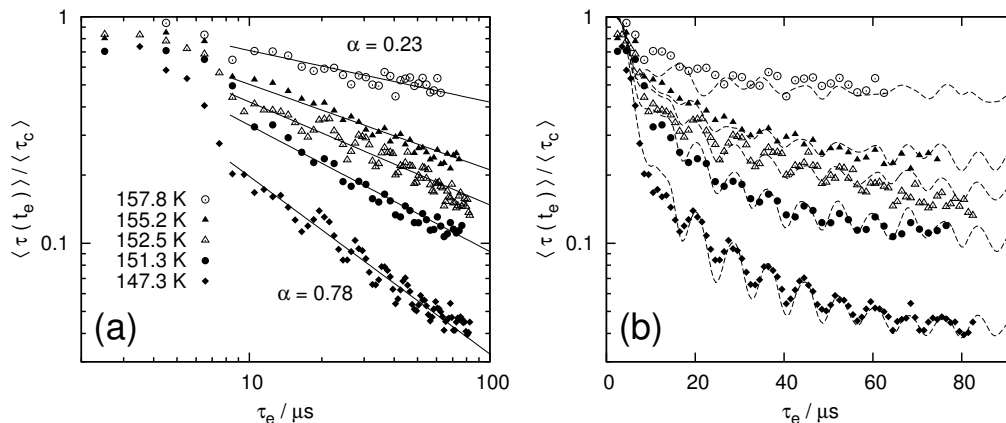


**Figure 6.34 (a):** Double logarithmic representation of  $\langle \tau(t_e) \rangle / \langle \tau_c \rangle$ : for long evolution times a power law  $\langle \tau(t_e) \rangle \propto t_e^{-\alpha}$  emerges, whereby the exponent  $\alpha$  exhibits a strong temperature dependence. **(b):** Normalized stimulated echo decay time constants resulting within the model of a distribution of small angular jumps and a fraction of  $40^\circ$  jumps (lines, fraction of large angles: 0.7, 0.3, 0.19, 0.11, 0.036 from top to bottom) in comparison with experimental results.

$\alpha$ -process also.

Figure 6.34 (a) displays the  $t_e$ -dependent correlation times of cyanocyclohexane at different temperatures in a  $\log(\langle \tau(t_e) \rangle / \langle \tau_c \rangle)$  vs.  $\log t_e$  representation. On this scale it becomes evident that at all temperatures a power law  $\langle \tau(t_e) \rangle \propto t_e^{-\alpha}$  emerges for  $t_e \geq 10 \mu\text{s}$ , whereby the exponent changes from  $\alpha = 0.78$  at 147.3 K to  $\alpha = 0.23$  at 157.8 K. Hence the motion resembles at neither temperature the limiting cases of rotational diffusion ( $\alpha = 2$ ) or random jump type reorientation ( $\alpha = 0$ ). Consequently the scenario of reorientation via fractions of large and small angular jumps introduced in previous sections and employed in the literature [Hinze 1998, Jörg 2000, Baldus 2005] appears applicable. To quantify the change in mechanism for the present assessment, we present a refined fit of the normalized  $\langle \tau(t_e) \rangle$  values within this model in figure 6.34 (b). Hereby a (temperature independent) distribution of small angular jumps (centred around  $\gamma=2^\circ$ ) was used to model the initial decay in  $\langle \tau(t_e) \rangle$ , whereas the fraction of large angular reorientations ( $\gamma=40^\circ$ ) again defines the plateau observed at longest evolution times  $t_e$ . In addition the employed coupling constant has been altered to account for the reduced apparent spectral width observed due to the  $\beta$ -process in this temperature regime (best agreement was found for  $\bar{\delta}=127 \text{ kHz}$ ). This approach is versatile enough to model the experimental data for all evolution times and throughout the studied temperature range by adjusting the fraction of large angles from 0.036 at 147.3 K to 0.7 at 157.8 K.

Figure 6.35 (a) displays the distributions of correlation times in cyanocyclohexane as obtained by dielectric spectroscopy at the latter temperatures: for the lowest temperature studied, 147.3 K, the better part of the distribution  $G(\log \tau_\alpha)$  is within the 2D NMR time window marked by the grey area. At the highest temperature, 157.8 K, the distribution has almost left the window, with only the terminal relaxation time remaining accessible to the technique. Furthermore it becomes evident in this

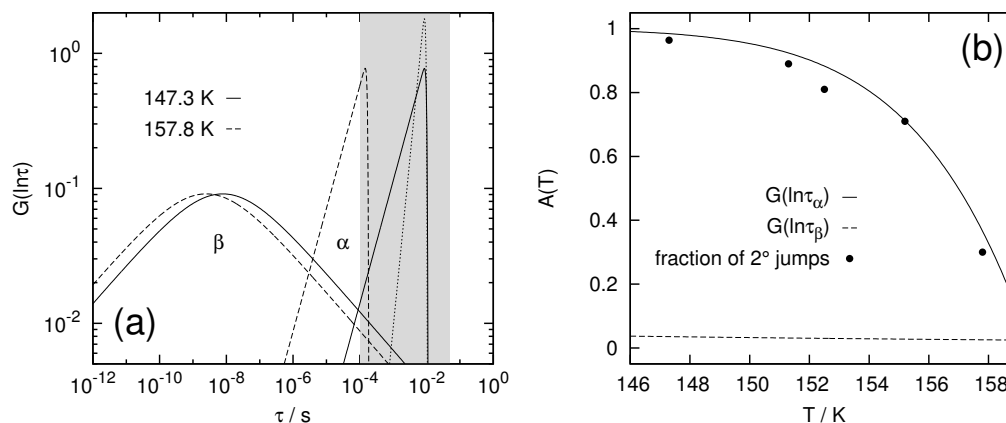


**Figure 6.35 (a):** Distributions of correlation times  $G(\log \tau)$  for the experimentally accessible temperature window in 2D  $^2\text{H}$  NMR.  $G_\alpha$  and  $G_\beta$  distributions were used for  $\alpha$ - and  $\beta$ -process respectively, distribution parameters from Tschirwitz et al. [Tschirwitz 2002a]. **(b):** Integral of  $G(\log \tau_\alpha)$  over the 2D  $^2\text{H}$  NMR time window  $A(T)$  in comparison with the small angular jump fractions obtained in the afore described model from experimental data.

representation that the  $\beta$ -process of cyanocyclohexane is not expected to contribute to any 2D NMR observables in the temperature regime under discussion.

To quantify the fraction of  $G(\log \tau_\alpha)$  within the time window of 2D NMR we will follow the approach presented in section 6.3.6:

$$A(T) = \int_{\log 100\mu\text{s}}^{\log T_1} d \log \tau G(\log \tau_\alpha, T). \quad (6.15)$$

As in case of the  $\beta$ -process before we assume a certain degree of heterogeneity in the  $\alpha$ -process here, i.e. exchange within the distribution  $G(\log \tau_\alpha)$  is neglected: if the respective dynamics of a certain sub-ensemble is too slow, no decay other than  $T_1$  or  $T_{1Q}$  is observed. If  $\tau_\alpha$  is too fast, a constant is obtained for all mixing times (one in case of the cosine-cosine correlation and zero in case of sine-sine).

The quantity  $A(T)$  for cyanocyclohexane is plotted in figure 6.35 (b): the distribution  $G(\log \tau_\alpha)$  traverses the 2D NMR time window in the temperature region from 145 K to 160 K, i.e.  $A(T)$  drops from one to zero in this regime. The temperature dependence of  $A$  remarkably resembles the one found for the small angle jump fraction from the fit in figure 6.34 (b), represented by the points in the same figure. Consequently the experimentally observed  $\langle \tau(t_e) \rangle$  dependence can be explained via  $A(T)$  without the need for a change in the mechanism of motion: the stimulated echo amplitude is characterized by a temperature independent fraction of large angular reorientations and a fraction of small angular jumps that is weighted via  $A(T)$ . Whether this assumption holds and possible reasons for the different impact of  $A(T)$  on the respective fractions will be discussed in the remainder of this section.

### Comparison with literature data for structural glass formers

First we will however repeat the present analysis for literature data of structural glass formers to ascertain that the proportionality of  $A(T)$  and the fraction of small angular

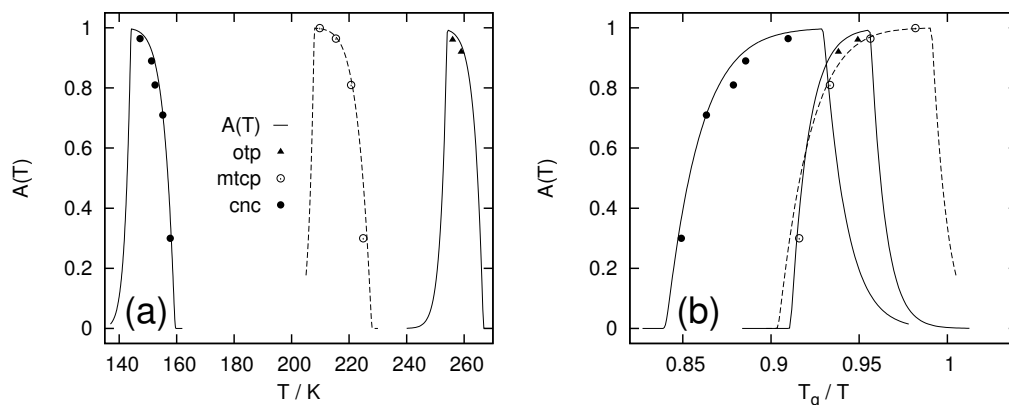


**Figure 6.36 (a):** Integral of  $G(\log \tau_\alpha)$  over the 2D NMR time window ( $A(T)$ , lines) for three glass forming substances in comparison with the small angle fraction extracted from corresponding stimulated echo experiments (symbols): ortho-terphenyl ( $^2\text{H}$  NMR, [Jörg 2000]), m-tricresylphosphate ( $^{31}\text{P}$  NMR, [Baldus 2005]) and cyanocyclohexane (this work). **(b):** Same data represented on the reduced temperature scale  $T_g/T$ .

jumps does not represent a peculiarity of cyanocyclohexane. We have chosen the systems m-tricresylphosphate (m-TCP) and ortho-terphenyl, as for both compounds temperature dependent measurements of  $F_{t_e}^{\text{SS}}$  are available. Ortho-terphenyl was studied by means of  $^2\text{H}$  NMR by Jörg et al. [Jörg 2000], corresponding dielectric data for the calculation of  $A(T)$  was taken from Gainaru et al. [Gainaru 2007a]; m-TCP  $^{31}\text{P}$  NMR data originates from Baldus et al., corresponding dielectric results from Gainaru et al. [Gainaru 2007b]. In both cases the  $t_e$ -dependence of the stimulated echo was fitted in a similar model as employed for cyanocyclohexane in this work, hence the extracted small angular jump fractions are directly comparable. Figure 6.36 (a) displays the reported fractions alongside with  $A(T)$  from equation 6.15, calculated from the corresponding  $G(\log \tau_\alpha)$  extracted from dielectric results. For both system the agreement of  $A(T)$  with the fraction of small angular jumps observed in the stimulated echo is equally well as in the case of cyanocyclohexane. Consequently the proportionality of the latter quantities does neither represent a peculiarity of cyanocyclohexane nor of the employed  $^2\text{H}$  NMR technique, as the results from  $^{31}\text{P}$  NMR are virtually the same. Figure 6.36 (b) present the same data on the  $T_g/T$  scale: the change in the  $t_e$ -dependence of the stimulated echo is apparently not linked to  $T_g$ , it solely reflects the time scale of the  $\alpha$ -process and is hence shifted according to the fragility  $m$  in this representation.

Consequently the present results render the assumption of a universal change in the mechanism of the  $\alpha$ -process in the regime  $\tau_\alpha \approx 10^{-4} \dots 10^{-1}$  s rather unlikely and are clearly in favour of an explanation via the time window of the employed technique.

## Discussion

To conclude the present analysis, we will briefly review its implications on the microscopic mechanism of the  $\alpha$ -process. When discussing a motion connected with

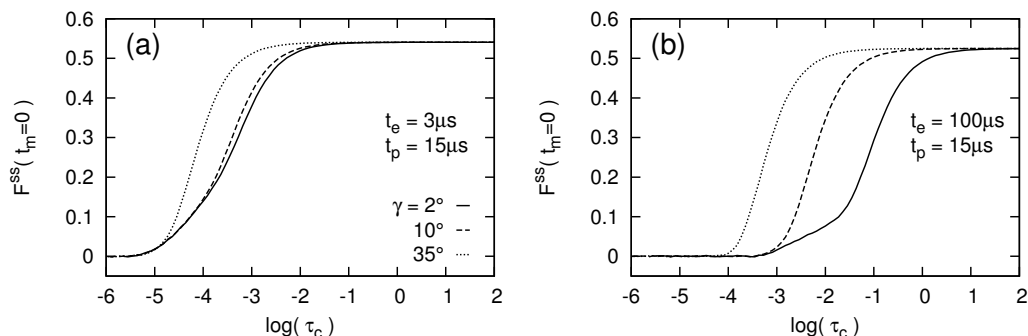


**Figure 6.37 (a):** Initial amplitude of  $F_{t_e}^{ss}$  in the four-pulse sequence with  $t_e=3\mu\text{s}$  and  $t_p=15\mu\text{s}$  for random walk simulations of different discrete  $\gamma$ -jump motions. **(b):** Same representation for an evolution time of  $t_e=100\mu\text{s}$ .

the  $\alpha$ -process that agitates via small angular displacements, at first the excess wing comes to mind. This feature, observed as a power law on the high frequency flank of the  $\alpha$ -process in dielectric spectroscopy, was shown to exhibit such a motional process [Gainaru 2008] and is also found in cyanocyclohexane (cf. figure A.1 (b)). Yet the excess wing was neglected in the calculation of  $A(T)$ , but still the agreement with the observed small angle fraction is remarkable. Furthermore it remains questionable that this subtle feature may account for the large amount of small angular reorientations observed at low temperatures, where  $A(T) \approx 1$ .

On the other hand the observed behaviour arises naturally if the distribution  $G(\log \tau_\alpha)$  is heterogeneous with regard to the geometry of the process. Therefore we assume a scenario in which the  $\alpha$ -process of molecules that are found in a rather “flat” area of the energy landscape, is fast and agitates via small angular displacements, whereas a small fraction of molecules are “trapped” and only reorient on longest times via large angular jumps when the surrounding structure has relaxed. Then the observed temperature dependence of the stimulated echo arises directly due to the suppression of the fast fraction, which exits the time window first.

The random walk simulation discussed in chapter 4 offer however an even simpler explanation: due to the separation of time scales  $\tau_j/\tau_c$  for a motion progressing via small angles, the contribution of such a fraction is inherently reduced at longer times  $\tau_c$  even if the correlation times are identical to the fraction progressing via large angle reorientations. Figure 6.37 (a) presents the initial amplitude ( $t_m \rightarrow 0$ ) of  $F_{t_e}^{ss}$  from random walk simulations for different discrete  $\gamma$ -jump motions: for an evolution time of  $t_e=3\mu\text{s}$  the contribution from molecules undergoing  $2^\circ$ -jumps is reduced for  $\tau_c < 10^{-2}\text{s}$ , whereas in case of  $35^\circ$ -jumps the reduction sets in only around  $10^{-3}\text{s}$ . For  $t_e=100\mu\text{s}$  the effect becomes even more pronounced, as the reduction factor is shifted more than two decades in  $\tau_c$  between the two cases (figure 6.37 (b)). With regard to these findings the  $t_e$ -dependence in the stimulated echo for the  $\alpha$ -process can be explained in the previously introduced model without any change in the mechanism of reorientation with temperature or further undue assumptions.

A detailed study of the experimentally observed  $t_e$ -dependence by means of random walk simulations is however beyond the scope of this work: too many free parameters

arise in the model and the calculations are time consuming as fast dynamics during  $t_e$  and  $t_p$  have to be considered in the approach, opposed to the usually employed simulations in the slow motion limit. It remains unclear if the underlying distribution of jump geometries is indeed bimodal or continuous but strongly asymmetric. Furthermore possible spatial and temporal correlations between the small and large angle jumps remain an open question, as does the exchange rate between the two fractions.

Nevertheless we were able to rationalise the peculiar temperature dependence of the motional process within this work. A finding which is of great significance with regard to the universal nature of glassy dynamics: previously differences in the microscopic dynamics of miscellaneous glass-forming systems were identified via measurements at a single temperature (cf. [Böhmer 2001] and references therein), which – as we have demonstrated – can lead to undue conclusions.

## 6.5 Summary and conclusions

In the present part of this work we have studied the molecular motion in the plastic crystalline phase (PC) of cyanocyclohexane by means of different  $^2\text{H}$  NMR methods. Cyanocyclohexane was affirmed to form a plastic crystal below  $T_m=285\text{ K}$  with a (possibly) face-centred cubic structure and a lattice constant of  $a=9.1\text{ \AA}$ . This translational order is however not reflected in the molecular motion in the supercooled and glassy PC phase of the system: 2D  $^2\text{H}$  NMR experiments for the  $\alpha$ -process have demonstrated that the motion progresses via the same mechanism as reported for structural glass formers, i.e. a model comprised of small and large angular jumps is applicable. This finding is in contrast to other plastic crystalline system like cyanoadamantane for example, where a  $90^\circ$  jump process is observed which directly reflects the symmetry of the cubic lattice [Lusceac 2004] – although also in the case of cyanocyclohexane the motion of a molecule around its lattice position has to be of cooperative nature, as it is constrained by the neighbouring molecules.

By means of random walk simulations and a joint approach with dielectric spectroscopy, we were able to demonstrate that the fractions of small and large angular jumps in the model for the  $\alpha$ -process not necessarily exhibit a temperature dependence slightly above  $T_g$ , although such a behaviour is clearly reflected in the  $t_e$ -dependence of the stimulated echo. The observed change can rather be rationalized by time window effects of the employed 2D  $^2\text{H}$  NMR techniques, which yield a suppression of the small angular motion in the experiment at relatively lower temperatures. This explanation was also shown to hold in the case of previously studied structural glass formers.

Due to the fast and non-merging characteristics of the  $\beta$ -process in cyanocyclohexane pronounced fast motion limit effects were observed in the  $^2\text{H}$  NMR observables at high temperatures. Below  $T_g$  however the mechanism of the  $\beta$ -process in the present system was shown to be virtually identical to the one observed in structural glass formers like toluene for example, i.e. also the secondary relaxation does not exhibit any peculiarities reflecting the translational order of the PC phase. Above  $T_g$  a pronounced minimum in  $T_1$  was observed for the  $\beta$ -process – for the first time in a glass

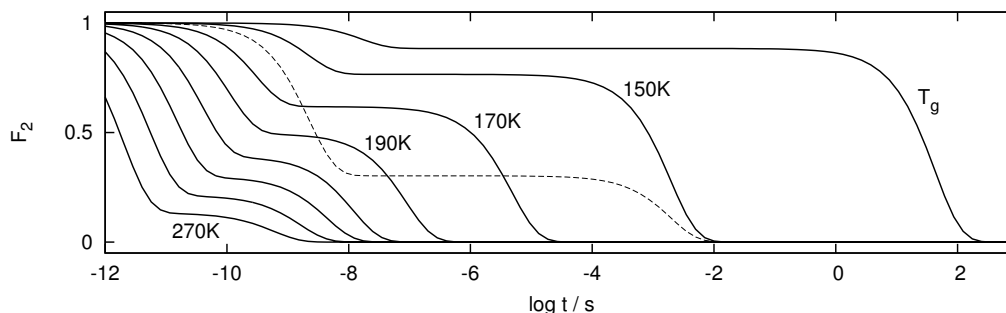


**Figure 6.38:** Sketch of single particle correlation functions  $F_2$  in cyanocyclohexane. A purely heterogeneous scenario was assumed, wherefore the decays due to  $\alpha$ - (long time decay) and  $\beta$ -process (decay at short times) are exponential with  $\tau = \langle \tau_{\alpha/\beta} \rangle$  at the respective temperatures. The relaxation strength  $1-S$  of the  $\beta$ -process is obtained from the  $T_1$  analysis. The dashed line marks  $F_2$  at 150 K for the largest opening angles  $\chi$  observed in the analysis of the fast motion limit line shape.

forming system.  $T_1$  was successfully modelled in the whole accessible temperature range by means of  $G(\log \tau)$  from dielectric spectroscopy and the assignment of the second minimum to the  $\beta$ -process was verified.

Furthermore the solid echo line shape showed strong and characteristic deviations from a Pake pattern in a large temperature regime above  $T_g$ . The spectra were successfully modelled via a motion restricted to the circumference of a cone with a Gaussian distribution of opening angles  $G(\chi)$  within an approach that directly arises from the behaviour observed below  $T_g$  by a growing relaxation strength, i.e. via changes in the maximum and width of the distribution  $G(\chi)$ . Consequently the distribution of restricting geometries for the  $\beta$ -process,  $G(\chi)$ , was for the first time directly accessible to  $^2\text{H}$  NMR via the fast motion limit line shape, which allowed for a confirmation of previously developed models for structural glass formers below  $T_g$ , where  $G(\chi)$  can not be quantified in straightforward manner. Whereas the temperature dependence of the dielectric relaxation strength was shown to be in agreement with our  $^2\text{H}$  NMR results, the magnitude of  $1 - S^{(1)}$  strongly varies among glass formers. As  $^2\text{H}$  NMR detects a rather universal  $\beta$ -process in the studied systems, our results indicate that  $1 - S^{(1)} = \Delta\epsilon_\beta/\Delta\epsilon$  may not represent a valid quantity to determine the relaxation strength of the  $\beta$ -process.

Apart from an extension and refinement of the microscopic model for the dynamics of the  $\beta$ -process, the present study demonstrates the significance of the latter for glassy dynamics. No plateau was observed in the extracted  $1-S$ : the relaxation strength was shown to grow until  $T_m$  in the analysis of  $T_1$ . Figure 6.38 presents a simple sketch of the correlation function  $F_2$  in a purely heterogeneous scenario employing  $1-S$  as obtained from the  $T_1$  analysis: at  $T_g$  the  $\beta$ -process accounts in accordance with common perception only for a subtle correlation loss, at higher temperatures however  $1-S$  grows and the correlation function is rendered distinctively bimodal. The dashed line demonstrates that already at 150 K the  $\beta$ -process yields a decay of  $F_2$  to about 0.3 for a small fraction of molecules. Around the melting point the  $\beta$ -process finally accounts for the better part of correlation loss in this representation.

This finding is in accordance with the random first-order transition theory of glasses, which predicts that the  $\beta$ -process becomes the dominant mode of structural relaxation at high temperatures [Stevenson 2010], and again raises questions with regard to the dynamics in structural glass formers at temperatures above the merging of  $\alpha$ - and  $\beta$ -process.

## Part II

# Binary Glass Forming Systems



# Introduction

## Contents

<b>7.1 Digest</b> . . . . .	<b>117</b>
<b>7.2 Spectroscopic amendments</b> . . . . .	<b>121</b>

Binary mixtures of glassy or supercooled substances have taken on a mayor role in soft matter research during the last decades and are still gaining in importance. The vast interest in this specific class of substances esteems not only from the bright prospects with regard to a deeper understanding of the glass transition phenomenon, but rather from the industrial application of (polymer-) blending and the large number of material properties that can be tailored thereby.

With the numerous oportunities that studies of binary systems provide, comes along however the drawback of a distinct step-up in complexity. Therefore the scope of this chapter is not only to present an introduction to the field – including remarks on present literature – but to discuss the most prominent problems from an (NMR-) spectroscopists angle of view, to guide the reader through the extensive results presented in the next chapter. As for the case of cyanocyclohexane presented in part I of this work, it is not expected to gain substantial insight from a single, decisive experiment – rather the dynamics in the studied system have to be discussed regarding the  $^2\text{H}$  NMR experiments as a whole in combination with results from other techniques, which is why at certain points novel and phenomenological approaches have to be considered.

## 7.1 Digest

The most prominent feature observed when blending a substance  $A$  with a high glass transition temperature  $T_g^A$  with an additive  $B$  exhibiting a significantly lower  $T_g^B$ , is the acceleration of dynamics for the low mobility component<sup>1</sup>. This so-called plasticizer effect has great industrial significance with respect to tailoring the material properties at a certain temperature defined by the desired application. Figure 7.2 (a) provides a sketch of the described scenario and figure 7.1 illustrates an example for a 50 % mixture of PMMA- $\text{d}_3$  and m-TCP [Bingemann 2007]: the line shape collapse in the  $^2\text{H}$  NMR solid echo spectra of PMMA- $\text{d}_3$  (i.e. the dynamics of PMMA in the mixture is selectively probed) is shifted approximately 100 K towards lower

<sup>1</sup>Throughout this work we will synonymous use the terms “low mobility component” or “high  $T_g$  component” to denote the slower component in dynamically asymmetric mixtures and “high mobility component”, “low  $T_g$  component”, “additive” or “plasticizer” for the substance exhibiting relatively faster dynamics.

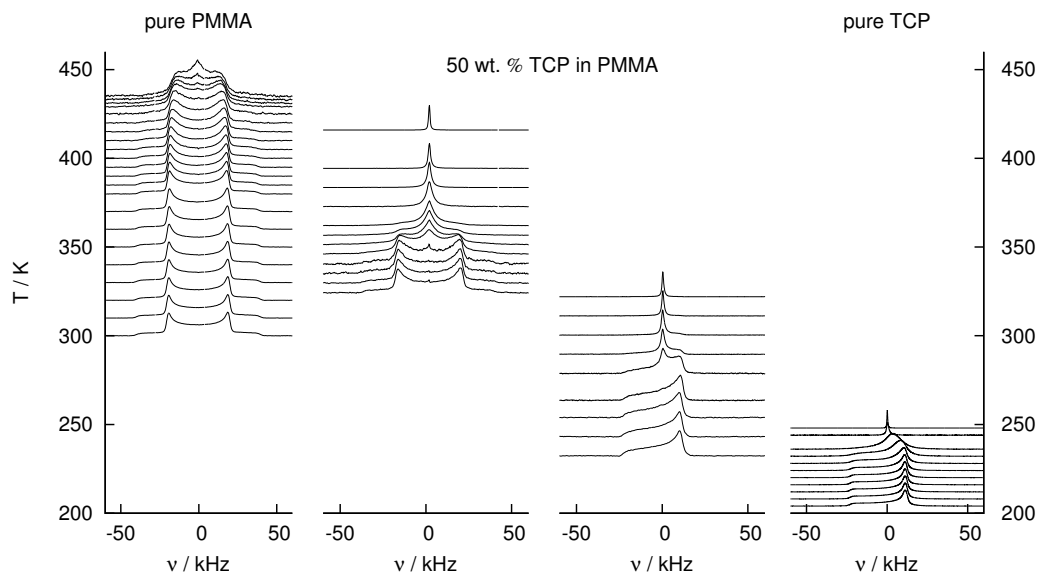


**Figure 7.1:**  $^2\text{H}$  NMR solid echo spectra of neat poly(methyl methacrylate)- $\text{d}_3$  (PMMA, left) and PMMA- $\text{d}_3$  in a 50% (by weight) mixture with tri-*m*-cresyl phosphate (m-TCP, center left); right part presents the corresponding  $^{31}\text{P}$  NMR Hahn-echo spectra of tri-*m*-cresyl phosphate (neat: right, in the 50% mixture: center right). Figure adapted from [Bingemann 2007].

temperatures in the mixture with m-TCP, i.e. the condition  $\tau_\alpha \simeq 1/\delta$  is approached at significantly lower temperatures.

Even though there exists no accepted microscopic theory, the dynamics of the high- $T_g$  component upon blending is mostly subject to mutual consent in present literature: although maybe drawing slightly different conclusions in detail, most studies (by means of DS [Hirose 2003, Alegria 1994, Blochowicz 1999b, Blochowicz 2011], DSC [Ceccorulli 1987, Taniguchi 2004], NMR [Vogel 1998, Medick 2002b, Medick 2002a] etc.) agree that the dynamics of the high- $T_g$  component is accelerated, albeit still follows a VFT temperature dependence. The dielectric spectra and correlation functions exhibit typically a slight broadening, respectively stretching compared to the neat component upon high additive concentrations (cf. sketch in figure 7.2 (b)), which can be understood in the framework of concentration fluctuations [Zetsche 1994, Kumar 1996, Kant 2003].

The dynamics of the additive or high mobility component in such mixtures on the other hand is still a matter of great debate. The  $^{31}\text{P}$  spectra of m-TCP in figure 7.1 clearly demonstrate that a dynamic decoupling of the components is found in mixtures with PMMA: compared to the neat system the line shape collapse of m-TCP in the 50% mixture is shifted about 50 K towards higher temperatures due to the anti-plasticizer effect, i.e. dynamics is significantly slowed down. At temperatures where a liquid line is observed for m-TCP (i.e.  $\tau \leq 1/\delta$ ), PMMA- $\text{d}_3$  in the same mixture yet still yields a solid state spectrum which only collapses at significantly higher temperatures. Furthermore “two-phase” spectra arise for m-TCP in the mixture, which are a fingerprint of pronounced dynamic heterogeneities. Hence it appears

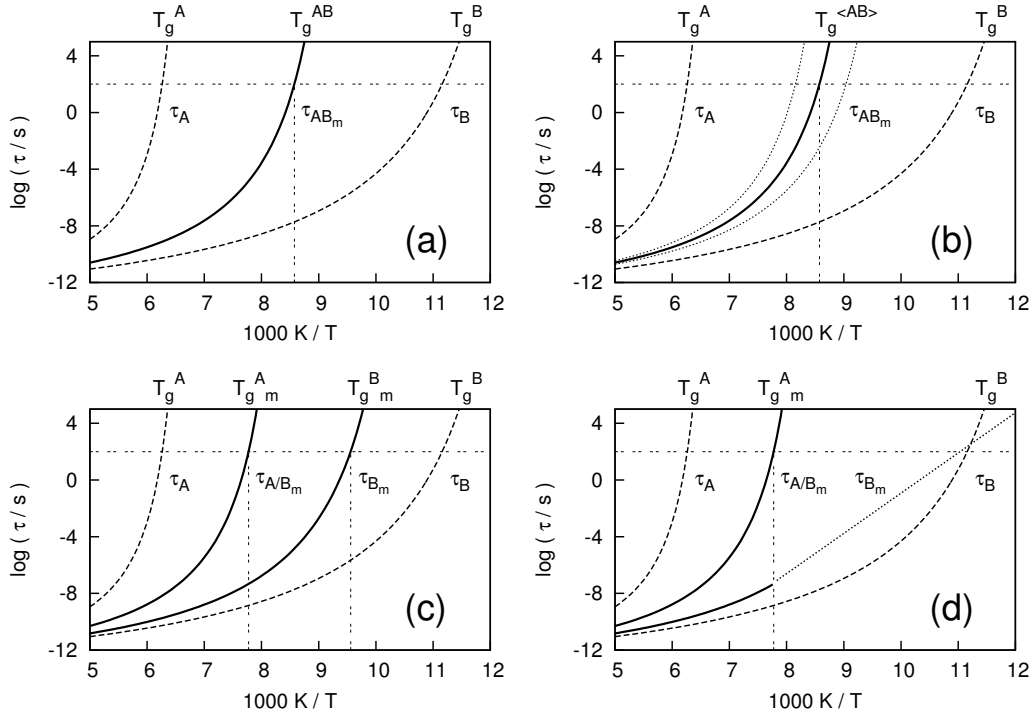


**Figure 7.2** (a): Plasticizer effect: the low mobility component A exhibits accelerated dynamics after blending with the high mobility component B. (b): Dynamic heterogeneities: the distribution of relaxation times is significantly broadened in the mixture. (c): Dynamic decoupling: time scales of high and low  $T_g$  component are decoupled in the mixture. (d): Intrinsic confinement effects: below  $T_g^A$  the dynamics of component B changes due to the confining geometry of the rigid matrix A. Figure adapted from [Blochowicz 2010].

that the scenarios proposed in figures 7.2 (a) and (b) do not hold for binary mixtures of the latter compounds. Dynamic decoupling has been reported for mixtures of polymers with small molecular additives [Bingemann 2007] and for mixtures of small molecular glass formers [Blochowicz 1999b, Medick 2002b, Schramm 2010]. If we hence assume a scenario as sketched in figure 7.2 (c), i.e. the time scale of relaxation is distinctively decoupled for both components, one would expect to observe two glass transition temperatures in DSC measurements. Yet in most DSC studies of binary mixtures and polymer blends a single glass transition step was observed, which typically becomes very broad at intermediate concentrations. The arise of a single step in DSC measurements was even regarded as a criterion for full miscibility of the compounds [Utracki 1990], in recent publications however two  $T_g$ s were reported for certain binary mixtures [Gaikwad 2008, Taniguchi 2004, Blochowicz 2011]. The second step, arising at relatively low temperatures and presumably connected to the decoupled dynamics of the low- $T_g$  component, becomes stronger for higher cooling rates – hence it does not reflect a phase separation process.

In contrast to the high- $T_g$  component, the dynamic heterogeneities arising for the high mobility additive are typically very pronounced in binary mixtures. The correlation functions become particularly broad and even logarithmic decays have been observed

in the experiment [Bingemann 2007] and in simulation works [Moreno 2006], which are in agreement with a higher order singularity predicted by mode-coupling theory [Krakoviack 2007].

In a recent publication Blochowicz et al. demonstrated for a mixture of methyltetrahydrofuran (M-THF) and tristyrene [Blochowicz 2011] that the low- $T_g$  component M-THF exhibits bimodal relaxation behaviour: due to the low dipole moment of tristyrene two loss peaks of M-THF were observed in the dielectric spectra (in addition to the  $\beta$ - and  $\gamma$ -process of M-THF). The low frequency loss peak coincides with the  $\alpha$ -process of tristyrene in the mixture ( $\tau_\alpha$  of tristyrene was determined by means of depolarized dynamic light scattering) and the high frequency peak corresponds to the dynamically decoupled M-THF reorientation in the mixture: the so-called  $\alpha'$ -process. Hence a scenario according to figure 7.2 (c) was proposed, in which two dynamically distinct M-THF fractions exist: a mobile fraction still isotropically reorienting in the “frozen matrix” of tristyrene at temperatures below the upper  $T_g$  and a fraction of M-THF immobilized in the vicinity of tristyrene molecules. The weight of the latter fractions is strongly temperature dependent (the slow fraction grows in relaxation strength with decreasing temperature), i.e. frequency-temperature-superposition is clearly not fulfilled for the low- $T_g$  component. The temperature dependence of  $\tau_{\alpha'}$  was furthermore reported to change at the upper  $T_g$  from a VFT behaviour above to temperature activated behaviour below, i.e. a fragile-to-strong transition was observed which was explained via intrinsic confinement effects [Colmenero 2007].

In NMR studies so far no bi-exponential relaxation behaviour was reported for the high-mobility component in binary mixtures, rather the obtained results are typically rationalized via a single, broad distribution of correlation times due to the pronounced dynamic heterogeneities in the mixture. The finding that the loss peaks observed for M-THF are both broadened with respect to the neat system, exhibit a strong temperature dependence of the relative weight and presumably show exchange, might conflict with the time window of NMR techniques and hence hamper the observation of pronounced effects.

Apart from the changes in time scale and the possible arise of bimodal relaxation behaviour, also an alteration in the microscopic mechanism for the structural relaxation was reported in binary mixtures. By addition of 15% water to glucose [van Dusschoten 1999, Wachner 1999], the jump mechanism observed via the  $t_e$ -dependence of the stimulated echo was reported to change: a greater fraction of large-angular jumps was found. With regard to the strong temperature dependence of the experiment, which we rationalized by means of time window effects in part I of this work, great care has however to be taken in the interpretation of such results. Whereas the high temperature dynamics of the  $\alpha'/\alpha$ -process in binary mixtures is intensively discussed in present literature, publications regarding the role of the Johari-Goldstein  $\beta$ -process for the dynamics in such systems on the other hand are sparse. Blochowicz et al. [Blochowicz 2004] have demonstrated that the excess wing in 2-picoline emerges to a  $\beta$ -peak in mixtures with tri-styrene and the  $\alpha'$ -process arising in different binary mixtures was interpreted in terms of a (submerged)  $\beta$ -process [Ngai 2010].  $^2\text{H}$  NMR studies of binary glass formers revealed dynamics of the secondary relaxation comparable to neat systems and for a mixture of chlorobenzene and decalin it was demonstrated that both components contribute to the  $\beta$ -process

[Vogel 2002]. Nevertheless a detailed assessment of the concentration dependence of the  $\beta$ -process in such systems is lacking, although it is of particular interest not only for the general dynamics in mixtures of glass formers but also with regard to a possible cooperativeness of the process.

## 7.2 Spectroscopic amendments

Before the results obtained in binary mixtures of toluene and a polychlorinated biphenyl are discussed in the next chapter, we need to address some characteristics regarding dielectric studies of binary mixtures.

The  $^2\text{H}$  NMR experiments in the latter mixture can be analysed in straightforward manner as only one of the components is selectively deuterated: the changes in the relaxation strength of different processes upon mixing are directly accessible and hence a contribution of the monitored component to a certain dynamic processes is explicitly clear, as otherwise no motion is detected on the time scale under discussion. In dielectric spectroscopy on the other hand always the response of both quantities is probed and even if one of the components exhibits a negligible dipole moment, the contributions have to be de-convoluted in the limit of high concentration of the latter substance.

Regarding the  $\alpha$ -process, the individual contributions in terms of  $\Delta\epsilon$  are obtained from a linear extrapolation [Benkhof 1999]:

$$\Delta\epsilon = x \cdot \Delta\epsilon_0^A + (1-x) \cdot \Delta\epsilon_0^B, \quad (7.1)$$

with  $\Delta\epsilon_0$  denoting the relaxation strength of the neat substance. Hence the contribution of species  $A$  to the dielectric spectrum reads:

$$\Delta\epsilon^A(x) = \frac{x \cdot \Delta\epsilon_0^A}{x + (1-x) \cdot \Delta\epsilon_0^B / \Delta\epsilon_0^A}. \quad (7.2)$$

The relaxation strength of the  $\beta$ -process on the other hand is generally obtained from:

$$1 - S(T) \approx \frac{\Delta\epsilon_\beta}{\Delta\epsilon} = \frac{\Delta\epsilon_\beta^A + \Delta\epsilon_\beta^B}{\Delta\epsilon^A + \Delta\epsilon^B}. \quad (7.3)$$

All binary systems discussed within this work consist of mixtures between type-A and type-B glass forming systems, i.e. only one of the systems exhibits a  $\beta$ -peak in the dielectric spectrum of the neat substance. Consequently we can divide the mixture into two sub-ensembles, of which only one contributes to the  $\beta$ -process. In case of  $\Delta\epsilon_\beta^B = 0$  equation 7.3 reads [Benkhof 1999]:

$$1 - S(T) \approx \frac{x \cdot (1 - S_0^A(T))}{x + (1-x) \cdot \Delta\epsilon_0^B / \Delta\epsilon_0^A} \quad (7.4)$$

Here we assume a linear interpolation of the relaxation strengths of species  $A, B$  and of  $1 - S_0^A(T)$  from the neat component  $A$ . As  $1 - S$  also for binary systems presumably couples to  $T_g$  of the mixture, the latter quantity is a-priori only known below  $T_g$

of the neat component *A*. Furthermore we have neglected a potential contribution of species *B* to the  $\beta$ -process of *A*, nevertheless equation 7.4 will be employed (and extended to account for the latter scenario when appropriate) when comparing prior dielectric results to our  $^2\text{H}$  NMR studies in the following chapters.

## Toluene in PCB

---

**Contents**


---

<b>8.1 Introduction</b> . . . . .	<b>123</b>
<b>8.2 Dielectric Spectroscopy</b> . . . . .	<b>124</b>
<b>8.3 Experimental details</b> . . . . .	<b>127</b>
<b>8.4 Thermal analysis</b> . . . . .	<b>128</b>
<b>8.5 NMR results – an overview</b> . . . . .	<b>130</b>
8.5.1 Spin lattice relaxation . . . . .	130
8.5.2 Solid echo spectra – high temperature regime . . . . .	135
8.5.3 2D exchange spectra . . . . .	139
8.5.4 Stimulated echoes – high temperature regime . . . . .	141
8.5.5 Solid echo line shape – low temperature regime . . . . .	147
8.5.6 Stimulated echoes – low temperature regime . . . . .	152
8.5.7 Spin lattice relaxation – revisited . . . . .	155
<b>8.6 Plausibility check</b> . . . . .	<b>160</b>
8.6.1 Modelling the toluene dynamics in mixtures with PCB . . . . .	161
8.6.2 Models for two dynamically distinct toluene sub-ensembles . . . . .	165
8.6.3 Discussion . . . . .	171

---

**8.1 Introduction**

The present chapter focuses on mixtures composed of two small molecular glass formers: toluene and a polychlorinated biphenyl (PCB). The compounds are in-

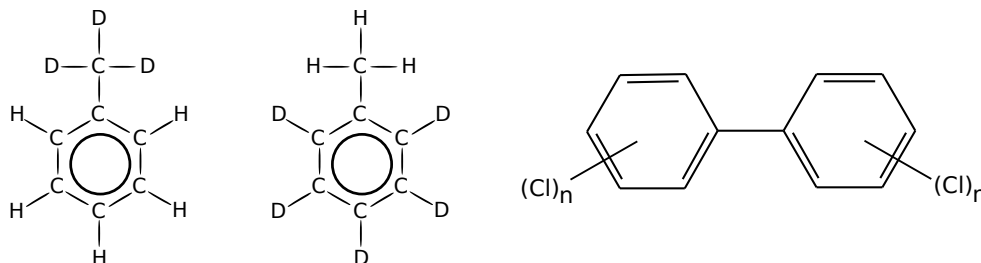


**Figure 8.1 left:** Sketch of a toluene- $d_3$  molecule deuterated at the methyl group. **Center:** ring deuterated toluene- $d_5$ . **Right:** general sketch of a polychlorinated biphenyl. Here  $n$  denotes the number of chlorine atoms per phenyl ring, for the present samples composed of PCB54  $2n = 4 \dots 5$  holds.

	toluene-d <sub>3</sub>	toluene-d <sub>5</sub>	PCB54
full name	toluene- $\alpha, \alpha, \alpha$ -d <sub>3</sub>	toluene-2,3,4,5-d <sub>5</sub>	aroclor 1254
$M_n$ [g/mole]	95.16	97.17	327
$\rho$ [g/cm <sup>3</sup> ]	0.895	0.912	1.51
$T_g$ [K]	117 [Levy 1983]	117 [Levy 1983]	241
chemical purity [%]	99.7	99.2	tech.
% atom D	99.9	99.6	-

**Table 8.1:** Material characteristics of the components. For PCB54 the molecular weight denotes an average value, as the number of chlorine atoms per molecule varies.

interesting candidates for an in-depth <sup>2</sup>H NMR study for numerous reasons: the components are miscible in the whole concentration range, both consist of rigid molecules and are good glass formers that provide a relatively large contrast in  $T_g$  ( $\Delta T_g = 124$  K). Furthermore there exist contemporary dielectric measurements from Cangialosi et al. [Cangialosi 2008], which however lack to provide conclusive answers to the questions raised in the introduction to this part, as the results regarding toluene are somewhat ambiguous due to the low dipole moment of the system. The high mobility component in the mixtures, the glass former toluene, was intensively studied by different techniques in our group before – besides dielectric measurements [Kudlik 1997b, Kudlik 1999, Blochowicz 2003] there exists a detailed NMR study on the  $\beta$ -process in toluene by M. Vogel [Vogel 2001a], which provides us with the aptitude to monitor even subtle changes in the secondary relaxation of toluene upon mixing with PCB – if present. The low mobility component is Monsanto’s Aroclor 1254 or PCB54: a polychlorinated biphenyl with a chlorine weight fraction of 54 %, which corresponds to four to five statistically distributed chlorine atoms per biphenyl ring. This somewhat random structure of the PCB molecules has the benefit that the tendency towards crystallization of the component is reduced in comparison to isomers with well defined chlorine bonding sites. PCB54 is toxic and carcinogenic but was widely used in capacitors and as plasticizer in paints and plastics<sup>1</sup> before being banned under the Stockholm convention in 2001.

This chapter is organized as follows: after a brief discussion of the dielectric results from Cangialosi et al., we will present our own DSC and NMR results – a refined discussion and interpretation of the data will be part of the next chapters, where the results are compared to other binary glass forming systems containing toluene as mobile component, in the attempt to draw conclusions of more general validity.

## 8.2 Dielectric Spectroscopy

In the following section we briefly review the results from dielectric spectroscopy on mixtures of toluene and PCB54 as on the neat components themselves. Dielectric spectra and time constants of toluene are presented and discussed in the introduction and part I of this thesis, as previously all dielectric results on neat toluene are adapted

<sup>1</sup>In the present mixture PCB54 is the low mobility component, whereas it was mainly used as high mobility additive to polymers with an even higher  $T_g$ .

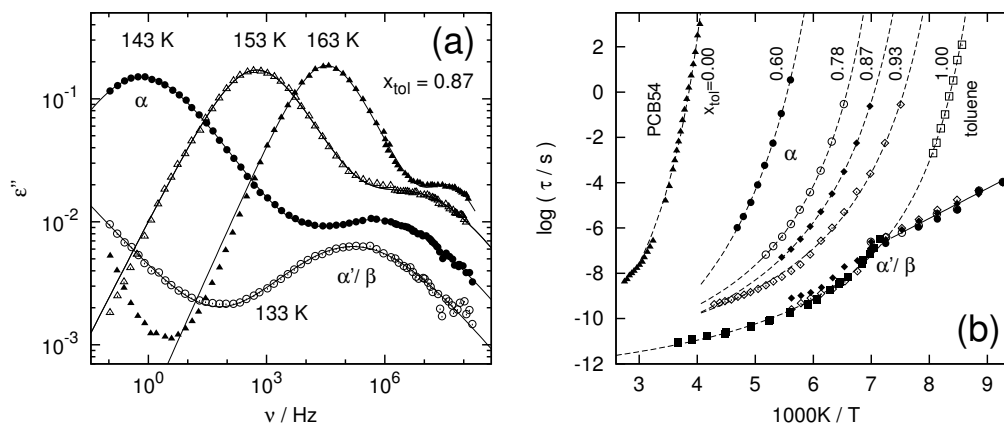
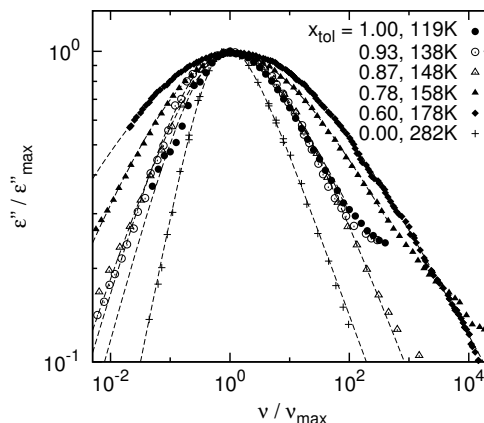


**Figure 8.2 (a):** Loss part of the dielectric permittivity for a concentration of  $x_{\text{tol}}=0.87$  toluene in PCB54 [Cangialosi 2008] at different temperatures. For all temperatures two distinct loss peaks are discernible: a low frequency ( $\alpha$ -) peak and a high frequency peak with lower intensity (denoted  $\alpha'/\beta$ ). **(b):** Corresponding time constants of both processes for different toluene concentrations [Cangialosi 2008] including neat PCB54 [Casalini 2002] and neat toluene data [Kudlik 1999] (DS,  $\square$ ) [Rössler 1984] (NMR,  $\blacksquare$ ).

from Kudlik et al. [Kudlik 1997b, Kudlik 1999]. Neat polychlorinated biphenyls were studied by Casalini et al. [Casalini 2002]: the systems are so-called type-A glass formers [Kudlik 1999], i.e. the dielectric loss exhibits an  $\alpha$ -peak with an excess-wing but lacks a distinct  $\beta$ -process. The time constants of the  $\alpha$ -process follow a VFT-behaviour (cf. figure 8.2 (b)) and are highly dependent on the degree of chlorination:  $T_g$  drops about 48 K with the chlorine content from PCB62 to PCB42 (i.e. from 62 to 42 weight percent). The high frequency wing in contrast appears almost unchanged, which may be explained via an interpretation of the excess wing as a submerged  $\beta$ -process [Blochowicz 2004].

Dielectric measurements on mixtures of toluene and PCB54 were performed by Cangialosi et al. [Cangialosi 2008], the discussion of which makes up the remainder of this section. At this point we have to remind the reader that dielectric spectroscopy on binary mixtures – in contrast to NMR – always measures a bulk quantity, i.e. the response of both components in the mixture. As the dipole moment of PCB54 is however significantly larger than the one of toluene, the main response is expected to arise from PCB even at relatively high toluene concentrations. Figure 8.2 (a) displays the loss part of the dielectric permittivity for a mole fraction of  $x_{\text{tol}}=0.87$  toluene in PCB54. At all displayed temperatures two discernible peaks are observed in the spectra of the mixture: a low frequency peak with a strong temperature dependence (denoted “ $\alpha$ ”) and a high frequency peak of lower intensity (denoted “ $\alpha'/\beta$ ”), exhibiting a weaker temperature dependence. The time constants corresponding to the  $\alpha$ -peak follow a VFT-law and are highly dependent on concentration, cf. figure 8.2 (b). The relaxation strength of the process approximately scales with the PCB54 content, as seen in figure 8.4 (b). Consequently the peak can be identified with the  $\alpha$ -process of PCB54 in the binary mixtures, which becomes faster upon higher concentrations of toluene due to the plasticizer effect imposed by the latter molecules. The width

**Figure 8.3:** Loss part of the dielectric permittivity of toluene / PCB54 [Cangialosi 2008] mixtures at different concentrations (including neat toluene [Kudlik 1997b] and PCB62 [Casalini 2002]). The data is scaled in frequency with respect to the dominant loss peak and normalized in amplitude. The temperatures were chosen to correspond to similar relaxation times (in all cases the applied frequency shift is less than 1.5 orders of magnitude). Full lines are fits via a HN-function.



of the  $\alpha$ -process exhibits a distinct concentration dependence, cf. figure 8.3. For concentrations  $x_{\text{tol}} \geq 0.87$  the high frequency flank is similar to the behaviour found in neat toluene, whereas a slight broadening is observed on the low frequency side of the peak. For lower concentrations the peak becomes very broad and almost symmetric, which contradicts the limit  $x_{\text{tol}} \rightarrow 0$ , as neat PCB54 exhibits a rather narrow loss peak.

The fast process is only resolved at lowest temperatures, where it follows an Arrhenius temperature dependence for  $T < 140$  K and coincides for all concentrations with the  $\beta$ -process of neat toluene (cf. figure 8.2 (b)). For the two samples with highest toluene content also time constants at temperatures above the merging of  $\alpha$ - and  $\beta$ -process in neat toluene are reported: in this regime they follow the  $\alpha$ -process of neat toluene, albeit slightly shifted towards higher temperatures in case of  $x_{\text{tol}} = 0.87$ . The universal (i.e. concentration independent) nature of this process is demonstrated in figure 8.4 (a): at 118 K in first approximation neither the maximum position, nor the width of the fast process depends on the concentration of PCB54 – instead the response of neat toluene is observed, i.e. the  $\beta$ -process of toluene persists in the mixtures. Its relaxation strength scales with the toluene content for concentrations above  $x_{\text{tol}} = 0.80$  (figure 8.4 (b)), at lower concentrations the experimentally observed relaxation strength is significantly higher than predicted by a linear extrapolation of  $\Delta\epsilon$  according to equation 7.2. In the same concentration range  $\Delta\epsilon$  of the  $\alpha$ -peak is somewhat smaller than predicted from equation 7.2.

Whereas the dielectric measurements serve to provide a convenient overview of the PCB54 related dynamics and were furthermore able to resolve the  $\beta$ -process of (neat) toluene in the mixtures, the technique fails to differentiate between the scenarios depicted in the introduction to this part (cf. figure 7.2): it remains unclear if the toluene related dynamics observed at relative high temperatures in the mixtures with  $x_{\text{tol}} = 0.93$  and 0.87 toluene content accounts for all toluene molecules or if a fraction reorients on the time scale of PCB54 in the mixtures (not observed due to the low dipole moment). Furthermore, as no time constants for the  $\alpha$ -process of toluene are reported below the merging temperatures of  $\alpha$ - and  $\beta$ -process in the mixtures, the attribution of the high temperature, high frequency loss peak to the structural relaxation of toluene by the authors remains speculative – it might still

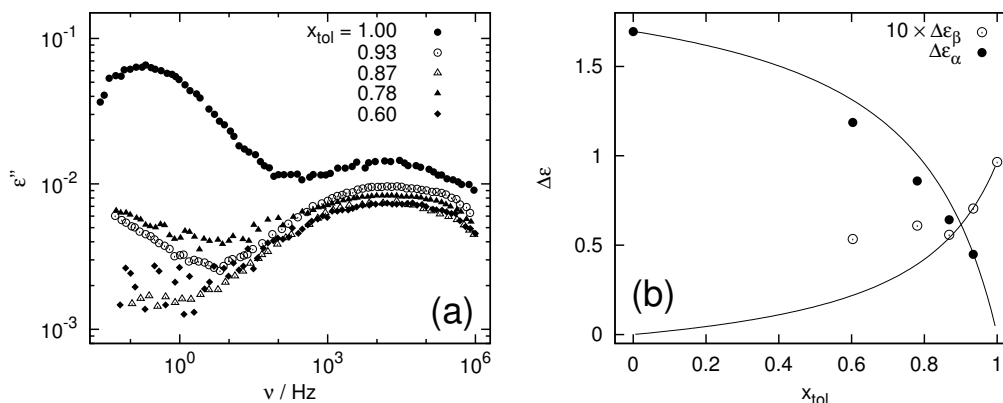


**Figure 8.4 (a):** Loss part of the dielectric permittivity of toluene / PCB54 mixtures for different concentrations at  $T=118$  K [Cangialosi 2008] including data of neat toluene [Kudlik 1999]. **(b):** Relaxation strength of the high ( $\circ$ ) and low ( $\bullet$ ) frequency loss peak in the toluene / PCB mixtures [Cangialosi 2008, Cangialosi 2009]. The lines represent a linear extrapolation of the relaxation strengths of PCB54 and toluene via equation 7.2 respectively.

be the  $\beta$ -process with the  $\alpha$ -peak submerged under the loss peak of PCB54.

The  $^2\text{H}$  NMR measurements carried out in this work, which selectively probe the dynamics of the deuterated toluene molecules, will help to elucidate the behaviour of toluene in the present mixtures as well as provide further insight on the mechanism of reorientation.

### 8.3 Experimental details

Having summarized the dielectric results of Cangialosi et al., we will now focus on our own studies of the aforementioned mixtures by means of differential scanning calorimetry (DSC) and  $^2\text{H}$  NMR. After a brief parenthesis on experimental details and sample preparation, the section will begin with a discussion of the DSC results, as they provide rapid means of comparison with regard to the sample preparation process of Cangialosi et al. and the one used in this work.

The deuterated toluene samples were obtained from CDN isotopes and used without further purification (for purities and other material properties see table 8.1). The first set of PCB54 samples (dissolved in the mixtures with  $x_{\text{tol}}=0.87, 0.74$  and  $0.36$  toluene- $\text{d}_3$ ) are courtesy of Daniele Cangialosi and originate from Ultra Scientific, the remainder of PCB54 was obtained from Supelco Analytical with the same purity as the aforementioned.

For sample preparation we pursued the following scheme: PCB was supplied in ampoules of 50 mg, the contents of which were dissolved with the appropriate amount of toluene- $\text{d}_x$ <sup>2</sup> to obtain the desired concentration. After agitation and annealing for several hours at  $50^\circ\text{C}$  in the closed ampoule to assure thorough mixing, the

<sup>2</sup>Whenever in order we will differentiate between the various labelled toluene samples by denoting the degree of deuteration, the term toluene- $\text{d}_x$  will be employed when discussing NMR arguments of general validity, i.e. independent of the labelling site.

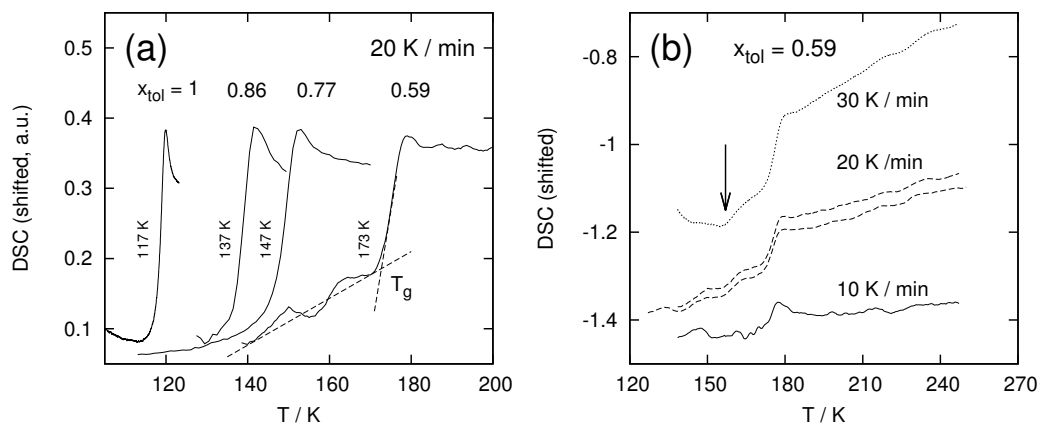


**Figure 8.5 (a):** Temperature dependent heat flow from DSC scans of toluene / PCB54 mixtures for different concentrations and a heating rate of 20 K/min. The dashed lines mark  $T_g$  defined as the onset of the step for  $x_{\text{tol}}=0.59$ . **(b):** DSC scans of  $x=0.59$  toluene in PCB54 for different heating rates. A second step in the heat flow (marked by the arrow) can be anticipated for higher heating rates.

samples were transferred to a 5 mm NMR glass tube which was subsequently sealed under light vacuum. Afterwards the ampoules were purged with acetone and dried to acquire the accurate initial weight of PCB for a refined declaration of the obtained concentration. All concentrations given in the remainder of this part will denote the toluene mole fraction.

DSC measurements were conducted on a Netzsch DSC 200 cooled with liquid nitrogen and using helium as purging gas. All heat flow patterns displayed in this work were obtained upon heating after annealing the sample for 2 min at 80-90 K.  $^2\text{H}$  NMR measurements on the binary mixtures were conducted with the same experimental setup as employed in chapter 6, i.e. at a magnetic field strength of 7.05 T corresponding to a deuterium Larmor frequency of 46.07 MHz. Again a Bruker Avance DSX 300 console and a home built low temperature probe placed in a Cryovac static cryostat, which was controlled via an Oxford ITC 503 temperature controller were used<sup>3</sup>. For details cf. section 6.3.1.

## 8.4 Thermal analysis

Glass formers are conveniently characterized by DSC measurements, as a step in the temperature dependent heat flow, obtained while heating the sample, provides a convenient and reliable way of determining the glass transition temperature  $T_g$ . Following the discussion in chapter 7, DSC studies on the toluene / PCB54 mixtures are of interest for mainly two reasons: as mentioned above, the  $^2\text{H}$  NMR measurements are only sensitive on the deuterium labelled toluene molecules - as the dielectric studies provided mainly data on the PCB related dynamics, we have no direct means

<sup>3</sup>Temperature stability was again better than 0.2 K.

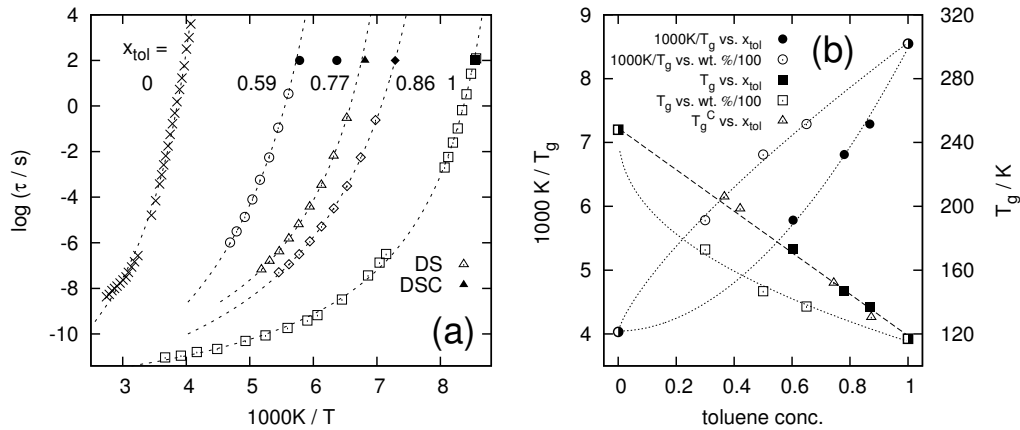


**Figure 8.6 (a):** Time constants extracted from the glass transition steps in figure 8.5 (a) ( $\tau(T_g) := 100s$ , full symbols) in comparison with dielectric results [Cangialosi 2008] (corresponding open symbols) for different concentrations of toluene in PCB54. For  $x_{tol}=0.59$  the  $T_g$  from the second step in figure 8.5 (b) for a heating rate of 30 K / min is also given. **(b):** Concentration dependence of  $T_g$  in the mixtures of toluene with PCB54 on various scales, see text.

of comparing the results in a straightforward manner. The DSC scans allow us to check the sample preparation process by comparing the  $T_g$ s of mixtures prepared by Cangialosi et al. and us, as we studied the same concentrations to employ the dielectric results in our analysis. Furthermore the measurements could give first hints on the toluene related dynamics via the possible arise of a second step in the heat flow, due to a process submerged under the dominant loss peak of PCB in the dielectric spectra.

Figure 8.5 (a) displays the DSC curves of toluene / PCB54 mixtures at different concentrations for a heating rate of 20 K/min. The anti-plasticizer effect, i.e. the slowing down of dynamics due to higher concentrations of PCB54 is clearly observed. Furthermore the glass transition steps in the mixtures appear to broaden with decreasing toluene concentration<sup>4</sup>.

For heating rates above 20 K/min a small, second step at  $T=157$  K becomes discernible in the sample with  $x_{tol}=0.59$  toluene content, cf. figure 8.5 (b) - a finding previously reported for other binary glass forming systems [Taniguchi 2004, Blochowicz 2011]. Due to problems with the baseline of the apparatus at low temperatures however, the measurements are not unambiguous – although the second step appeared in several different cooling runs. This feature was not observed in the samples with higher toluene content, possibly due the fact that the second step is submerged under the large high temperature step, which appears at lower temperatures as the PCB54 content is reduced.

Assuming  $\tau(T_g) = 100s$ <sup>5</sup>, the  $T_g(x)$  values (defined as the temperate of the onset of

<sup>4</sup>The reproducibility of the base line in the apparatus is however not sufficient for a quantitative discussion of the effect.

<sup>5</sup>This convention holds for a heating rate of 10 K/min. The measurements were done however with 20 K/min to improve the signal to noise ratio. For a comparison with dielectric results we will

the step) indicated in figure 8.5 (a) are plotted in figure 8.6 (a) alongside with the correlation times obtained by dielectric spectroscopy for the same concentrations ( $x_{\text{tol}}=0.59, 0.77$  and  $0.86$  [Cangialosi 2008]) and literature data of the neat components [Casalini 2002, Kudlik 1999, Rössler 1984]. The  $T_g$  values resulting from the large, upper step in the DSC curves are in good agreement with the VFT fits to the dielectric data, which validates agreement in the sample preparation processes (the point resulting from the small step in the  $x_{\text{tol}}=0.59$  sample will be discussed later in the framework of the NMR measurements).

The concentration dependence of  $T_g$  is plotted in figure 8.6 (b) in terms of weight and mole fraction: it becomes obvious that the Fox equation [Fox 1956]

$$\frac{1}{T_g} = \frac{w_A}{T_g^A} + \frac{w_B}{T_g^B} \quad (8.1)$$

is not fulfilled, i.e. no linear dependence of  $1/T_g$  on the weight fraction is observed ( $\circ$ ). In first approximation we found however a linear relation between  $T_g$  and the toluene mole fraction ( $\blacksquare$ ).

## 8.5 NMR results – an overview

We investigated mixtures of PCB54 with two different spin labelled toluene molecules: toluene- $d_3$  and toluene- $d_5$ . Since toluene is apart from the methyl group rotation a rigid molecule, the samples are expected to reflect similar dynamics except for the latter rotation, which is fast with respect to the NMR time scale at all investigated temperatures.

The first set of samples was composed of toluene- $d_3$ , which due to fast rotation of the methyl group exhibits considerable shorter spin-lattice relaxation times  $T_1$  at lowest temperatures (cf. figures 8.7) and therefore provides the benefit of convenient measurement times in this temperature range. This feature is however also a drawback of toluene- $d_3$ :  $T_1$  and the  $t_p$ -dependence of the solid echo spectra are governed by the methyl-group rotation at low temperatures and hence provide no direct insight on the dynamics of the molecule as a whole. Due to the short spin lattice relaxation time at low temperatures it is furthermore inapplicable to study the  $\beta$ -process of toluene- $d_3$  by means of 2D NMR, as the available time window is too small. To overcome these obstacles, samples with toluene- $d_5$  were prepared to conduct concerted measurements at low and lowest temperatures.

The following overview presents all data from the employed  $^2\text{H}$  NMR experiments, including preliminary analysis and a brief discussion of the results within each technique. This approach will facilitate a refined discussion in section 8.6, where all results are combined in the attempt to provide a coherent picture of the dynamics in mixtures of toluene and PCB54.

### 8.5.1 Spin lattice relaxation

We will begin the review of  $^2\text{H}$  NMR results with a discussion of spin-lattice relaxation measurements. The spin lattice relaxation times  $\langle T_1 \rangle$  of toluene- $d_x$  in PCB54 for

---

accept the resulting error for the time being.

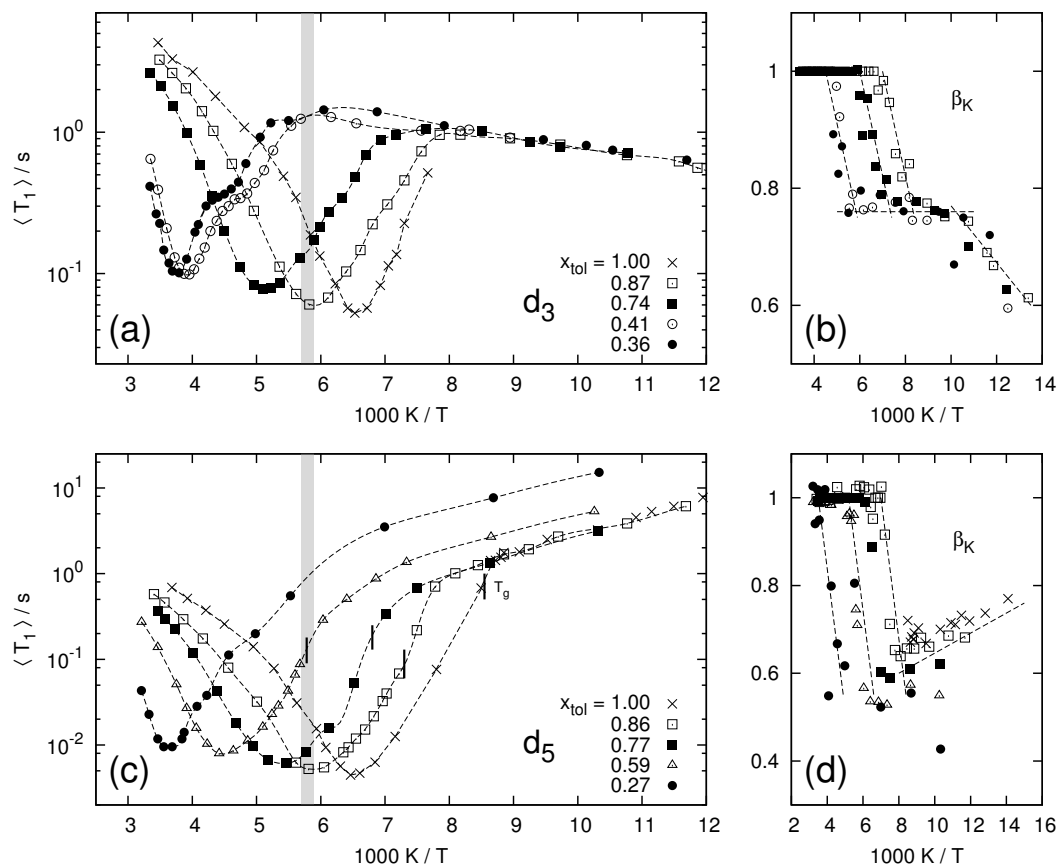


**Figure 8.7 (a):** Average spin lattice relaxation times  $\langle T_1 \rangle$  for different concentrations of toluene-d<sub>3</sub> in PCB54 at  $\omega_L=46.07$  MHz (neat toluene-d<sub>3</sub> (x) [Rössler 1984] recorded at  $\omega_L=55$  MHz). The lines serve as guide for the eye. **(b):** Corresponding stretching parameter  $\beta_K$ . Again, the lines are guide for the eye. **(c):** Average spin lattice relaxation times  $\langle T_1 \rangle$  for different concentrations of toluene-d<sub>5</sub> in PCB54 at  $\omega_L=46.07$  MHz (neat toluene-d<sub>5</sub> (x), above  $T_g = 117$  K: [Rössler 1984],  $\omega_L=55$  MHz, below  $T_g$ : [Vogel 2000a],  $\omega_L=46.07$  MHz). The lines serve as guide for the eye, the vertical bars mark the respective  $T_g$  of the mixture. **(d):** Corresponding stretching parameter  $\beta_K$ . Again, the lines are guide for the eye.

different concentrations are displayed in figure 8.7. As  $T_1$  becomes non-exponential at temperatures slightly below the minimum, the average spin lattice relaxation time  $\langle T_1 \rangle = T_1 / \beta_K \cdot \Gamma(\beta_K^{-1})$  from a Kohlrausch fit to the experimental magnetization curves is plotted. The  $\langle T_1 \rangle$  minimum, which according to the BPP condition  $\tau = 1/\omega_L$  marks an iso-kinetic point, is shifted more than 100 K towards higher temperatures as the toluene concentration is lowered from  $x_{\text{tol}}=1$  to 0.27. The corresponding time constants are displayed in figure 8.8. In contrast to the DSC measurements, where a mixed response from both components is probed, the selective <sup>2</sup>H NMR  $T_1$  measurements show a distinct decoupling of the time scale of toluene motion from the PCB54 dynamics observed in dielectric spectroscopy: for each concentration the average correlation time of toluene molecules at the temperature of the respective  $T_1$  minimum is about two orders of magnitude faster than the corresponding  $\tau_\alpha$

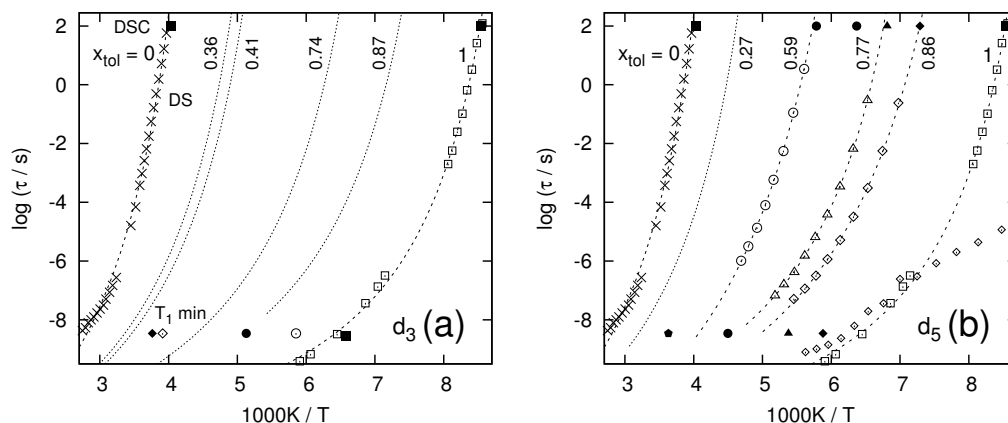


**Figure 8.8 (a):** Time constants extracted from the  $\langle T_1 \rangle$  minimum condition (symbols in the ns-regime) for different concentrations of toluene- $d_3$  in PCB54 in comparison with corresponding VFT-interpolations from dielectric spectroscopy (dotted lines, cf. section B.1). Dielectric and DSC results of the neat components are repeated from figure 8.6 (a),  $T_1$  minimum of neat toluene- $d_3$  from Rössler et al. [Rössler 1984]. **(b):** Same representation for mixtures of toluene- $d_5$  in PCB54: for the high concentrations in comparison with corresponding dielectric results [Cangialosi 2008], in case of  $x_{\text{tol}}=0.27$  a VFT-interpolation is plotted, as no dielectric data is available.

from dielectric spectroscopy<sup>6</sup>. The presented  $\langle T_1 \rangle$  data by itself (i.e. in a model-free approach) does not provide unambiguous information on the number or nature of the dynamical processes involved in the toluene motion. Nevertheless we will attribute the minimum in  $T_1$  for all concentrations with an isotropic motion of toluene molecules decoupled from the time scale of the PCB dynamics: the  $\alpha'$ -process. In section 8.6 we will corroborate this working hypothesis. Yet it remains unclear if a fraction of toluene reorients on the time scale of PCB54 in the mixtures, or if the observed decoupling holds for all sub-ensembles. Consequently the term “ $\alpha$ -process” will denote only the dynamics of the PCB54 fraction in the remainder of this part, unless explicitly stated otherwise.

The dynamic decoupling between  $\tau_\alpha$  and  $\tau_{\alpha'}$  appears concentration independent in first approximation, consequently the temperature of the  $T_1$  minimum (figure 8.9 (a)) exhibits comparable concentration dependence as observed for  $T_g$  in figure 8.6 (b): a linear dependence of  $T_{\text{min}}$  on  $x_{\text{tol}}$  is found. This behaviour does however not hold in the limit  $x_{\text{tol}} \rightarrow 0$ , i.e. the dielectric results of neat PCB54 yield a significantly higher temperature for  $\tau = 1/\omega_L$ .

### Low temperature regime

So far we discussed the high temperature region around the  $T_1$  minimum, where spin-lattice relaxation is presumably dominated by the  $\alpha'$ -process. In mixtures containing toluene- $d_3$   $T_1$  in the low temperature regime, i.e.  $T < T_g = 117$  K of neat

<sup>6</sup>As dielectric results are only available for some of the studied concentrations, the VFT parameters (obtained via a fit to  $\tau_\alpha(x)$  from DS) have been interpolated for a comparison with the remainder of concentrations. For details cf. section B.1.

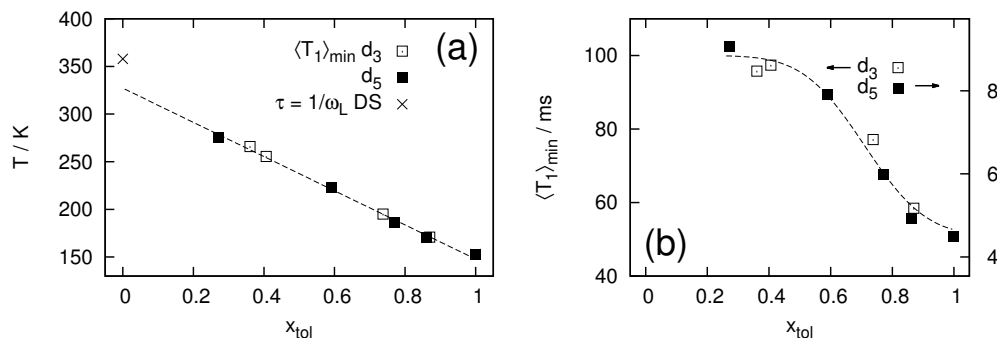


**Figure 8.9 (a):** Temperature of the spin lattice relaxation time minimum for mixtures of toluene- $d_x$  in PCB54, point for neat PCB54 extrapolated from  $\tau_\alpha$  [Casalini 2002]. The line serves as guide for the eye. **(b):** Concentration dependence of the average spin lattice relaxation time at the  $\langle T_1 \rangle$  minimum of toluene- $d_3$  and toluene- $d_5$  in PCB54. The y-margins are reduced by a factor of 11 in the case of toluene- $d_5$ , line serves a guide for the eye.

toluene, is dominated by the dynamics of the methyl group rotation and hence no unambiguous information regarding the  $\beta$ -process can be extracted from the latter samples. Yet the fact that all toluene- $d_3$  containing mixtures exhibit comparable spin lattice relaxation times at lowest temperatures is noteworthy, as it implies that the energy landscape probed by the tunnelling methyl group appears to be concentration independent in first order in this temperature regime, see section B.2 for details.

In neat toluene- $d_5$  on the other hand, the temperature dependence of  $\langle T_1 \rangle$  solely reflects the motion of the molecule as a whole and hence below  $T_g$  the relevant spectral density is governed by the  $\beta$ -process as the dominant motion in the NMR time window. The low temperature spin lattice relaxation times in the binary mixtures consequently yield information on a possible change of the  $\beta$ -process upon mixing: indeed there appears a distinct concentration dependence in figure 8.7 for  $T < 117$  K. Whereas  $\langle T_1 \rangle$  in the mixtures with  $x_{tol} \geq 0.77$  coincides with the data of neat toluene- $d_5$ , the  $x_{tol} = 0.59$  and  $0.27$  mixtures exhibit considerably longer average spin lattice relaxation times ( $\langle T_1 \rangle$  of the  $x_{tol} = 0.27$  mixture is almost an order of magnitude longer than in the neat system), following however the same temperature dependence. This observation raises two interesting points: on the one hand the spin lattice relaxation times in the mixtures containing  $x_{tol} \geq 0.77$  toluene- $d_5$  support the results from dielectric spectroscopy in the sense that the  $\beta$ -process of neat toluene is also present in the mixtures – with comparable relaxation strength  $1-S^7$  – whereas the lower concentrations exhibit a decrease of  $1-S$  not observed in dielectric spectroscopy. The last point is of considerable interest, as the dielectric results show the opposite trend, i.e. an increase in  $1-S$  (cf. figure 8.3), which could however also result from a contribution of PCB54 to the dielectric strength of the  $\beta$ -process, as the quantity represents an ensemble average.

In addition to  $\langle T_1 \rangle$ , the stretching parameter  $\beta_K$  also appears concentration dependent in toluene- $d_5$  below 117 K, whereas it is concentration independent at lowest

<sup>7</sup>As small changes in the spectral density can be precisely measured by  $T_1$ .

temperatures in toluene-d<sub>3</sub>. At intermediate temperatures  $\beta_K$  couples in both cases to the position of the  $T_1$  minimum, as the temperature at which the  $\alpha$ -process becomes so slow to render  $T_1$  exponential via effective exchange shifts in a proportional manner.

If we conclude that the  $\beta$ -process of toluene (albeit with a concentration dependence of the relaxation strength detectable below a certain toluene content) survives in the mixtures, as suggested by the dielectric and spin lattice relaxation results at low temperatures – then, following the arguments in part I of this work, a second, distinct minimum in  $T_1$  should be observed as the  $\alpha$ '-process of toluene slows down upon mixing and becomes more and more separated from the  $\beta$ -process. For concentrations above  $x_{\text{tol}}=0.7$  the minimum attributed to the  $\alpha$ '-process is yet not well separated from the region where one would expect to find such a second minimum (shaded in grey<sup>8</sup> in figure 8.7), but also for lower toluene concentrations no distinct second minimum like in cyanocyclohexane occurs that could be attributed to the  $\beta$ -process – only a slight *bend* around 230 K for concentrations below  $x_{\text{tol}}=0.5$  is observed. As pointed out in part I of this thesis, this could be due to an insufficient relaxation strength of the  $\beta$ -process in the mixtures: in ethanol-d<sub>2</sub> also no  $T_1$  minimum of the  $\beta$ -process was observed since the minimum condition is approached already below  $T_g$ , where the relaxation strength is rather limited.

In neat glass formers the relaxation strength is known to be virtually constant below  $T_g$  and to increase sharply at the glass transition temperature. If this behaviour is maintained in the mixtures of toluene and PCB54, it could serve to explain the observed  $T_1$  pattern: as the increase in relaxation strength couples to the  $\alpha$ -process, the onset is shifted towards higher temperatures with decreasing toluene concentration. Hence for lowest concentrations the same argument as in ethanol-d<sub>2</sub> holds, whereas for intermediate concentrations effects in  $T_1$  are expected that result from an interplay of time scale and relaxation strength – which could account for the saddle point observed in samples with  $x_{\text{tol}}<0.5$ . For a modelling of  $T_1$  as employed in part I, i.e.  $T_1$  calculations based on  $G(\log \tau)$ , we first need to gain further insight on the toluene dynamics in the present mixtures, as no unambiguous distributions of correlation times from dielectric spectroscopy are available in the present case.

Briefly summarizing this section, we state that a dramatic slowing down of the toluene dynamics in the present mixtures was observed, whereat the toluene motion appears decoupled from the PCB54 dynamics observed in dielectric spectroscopy. The  $\beta$ -process of pure toluene persists in the mixtures and shows little concentration dependence for concentrations  $x_{\text{tol}}\geq 0.77$ . At lower concentrations effects in the spin lattice relaxation time of the mixtures are observed that in a first approach can be explained by a reduction in the relaxation strength of the  $\beta$ -process with respect to the neat system – the nature of which can not be ascertained at this point. Especially it remains unclear if the  $\beta$ -process of (virtually) all toluene molecules is altered upon mixing or if a fraction arises in which the secondary relaxation is suppressed (“islands of mobility” concept).

<sup>8</sup>Under the assumption that  $\tau_\beta$  retains an Arrhenius temperature dependence above the merging temperature in neat toluene. If the  $\beta$ -process would exhibit a VFT like behaviour at high temperatures the minimum should appear at relative lower temperatures.

### 8.5.2 Solid echo spectra – high temperature regime

We will begin the discussion of the solid echo line shape in mixtures of toluene with PCB54 with the most prominent effect: the arise of so-called “two phase” spectra in the high temperature regime. This peculiar spectral pattern in the region of the line shape collapse is not observed in pure toluene, as being the case for the majority of neat glass forming systems. The spectra of toluene in PCB54, as demonstrated by the inset in figure 8.10, can be described by a superposition of a Lorentzian line, stemming from a mobile fraction ( $\tau \ll 1/\delta$ ) of molecules, and an in first approach undistorted Pake pattern ( $\tau \gg 1/\delta$ ) resulting from relatively slow molecules. Consequently two phase spectra are only observed if a sufficiently broad distribution of correlation times with a fairly slow exchange rate is present (cf. section 4.2.2).

#### Two phase spectra

Figure 8.10 displays solid echo spectra in the high temperature regime around the collapse of the solid line for each studied concentration of toluene-d<sub>x</sub> in PCB54. Again, the slowing down of toluene dynamics upon mixing is clearly reflected in a shift of the line shape collapse towards higher temperatures: at 215 K the sample with  $x_{\text{tol}}=0.36$  toluene-d<sub>3</sub> still exhibits a solid state spectrum, whereas the spectrum of the  $x_{\text{tol}}=0.87$  concentration has collapsed to a liquid line already 70 K below at around 145 K – the same trend is observed in the samples containing toluene-d<sub>5</sub>. In neat toluene the solid state spectrum vanishes at about 130 K (extrapolated from DS [Kudlik 1999]) in an unfavourable temperature region with regard to <sup>2</sup>H NMR measurements, as the sample exhibits a high tendency towards crystallization here. Due to the lack of data for toluene, spectra of glycerol around the temperature of the line shape collapse are displayed in figure 8.10 as a typical example for the behaviour of a neat glass former.

In addition to the slowing down of toluene dynamics with increasing PCB concentration, also the temperature range in which two phase spectra are observed broadens significantly. For a more quantitative analysis the individual spectra were fitted in a phenomenological approach via the superposition of a Pake pattern  $S(\omega; \delta)$  and a Lorentzian line, as sketched in figure 8.10:

$$S'(\omega, T) = (1 - W(T)) S(\omega; \delta(T)) + \frac{W(T)}{\pi} \left[ \frac{\gamma(T)}{\omega^2 + \gamma(T)^2} \right]. \quad (8.2)$$

The resulting temperature dependent weighting factor of the liquid line  $W(T)$  is displayed in figure 8.11 (b) for all investigated concentrations. In this representation the aforementioned effects become more apparent: the inflection point of the curves at  $W(T)=0.5$  shifts about 100 K towards higher temperatures from neat toluene to the  $x_{\text{tol}}=0.36$  mixture and the slopes of the individual curves decline in the process<sup>9</sup>. As the  $W(T)$  progression appears rather symmetric, a straightforward approach is to take the inflection point in the fit as the temperature at which the average correlation time  $\langle \tau \rangle$  is on the order of the inverse coupling constant  $\delta$ . Hence we

<sup>9</sup>As guide for the eye the points were fitted via a stretched error function,  $1-1/2 \cdot \text{erfc}([T - T_W]^\beta)$ , the stretching parameter  $\beta$  drops from  $\approx 0.3$  for  $x_{\text{tol}}=0.87$  to 0.08 in case of the  $x_{\text{tol}}=0.36$  concentration.

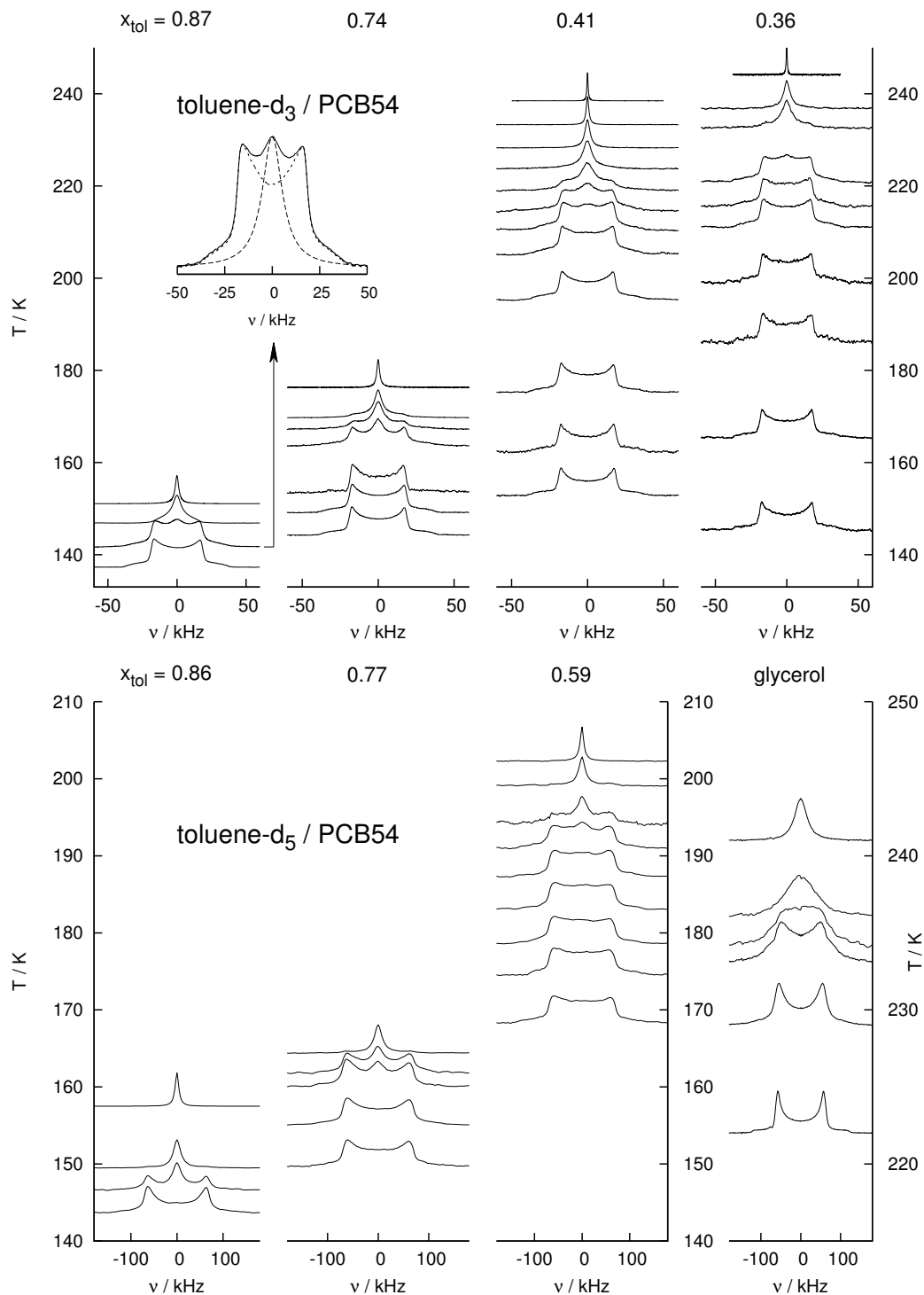


**Figure 8.10:** Solid echo spectra of toluene-d<sub>3</sub> and toluene-d<sub>5</sub> in PCB54 in the high temperature regime for different concentrations. All spectra are recorded with an inter pulse delay of 20  $\mu$ s. For comparison spectra of glycerol at temperatures around the line shape collapse are displayed [Vogel 2000a]. The inset in the upper figure demonstrates a fit via equation 8.2.

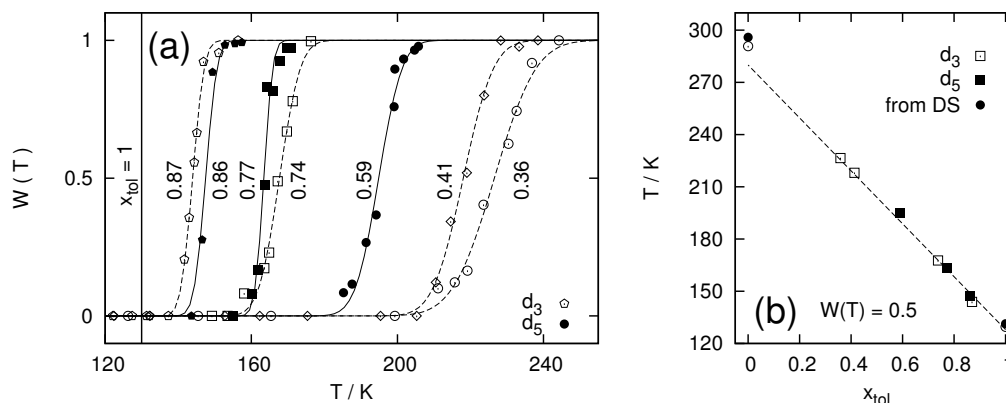


**Figure 8.11 (a):** Weighting factor of the liquid line in solid echo spectra of toluene- $d_3$  (open symbols) and toluene- $d_5$  (full symbols) in PCB54 (all  $t_p=20\ \mu\text{s}$ ). The lines result from fits with a stretched error function. **(b):** Temperature of the inflection point in  $W(T)$  taken from the fits in figure (a). In case of the neat systems the temperatures have been extrapolated from  $\tau_\alpha$  (DS, [Kudlik 1999, Casalini 2002]).

obtain another iso-kinetic point for each concentration, as in case of the  $T_1$  minimum and the DSC studies. In contrast to the analysis of the  $T_1$  minimum, where the different toluene samples could be treated alike, the reduced coupling constant  $\delta$  in toluene- $d_3$  leads to a difference in the obtained correlation times for the present line shape analysis. Due to the fragile temperature dependence of the correlation times this shift by a factor of three is hardly noticeable in figure 8.11 (b), where the temperatures corresponding to  $W(T)=0.5$  are plotted. For reasons of comparison the temperatures of the (fictive) line shape collapse in the neat components have been determined via  $\tau_\alpha$  from dielectric spectroscopy (employing the coupling constants for toluene- $d_3$  and toluene- $d_5$ ). The observed concentration dependence is similar to the one found for the temperature of the  $T_1$  minimum: a linear dependence between the temperature of the inflection point in  $W$  and the toluene mole fraction is found, which again does not apply to the limit  $x_{tol}\rightarrow 0$ , i.e.  $\tau_\alpha$  of neat PCB54 is slower than predicted by this simple extrapolation.

The time constants for the line shape collapse again exhibit a distinct decoupling from the PCB54 dynamics observed in dielectric spectroscopy ( $\alpha$ -process): by defining  $\langle\tau(T)\rangle = 1/\delta$  at the temperature of the inflection point in  $W(T)$ , toluene dynamics about 1.5 - 2 orders of magnitude faster than the corresponding  $\tau_\alpha$  of PCB are obtained, cf. figure 8.12. This finding is in agreement with the correlation times extracted from the  $T_1$  minima plotted in the same figure, albeit the decoupling appears even larger in the case of  $T_1$ . Apart from the inflection point also the temperature span  $0 < W(T) < 1$ , i.e. the range in which sub ensembles with correlation times in the microsecond regime can be found, is of considerable interest for the present discussion. This region is marked by the horizontal bars in figure 8.12: in this representation it becomes evident that the slowest toluene molecules in the mixtures with  $x_{tol}\leq 0.77$  reorient on the time scale of PCB54, as the high temperature end of the  $W(T)$  bar coincides with  $\tau_\alpha$  from DS for the respective concentration. Hence  $\tau_\alpha$

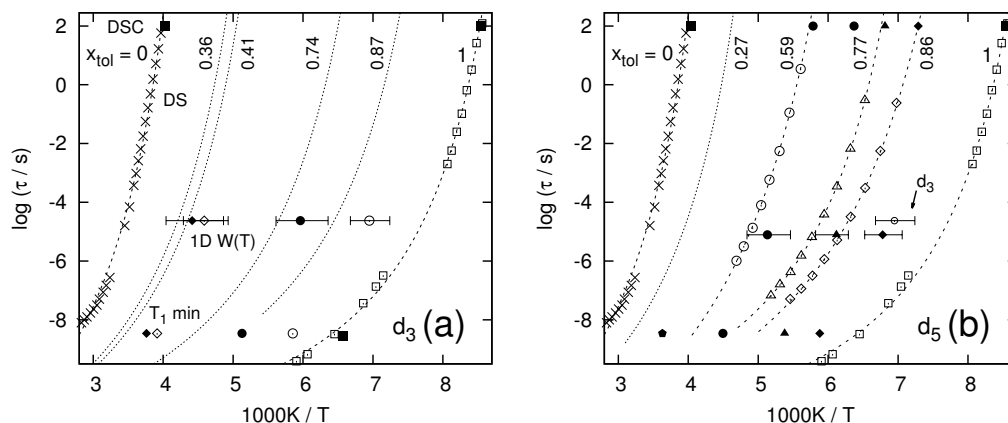


**Figure 8.12 (a):** Time constants extracted from the line shape weighting factor  $W$  (the errorbar marks beginning and end of the two-phase region:  $W(T)=0.01-0.99$ ) for different concentrations of toluene- $d_3$  in PCB54 in comparison with corresponding VFT-interpolations from dielectric spectroscopy (cf. section B.1). For comparison previous results and literature data is repeated from figure 8.8. **(b):** Same representation for mixtures of toluene- $d_5$  in PCB54.

of PCB serves as an upper bound for the correlation time of toluene in the mixtures. The samples with  $x_{tol}=0.87$  toluene- $d_3$  and  $x_{tol}=0.86$  toluene- $d_5$  exhibit a slightly different behaviour: here the time constant for the high-temperature end of the two phase region does not coincide with  $\tau_\alpha$  from DS. Instead a consistent decoupling of dynamics also for the slowest toluene sub ensembles is observed in both mixtures. As it may seem plausible that the motion of the PCB molecules in the mixtures provides a terminal relaxation time for the toluene molecules, this finding is nevertheless non-trivial. It demonstrates clearly that a number of toluene molecules find themselves in the vicinity of PCB molecules with a residence time defined by the motion of the high- $T_g$  component. Whereas the majority of toluene molecules reorient on a significantly faster time scale, i.e. the first coordination shell of toluene on PCB appears not to be subject to fast exchange any more in the microsecond regime.

### Fast motion limit effects

In the last paragraph the solid echo line shape observed in mixtures of toluene with PCB was analysed with regard to the “two phase” characteristic. In this approach any (subtle) change in the solid fraction of the spectra, i.e. the Pake pattern, was neglected.

Figure 8.13 displays the apparent spectral widths  $C_x$  (cf. section 4.2.2) for mixtures of toluene- $d_3$ , which was determined from the solid fraction of the spectra, i.e. by neglecting the central line in the two phase spectra at high temperatures. For lowest temperatures (below about 120 K) the line shape parametrized by the apparent spectral widths displays a universal, concentration independent behaviour. The change in  $C_x$  with temperature is more pronounced than in the case of toluene- $d_5$  (cf.

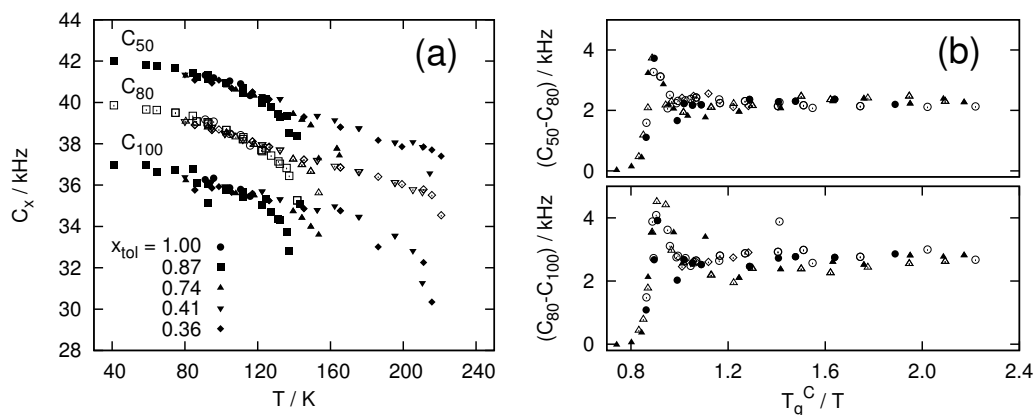


**Figure 8.13 (a):** Apparent spectral width  $C_x$  of solid echo spectra for toluene- $d_3$  in PCB54 (full symbols bottom:  $C_{100}$ , open symbols:  $C_{80}$ , full symbols top:  $C_{50}$ ). **(b):** Slope of the outer flank of the spectra quantified via  $C_{80} - C_{100}$  (bottom) and  $C_{50} - C_{80}$  (top) on a reduced temperature scale.

figure 6.31 for example), since in toluene- $d_3$  the fast methyl group rotation imposes a strong effect on the width of the spectra at lowest temperatures, whereas the line shape in toluene- $d_5$  is dominated by the  $\beta$ -process in this regime.

Around 120 K the values for the highest concentration ( $x_{\text{tol}}=0.87$ ) start to deviate from this common envelope as  $T_g$  of the mixture is approached and the spectral width is reduced more effectively by a stronger  $\beta$ -process. At higher temperatures the  $\alpha$ -process leads to a more effective narrowing of the spectra before the solid part of the two phase spectra finally vanishes. This behaviour is found in all concentrations, albeit shifted towards higher temperatures for lower toluene concentrations. Consequently the temperature of the “kink” observed in  $C_x$  yields a measure analogous to  $T_g$ :  $T_g^C$ . The finding that  $T_g^C \approx T_g$  holds for all concentrations ( $\Delta$  symbols in figure 8.6 (b)), again demonstrates that a fraction of toluene molecules reorient on the time scale of PCB in the mixtures.

The shape of the spectra determined by relative differences in  $C_x$  taken at different intensities neglects the influence of the methyl group rotation, as the latter only affects the overall width. Hence when plotted on a reduced temperature scale  $T_g^C / T$  (cf. figure 8.13 (b)), the spectral evolution with temperature appears concentration independent. Consequently the mechanism of motion appears not to be concentration dependent for the slowest toluene molecules in the mixtures.

### 8.5.3 2D exchange spectra

In the next step we address the time scale and mechanism of toluene dynamics in the millisecond regime for the present mixtures, i.e. by means of 2D  $^2\text{H}$  NMR. Hereby 2D exchange spectra will serve to provide a first overview on the mechanism of the reorientation.

In figure 8.14 the spectra of  $x_{\text{tol}}=0.74$  toluene- $d_3$  in PCB54 recorded at two tem-

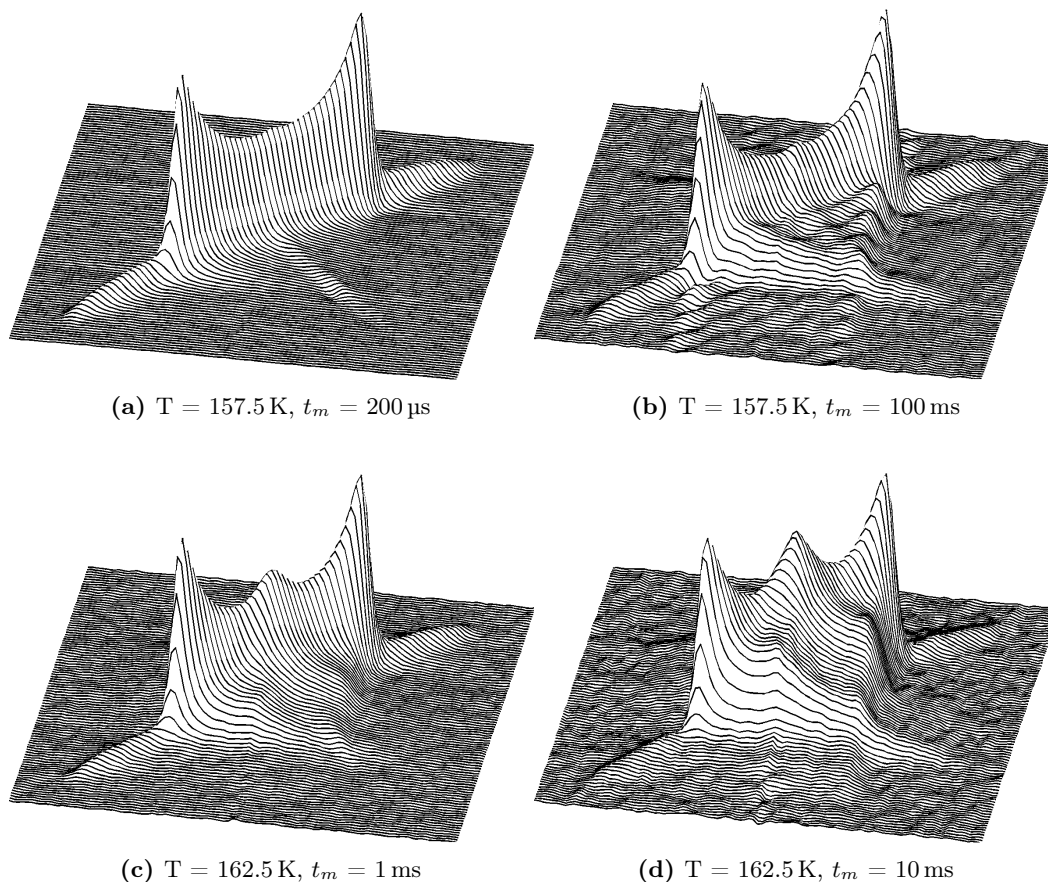


**Figure 8.14:** 2D exchange spectra of  $x_{\text{tol}}=0.74$  toluene- $\text{d}_3$  in PCB at two temperatures for various mixing times  $t_m$ .

peratures and for various mixing times  $t_m$  are displayed. At 157.5 K (figures (a) and (b)) the corresponding solid echo line shape still resembles a Pake pattern, as observed along the main diagonal of the 2D spectra. The spectrum recorded for a short mixing time of  $t_m=200\ \mu\text{s}$  exhibits no discernible exchange intensity, apart from a weak broadening of the diagonal, hence the  $\alpha'$ -process has imposed no significant correlation loss on the latter time scale. At  $t_m=100\ \text{ms}$  on the other hand the exchange intensity covers the full plane of the spectrum: the observed process is isotropic (as all possible orientations of a  $\text{C}-^2\text{H}$  bond with respect to  $\vec{B}_0$  are captured) and the spectra resemble those known from neat structural glass formers (cf. the results of cyanocyclohexane in section 6.3.7 for example). With regard to limitations due to  $T_1$  it is not feasible to obtain spectra for longer mixing times at the present temperature, i.e. we can not determine if and on which time scale full exchange of all molecules is observed.

At 162.5 K the solid echo line shape in the  $x_{\text{tol}}=0.74$  mixture exhibits already a two phase characteristic, i.e. a liquid line is observed in combination with a solid state spectrum (cf. figure 8.10), as seen again along the main diagonal in figures (c)

and (d). The observed exchange pattern in the spectra allow to draw the following conclusions regarding the dynamics of toluene in the mixtures:

- Also at 162.5 K the slowly reorienting toluene molecules undergo isotropic motion, as the arising exchange pattern covers the full 2D frequency range. The relatively faster motion, contributing to the central liquid line and intermediate spectral patterns, can however not be tracked by this type of experiment.
- The sub-ensembles with relatively fast (central line) and slow dynamics (Pake pattern) show exchange on the millisecond time scale, as distinct cross peaks between the central line and the singularities of the Pake pattern arise for both mixing times.
- Exchange between the sub ensembles takes place on the time scale of the slow motion, as the relative growth of cross peak and exchange intensity between the studied mixing times is comparable.

In conclusion the 2D exchange spectra have shown that essentially all toluene molecules reorient isotropically in the mixtures with PCB54, and that exchange between relatively fast and slow sub ensembles takes place on the same time scale. From the present analysis it is however not possible to differentiate between a scenario in which those sub ensembles are both part of a broad, continuous distribution  $G(\log \tau)$  on the one hand, or reflect a bimodal scenario on the other hand.

#### 8.5.4 Stimulated echoes – high temperature regime

For each of the prepared samples (except for the  $x_{\text{tol}}=0.27$  toluene-d<sub>5</sub> / PCB mixture) stimulated echo decays were measured for an evolution time of  $t_e=3 \mu\text{s}$  to obtain correlation times for the tumbling motion of the toluene molecules in the millisecond to second regime. Phase cycling was chosen as such that the sine-sine correlation was measured, as it allows for an extraction of  $\tau_2$  in the limit  $t_e \rightarrow 0$  (cf. section 3.4.4 for details). As typically found in mixtures of glass forming substances, a broadening of the correlation functions is also observed in the present case.

This is well seen in figure 8.15 (a), where the  $F_{t_e}^{\text{ss}}$  decays for three different toluene-d<sub>3</sub> / PCB54 mixtures are plotted: in all cases the correlation function spans the whole accessible time window, i.e. no distinct initial or final state plateau value is observed. For all three combinations of concentration and temperature  $T_1$  is approx. 40 ms and nearly exponential.  $T_{1Q}$ , the relaxation time of the spin alignment state prepared in the present pulse sequence, which can not be determined individually, is typically shorter. As  $F_{t_e}^{\text{ss}}$  has not decayed to  $F_\infty$  in any of the samples on this time scale, a reliable determination of the latter quantity is not feasible. Since the 2D exchange spectra presented in the last section however exhibited clear signs of isotropic motion in the same temperature regime and an assessment of the residual amplitude via a free fit in the stimulated echo decays of toluene-d<sub>3</sub> and toluene-d<sub>5</sub><sup>10</sup> in the present

<sup>10</sup>It is noteworthy to mention here that toluene-d<sub>5</sub> – in contrast to the low temperature regime – provides no advantage in terms of the available time window for the present experiments:  $T_1$  and  $T_{1Q}$  are typically an order of magnitude shorter in the temperature regime where  $100 \mu\text{s} < \tau < T_{1Q}$  holds (i.e. in which  $F_{t_e}^{\text{ss}}$  can be measured), as compared to  $T_1$  in mixtures with toluene-d<sub>3</sub>.

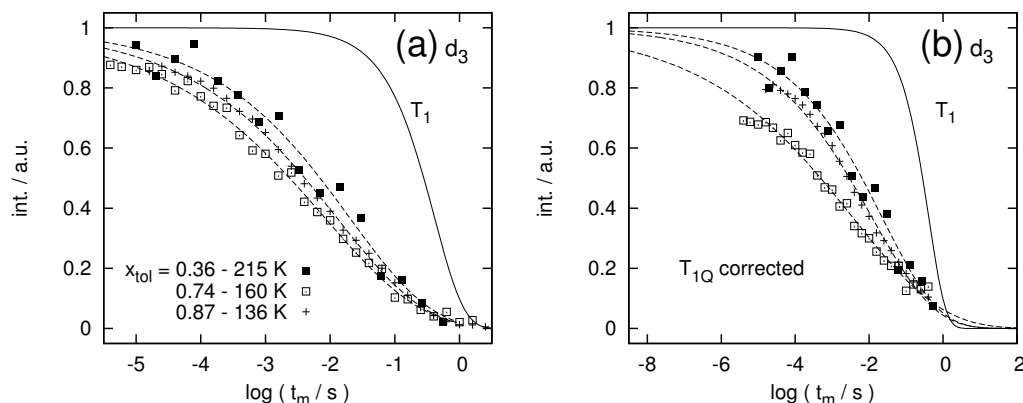


**Figure 8.15 (a):** Stimulated echo decay curves for three toluene-d<sub>3</sub> / PCB mixtures (sine-sine correlation,  $t_e = 3 \mu\text{s}$ ) at different temperatures but comparable correlation times. The solid line represents approximately  $T_1$  in all cases, the dashed lines are fits via equation 8.3. **(b):** Data of figure (a) corrected for  $T_{1Q}$  decay during  $t_m$ . The dashed lines represent (single) stretched exponential fits.

mixtures purveyed values well below 0.2, and hence on the order of what is expected for an isotropic motion (cf. figure 3.6),  $F_\infty$  was fixed to the theoretical value for an effective evolution time of  $t_e = 4.5 \mu\text{s}$  (cf. section 6.3.8) to reduce the number of free parameters.

As furthermore no distinct bi-modal behaviour was observed in any of the experiments, the stimulated echo decays were fitted via a function comprised of two stretched exponential decays:

$$F_{t_e}^{ss}(t_m) = A_0 \left[ (1 - F_\infty^{ss}) \cdot e^{(-\tau/t_m)^{\beta\tau}} + F_\infty^{ss} \right] \cdot e^{(-T_{1Q}/t_m)^{\beta T_{1Q}}}, \quad (8.3)$$

including four parameters:  $A_0$ ,  $\tau$ ,  $\beta\tau$  and  $T_{1Q}$ , as  $\beta T_{1Q}$  was fixed to the stretching observed in  $T_1$  at the same temperature. Figure 8.15 (b) displays the resulting correlation functions, i.e. the stimulated echo decays in figure (a) have been fitted via equation 8.3 and subsequently corrected for  $T_{1Q}$  decay during  $t_m$ : in this representation it becomes evident that the correlation loss spans a significantly larger time window than accessible to the experiment. Nevertheless consistent correlation times could be extracted for all investigated concentrations, cf. figure 8.16: interestingly  $\langle\tau\rangle$  of  $x_{\text{tol}} \leq 0.77$  coincides with  $\tau_\alpha$  (of the PCB54 component) from dielectric spectroscopy. This experimental finding is in contrast to our previous <sup>2</sup>H NMR results, as the correlation times determined from the  $T_1$  minimum and the two phase spectra in the region of the line shape collapse exhibited a distinct decoupling from  $\tau_\alpha$  of PCB54. In the analysis of the solid echo line shape we found that  $\tau_\alpha$  of PCB54 provides an upper bound for  $\tau_{\alpha'}$  of toluene, whereas the present experiment yields  $\langle\tau_\alpha\rangle \approx \langle\tau_{\alpha'}\rangle$ . The finding that this relation does not hold for the mixtures with  $x_{\text{tol}} = 0.86-0.87$  is however in accordance with our previous results: the apparent decoupling between  $\langle\tau_\alpha\rangle$  and  $\langle\tau_{\alpha'}\rangle$  observed here is consistent with the observations made in the line shape analysis, where the temperature for the first

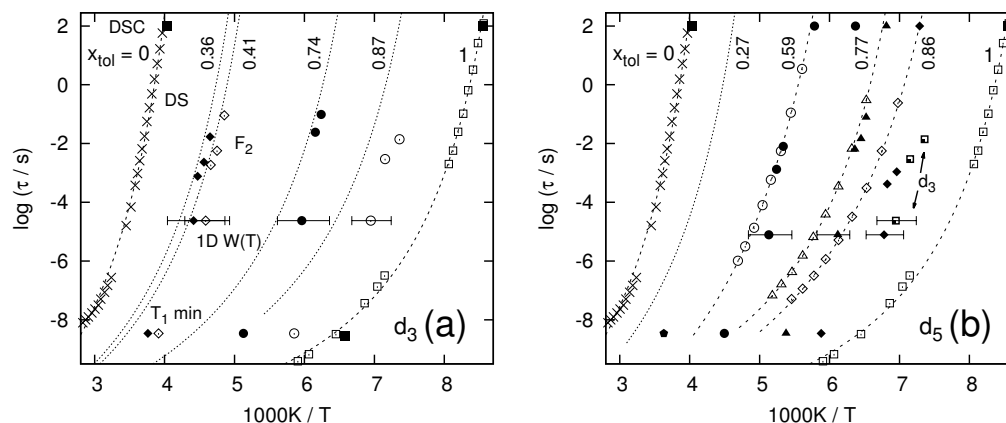


**Figure 8.16 (a):** Average correlation times from stimulated echo decays ( $\tau$  in the millisecond to second regime, sine-sine correlation,  $t_e = 3 \mu\text{s}$ ) for mixtures of toluene- $d_3$  in PCB. Additionally plotted are the corresponding correlation times from  $W(T)$  and the  $T_1$  minimum for each concentration. The dotted lines represent an interpolation of  $\tau_\alpha$ , cf. figure B.1. **(b):** Same representation for toluene- $d_5$  in PCB in comparison with dielectric results. The results of  $x_{\text{tol}}=0.87$  toluene- $d_3$  from figure (a) are repeated as partially filled squares.

appearance of a solid state spectrum did also not coincide with  $\tau_\alpha(T) = 1/\delta$  from dielectric spectroscopy for concentrations of  $x_{\text{tol}}=0.86-0.87$ .  $\tau_\alpha'$  furthermore exhibits lower temperature dependence, i.e. appears less fragile, in the latter concentrations compared to mixtures with lower toluene content.

As mentioned at the beginning of this section, the correlation functions of toluene in the mixtures are more stretched with respect to the data of neat toluene: figure 8.17 displays the stretching parameters  $\beta_K$  from the  $F^{\text{ss}}$  measurements vs. the corresponding correlation time  $\langle\tau\rangle$ . Although the data exhibit rather large spread, a distinct concentration dependence can be observed: the samples with highest toluene content ( $x_{\text{tol}}=0.86$  and  $0.87$ ) exhibit slightly broader correlation functions than observed in the neat system ( $\beta_K \approx 0.45$  opposed to  $0.5$  in neat toluene). For

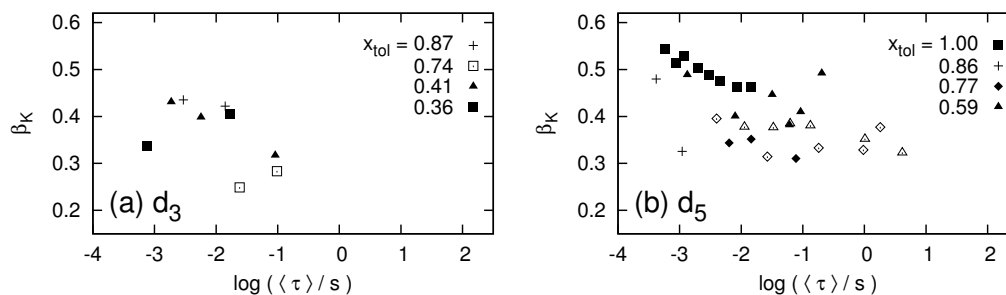


**Figure 8.17 (a):** Stretching parameters  $\beta_K$  from a fit via equation 8.3 to  $F^{\text{ss}}$  for mixtures of toluene- $d_3$  in PCB54, plotted versus the corresponding correlation time  $\langle\tau\rangle$ . **(b):** Same representation for the toluene- $d_5$  containing mixtures. Open symbols from  $F^{\text{cc}}$  measurements, data of neat toluene from Hinze et al. [Hinze 1998].

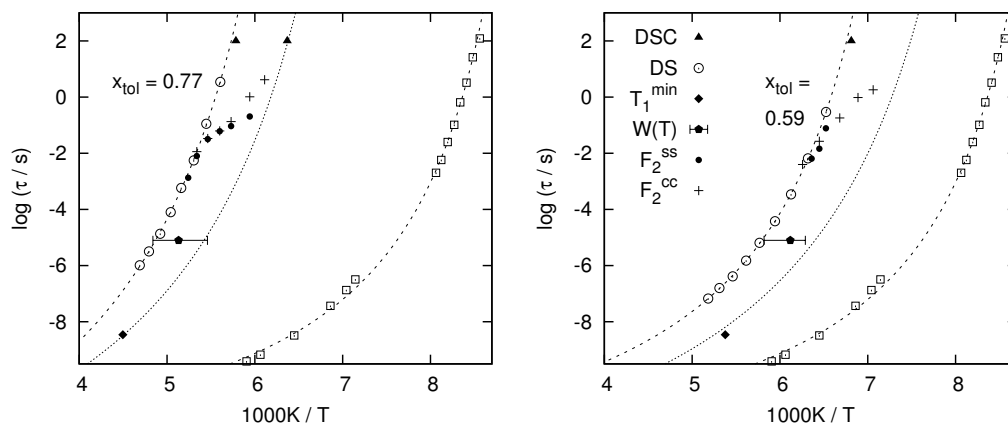


**Figure 8.18:** Repetition of figure 8.16 (b) with additional time constants extracted from  $F_{t_e}^{cc}$  ("+", cosine-cosine correlation,  $t_e=3\ \mu\text{s}$ ) for two concentrations of toluene-d<sub>5</sub> in PCB54. The key holds for both figures.

intermediate concentrations the broadening effect becomes more pronounced, with stretching parameters  $\beta_K$  of about 0.25 to 0.35 for  $x_{\text{tol}}=0.74$  and 0.77 – at lower concentrations however this trend reverses and the mixtures with  $x_{\text{tol}}\leq 0.59$  yield again  $\beta_K$  values of about 0.4 and above. This effect can also be seen in the correlation functions displayed in figure 8.15, as the  $F_{t_e}^{ss}$  decay in the mixture with  $x_{\text{tol}}=0.74$  appears broader than in the case of  $x_{\text{tol}}=0.87$  and 0.36.

This experimental finding is rather surprising as it contradicts the results from dielectric spectroscopy and the analysis of the two phase spectra: in DS the width of the  $\alpha$ -peak increases<sup>11</sup> towards lower toluene concentrations, cf. figures 8.4 and B.2<sup>12</sup>, the same holds for the temperature range in which two phase spectra are observed, cf. figure 8.11 (a). The mixture of  $x_{\text{tol}}=0.59$  toluene-d<sub>5</sub> in PCB54 for example yields stretching parameters comparable to the ones found in neat toluene-d<sub>5</sub>, cf. figure 8.17 (b), the mixture however exhibits two phase spectra over a broad temperature range, whereas the neat system (presumably) does not. One plausible explanation of this finding lies in the time window of the stimulated echo technique: as demonstrated in figure 8.15 we are not able to ascertain that the full correlation loss of all toluene molecules is tracked by the experiment.

To slightly extend the time window of the experiment towards longer times  $t_m$ , also cosine-cosine correlation functions  $F^{cc}$  were measured in the toluene-d<sub>5</sub> containing samples. Apart from  $T_1$  being (slightly) longer than  $T_{1Q}$ , the former can be obtained via a different experiment – whereas  $T_{1Q}$  is only accessible from  $F^{ss}$ . Therefore a straightforward correction of the damping via spin-lattice relaxation during  $t_m$  is obtained and hence the correlation function can be monitored towards longer times and the stretching parameter  $\beta_K$  is determined with better accuracy. One drawback of the cosine-cosine correlation in the stimulated echo experiment is however, that it

<sup>11</sup>Again: the  $\alpha'$ -process of toluene was not unambiguously resolved by means of dielectric spectroscopy due to the low dipole moment of toluene.

<sup>12</sup>Which however poses a contradiction to the rather narrow dielectric loss peak observed in neat PCB54.

does not yield  $F_2$  in the limit  $t_e \rightarrow 0$ <sup>13</sup>. We measured the cosine-cosine part of the stimulated echo for an evolution time of  $t_e = 3 \mu\text{s}$ <sup>14</sup> and fitted the decay via

$$F_{t_e}^{cc}(t_m) = A_0 \left[ (1 - F_{\infty}^{cc}) \cdot e^{(-\tau/t_m)^{\beta\tau}} + F_{\infty}^{cc} \right] \cdot e^{(-T_1/t_m)^{\beta T_1}}. \quad (8.4)$$

As again the theoretical value of  $F_{\infty}$  was employed and  $T_1, \beta T_1$  at the given temperatures are known, equation 8.4 contains only three free parameters:  $\tau, \beta$  and  $A_0$ . The resulting correlation times are displayed in figure 8.18: at high temperatures we found  $\langle \tau \rangle$  and  $\beta_K$  (open symbols in figure 8.17 (b)) from  $F^{cc}$  to be in agreement with our previous results from  $F^{ss}$ , i.e. also  $F_{t_e}^{cc}$  yields  $\langle \tau_{\alpha} \rangle \approx \langle \tau_{\alpha'} \rangle$  at high temperatures. At lower temperatures (where in the case of  $F^{ss}$  a stable correction for  $T_{1Q}$  is no longer possible) the time constants from the cosine-cosine decays deviate from the VFT behaviour of  $\tau_{\alpha}$  and follow an almost Arrhenius temperature dependence, whereas the stretching  $\beta_K$  remains comparable to the high temperature values. This clearly demonstrates that also at low temperatures a fraction of toluene molecules exhibits dynamics on a time scale considerably shorter than the PCB motion observed in dielectric spectroscopy. Albeit reported for other binary glass forming systems [Blochowicz 2011], the observed temperature dependence of  $\langle \tau \rangle$  not necessarily reflects a fragile-to-strong transition of the toluene dynamics in this regime: also in case of  $F^{cc}$  we can not ascertain that the full correlation loss is captured by the experiment, the temperature dependence of  $\langle \tau \rangle$  may as well be explained by time window effects. Interestingly however, an extrapolation of  $\langle \tau \rangle$  from  $F^{cc}$  in the mixture with  $x_{\text{tol}} = 0.59$  is in agreement with the second  $T_g$  obtained from the low temperature step in the heat capacity of the same concentration.

### Geometry of the toluene dynamics upon mixing

In section 8.5.3 we demonstrated by means of 2D exchange spectra that the dynamics of toluene in the mixtures with PCB54 remains isotropic. To obtain further information on the detailed mechanism of reorientation, we will employ the evolution time dependence of the stimulated echo experiment (cf. sections 3.4.4 and 4.2.1 for details) for the sample with  $x_{\text{tol}} = 0.77$  toluene- $d_5$  in PCB54. Again the cosine-cosine correlation was chosen, as  $F_{t_e}^{cc}$  data for neat toluene is available in literature [Hinze 1998]. Due to the broadening of the correlation functions in the present mixtures, it is again not feasible to extract the residual amplitude  $F_{\infty}$  of the stimulated echo due to interference with  $T_1$ , as demonstrated in figure 8.19 (a). Hence again the theoretical value of  $F_{\infty}^{cc}(t_e; \delta)$  (cf. figure 3.6) for each effective evolution time<sup>15</sup> was employed to reduce the number of free parameters and obtain a stable fit. Consequently all stimulated echo curves were fitted via equation 8.4

<sup>13</sup> $F_{\infty}$  of the cosine-cosine correlation approaches one in this limit and hence no correlation loss can be observed, cf. section 3.4.4 for details.

<sup>14</sup>Which for the used pulse lengths corresponds to an effective evolution time of  $4.5 \mu\text{s}$ , i.e. the theoretical residual amplitude of  $F^{cc}$  for an isotropic motion is about 0.05 and hence correlation loss can be measured.

<sup>15</sup>For the applied sequence and pulse lengths the effective evolution time was determined via  $F_{\infty}^{ss}(t_e; \delta)$  of cyanocyclohexane in section 6.3.8. We found that for the present set-up the effective evolution time is  $1.5 \mu\text{s}$  longer than  $t_e$  applied in the pulse sequence.

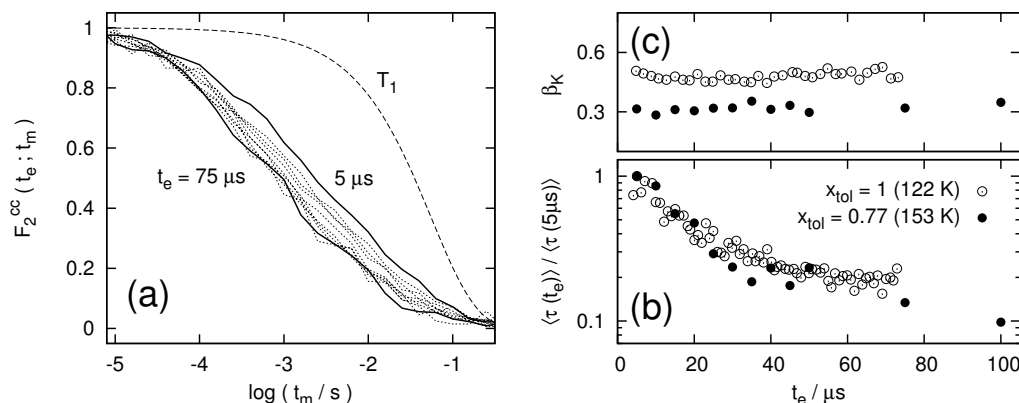


**Figure 8.19 (a):** Stimulated echo decay curves (Zeeman) for different evolution times  $t_e$  of the  $x_{\text{tol}}=0.77$  toluene- $d_5$  in PCB54 sample recorded at 153.3 K (the dashed line symbolises the magnetization curve at that temperature). **(b):** Normalized  $t_e$  dependent correlation times from stretched exponential fits to the curves presented in (a) ( $\langle \tau_c \rangle \approx 240$  ms) in comparison with data of neat toluene [Hinze 1998] recorded at a different temperature ( $\langle \tau_c \rangle \approx 15$  ms). **(c):** Corresponding stretching parameters  $\beta_K$ .

with the parameters  $\tau$ ,  $\beta_K$  and  $A_0$ . The resulting  $\langle \tau \rangle$  and  $\beta_K$  values obtained in this manner are displayed in figure 8.19 (b) and (c) respectively.  $\langle \tau(t_e) \rangle$  of neat toluene shows the typical behaviour of a supercooled liquid, which is similar to the one discussed in the case of cyanocyclohexane, i.e. can be modelled by a weighted superposition of small- and large-angular reorientation, as suggested by Hinze et al. The obtained  $\beta_K$  values for the  $x_{\text{tol}}=0.77$  toluene- $d_5$  / PCB mixture are again considerably lower at all evolution times with respect to the neat system and in agreement with our previous results. The individual correlation times  $\langle \tau(t_e) \rangle = \tau / \beta \cdot \Gamma(\beta^{-1})$  are normalized with respect to  $\langle \tau(5\mu s) \rangle$  in figure 8.19 (b): in this representation it becomes obvious that both samples exhibit almost identical evolution time dependence in the stimulated echo decay. Hence the microscopic mechanism of toluene reorientation appears unaltered in mixtures with PCB54: any model applicable for the  $\alpha$ -process of neat toluene also holds for the observed dynamics in the present mixtures<sup>16</sup>.

## Conclusions

In summary the presented 2D  $^2\text{H}$  NMR experiments elucidate a number of points regarding the dynamics of toluene in the mixtures with PCB54, but also raise further questions: in the millisecond regime a substantial fraction of toluene molecules reorients on the time scale of the  $\alpha$ -process, i.e. a sub ensemble of toluene is no longer decoupled from the PCB54 motion at this temperature. This does however not hold for all toluene molecules, as the  $F^{\text{cc}}$  measurements detected dynamics substantially

<sup>16</sup>In part I of this work we have demonstrated that the  $t_e$ -dependence of the stimulated echo is very sensitive with regard to the time window of the experiment, as  $\langle \tau \rangle$  and  $T_1$  of neat toluene and the  $x_{\text{tol}}=0.77$  mixture are however comparable at the selected temperatures, the results nevertheless clearly rule out any drastic change in the motional process.

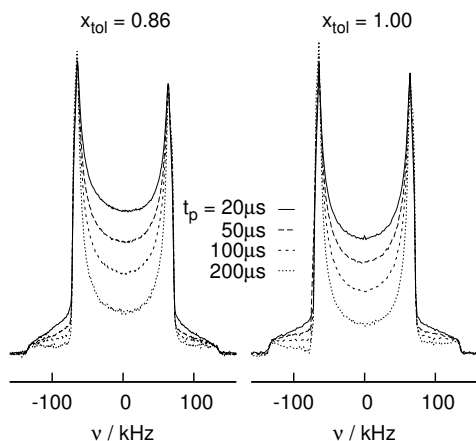


**Figure 8.20:** Solid echo spectra of  $x_{\text{tol}}=0.86$  toluene- $d_5$  in PCB54 and neat toluene- $d_5$  [Vogel 2000a] at  $T=107$  K for different inter pulse delays  $t_p$ . The  $t_p$ -dependent line shape changes imposed by the  $\beta$ -process are similar in both samples.

faster than  $\tau_\alpha$  at lower temperatures. The mechanism via which the tumbling motion of toluene agitates (in the ms regime) appears unchanged in the  $x_{\text{tol}}=0.77$  mixture with respect to the neat system.

The correlation functions in the mixtures are slightly broadened with respect to neat toluene, an effect which appears to retract again at low toluene concentration. Albeit we were unable to observe any bi-modal behaviour in  $F^{\text{ss}}$ , this does however not exclude a scenario with two distinct toluene relaxations in the mixtures: due to the narrow time window of the technique potentially not all toluene molecules are observed in a single experiment.

Before any conclusions can be drawn, we will analyse the dynamics of the  $\beta$ -process at low temperatures. Due to the lack of a fast exchange mechanism, this analysis is promising with regard to the observation of a distinct bimodal behaviour of toluene in the present mixtures.

### 8.5.5 Solid echo line shape – low temperature regime

So far we have intensively discussed the high temperature  $^2\text{H}$  NMR results in the mixtures of toluene with PCB54, i.e. at  $T > T_g$ , where a pronounced decoupling of the toluene dynamics from the dielectric results of PCB54 was observed for a fraction of molecules in all experiments. The two phase spectra in section 8.5.2 and the stimulated echo measurements in section 8.5.4 on the other hand demonstrated that some toluene molecules reorient on the time scale of  $\tau_\alpha$ , i.e. of PCB54, whereas the 2D exchange spectra in section 8.5.3 showed that exchange between the different sub ensembles exists. Although the results point towards a bi-modal scenario with the arise two toluene fractions, it is possibly due to this effective exchange mechanism at high temperatures in combination with the limited time window of  $^2\text{H}$  NMR that no distinct bi-modality was observed so far. In the remainder of this chapter we will now focus on the low temperature dynamics in the system, i.e. the concentration dependence of the  $\beta$ -process. In the temperature regime  $T \leq T_g$  no effective exchange takes place on the experimental time scale and as the  $\alpha$ - and  $\beta$ -process in glass formers are suspected to be coupled [Böhmer 2006], a detailed study of the  $\beta$ -process could serve to answer some of the open questions with regard to the microscopic

dynamics in binary mixtures.

At temperatures  $T \leq T_g = 117$  K of neat toluene all samples exhibit a broad solid state spectrum with only subtle temperature dependence in this regime. As demonstrated in sections 4.3 and 6.3.4 line shape effects due to the restricted, small angular motion of the  $\beta$ -process can be observed by prolonging the inter pulse delay  $t_p$ . Figure 8.20 displays the solid echo spectra of  $x_{\text{tol}}=0.86$  toluene-d<sub>5</sub> in PCB54 and neat toluene-d<sub>5</sub> at  $T=107$  K for different inter pulse delays: the observed  $t_p$ -dependence in both samples is analogous. This finding is in accordance with the results from dielectric spectroscopy and  $T_1$  measurements of toluene-d<sub>5</sub> in PCB, which detected the unaltered  $\beta$ -process of neat toluene for  $x_{\text{tol}} \geq 0.77$ . At lower toluene contents however the spin lattice relaxation time exhibits a distinct concentration dependence, which is also reflected in the  $t_p$ -dependence of the solid echo line shape. Figure 8.21 displays spectra for different concentrations (columns) and temperatures (rows) of toluene-d<sub>3</sub><sup>17</sup> in PCB54 for inter pulse delays of  $t_p=20$   $\mu\text{s}$  (full lines) and 200  $\mu\text{s}$  (dashed lines): the samples with  $x_{\text{tol}}=0.87$  and 0.74 exhibit a  $t_p$ -dependence analogous to the one of neat toluene at all given temperatures, and therefore clear signs for the presence of an unaltered (in terms of time scale and geometry)  $\beta$ -process in the mixtures. Although for samples with lower toluene content the change with temperature is qualitatively the same, the magnitude of the effect decreases noticeably with lowering the toluene concentration: in case of  $x_{\text{tol}}=0.41$  still a difference in the intensities around zero frequency of the spectra recorded for  $t_p=20$   $\mu\text{s}$  and 200  $\mu\text{s}$  exists, although much more subtle than observed for higher concentrations. In the sample containing  $x_{\text{tol}}=0.36$  toluene-d<sub>3</sub>, the lowest concentration studied, the effect is however no longer apparent – although the signal to noise ratio is comparable.

To quantify the spectral evolution with temperature and  $t_p$  we will again employ the line shape parameter  $R(t_p)$ , which measures the relative spectral intensity at zero frequency (cf. sections 4.2.2 and 4.3) and provides a measure analogous to  $T_2$  in the low temperature regime. As demonstrated in figure 8.22 (a) and (b), the  $R(t_p)$  and  $\langle T_2 \rangle$  values in all concentrations coincide at lowest temperatures with results for the neat system. At higher temperatures a distinct minimum arises in both quantities at about 110 K, where the condition  $\tau_\beta = 1/\delta$  for the  $\beta$ -process of neat toluene is approached. In the neat system the observation of such a minimum is obscured by the onset of the  $\alpha$ -process, which leads to a collapse of the solid state spectrum and a strong reduction in  $T_2$ . Apart from the obvious shift in  $T_g$ , and consequently the temperature at which effects of the  $\alpha$ -process are observed in  $R(t_p)$  and  $T_2$ , a distinct concentration dependence is observed in both quantities: whereas the temperature of the minimum remains constant, the minimum value grows significantly at low toluene concentrations, i.e.  $T_2$  becomes longer and the line shape changes less pronounced. This behaviour is anticipated if the time scale of the  $\beta$ -process appears unaltered in the mixtures, whereas the relaxation strength changes with concentration.

For a more detailed analysis of the concentration dependence we present a series of  $R(t_p)$  decays for three concentrations of toluene-d<sub>5</sub> in PCB measured at the same temperature (107 K) in figure 8.23 (a). As the decay in  $R(t_p)$  appears concentration

<sup>17</sup>Most of the line shape analysis at low temperatures is conducted on the samples containing toluene-d<sub>3</sub> due to the conveniently short spin lattice relaxation time of the compound.

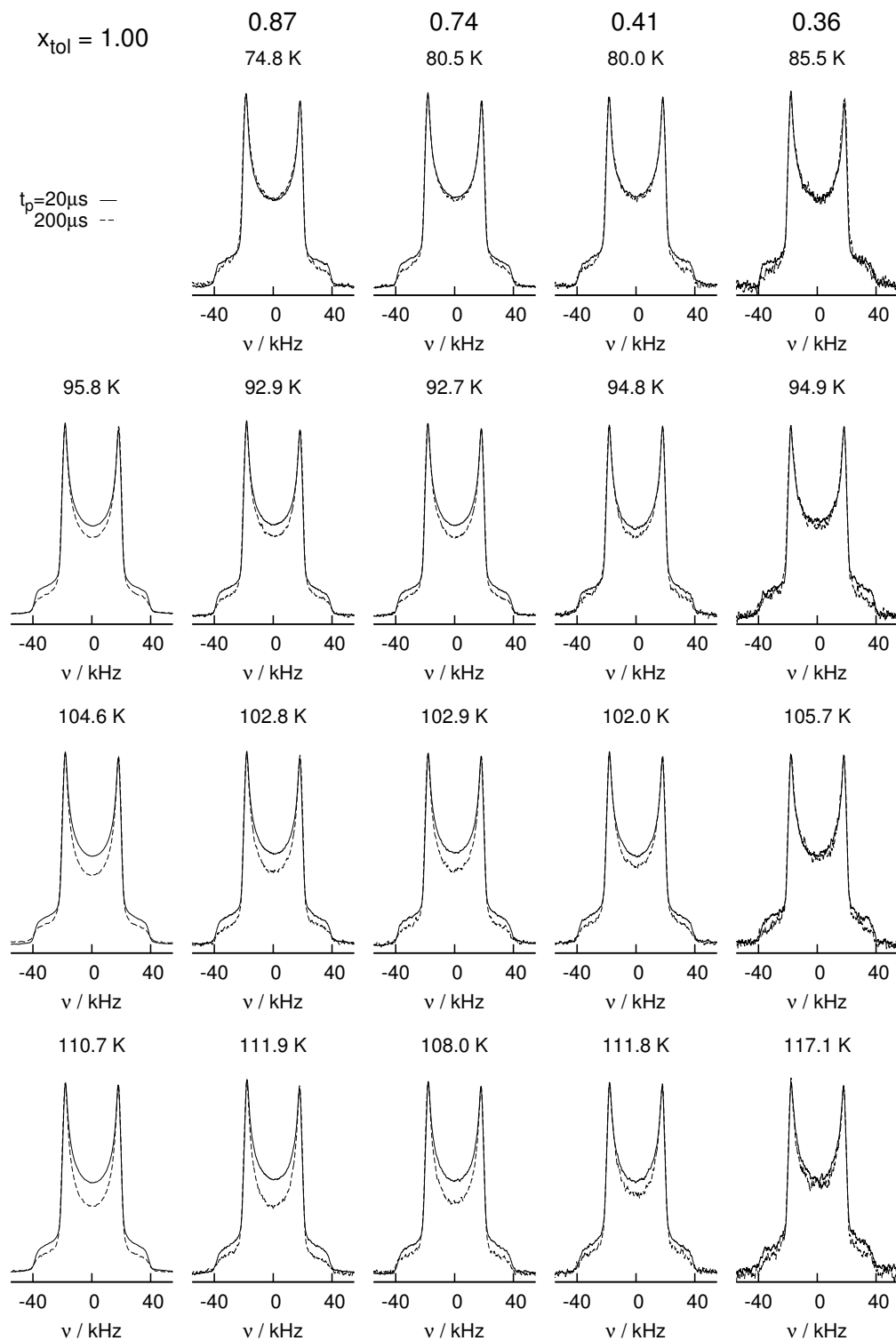


**Figure 8.21:** Solid echo spectra of toluene-d<sub>3</sub> in PCB54 for different concentrations (columns) at similar absolute temperatures (rows), each for  $t_p = 20 \mu\text{s}$  (solid line) and  $t_p = 200 \mu\text{s}$  (dashed line).

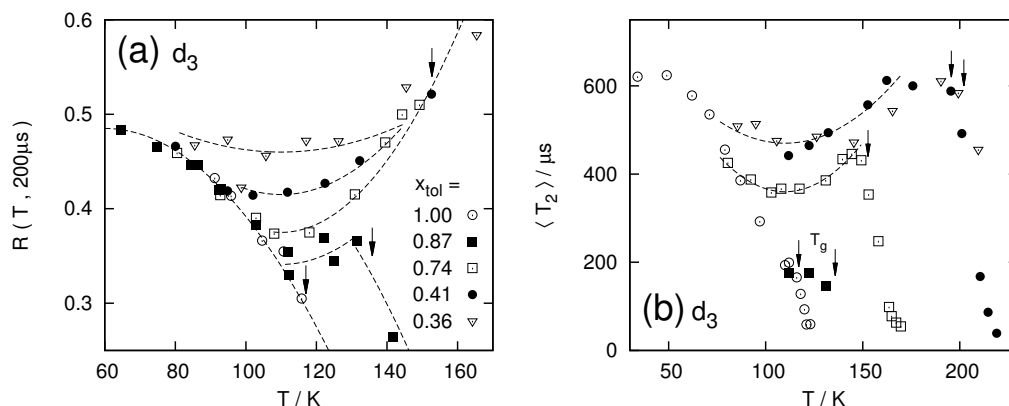


**Figure 8.22 (a):** Relative spectral intensity at zero frequency  $R(t_p=200 \mu\text{s})$  for different concentrations of toluene- $d_3$  in PCB54. The arrows mark  $T_g$  for  $x_{\text{tol}}=1, 0.87$  and  $0.74$ . The lines serve as guide for the eye. **(b):** Average spin-spin relaxation times  $\langle T_2 \rangle$  of toluene- $d_3$  in PCB54. Data of neat toluene ( $\circ$ ) [Vogel 2000a] from toluene- $d_5$ , lines serve as guide for the eye. For corresponding stretching parameters  $\beta_K$  see section B.3.

independent except for a plateau arising at long  $t_p$  and low toluene contents, the data were fitted in a phenomenological approach via the superposition of a stretched exponential function and a plateau value  $1-f_\beta$ :

$$R'(t_p, x_{\text{tol}}) = R_0 \left[ f_\beta(x_{\text{tol}}) \cdot \exp\left(-\left(\frac{t_p}{\tau}\right)^\beta\right) + (1 - f_\beta(x_{\text{tol}})) \right]. \quad (8.5)$$

$\tau$  and  $\beta$  are fit parameters,  $R_0$  accounts for the rigid limit spectrum at  $t_p \rightarrow 0$  and the (presumably temperature dependent) parameter  $f_\beta(x_{\text{tol}})$  denotes any concentration dependence in the relaxation strength of the  $\beta$ -process. As demonstrated in figure 8.23 (a) the description via a single set of  $\tau, \beta$  (dashed lines) works well in all concentrations, affirming concentration independence of  $\tau_\beta$ . The obtained fit parameter  $f_\beta$  allows us to quantify the change regarding the secondary relaxation upon mixing. The values in figure 8.23 (b) show that the relaxation strength  $1-S$  of the  $\beta$ -process in pure toluene is virtually maintained down to a threshold concentration of about  $x_{\text{tol}}=0.8$ , at lower toluene content  $1-S$  exhibits a strong concentration dependence.

A similar analysis has been conducted for the mixtures containing toluene- $d_3$ , where the minimum values of  $R(t_p)$  (from the dashed lines in figure 8.22 (a)) were modelled via equation 8.5 (open circles in figure 8.23 (b)), furthermore random walk simulations of the spectra at 103 K have been conducted to determine  $f_\beta$  (filled triangles). The obtained results exhibit in both cases the same concentration dependence as found in mixtures of toluene- $d_5$  at 107 K. Hence so far all  $^2\text{H}$  NMR results in the low temperature regime,  $T \leq T_g=117 \text{ K}$  of neat toluene, yield indications for a heterogeneous nature of the  $\beta$ -process in mixtures with  $x_{\text{tol}} \leq 0.77$ .

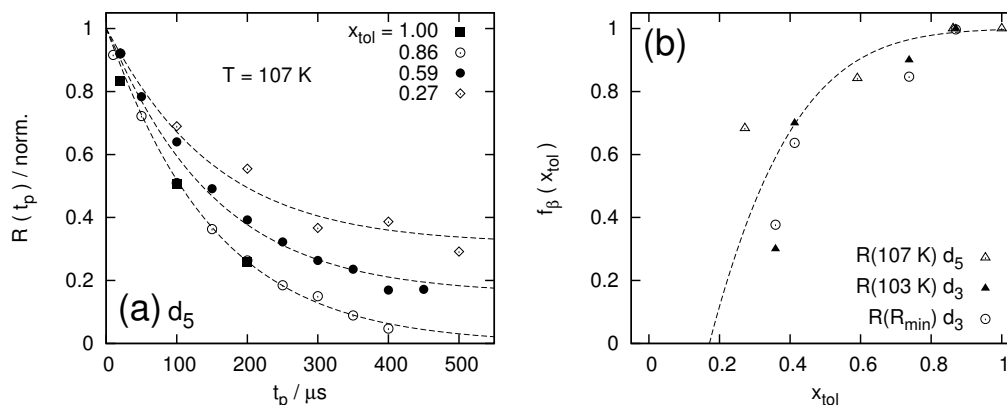


**Figure 8.23 (a):** Normalized inter pulse dependence of the  $R(t_p)$  value for different concentrations of toluene- $d_5$  in PCB54 at  $T=107 \text{ K}$ . Data of neat toluene from C. Tschirwitz [Tschirwitz 2001]. The lines represent fits via equation 8.5. **(b):** Concentration dependence of the toluene fraction  $f_\beta$ , which exhibits the unmodified  $\beta$ -process of neat toluene in the mixtures at low temperatures.

### Fast motion limit effects

We end the discussion of the solid echo line shape in mixtures of toluene and PCB54 with an outlook regarding the fast motion limit line shape effects of the  $\beta$ -process. In cyanocyclohexane we observed, due to the fast and non-merging  $\beta$ -process in the system, in addition to the  $R(t_p)$  minimum at  $T < T_g$  also pronounced fast motion limit effects of the  $\beta$ -process above  $T_g$  (cf. figure 6.9 (c)). This peculiar line shape for  $t_p=20 \mu\text{s}$  was accompanied by a distinct effect in the  $t_p$ -dependence of the solid echo experiment: for prolonged inter-pulse delays the rigid limit slope of the inner singularities was (partially) recovered. We attributed this behaviour to small angular displacements due to the  $\alpha$ -process (cf. section 6.4.3), that are only observed if the spectra for short  $t_p$  significantly deviate from the rigid limit Pake spectrum (i.e. if a fast and strong  $\beta$ -process is present). The same effect is also observed in the mixtures of toluene with PCB54, although less pronounced. Figure 8.24 displays a detail around the inner singularity of spectra for  $x_{\text{tol}}=0.87$  toluene- $d_3$  in PCB: the subtle effects around the inner singularities resemble those observed in cyanocyclohexane slightly above  $T_g$ . For lower concentrations ( $x_{\text{tol}}=0.41$ , right part of the figure) the effect is absent at even much higher temperatures, as the respective temperature is still below  $T_g$  in this mixture.

Consequently the analysis of the  $\beta$ -process in cyanocyclohexane remains valid also for the present mixtures of toluene: spectra recorded at temperatures above  $T_g$ , where the relaxation strength of the  $\beta$ -process is enhanced and  $\tau_\beta \ll 1/\delta$ ,  $\tau_\alpha > 1/\delta$  holds, exhibit distinct and rather universal effects. For most neat glass forming systems it is however not possible to fulfil all three conditions at the same temperature, hence the observation of such line shapes is hampered.

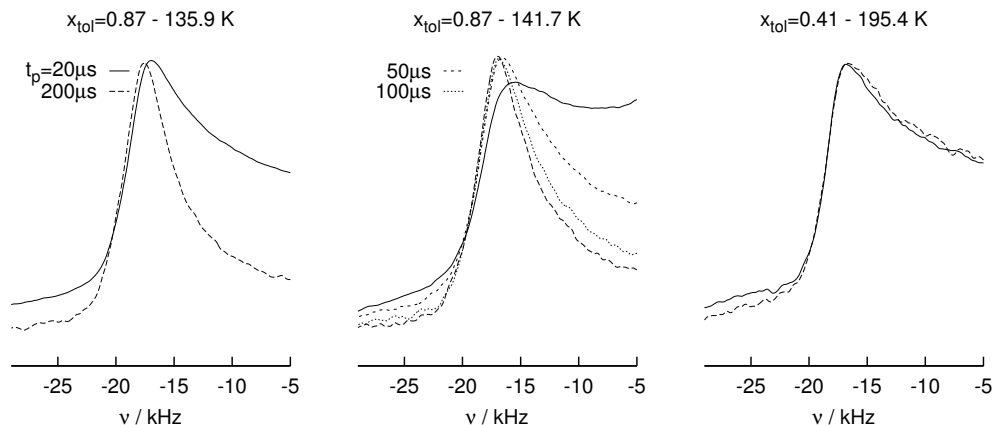


**Figure 8.24:** Detail around the lower inner singularity of solid echo spectra of toluene- $d_3$  in PCB54 for different concentrations and inter pulse delays  $t_p$ . The  $t_p$ -dependent line shape in the high concentrations resembles the behaviour observed in cyanocyclohexane.

### 8.5.6 Stimulated echoes – low temperature regime

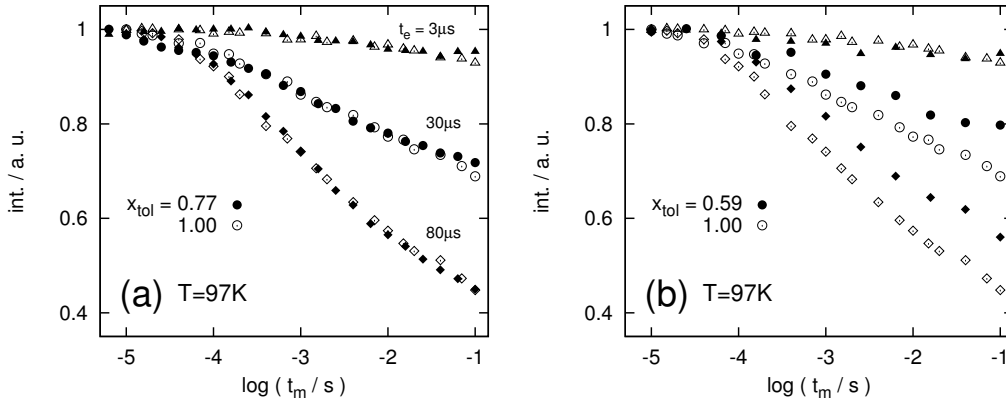
To further analyse the concentration dependence of the  $\beta$ -process – especially to differentiate between a heterogeneous and a homogeneous scenario – the cosine-cosine part of the stimulated echo was measured for a set of evolution times at low temperatures, i.e. we repeated the analysis of neat toluene by M. Vogel [Vogel 2000a] (cf. section 6.3.6 in part I of this work) in the present mixtures.

Figure 8.25 displays the stimulated echo decay curves for three different evolution times in case of the  $x_{\text{tol}}=0.77$  and 0.59 toluene- $d_5$  in PCB54 samples in comparison with data of neat toluene, recorded at the same absolute temperature  $T=97$  K. Whereas the  $x_{\text{tol}}=0.77$  mixture yields the same results as neat toluene, the sample with lower toluene content shows a larger residual amplitude for long evolution times, i.e. less correlation loss due to the  $\beta$ -process. An analysis in the scope of section 6.3.6, i.e. application of  $T_1$  correction and subsequent fit via a bi-modal, stretched exponential decay<sup>18</sup>

$$F_{t_e}^{\text{cc}}(t_m) = A_0 \left[ (1 - C_{t_e}^{\text{cc}}) \cdot e^{(-\tau/t_m)^\beta} + C_{t_e}^{\text{cc}} \right] \cdot e^{(-\tau_{SD}/t_m)^{\beta_{SD}}}, \quad (8.6)$$

yields comparable time constants  $\langle \tau \rangle$  for all measured concentrations ( $x_{\text{tol}}=0.27, 0.59$  and 0.77):  $9.2 \pm 2.4$  ms for an evolution time of  $30 \mu\text{s}$  and  $5.2 \pm 0.7$  ms for  $t_e=80 \mu\text{s}$ . In case of the neat system Vogel et al. found 10.5 ms for  $t_e=30 \mu\text{s}$  and 4.1 ms for  $80 \mu\text{s}$  – which demonstrates again the concentration independence of  $G(\log \tau_\beta)$ . The residual amplitude  $C_{t_e}^{\text{cc}}$  in equation 8.6 however exhibits a strong concentration dependence below  $x_{\text{tol}}=0.77$ , as seen in figure 8.26 (a): while  $C_{t_e}^{\text{cc}}$  for  $x_{\text{tol}}=0.77$  at 97 K coincides with the data of neat toluene, the samples with lower toluene content exhibit a significantly weaker short time decay in  $F^{\text{cc}}$  (the concentration dependence is depicted again in figure 8.26 (c)). At 115 K the quality of data is worse, furthermore

<sup>18</sup>The long time decay due to spin diffusion at  $t_m \geq 100$  ms is omitted in figure 8.25, cf. figure 6.14 for the full data set of neat toluene.



**Figure 8.25 (a):** Stimulated echo decay curves ( $F_{t_e}^{cc}$ ) of  $x_{\text{tol}}=0.77$  toluene- $d_5$  in PCB54 for different evolution times recorded at 97 K in comparison with data of neat toluene [Vogel 2000a]. **(b):** Same representation in case of the  $x_{\text{tol}}=0.59$  sample.

are the different samples expected to show in addition a concentration dependent contribution of the (elementary step of the)  $\alpha'$ -process, consequently we will restrict further discussion to the results obtained at 97 K.

For a detailed analysis of the concentration dependence of  $C_{t_e}^{cc}$  we have to remind the reader that the decay observed for relatively short evolution times ( $t_e=30 \mu\text{s}$ ) is mostly determined by the geometry of the process and hence – in case of a motion on or within a cone – defined by the distribution of opening angles  $G(\chi)$  (as demonstrated by M. Vogel [Vogel 2000a] by means of random walk simulations, cf. also chapter 4). Whereas the experiment becomes increasingly sensitive on the elementary step of the motion for longer evolution times. Consequently the initial decay at  $t_e=30 \mu\text{s}$  can be modelled by a simple random jump process with according geometry, whereas the model for  $t_e=80 \mu\text{s}$  has to account for the small angular jumps via which the  $\beta$ -process is suspected to progress in the system.

This behaviour can be exploited to elucidate the nature of the concentration dependence of the  $\beta$ -process observed so far, i.e. to differentiate between a homogeneous and a heterogeneous scenario. In a homogeneous scenario the geometry (and probably mechanism) of the  $\beta$ -process changes in a uniform manner for all molecules at low toluene concentrations, a heterogeneous model on the other hand depicts the arise of a fraction of molecules which are “rigid” on the time scale of the experiment, i.e. do no longer exhibit the  $\beta$ -process of pure toluene, whereas the remainder of molecules maintains the exact behaviour of the neat system. If the latter scenario is found, then the overall concentration dependence can be described in terms of the mobile fraction  $f_\beta$ :

$$C_{t_e}^{cc}(x_{\text{tol}}) = f_\beta(x_{\text{tol}}) C_{t_e}^{cc}(x_{\text{tol}} = 1). \quad (8.7)$$

Consequently the geometrical factor  $p(t_e)$  (cf. section 6.3.6), quantifying the evolution time dependence of  $C_{t_e}^{cc}$ , remains constant as the factor  $f_\beta$  is presumably the same

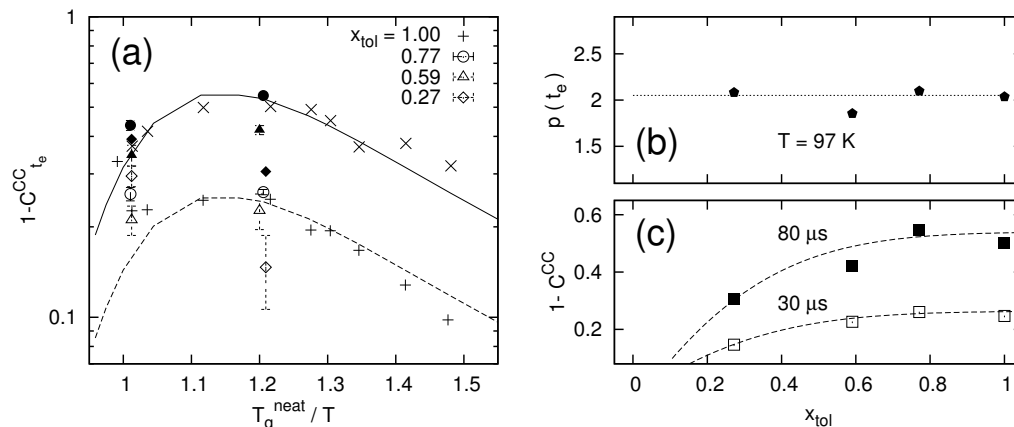
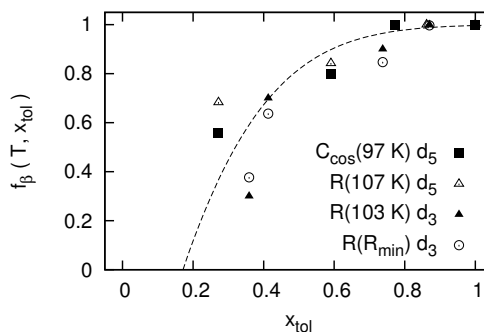


**Figure 8.26 (a):** Amplitude of the  $F^{cc}$  decay in different mixtures of toluene- $d_5$  in PCB54 versus reduced temperature ( $T_g = 117 \text{ K}$ )/ $T$  (open symbols:  $t_e = 30 \mu s$ , full symbols:  $80 \mu s$ ). The lines represent  $p(t_e)(1 - A(T))$  calculated employing dielectric results of neat toluene. Data of neat toluene from Vogel et al. [Vogel 2000a]. **(b):** Concentration dependence of the geometrical factor  $p(t_e)$ . **(c):** Concentration dependence of the residual amplitude  $C_{t_e}^{cc}$  at  $97 \text{ K}$ , a clear trend is seen for concentrations below  $x_{tol} = 0.77$ . Lines serve as guide for the eye.

**Figure 8.27:** Concentration dependence of the toluene fraction in the mixtures exhibiting the unmodified response of neat toluene at low temperatures (i.e. its  $\beta$ -process).



for all evolution times:

$$p(t_e; x_{tol}) = \frac{1 - f_\beta(x_{tol}) C_{80\mu s}^{cc}(1)}{1 - f_\beta(x_{tol}) C_{30\mu s}^{cc}(1)} = \frac{1 - C_{80\mu s}^{cc}(1)}{1 - C_{30\mu s}^{cc}(1)} = p(t_e). \quad (8.8)$$

As seen in figure 8.26 (b) this assumption holds for the present binary mixtures of toluene with PCB54:  $p(t_e)$  remains constant in the whole concentration range with a value of about two (as also found in cyanocyclohexane).

The mobile fraction  $f_\beta$  determined from  $C_{t_e}^{cc}$  at  $97 \text{ K}$  (cf. figure 8.26 (c)) in this manner is plotted with the results from line shape measurements in figure 8.27: the concentration dependence of  $f_\beta$  manifests itself in a uniform way in the different experiments for temperatures below  $T_g = 117 \text{ K}$  of neat toluene. Regarding the constant geometrical factor  $p(t_e)$  observed in the stimulated echo experiments, we can now ascertain that a heterogeneous scenario for the  $\beta$ -process is found in the present mixtures: upon concentrations lower than  $x_{tol} = 0.77$  a fraction of molecules

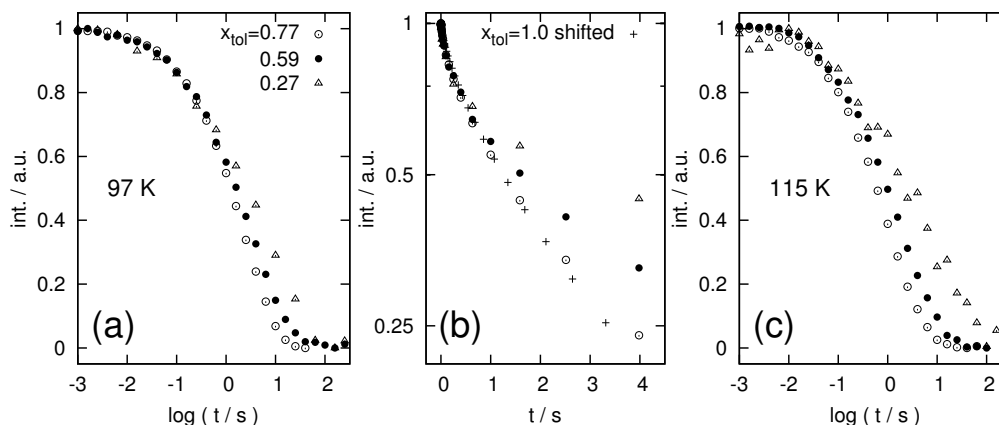


**Figure 8.28** (a): Magnetization curves for samples with different concentrations of toluene- $d_5$  in PCB54 recorded at 97 K. Whereas the initial slope appears to be concentration independent, the long time “tail” and hence the stretching of the curves differs significantly. (b): Same set of data in log/linear representation. The data of neat toluene [Vogel 2000a] is scaled by a factor of 1.2 as it was obtained at a slightly higher temperature. (c): Magnetization curves of different concentrations of toluene- $d_5$  in PCB54 recorded at 115 K.

arises which no longer exhibits the  $\beta$ -process of neat toluene. The “islands of mobility” concept, refuted in the case of neat systems [Vogel 2005], appears to be a valid description in the case of binary mixtures of toluene.

### 8.5.7 Spin lattice relaxation – revisited

The analysis in the previous sections depicted a scenario in which a fraction of toluene molecules in the mixtures do no longer exhibit the  $\beta$ -process of the neat system. If this holds, one would consequently expect to observe the different fractions also in the spin-lattice relaxation at low temperatures, where  $T_1$  is governed by the  $\beta$ -process.

As a potential bimodal behaviour is only observable when  $T_1$  is non-exponential (i.e. exchange between the dynamically different species is sufficiently slow) and governed by the  $\beta$ -process, the present analysis is limited to temperatures below about  $T_g + 15$  K in mixtures containing toluene- $d_5$ . Figure 8.28 displays the magnetization curves of toluene- $d_5$  in PCB54 for different concentrations at the temperatures of the  $F_{te}^{cc}$  measurements in section 8.5.6, i.e. below  $T_g$  of neat toluene. Aside from the finding that the stretching is more pronounced in case of the samples with higher PCB content, one notices the apparent concentration independence of the initial decay in the displayed magnetization curves<sup>19</sup>. This finding is in agreement with the previous result that a sustainable number of toluene molecules in the mixtures

<sup>19</sup>The resemblance is better in case of the lower temperature,  $T=97$  K, where the three curves are indistinguishable during the first 30% of magnetization decay (this is better seen in the log/linear representation in figure 8.28 (b)). At 115 K (figure (c)) the agreement is still distinguished, however the relaxation strength  $1-S$  of the  $\beta$ -process may already be higher in the samples with high toluene content, as the respective  $T_g$  is approached.

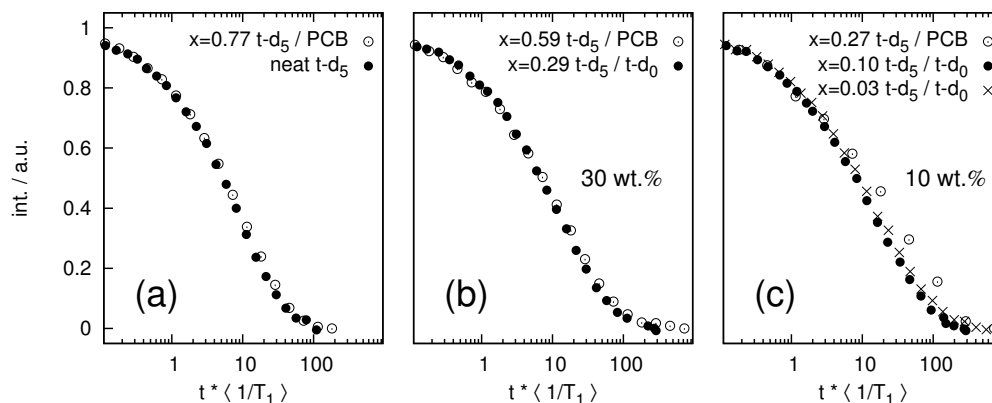


**Figure 8.29:** Magnetization curves from figure 8.28 (a) ( $T=97\text{ K}$ ) and of toluene- $d_5$  in toluene- $d_0$  recorded at  $110\text{ K}$ , data from [Hinze 1996]. For comparison the curves are scaled with respect to the initial decay. The dilution effect (i.e. stretching), in the system toluene- $d_5$  / PCB appears more pronounced at low concentrations.

exhibit the unaltered  $\beta$ -process of the neat system, which dominates  $T_1$  at the selected temperatures. Consequently one approach to explain the concentration dependent effects, i.e. the changes in the long time “tail” due to a more pronounced stretching, is via the fraction  $1-f_\beta$  of molecules without a  $\beta$ -process.

As discussed above (cf. section 6.3.6 for example), the long time end of the magnetization curves at  $T < T_g$  in all of our samples is governed by spin diffusion. Hence  $\langle T_1 \rangle$  at lowest temperatures always reflects a mixed quantity with contributions from the spectral density of the  $\beta$ -process and the time scale of spin diffusion in the respective sample, whereas the initial magnetization decay  $\langle 1/T_1 \rangle$  solely reflects the spectral density and is suspected to be free of spin diffusion artefacts. As spin diffusion rates vary upon dilution with a protonated compound such as PCB54, changes in the stretching of the magnetization curves at low temperatures are inherent to binary systems. Hence we expect to observe a superposition of effects due to changes in the spectral density (due to the fraction  $1-f_\beta$  without a  $\beta$ -process) on the one hand and a modified spin diffusion rate on the other hand.

For a qualitative argument regarding the concentration dependence of spin diffusion rates in mixtures of toluene with PCB54, we will compare the magnetization curves of the former with those of an isotope dilution series of toluene- $d_5$  in toluene- $d_0$  [Hinze 1996]. Figure 8.29 displays the low temperature magnetization curves of figure 8.28 (a) in comparison with different concentrations of toluene- $d_5$  in toluene- $d_0$  at  $T < T_g$ . As the temperatures of the measurements differ about  $10\text{ K}$ , the  $x$ -axis is scaled with respect to the initial decay. The stretching parameter  $\beta_K$  for the magnetization curves of neat toluene remains however comparable at the two temperatures, hence the curves of  $x_{\text{tol}}=0.77$  toluene- $d_5$  in PCB and neat toluene almost coincide in figure (a). The mixtures of  $x_{\text{tol}}=0.59$  toluene- $d_5$  in PCB and  $x_{\text{tol}}=0.29$  toluene- $d_5$  in toluene- $d_0$  (which both correspond to a concentration of about 30 wt. %) still exhibit comparable magnetization curves, albeit the stretching at long times is slightly more pronounced in the mixture with PCB. The  $x_{\text{tol}}=0.27$  toluene/PCB

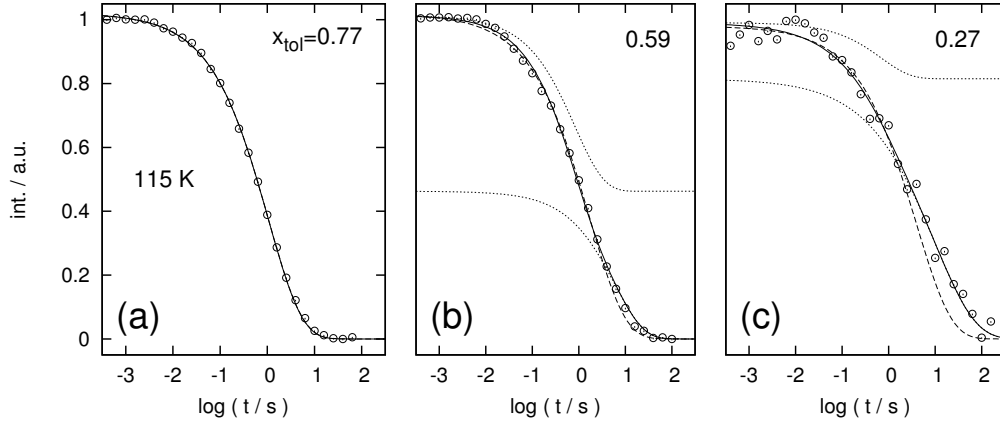


**Figure 8.30:** Demonstration of different fitting strategies on the magnetization curves for samples with different concentrations of toluene-d<sub>5</sub> in PCB54 recorded at 115 K. The dashed line represent a fit via a single stretched exponential function, the full line results from a bi-exponential fit (the dotted lines are the respective fast and slow fractions).

sample finally exhibits a more pronounced long time “tail” in the magnetization curves than observed in toluene-d<sub>5</sub> / toluene-d<sub>0</sub> down to  $x_{d5}=0.03$  (figure 8.29 (c)). Dilutions of toluene-d<sub>5</sub> in PCB54 and toluene-d<sub>0</sub> are not strictly quantitatively comparable with regard to spin diffusion effects. As the present results are however recovered in mixtures of toluene-d<sub>5</sub> with picoline-d<sub>0</sub> (cf. section 9.2), which mimic the system toluene-d<sub>5</sub>/toluene-d<sub>0</sub> much closer in terms of proton/deuteron density, molecular size and hence inter-nuclear distances, we can state that the deviations arising in the magnetization curves upon low toluene-d<sub>5</sub> concentrations in PCB54 originate in the spectral density of the system, whereas the contributions from a modified spin diffusion rate are minor in first approximation.

If however two distinct toluene fractions with regard to the  $\beta$ -process are discernible in the magnetization curves, a simple stretched exponential description is no longer justified. With respect to figure 8.28 (a) it is obvious that a single Kohlrausch function is not versatile enough to capture the concentration independent initial decay and simultaneously the ample changes in the behaviour at long times. This is demonstrated in figure 8.30, where a single stretched exponential fit (dashed line) clearly fails to reproduce all features in the lower concentrations (figures (b) and (c)). Consequently a bi-exponential fitting procedure via the sum of two Kohlrausch functions was applied to the magnetization curves:

$$\psi(t) = W_{T_1} \cdot \exp\left(-\left(\frac{t}{T_1^f}\right)^{\beta_K^f}\right) + (1 - W_{T_1}) \cdot \exp\left(-\left(\frac{t}{T_1^s}\right)^{\beta_K^s}\right), \quad (8.9)$$

where  $T_1^f, \beta_K^f$  and  $T_1^s, \beta_K^s$  denote the relatively fast and slow fractions and  $W_{T_1}$  the weighting of the fast component. The magnetization curves in figure 8.28 suggest that  $1/T_1^f$  coincides with  $\langle 1/T_1 \rangle$  of neat toluene below  $T_g=117$  K, at higher temperatures the quantity is however also a-priori unknown. Hence five independent parameters have to be optimized in the fitting procedure. Nevertheless stable fits were obtained,

as exemplarily demonstrated in figure 8.30. In case of  $x_{\text{tol}}=0.77$  the bi-exponential fit yields no considerable improvement to a single stretched exponential description of the magnetization curve, whereas for lower toluene content the fit via equation 8.9 models the experimental results significantly better. A bi-modal description of the experimental magnetization curves appears therefore justified.

The results from fits in this manner to all magnetization curves<sup>20</sup> are displayed in figure 8.31. For all concentrations bi-modal Kohlrausch decays were found at temperatures where a single Kohlrausch fit yields  $\beta_K \neq 1$ , i.e. at temperatures lower than  $T \approx T_g + 15$  K. Slightly above  $T_g$  the magnetization curves are well described mainly via the fast portion with  $\beta_f \approx 0.9 - 1$  and  $T_1^f$  in agreement with an extrapolation of the low temperature  $\langle 1/T_1 \rangle^{-1}$  of the neat system ( $\times$  symbols in figure 8.31). Towards lower temperatures the relative weighting of the fast fraction is reduced and the magnetization curves are more and more dominated by the slow fraction with pronounced stretching ( $\beta_s \approx 0.75$ ) until at about 90-100 K a bi-exponential adaptation is no longer possible as  $W_{T_1}(T) \rightarrow 0$  and  $T_1$  is again well described by a single Kohlrausch function due to the strong influence of spin diffusion (as in the neat system, where  $\beta_K$  is reduced in this region).

The temperature dependence of the weighting factor  $W_{T_1}(T)$  between the different contributions to  $T_1$  traverses two distinct regimes, as seen in figure 8.32. Around  $T_g$  of the individual mixtures  $W_{T_1}$  drops from 1 to below 0.5 in a rather narrow temperature region, which appears universal when plotted on a reduced temperature scale  $T_g/T$  (cf. figure 8.32 (b)). This initial decay is dominated by the slowing down of isotropic dynamics and hence the arise of non-exponential  $T_1$ , which is crucial for the observation of the effects. In this regime neither the  $\alpha$ - nor the  $\alpha'$ -process can mediate efficient exchange on the time scale of  $T_1$  anymore and hence different (local) spin-lattice relaxation times of the sub-ensembles become observable. At lower temperatures the progression of  $W_{T_1}(T)$  is no longer coupled to the collective motion in the mixtures, but collapses on a single envelope, i.e. displays universal features on an absolute temperature scale – here the different sub ensembles are mediated via spin diffusion.

The fact that a fit via equation 8.9 yields consistent results in all studied concentrations affirms the bi-modal scenario sketched in the last sections. The model used to describe the low temperature magnetization curves was based on two dynamically different fractions with regard to the  $\beta$ -process, the finding that bi-modal decays are observed for all temperatures with non-exponential magnetization curves, i.e. even at temperatures above  $T_g$ , where  $T_1$  is no longer (solely) governed by the  $\beta$ -process, has to be explained in a different scope. This behaviour is related to the bi-modal behaviour introduced by the  $\alpha$ - and  $\alpha'$ -process, which is however closely related to the fractions observed for the  $\beta$ -process – as we will demonstrate in the next section.

<sup>20</sup>The signal-to-noise ratio in the  $x_{\text{tol}}=0.27$  toluene-d<sub>5</sub>/PCB45 sample is too poor for a stable bi-exponential fit at temperatures other than the ones displayed in figure 8.28.

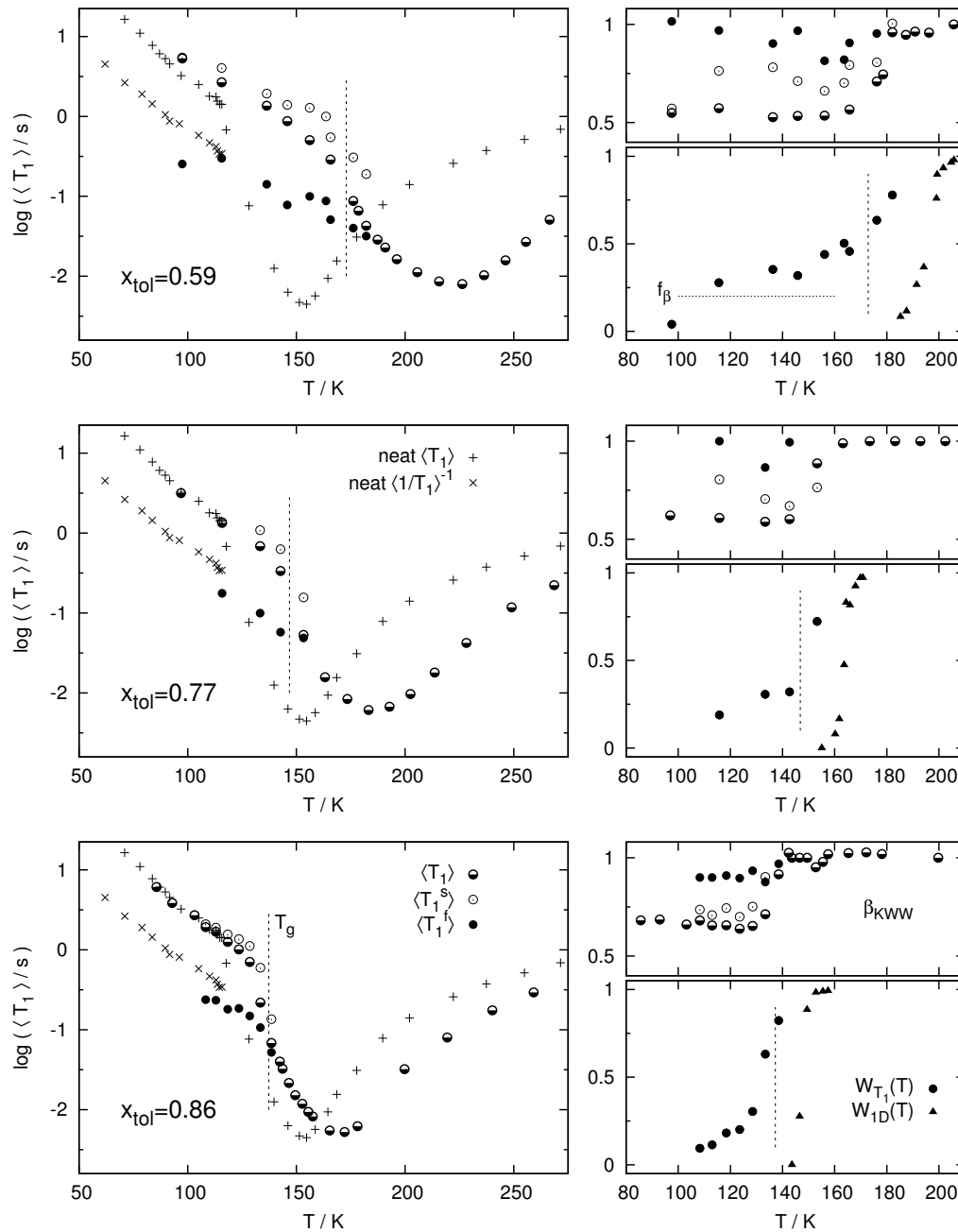


**Figure 8.31:** Average spin lattice relaxation times  $\langle T_1 \rangle$  from figure 8.7 (single stretched exponential fit, partially filled circles) and results from a bi-exponential fit via equation 8.9 ( $\circ$ ,  $\bullet$ ) to the same magnetization curves in the applicable temperature regions. The relative weighting of the fast portion (alongside with  $W(T)$  from the line shape studies) as well as the stretching parameters  $\beta_K$  are given in the right-hand part of the figure. The dashed lines mark the upper  $T_g$  attributed to the prominent step in the DSC measurements (cf. figure 8.6 (a)).

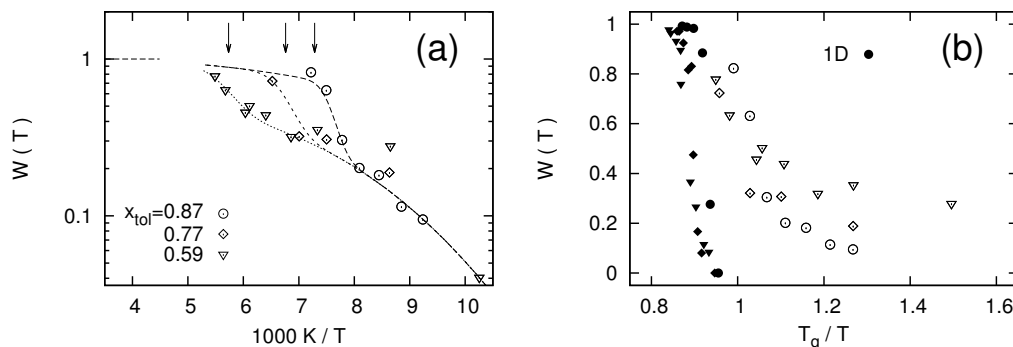


**Figure 8.32 (a):** Relative weighting of the fast  $T_1$  component in the different toluene- $d_5$ /PCB mixtures. The lines serve as guide for the eye, the arrows mark the respective  $T_g$ s. **(b):** The high temperature onset of  $W(T)$  roughly scales with the upper  $T_g$  in the mixtures, as found for the weighting factor of the 1D two phase spectra (corresponding full symbols).

## 8.6 Plausibility check

In the previous sections we observed dynamically distinct sub-ensembles of toluene with regard to the  $\beta$ -process in the present mixtures. This finding provides strong arguments for the presence of a bimodal scenario for toluene dynamics in mixtures with PCB54. As it was however not feasible to observe such a bimodal behaviour in a single experiment – via bi-exponential decays in the stimulated echo measurements for example – we have to divert from a model-free analysis and probe the multitude of  $^2\text{H}$  NMR results for consistency with a hypothetical mono- respectively bimodal behaviour of toluene. Before doing so, we will briefly summarize the previous results and open questions:

- At lowest temperatures ( $T < T_g = 117\text{ K}$  of neat toluene) the results from line shape analysis and stimulated echo studies with regard to the  $\beta$ -process concertedly depict a scenario with a (concentration and presumably temperature dependent) fraction  $1 - f_\beta$  of molecules, that no longer participate in the  $\beta$ -process of the neat system – whereas the remainder of molecules exhibits the unaltered secondary relaxation of neat toluene.
- In the same temperature region the initial decay of the magnetization curves for all toluene- $d_5$  in PCB samples coincides with the one observed in the neat system, whereas a more pronounced stretching is observed at longer times for low toluene concentrations. This behaviour is in agreement with the concentration dependence  $f_\beta$  of the  $\beta$ -process described above.
- Time constants determined at  $T \geq T_g$  depict a slightly different scenario for the toluene dynamics depending on the time scale of the experiment:  $\tau_{\alpha'}$  at the  $T_1$  minimum is about two orders of magnitude faster than the corresponding  $\tau_\alpha$  from dielectric spectroscopy (i.e. of PCB54). The analysis of the two phase spectra also shows dynamics that is on average faster than  $\tau_\alpha$ , the slowest toluene molecules (for concentrations  $x_{\text{tol}} \leq 0.77$ ) however reorient on

the time scale of PCB54 in the  $\mu\text{s}$ -regime. In the ms-regime stimulated echo measurements ( $F^{\text{ss}}$ ) yield  $\langle\tau_{\alpha'}\rangle = \langle\tau_{\alpha}\rangle$  for  $x_{\text{tol}} \leq 0.77$ , whereas by means of  $F^{\text{cc}}$  measurements at relatively lower temperatures (due to the slightly enhanced time window) again  $\langle\tau_{\alpha'}\rangle < \langle\tau_{\alpha}\rangle$  was found. The latter time constants furthermore exhibit an apparent fragile-to-strong transition.

- For concentrations  $x_{\text{tol}} > 0.77$  we found in contrast to lower toluene contents  $\langle\tau_{\alpha'}\rangle \ll \langle\tau_{\alpha}\rangle$  in all experiments.
- In case of  $x_{\text{tol}} = 0.59$  a second step in the DSC curves was observed at lower temperatures, the corresponding  $T_g$  is in agreement with an extrapolation of  $\tau_{\alpha'}$  from  $F^{\text{cc}}$  measurements.

### 8.6.1 Modelling the toluene dynamics in mixtures with PCB

The concept of the present analysis follows the ansatz in section 6.4.1: in a first step the evolution of  $T_1$  with temperature will be modelled according to equation 3.29 via the spectral density constructed for a number of simple scenarios. The parameters for which best agreement with the experimental results is obtained, will then subsequently be tested against the results of the line shape analysis (i.e. the weighting factor  $W(T)$  obtained from the two phase spectra), stimulated echo measurements and dielectric data obtained for the same concentration.

We will start the present discussion with the simplest assumptions: all toluene molecules reorient on the time scale of  $\tau_{\alpha}$  (i.e. of PCB54) and the concentration dependence of the  $\beta$ -process is homogeneous (i.e. only one fraction of toluene molecules is present,  $f_{\beta}$  will be neglected). To calculate the spectral density we employed a generalized gamma (GG, equation C.12) distribution in case of the  $\alpha$ -process and a (symmetric)  $G_{\beta}$  distribution (equation C.17) for the  $\beta$ -process. Both distributions have the advantage that parameters for neat toluene are available [Blochowicz 2003] and have proven to be versatile enough to describe also the dynamics in the present mixtures.

In a first step  $\langle 1/T_1 \rangle$  of pure toluene- $d_5$  [Vogel 2000a] was fitted in a Williams-Watts approach

$$G(\log \tau) = S \cdot G_{GG}(\log \tau_{\alpha}) + (1 - S) \cdot G_{\beta}(\log \tau_{\beta}), \quad (8.10)$$

via equation 3.29 [Resing 1965]:

$$\frac{1}{T_1} = \int_{-\infty}^{\infty} \frac{1}{T_1(\tau)} G(\log \tau) d \log \tau. \quad (8.11)$$

The only free fit parameter in equation 8.11 is  $1-S$  (cf. section 6.4.1 for details), as the parameters  $\tau_{\beta}, a, b$  of the  $G_{\beta}$  distribution and  $\tau_{\alpha}$  of the  $G_{GG}$  distribution were obtained from dielectric spectroscopy and the shape parameters of  $G_{GG}$  were kept constant (i.e. assuming frequency-temperature superposition) at the values reported for  $T = T_g + 10 \text{ K}$  [Blochowicz 2003] ( $\alpha = 1, \beta = 0.65$ ). The results are displayed in figure 8.33 (dashed line): in the temperature region of interest for the present approach, i.e. around and below the  $T_1$  minimum, the deviations resulting from the assumption of

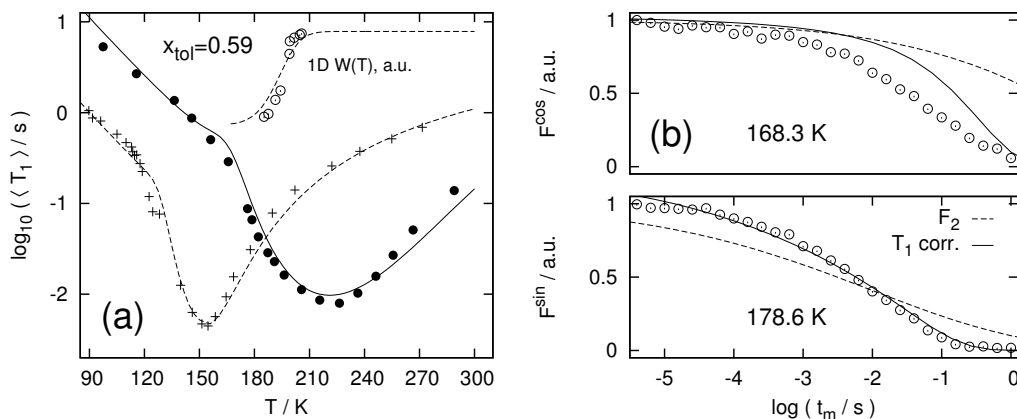


**Figure 8.33 (a):**  $T_1$  (●) and the 1D weighting factor (○) calculated for a model in which the toluene and PCB54 time scales are not decoupled and only a single toluene fraction exists in the mixtures. In addition  $\langle 1/T_1 \rangle$  of neat toluene- $d_5$  (+) [Vogel 2000a, Rössler 1984] is shown with a corresponding fit via equation 8.11 by assuming FTS. **(b):** Experimental correlation functions in comparison with results of equation 8.15 for the parameters found in (a) (dashed line). The full line results from a  $T_1$  correction and normalization with respect to the experimental data.

FTS are negligible in the neat system.

For the binary mixtures of toluene- $d_5$  with PCB54 we have demonstrated by means of the bi-modal fits in section 8.5.7 that  $\langle 1/T_1 \rangle$  does not represent a measure for all toluene molecules in the sample. Consequently we will employ  $\langle T_1 \rangle$  for the remainder of calculations: as equation 8.11 does not strictly hold in this case due to the influence of spin diffusion, the adaptation at temperatures where  $T_1$  is non-exponential (i.e. below the  $T_1$  minimum) will be phenomenological and the obtained relaxation strength of the  $\beta$ -process (1- $S$ ) will contain a systematic deviation. The error made in case of the  $\alpha$ -process, which dominates  $T_1$  at high temperatures, will however be marginal and this approach is the only possibility to account for the observed concentration dependence in  $T_1$  at low temperatures (since  $\langle 1/T_1 \rangle$  below 117 K remains concentration independent in first approximation, as demonstrated in section 8.5.7).

For the present model, in which all toluene molecules participate in the  $\beta$ -process, the parameters of  $G_\beta$  were again obtained from the neat system. As  $\tau_\alpha$  is fixed to the dielectric results of PCB, the only fit parameters are  $\alpha, \beta$  of the GG distribution and 1- $S$ . The results for  $x_{\text{tol}}=0.59$  toluene- $d_5$  in PCB are displayed in figure 8.33 (solid line). As the experimentally observed minimum position appears at temperatures lower than  $\tau_\alpha(T)=1/\omega_L$ , an adaptation is only possible via a very broad and distorted GG distribution ( $\alpha=0.15, \beta=0.3$ ). Still the agreement for the present model is not satisfying – as expected with respect to our previous results. Nevertheless we will compare the predictions of this model with the remainder of  $^2\text{H}$  NMR results. From the parameters obtained in modelling  $T_1$  we can subsequently calculate the

theoretical weighting factor of the liquid line in the solid echo spectra<sup>21</sup>:

$$W(T) = \int_{-\infty}^{\log 1/\delta} G_{GG}(\log \tau) d \log \tau. \quad (8.12)$$

As we have demonstrated however in section 4.2.3 by means of random walk simulations, that correlation times on the order  $\tau=0.5\text{-}13.5\ \mu\text{s}$  are effectively suppressed in the two phase spectra<sup>22</sup>, we will employ a slightly modified equation:

$$W(T) = \frac{1}{N} \int_{-\infty}^{\log 0.5\mu\text{s}} G_{GG}(\log \tau) d \log \tau \quad (8.13)$$

with the normalization factor

$$N = \int_{\log 13.5\mu\text{s}}^{\infty} G_{GG}(\log \tau) d \log \tau + \int_{-\infty}^{\log 0.5\mu\text{s}} G_{GG}(\log \tau) d \log \tau. \quad (8.14)$$

The results are given as inset in figure 8.33 (a): due to the broad GG distribution the calculated weighting factor predicts a wider temperature range of two phase spectra than observed in the experiment, albeit the high temperature end is roughly captured. In addition to  $W(T)$  the corresponding correlation functions  $F_2$  are accessible via Laplace transformation:

$$F_2(t) = \int_{-\infty}^{\infty} \exp\left(-\frac{t}{\tau}\right) G_{GG}(\log \tau) d \log \tau. \quad (8.15)$$

The obtained correlation functions  $F_2$  are very broad, as demonstrated in figure 8.33 (b), where the calculations are compared to experimental stimulated echo decays at the respective temperatures. At  $T=178.6\ \text{K}$  the resulting  $F_2$  (dashed line) exhibits a significantly broader decay than observed in the experiment (open symbols). Applying a damping via  $T_1$ <sup>23</sup> to the calculated curve (full line), yields however good agreement with the experimental data. Since the analysis of the stimulated echo at the given temperature (section 8.5.4) purveyed  $\tau_2 = \tau_\alpha$ , this finding is trivial. It is noteworthy however that – in the present scenario – it appears that not all toluene molecules are observed in the experiment and the stretching  $\beta_K$  is systematically underestimated. The cosine-cosine correlation function, measured at  $T=168.3\ \text{K}$  and displayed in the same figure, can no longer be reproduced in the present approach, as the assumed time scale of toluene dynamics is already too slow. Consequently the present model fails to describe any of the  $^2\text{H}$  NMR results sufficiently.

In an attempt to improve the agreement of the model with our experimental results,

<sup>21</sup>For the calculation of the 1D weighting factor and the stimulated echo decay any possible influence of the  $\beta$ -process will be neglected.

<sup>22</sup>For coupling constants on the order of  $\delta=125\ \text{kHz}$ , as typically observed for C-D bonds.

<sup>23</sup>For the  $T_1$  damping in all cases the resulting spin-lattice relaxation time from the calculations at the respective temperature was used, the stretching parameter  $\beta_K$  was interpolated from experimental results in the given region.

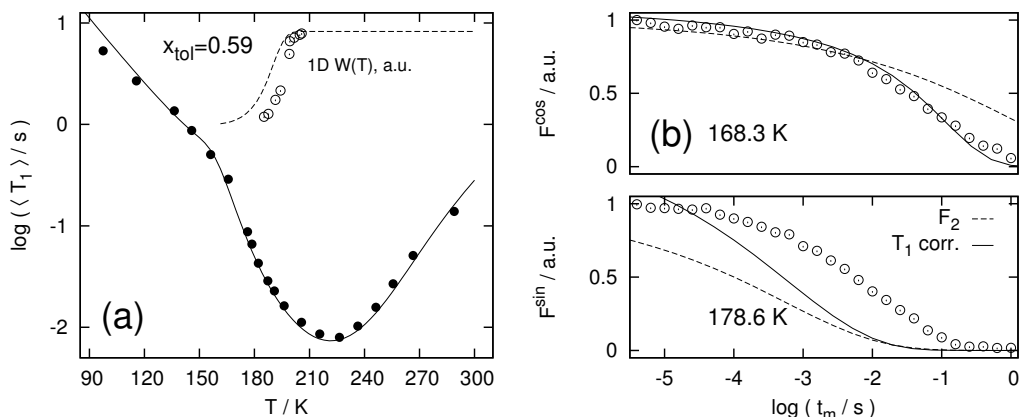


**Figure 8.34 (a):**  $T_1$  (●) and the 1D weighting factor (○) calculated for a model in which the toluene and PCB54 time scales are decoupled (cf. figure 8.35 (a)) but only a single toluene fraction exists in the mixtures. **(b):** Experimental correlation functions in comparison with results of equation 8.15 for the parameters found in (a) (dashed line). The full line results from a  $T_1$  correction and normalization with respect to the experimental data.

we introduce a scenario in which  $\tau_{\alpha'} = \tau_{\alpha}$  no longer holds, i.e. the temperature dependence of  $\tau_{\alpha'}$  becomes an additional fit parameter. The assumption of a single toluene fraction is yet maintained for the moment. A shift of  $\tau_{\alpha'}$  (cf. dotted line in figure 8.35 (a)) yields better agreement of equation 8.11 with the experimental results by means of a narrower distribution  $G_{GG}(\log \tau)$  ( $\alpha = 0.58$ ,  $\beta = 0.21$ ), as demonstrated in figure 8.34 (a). Due to the toluene dynamics being significantly faster, the low temperature stimulated echo measurements are now well reproduced by means of the employed GG distribution ( $T = 168.3 \text{ K}$  in figure 8.34 (b)). At  $T = 178.6 \text{ K}$  however  $\tau_{\alpha'}$  is now too fast in the present model: in contrast to the previous approach the  $F^{\text{ss}}$  decay at the given temperature can not be explained in the present scenario. The same holds for the calculated weighting factor of the two phase spectra: the predicted transition in  $W(T)$  is shifted about 10 K towards lower temperatures with respect to the experimental values.

With regard to dielectric spectroscopy however both models are in agreement with experimental data, cf. figure 8.35: as the dipole moment of toluene is substantially smaller than the one of PCB, the loss peak of toluene is in both cases completely submerged under the one of PCB.

Although the selected models represent two rather arbitrary limiting cases, the calculations demonstrated that any simple model for a single dynamic process of toluene is incapable of reproducing the obtained  $^2\text{H}$  NMR results in the whole temperature range<sup>24</sup>. Consequently we will now focus on bi-modal scenarios for the toluene dynamics in the present mixtures, as indicated by the experimentally observed “islands of mobility” with regard to the  $\beta$ -process.

<sup>24</sup>Slight refinements are certainly possible, i.e. by neglecting FTS and introducing a temperature dependence for the shape of the GG distribution. The overall agreement will however not be altered significantly.

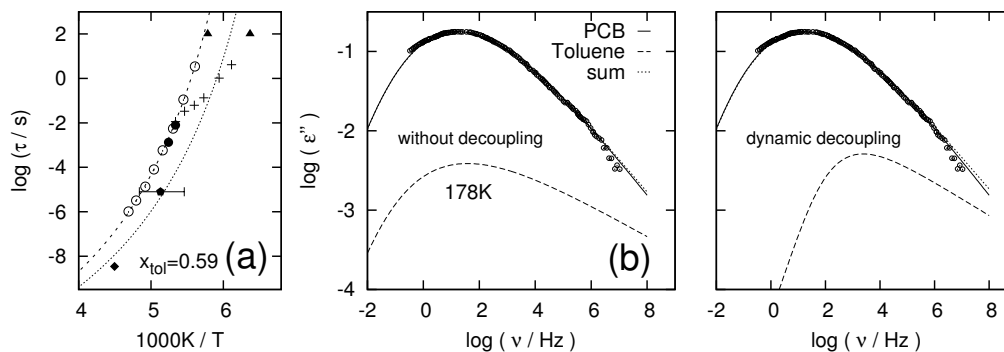


**Figure 8.35 (a):** Time constants for the mixture of  $x_{tol}=0.59$  toluene in PCB54: the dashed line, i.e. the VFT fit to  $\tau_\alpha$  from dielectric spectroscopy [Cangialosi 2008], corresponds to  $\tau_{\alpha'}$  employed in the non-decoupled scenario (figure 8.33), the dotted line was used in the model for a dynamic decoupling in figure 8.34. **(b):** Dielectric loss spectra of  $x_{tol}=0.59$  toluene in PCB [Cangialosi 2008] in comparison with the GG distributions used for the calculation of  $T_1$ .  $\Delta\epsilon$  of the toluene fraction was obtained from the neat system [Kudlik 1997b].

### 8.6.2 Models for two dynamically distinct toluene sub-ensembles

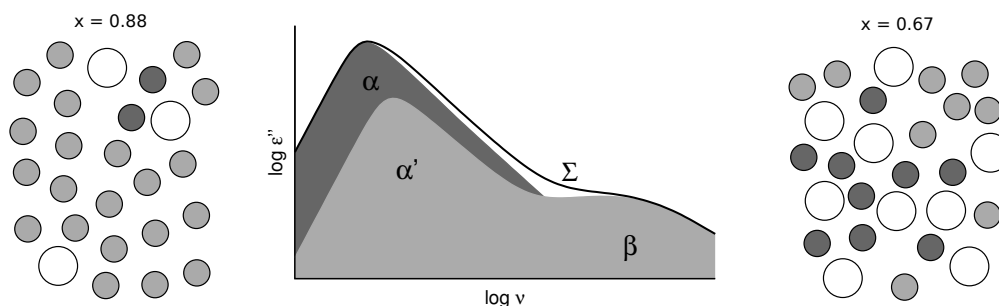


**Figure 8.36 :** Sketch of the proposed bi-modal scenario for the toluene dynamics in mixtures with PCB54. Toluene molecules (small shaded circles, the shading corresponds to the respective loss peaks sketched in the center) found in a PCB54 (large open circles) rich environment participate only in the  $\alpha$ -process of the PCB molecules and consequently do not exhibit a  $\beta$ -process. Toluene molecules in a toluene rich environment exhibit a (faster)  $\alpha'$ -process and participate in the  $\beta$ -process of the neat system.

Models incorporating two distinct dynamic processes of toluene in binary mixtures are per se more versatile in the description of experimental data, as they contain more adjustable parameters. As however stressed in the introduction to this analysis we have observed strong hints for the presence of such a scenario in the mixtures with PCB. Figure 8.36 sketches the heterogeneous model that will be applied in the present section: toluene molecules found in a (local) PCB54 rich environment participate only in the  $\alpha$ -process of the PCB molecules and consequently do not exhibit a  $\beta$ -process (i.e. appear “frozen” on the high  $T_g$  component). Toluene molecules in a toluene rich environment exhibit a (faster, i.e. decoupled)  $\alpha'$ -process and participate in the  $\beta$ -process of the neat system.

The approach is as follows: for each of the fractions  $T_1$  is calculated individually according to equation 8.11 from the distributions of correlation times. For the (relatively fast) fraction of molecules in an environment with high local toluene concentration again a Williams Watts approach was employed: the parameters of the distribution  $G_\beta$  for the  $\beta$ -process were obtained from the dielectric results of the neat system, including the relaxation strength  $1-S$  employed in modelling  $\langle 1/T_1 \rangle$  of neat toluene (as  $T_1$  of the fast fraction approximately coincides with  $\langle 1/T_1 \rangle^{-1}$  of neat toluene below 117 K, cf. figure 8.31). The shape parameters of the GG distribution for the  $\alpha'$ -process are free fit parameters (again assuming FTS) and  $\tau_{\alpha'}$  was chosen to mimic the previous results, i.e. to coincide with the values reported for the  $T_1$  minimum, the low temperature end of the line shape collapse and  $T_{g2}$  where applicable (cf. figure 8.38 (a)). The parameters  $\tau_\alpha, \alpha, \beta$  of the distribution  $G_{GG}(\log \tau_\alpha)$  for the (slow) toluene fraction in the neighbourhood of PCB molecules were obtained from dielectric spectroscopy, where again the shape parameters  $\alpha$  and  $\beta$  were chosen to mimic the dielectric loss (of PCB) at temperatures slightly above  $T_g$ <sup>25</sup>. To account for  $T_1$  at low temperatures, where spin-lattice relaxation of the slow fraction (due to the lack of a  $\beta$ -process) is mediated via spin diffusion from the fast fraction, we introduced  $G_\beta$  (with the same parameters) also for the slow sub ensembles. In this phenomenological approach the (relatively smaller) relaxation strength  $1-S$  models magnetization transfer via spin diffusion, consequently we can not quantify the relative weighting of the fractions below  $T_g$ .

The resulting  $T_1$  values from an adaptation in the described manner are plotted in figure 8.37 (a):  $T_1$  of the  $\alpha$ -process (dotted line) and the  $\alpha'$ -process (dashed line) roughly coincide with the slow respectively fast  $\langle T_1 \rangle$  values obtained from the bi-modal fits to the experimental magnetization curves.  $T_1$  of the fast fraction furthermore reproduces the high temperature flank of the minimum quite well (via  $\alpha = 1, \beta = 0.18$ ). As we have demonstrated by means of the 2D exchange spectra in section 8.5.3 that dynamical exchange between the relatively fast and slow toluene sub-ensembles exists, the processes contributing to  $T_1$  are not statistically independent and hence the mean spin lattice relaxation time in the model is calculated from the rate via the relative weighting  $W_{T_1}$ :

$$\frac{1}{T_1} = (1 - W_{T_1}) \cdot \frac{1}{T_1^\alpha} + W_{T_1} \cdot \frac{1}{T_1^{\alpha'}}, \quad (8.16)$$

where  $W_{T_1}$  was modelled via a stretched error function. The results are represented by the solid line in figure 8.37 (a), which fits the experimental  $\langle T_1 \rangle$  sufficiently at all temperatures<sup>26</sup>. The employed weighting  $W_{T_1}$  is plotted in figure 8.37 (b): as found for the bi-modal fits in the experiment, a broad transition is observed from the high temperature regime, where  $T_1$  is dominated by the  $\alpha'$ -process, towards low temperatures, where the relaxation is governed by the  $\alpha$ -process<sup>27</sup>.

<sup>25</sup>We found  $\alpha=0.18, \beta=0.52$  in the  $x_{\text{tol}}=0.59$  concentration,  $\alpha=0.18, \beta=0.65$  in case of  $x_{\text{tol}}=0.77$  and  $\alpha=0.35, \beta=0.9$  for the  $x_{\text{tol}}=0.86$  sample, cf. figure 8.3.

<sup>26</sup>The deviations arising at low temperatures result from spin diffusion artefacts, as the experimental  $\langle T_1 \rangle$  instead of  $\langle 1/T_1 \rangle$  is considered.

<sup>27</sup>The high and low temperature limits of  $W_{T_1}$  represent an artefact of the simple assumptions made in the present model (no exchange between the fractions,  $\beta$ -process for the slow fraction to model spin diffusion etc.).

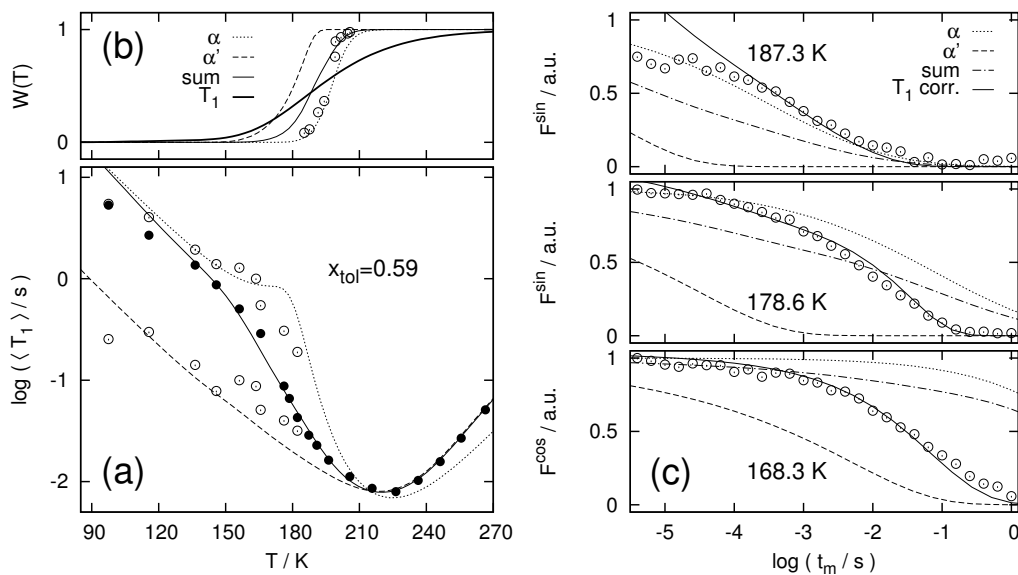


**Figure 8.37 (a):** Calculations in the present model in comparison with results from a bi-exponential fit to  $T_1$ . **(b):** Corresponding weighting factor of  $\alpha$ - and  $\alpha'$ -process (thick line) and calculations for the weighting factor of the liquid line in solid echo spectra. **(c):** Experimental correlation functions in comparison with results of the present model, for the weighting of the single contributions again  $W_{T_1}$  was employed.

The weighting factor of the two phase spectra and  $F_2$  were obtained via equations 8.13 and 8.15 for each toluene fraction individually and subsequently weighted via  $W_{T_1}$ , i.e. the only additional fitting parameters in the present model are  $W_{T_1}$  and  $1-S$  in the slow fraction (to account for spin diffusion effects), as all other parameters of the distributions are fixed to previous dielectric and  $^2\text{H}$  NMR results. The obtained 1D weighting factors are given in figure 8.37 (b): the weighted sum of the contributions from  $\alpha$ - and  $\alpha'$ -process fits the high temperature onset in  $W(T)$  rather well, whereas the width is again over-estimated in the present model, as the low temperature behaviour is better modelled by the  $\alpha$ -process alone. One explanation for this deviation might be found in the neglecting of exchange processes in the present calculation.

The agreement of the model with stimulated echo measurements, presented in figure 8.37 (c), on the other hand is remarkable: in contrast to the mono-modal scenarios the present approach captures the stimulated echo decays in the whole temperature range (after a  $T_1$  correction has been applied, full line<sup>28</sup>). The outcome of the present model also demonstrates that the time constants obtained via  $F^{\text{ss}}$  and  $F^{\text{cc}}$  always represent a mixed quantity with weighted contributions from both processes and are at all temperatures affected by the time window of the experiment, i.e. only a (temperature dependent) fraction of toluene molecules is observable in the experiment. Consequently the time constants extracted from  $F^{\text{ss}}$  and  $F^{\text{cc}}$  only reflect a certain sub ensemble and hence the apparent fragile-to-strong transition in figure

<sup>28</sup>The deviations in the initial decay at 187.3 K presumably result from the effective suppression of dynamics faster than 100  $\mu\text{s}$  in the experiment.

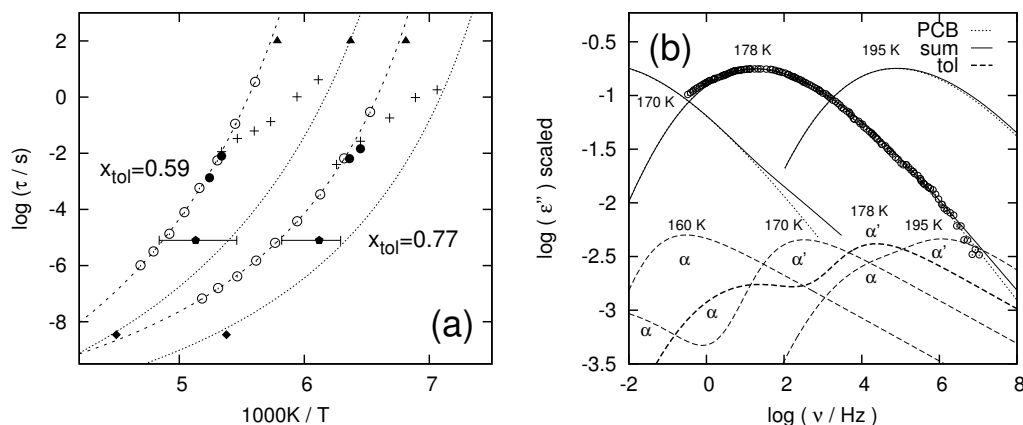


**Figure 8.38 (a):** Time constants for the mixtures of  $x_{tol}=0.59$  and  $0.77$  toluene in PCB: open symbols correspond to the low frequency peak observed in dielectric spectroscopy [Cangialosi 2008]. The dashed and dotted lines represent  $\tau_\alpha$  and  $\tau_{\alpha'}$  employed in the present models. **(b):** Dielectric loss spectra of  $x_{tol}=0.59$  toluene in PCB [Cangialosi 2008] in comparison with the GG distributions used in the calculation of  $T_1$ .  $\Delta\epsilon$  of the toluene fraction was obtained from the neat system [Kudlik 1997b].

8.18 represents an artefact.

As in case of the previous models we briefly discuss the compatibility with dielectric spectroscopy by means of figure 8.38 (b): also in the bi-modal scenario the toluene contribution to the dielectric loss is negligible due to the low dipole moment of the molecule. Again (cf. curves for  $T=178$  K) only the high frequency flank of the  $\alpha$ -process is suspect to very subtle changes when the two loss peaks of toluene are added to the one of PCB. As only the dielectric spectrum at  $T=178$  K is reported in literature, no comparisons can be made at lower temperatures where the model predicts a wing on the high frequency flank of the  $\alpha$ -process (at  $T=170$  K).

The same model was applied to the data of the  $x_{tol}=0.77$  mixture: the GG distribution of the  $\alpha$ -process was again obtained from dielectric,  $\tau_{\alpha'}$  was chosen to mimic the previous  $^2\text{H}$  NMR results (i.e. time constants from the  $T_1$  minimum, the line shape collapse and  $F^{cc}$ , cf. figure 8.38 (a)) and the shape parameters of  $G_{GG}(\log \tau_{\alpha'})$  were adopted from the  $x_{tol}=0.59$  concentration, hence only the parameters  $W_{T_1}$  and  $1-S$  were altered. The results are virtually the same as in case of the lower concentration: again overall agreement with the experimental  $\langle T_1 \rangle$ , including fast and slow fractions obtained from the bi-modal fits, is achieved and the correlation functions are reproduced in the whole temperature range by means of the same parameters as employed for the calculation of  $T_1$ . The transition from  $\alpha'$ -process to  $\alpha$ -process via  $W_{T_1}$  is shifted towards lower temperatures and spans a slightly smaller temperature range. Again the high temperature onset of the experimental 1D weighting factor is captured via the weighted sum of both processes calculated in the model, whereas the low temperature end follows  $W(T)$  of the  $\alpha$ -process (cf. figure 8.39 (b)).

Higher toluene concentrations (i.e.  $x_{tol}=0.86$  toluene- $d_5$  and  $0.87$  toluene- $d_3$  in PCB) represent an exception with regard to our  $^2\text{H}$  NMR results: here the stimulated

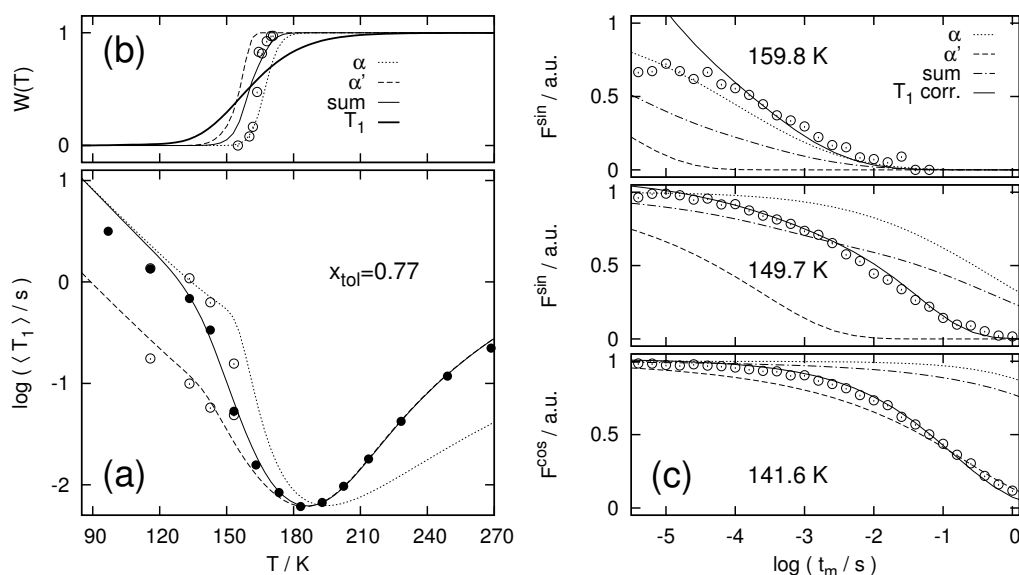


**Figure 8.39 (a):** Results of a fit within the bi-modal scenario to  $T_1$  data of  $x_{\text{tol}}=0.77$  toluene- $d_5$  in PCB54. **(b):** Corresponding weighting factor of the  $\alpha'$ -process (thick line) and calculations for the weighting factor of the liquid line in the two phase spectra. **(c):** Experimental correlation functions in comparison with results of the present model, for the weighting of the single contributions again  $W_{T_1}$  was employed.

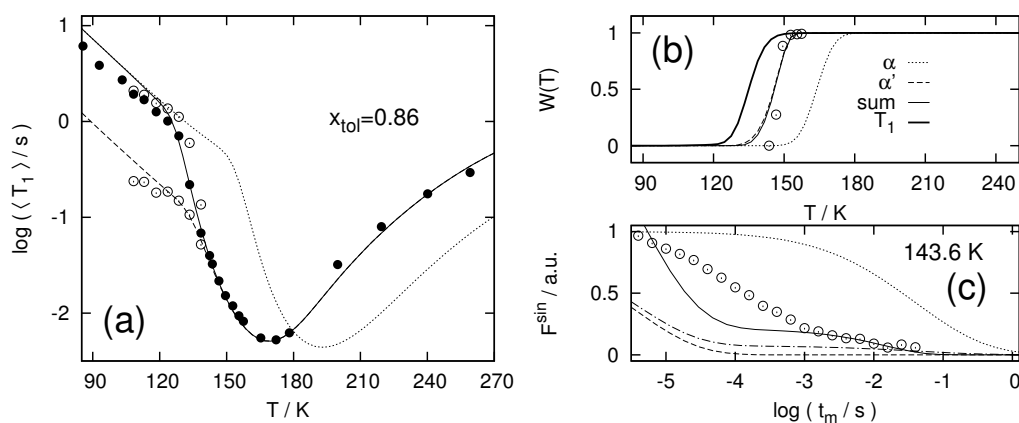


**Figure 8.40 (a):** Results of a fit within the bi-modal scenario to  $T_1$  data of  $x_{\text{tol}}=0.86$  toluene- $d_5$  in PCB54. **(b):** Corresponding weighting factor of the  $\alpha'$ -process (thick line) and calculations for the weighting factor of the liquid line in two phase spectra. **(c):** Experimental correlation function in comparison with results of the present model, key cf. figure 8.39 (c).

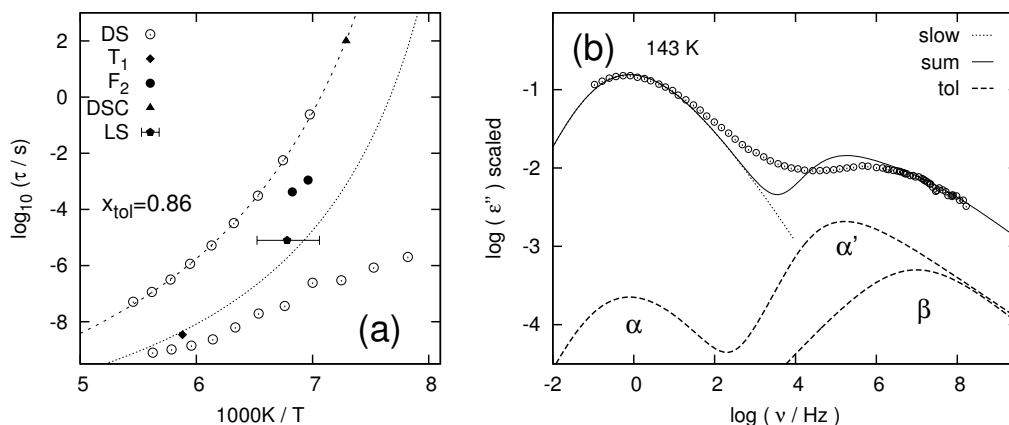


**Figure 8.41 (a):** Time constants for the mixture of  $x_{tol}=0.86$  toluene- $d_5$  in PCB: open symbols correspond to the high respectively low frequency peak observed in dielectric spectroscopy [Cangialosi 2008]. The dashed and dotted lines represent  $\tau_\alpha$  and  $\tau_{\alpha'}$  employed in the present model. **(b):** Dielectric loss spectra of  $x_{tol}=0.87$  toluene in PCB [Cangialosi 2008] in comparison with the GG and  $G_\beta$  distributions used for the calculation of  $T_1$  at different temperatures.

echoes at high temperatures already provided  $\tau_{\alpha'} \ll \tau_\alpha$  and the high temperature end of the 1D weighting factor did not coincide with  $\tau_\alpha$  from dielectric spectroscopy. This behaviour is also reflected in the outcome of the present approach: the experimental  $\langle T_1 \rangle$  is again reproduced well in the whole temperature range (cf. figure 8.40 (a)) by means of  $G_{GG}(\log \tau_\alpha)$  from dielectric,  $\tau_{\alpha'}$  given in figure 8.41 (b) and a slightly narrower distribution  $G_{GG}(\log \tau_{\alpha'})$  ( $\alpha=1$ ,  $\beta=0.35$ ).

In contrast to the mixtures with lower toluene content, the weighting factor  $W_{T_1}$  is one in the region of the line shape collapse, i.e. the  $\alpha$ -process does not contribute to the arise of two phase spectra at this concentration in the present model. Yet the agreement with experimental results is comparable to the mixtures of  $x_{tol}=0.59$  and  $0.77$  toluene- $d_5$  in PCB (i.e. the high temperature onset is captured, whereas the calculated weighting factor extends to lower temperatures than observed in the experiment). Hence the modelling of  $\langle T_1 \rangle$  readily explains the finding that the time constants extracted from the first arise of a solid state spectrum do not coincide with  $\tau_\alpha$  from dielectric spectroscopy, cf. figure 8.41 (a). For the present concentrations only two  $F^{ss}$  correlation functions were measured, and albeit the agreement with the calculated decays is significantly worse than for lower toluene contents, the model predicts a bi-modal decay at  $T=143.6\text{ K}$ , which – to certain degree – can also be observed in the experimental data.

The distinctiveness of the  $x_{tol}=0.86$  mixture is also observed in figure 8.42: when plotted versus  $\tau_{\alpha'}$  the obtained weighting factors  $W_{T_1}$  of the  $x_{tol}=0.59$  and  $0.77$  concentrations almost coincide, whereas the transition is shifted to considerably longer correlation times for the highest concentration. A comparison of the model with dielectric spectroscopy is facilitated in the present case, as for  $x_{tol}=0.87$  toluene in PCB dielectric spectra are available at different temperatures [Cangialosi 2008]: in figure 8.41 (b) it is seen that the predicted loss peak of the  $\alpha'$ -process agrees qual-

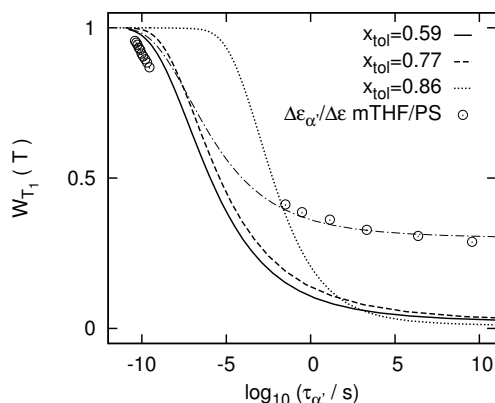


**Figure 8.42:** Weighting factors  $W_{T_1}$  obtained from a bi-modal adaptation to  $T_1$  vs.  $\tau_{\alpha'}$  employed in the model. Whereas the weighting factors of  $x_{\text{tol}}=0.59$  and  $x_{\text{tol}}=0.77$  toluene- $d_5$  in PCB are virtually universal in this representation, the high temperature onset in case of the  $x_{\text{tol}}=0.86$  mixture deviates significantly. The open symbols originate from the relative relaxation strength of the  $\alpha'$ -process in a 50% mixture of MTHF with polystyrene [Schramm 2011], cf. section 8.6.3.

itatively with the high frequency peak observed in dielectric spectroscopy (although FTS is clearly not fulfilled here), which is not seen in the literature data for the remainder of concentrations, as no spectra in the suitable temperature regime are reported.

In contrast to the remainder of concentrations, Cangialosi et al. reported time constants for the  $\alpha'$ -process in the  $x_{\text{tol}}=0.87$  toluene / PCB mixture (cf. figure 8.41 (a)):  $\tau_{\alpha'}$  from dielectric only mimics our  $^2\text{H}$  NMR results and the time constants employed in the present model at highest temperatures, as they deviate from a VFT behaviour around  $10^{-7}$  s and follow  $\tau_{\beta}$  of neat toluene below  $T_g$ . At 143 K  $\tau_{\alpha'}$  reported from dielectric spectroscopy is still about two orders of magnitude faster than found in the present model: as this temperature however lies in the regime where  $\alpha'$ - and  $\beta$ -process are suspected to merge, one possible explanation for this deviation can be found in a fitting procedure that covers both processes by means of a single peak. This is demonstrated in figure 8.41 (b): the submerged  $\beta$ -process ( $G_{\beta}$ , parameters of neat toluene,  $1-S=0.1$ ) significantly broadens the dielectric response and shifts the apparent peak position towards higher frequencies. Consequently no contradiction between a bimodal scenario and the dielectric results of Cangialosi et al. is found.

### 8.6.3 Discussion

The present section demonstrated that the proposed bimodal scenario for toluene dynamics in mixtures with PCB54 is not only in accordance with the low temperature findings regarding the  $\beta$ -process, but also models all high temperature results in a straightforward manner. Furthermore the approach illustrated that – in any possible scenario – the stimulated echo measurements only account for a certain fraction of toluene molecules within the distribution(s)  $G(\log \tau_{\alpha})$  and hence the extracted time constants require careful interpretation.

The solid echo weighting factor at low temperatures represents the only  $^2\text{H}$  NMR observable that was not sufficiently captured by the bimodal approach for toluene dynamics – and this deviation is probably resolved by the introduction of dynamic exchange, so far neglected in the model but observed in the experiment. The remainder of results are reproduced well via few and plausible assumptions. The relative

weighting between  $\alpha$ - and  $\alpha'$ -process resembles the weighting factor obtained from the bi-exponential fits to  $T_1$  and is virtually identical for  $x_{\text{tol}} \leq 0.77$  when plotted vs.  $\tau_{\alpha'}$ , cf. figure 8.42: at high temperatures all toluene molecules contribute to the fast  $\alpha'$ -process, when  $\tau_{\alpha'}$  approaches the ns-regime slower sub ensembles are detected by  $^2\text{H}$  NMR, which contribute to the  $\alpha$ -process of PCB54. Around  $\tau_{\alpha'} \approx 100$  s (i.e.  $T_{g2}$ ) the weighing factor decays to zero. This represents an artefact of the model, since for the sake of simplicity spin diffusion has been neglected in the present calculation of  $T_1$ . Regarding the proposed coupling of  $\alpha'$ - and  $\beta$ -process,  $W(T)$  is expected to approach a concentration dependent plateau  $\simeq f_{\beta}$  in the experiment, the observation of which is hampered by spin diffusion effects.

The mixture with the highest studied toluene concentration,  $x_{\text{tol}}=0.86$ , represents an exception with regard to  $W(T)$ : the initial decay for short  $\tau_{\alpha'}$  is shifted from the ns- to the  $\mu\text{s}$ -regime, which readily explains the finding that opposed to lower concentrations always  $\tau_{\alpha'} \ll \tau_{\alpha}$  was observed in the experiment. The qualitative progression of  $W(T)$  is however the same as for lower toluene concentrations.

As the loss peak(s) of toluene are not unambiguously resolved by dielectric spectroscopy due to the low dipole moment of the compound, a comparison of  $W(T)$  with  $\Delta\epsilon$  is not applicable, the proposed model is however consistent with dielectric results. Blochowicz et al. studied a 50% (by weight) mixture of methyltetrahydrofuran (M-THF) and polystyrene ( $M_w=60$  kg/mol), where the main dipole moment arises from the low- $T_g$  component M-THF [Blochowicz 2011, Schramm 2011]. In this sample two distinct peaks for the M-THF dynamics were resolved (in addition to the  $\beta$ -process) and the individual relaxation strengths are reported for certain temperatures. When normalized according to the proposed model, i.e.

$$W(T) = \frac{\Delta\epsilon_{\alpha'} + \Delta\epsilon_{\beta}}{\Delta\epsilon_{\text{tot}}}, \quad (8.17)$$

and plotted vs.  $\tau_{\alpha'}$  obtained from a VFT fit to the dielectric time constants, the results closely mimic the weighting obtained from an analysis of the present  $^2\text{H}$  NMR data, cf. open symbols in figure 8.42<sup>29</sup>. Hence it appears that the assumptions made in the present model are of more general validity and the extracted weighting factor does not represent a peculiarity of the employed  $^2\text{H}$  NMR technique arising from time window effects for example.

A comprehensive discussion and outlook on the presented results will be postponed however to chapter 10, as we will afore reassess literature data on further binary mixtures of toluene in the light of the present findings in the next chapter.

<sup>29</sup>The dash dotted line represents  $W(T)$  for the  $x_{\text{tol}}=0.59$  concentration with a plateau chosen to match the dielectric results of m-THF / polystyrene, as the plateau is neglected in the present model (vide supra) and presumably system dependent.

# Universal behaviour of toluene in binary mixtures

## Contents

<b>9.1 Motivation</b>	<b>173</b>
<b>9.2 Toluene in picoline</b>	<b>173</b>
9.2.1 Thermal analysis	174
9.2.2 Dielectric measurements	175
9.2.3 NMR results	177
<b>9.3 Toluene in polystyrene</b>	<b>181</b>
9.3.1 NMR results	184
<b>9.4 A model for the concentration dependence</b>	<b>185</b>
9.4.1 Application	186

## 9.1 Motivation

The scope of the present chapter is to reassess literature data on binary mixtures of toluene in the context of the findings presented in the last chapter. Special attention will be paid to the question if the concentration dependence of the  $\beta$ -process, observed in toluene / PCB54, can also be found in other binary mixtures of toluene.

We will thereby focus on two previously studied mixtures of toluene: toluene in picoline [Tschirwitz 2001] and toluene in polystyrene [Adachi 1975, Rössler 1985]. By means of a re-evaluation of the literature data we will obtain the justification for a more general treatment of our previous results in section 9.4. Of the two toluene mixtures presented in this chapter, the one comprising picoline is of considerable interest, as the data was previously unpublished and only preliminarily analysed.

## 9.2 Toluene in picoline

Picoline is a close relative of the toluene molecule, as only one carbon atom in the ring of toluene is replaced by nitrogen (and consequently one hydrogen is missing). Hence the high  $T_g$  component in the present case is very similar to toluene in terms of size, shape and structure and exhibits dynamics on a more comparable time scale, i.e. the  $T_g$  contrast is less pronounced than in mixtures of toluene and PCB ( $\Delta T_g \approx 16$  K in adverse to 124 K for toluene in PCB).

All experimental results presented within this section, unless otherwise noted, are

	2-picoline-d <sub>7</sub>	toluene-d <sub>5</sub>
full name	2-methylpyridine	toluene-2,3,4,5-d <sub>5</sub>
$M_n$ [g/mole]	100.17	97.17
$\rho$ [g/cm <sup>3</sup> ]	1.026	0.912
$T_g$ [K]	132.7	117

**Table 9.1:** Material characteristics of the components in the present mixture.

courtesy of C. Tschirwitz [Tschirwitz 2001] and have been acquired during his stay in our group. For the <sup>2</sup>H NMR and DSC measurements the same experimental setup as described in 6.3.1 was employed and hence the results are directly comparable. Only the raw data and preliminary analysis thereof (i.e. fits to the dielectric spectra, magnetization curves etc.) were readily available – any interpretation of the results is part of this work.

As the available results from <sup>2</sup>H NMR are rather limited in the present case, the

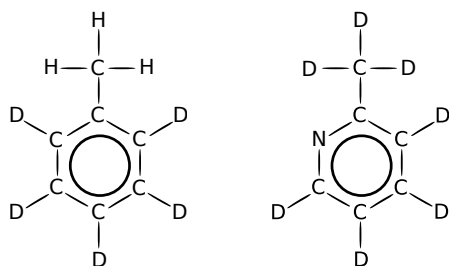


**Figure 9.1 left:** ring deuterated toluene-d<sub>5</sub>.  
**Right:** perdeuterated 2- or α-picoline-d<sub>7</sub>.

presentation will be brief and restricted to a comparison with regard to the prominent findings in mixtures of toluene with PCB – but nevertheless crucial, as we will demonstrate that the dynamics of toluene in mixtures with compounds as various as PCB and picoline are closely related.

### 9.2.1 Thermal analysis

Figure 9.2 (a) presents DSC curves for different concentrations of toluene in picoline, including measurements of the neat systems. For each sample a single glass transition step is observed which changes in position and width between the limits of the neat compounds. The fact that only a single glass transition temperature is observed, is probably related to the rather low heating rate of 10 K/min<sup>1</sup> and the low  $T_g$  contrast in the present mixture – it can not be waived at this point that a second, low temperature step in the DSC measurements is hidden beneath the larger one. The glass transition temperatures (extracted from the onset of the steps as sketched for neat picoline) are presented in figure (b). In contrast to the concentration dependence of  $T_g$  in the mixtures with PCB,  $T_g(x_{\text{tol}})$  of toluene in picoline does not exhibit a linear behaviour, instead a smooth, convex concentration dependence is observed.

<sup>1</sup>The measurements in section 8.4 and by Blochowicz et al. [Blochowicz 2011] demonstrated the arise of a second step at higher heating rates.

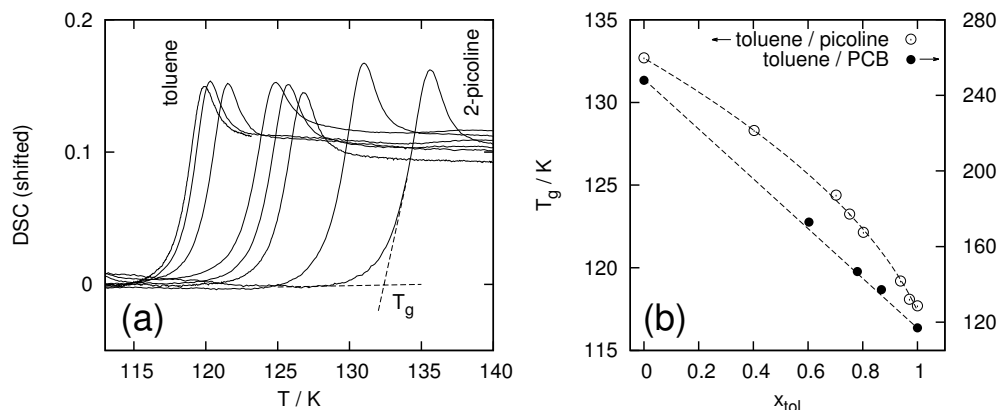
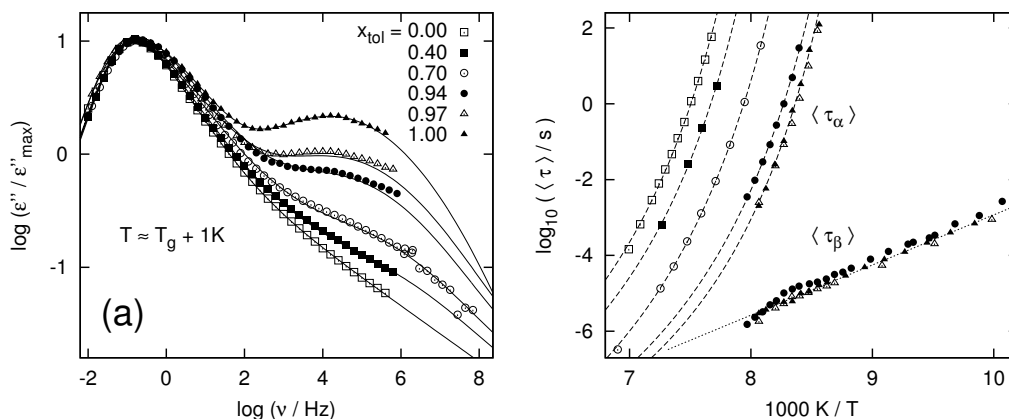


**Figure 9.2 (a):** Calorimetric measurements of different toluene / picoline mixtures: concentration dependence of the step in heat capacity accompanying the glass transition [Tschirwitz 2001]. **(b):** Corresponding glass transition temperatures determined from the onset of the steps in (a) [Tschirwitz 2001] in comparison with results obtained for mixtures of toluene in PCB. Line serves as guide for the eye.

### 9.2.2 Dielectric measurements

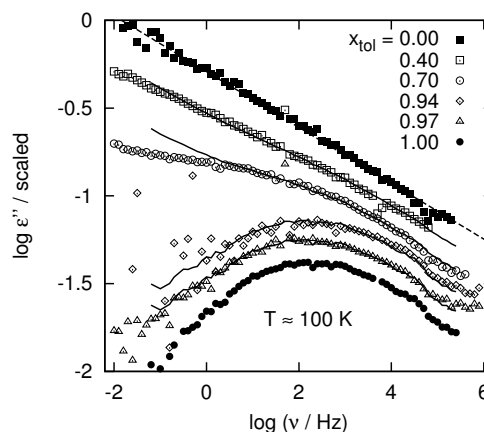
The vast amount of data available for analysis in the system toluene/picoline originates from dielectric measurements. The high concentration limit, i.e. mixtures with  $x_{tol}=0.97$  and  $0.94$  toluene were studied by S. Benkhof [Benkhof 1999], the remainder of concentrations ( $x_{tol}=1.0, 0.7, 0.4$  and  $0$ ) are adapted from C. Tschirwitz [Tschirwitz 2001]. With regard to dielectric measurements the mixtures of toluene and picoline are similar to the system toluene/PCB: in both cases the dipole moment of the high  $T_g$  component is substantially larger, i.e. even at relatively high toluene concentrations the main dielectric response arises already from the other component. Furthermore both high  $T_g$  components do not exhibit a  $\beta$ -process (in dielectric spectroscopy), yet in both cases there appears an excess wing on the high frequency flank of the  $\alpha$ -process.

Figure 9.3 (a) displays the dielectric spectra for each studied concentration at about  $T=T_g+1$  K, i.e. the  $\alpha$ -process appears in the same frequency range and has been normalized with respect to the peak height for comparison. Apart from the strong change in the contribution of the  $\beta$ -process, it is well seen in this representation that the low frequency flank of the  $\alpha$ -process retains its shape in first approximation. The width of the  $\alpha$ -process however steadily changes with concentration between the limits of neat picoline and toluene (cf. figure 9.5 (b)), i.e. no maximum of the broadening at intermediate concentrations as in toluene/PCB is observed (cf. figure 8.3). In contrast to common perception the loss peak of toluene becomes narrower in mixtures with picoline, i.e. the dynamic heterogeneities are apparently reduced. As the main dielectric response originates already at high  $x_{tol}$  from the picoline fraction, one should however not over-interpret this finding. Figure 9.3 (b) depicts the extracted time constants: as the fragilities of toluene and 2-picoline are comparable, the temperature dependence of the  $\alpha$ -process in the binary mixtures



**Figure 9.3 (a):** Loss part of the dielectric modulus for different concentrations of toluene in picoline recorded at similar reduced temperatures ( $T \approx T_g + 1$  K). The spectra are normalized with respect to the height of the  $\alpha$ -peak for comparison. Lines are fits in the William Watts approach ( $\alpha$ : Kohlrausch,  $\beta$ : log-Gaussian) [Tschirwitz 2001]. **(b):** Corresponding time constants of  $\alpha$ - and  $\beta$ -process from fits depicted in (a) [Tschirwitz 2001].

**Figure 9.4:** Loss part of the dielectric modulus (scaled) for different concentrations of toluene in picoline at  $T=100$  K [Tschirwitz 2001]. The full lines represent an interpolation of the excess wing in neat picoline (fit, dashed line) and the  $\beta$ -peak of neat toluene, demonstrating the concentration independence of the high frequency behaviour with respect to the time scale of the  $\beta$ -process.



appears simply shifted between the two limiting cases.  $\tau_\beta$  on the other hand exhibits no concentration dependence between  $x_{\text{tol}}=1$  and 0.94, for concentrations of  $x_{\text{tol}}=0.7$  and 0.4 a stable deconvolution of the excess wing, observed on the high frequency flank of the  $\alpha$ -process, and the weak loss peak of the  $\beta$ -process is no longer possible. As demonstrated in figure 9.4, the dielectric loss at  $T=100$  K can however be described in all concentrations via a superposition of the wing observed in neat picoline and the  $\beta$ -process of neat toluene (full lines), which provides strong arguments for a concentration independence of  $G(\log \tau_\beta)$  also for concentrations  $x_{\text{tol}} < 0.94$ .

The relaxation strength of the  $\beta$ -process ( $1-S$ ), determined from the dielectric spectra at 122 K for all concentrations, is displayed in figure 9.5 (a). The dotted line represents the result from equation 7.4, i.e. a linear interpolation in a scenario where all toluene molecules contribute to the  $\beta$ -process, the picoline molecules do not. The interpolation describes the experimental results for  $x_{\text{tol}}=0.97$  quite well, but clearly under-estimates the relaxation strength in the samples with  $x_{\text{tol}}=0.94$  and

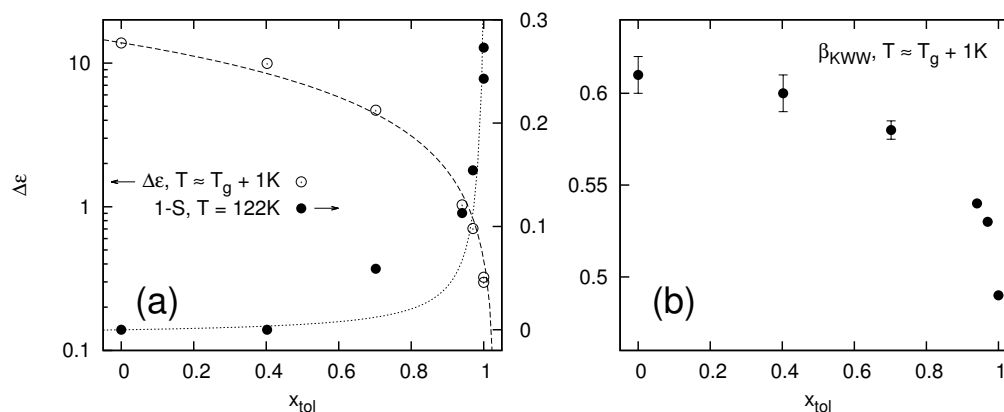


**Figure 9.5 (a):** Total dielectric strength  $\Delta\epsilon$  ( $T_g+1\text{K}$ ) and relaxation strength of the  $\beta$ -process 1-S [Tschirwitz 2001]. Lines represent linear interpolations via eq. 7.2 and 7.4. **(b):** Concentration dependence of the width of the  $\alpha$ -peak close to  $T_g$  [Tschirwitz 2001] from Kohlrausch fits to the spectra presented in figure 9.3 (a).

0.70 toluene. A similar excess strength in 1- $S$  was also observed for the toluene / PCB mixtures (cf. figure 8.4 (b)) – in the present case yet the quality of data is significantly better.

The relaxation strength  $\Delta\epsilon_\beta$  of the  $\beta$ -process observed at  $x_{\text{tol}}=0.70$  exceeds the total  $\Delta\epsilon$  of toluene for the given concentration, i.e. even for 1- $S=1$  the contribution of the  $\beta$ -process to the dielectric spectrum is too large. Consequently picoline molecules contribute to the  $\beta$ -process of toluene. In the next section we will affirm this observation by means of  $^2\text{H}$  NMR, which provides the ability to monitor the components in the mixture individually.

### 9.2.3 NMR results

The available  $^2\text{H}$  NMR results for the present system consist of a small number of spin-lattice relaxation and  $t_p$ -dependent solid echo line shape measurements at temperatures below  $T_g$  of neat toluene. Nevertheless the results are of considerable interest, as the “islands of mobility” with regard to the  $\beta$ -process in mixtures of toluene and PCB were mainly observed in this temperature regime. Especially since for the system toluene / picoline mixtures of toluene- $\text{d}_5$  in picoline and toluene- $\text{d}_0$  in picoline- $\text{d}_7$  were studied, i.e. the dynamics of high- and low- $T_g$  components could be monitored individually (which was not possible for the systems in the last chapter due to the lack of deuterium labelled PCB54).

The ring and methyl-group deuterated forms of 2-picoline, i.e. - $\text{d}_4$  and - $\text{d}_3$ , were not available, hence the fully deuterated form picoline- $\text{d}_7$  had to be used in the mixtures. This yields some drawbacks as contributions from the methyl-group rotation and the tumbling motion of the molecule as a whole are observed in each experiment, i.e. magnetization curves are inherently bi-exponential and solid echo spectra consist of a weighted sum of a broad powder pattern and a spectrum with reduced coupling constant due to the fast methyl group rotation in the observed temperature regime.

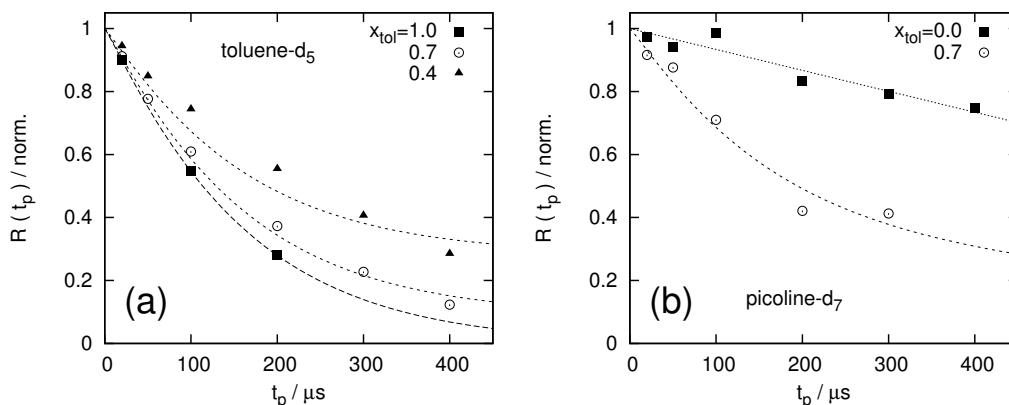


**Figure 9.6 (a):**  $t_p$ -dependence of the  $R$  value for different concentrations of toluene-d<sub>5</sub> in picoline at similar absolute temperatures ( $x_{\text{tol}}=1.0$ : 105 K, 0.7: 107 K, 0.4: 112 K) [Tschirwitz 2001]. The lines display fits via equation 8.5 for concentration independent parameters  $\tau, \beta$ . **(b):** Corresponding  $R(t_p)$  values of picoline-d<sub>7</sub> in toluene-d<sub>0</sub> for different concentrations ( $x_{\text{tol}}=0$ : 115 K, 0.7: 106 K) [Tschirwitz 2001]. The dashed line represents a fit via eq. 8.5, again the same  $\tau, \beta$  as in (a) plus a linear term depicted by the dotted line has been used.

In style of figure 8.23 (a) in the last chapter, figure 9.6 (a) presents the  $R(t_p)$  values of solid echo spectra for different concentrations of toluene in picoline for various inter pulse delays  $t_p$ . In section 8.5.5 we have demonstrated that in the system toluene / PCB the  $R(t_p)$  decays for different concentrations measured at the same temperature are well described via a stretched exponential with concentration independent parameters  $\tau, \beta$  (cf. equation 8.5). For concentrations lower than  $x_{\text{tol}}=0.77$  a plateau value  $f_\beta$  was observed at long  $t_p$ , which arises from the toluene fraction no longer participating in the  $\beta$ -process – a similar behaviour is observed in the data of toluene / picoline. The number and quality of data points is however rather low for the present system. As the analysis (in case of  $x_{\text{tol}}=1$  and 0.7) is conducted at (almost) the same temperature as in toluene / PCB, we will employ the parameters  $\tau, \beta$  obtained in the latter system also for the present case. Consequently a fit was performed via a single parameter:  $f_\beta$ . The results are displayed as dashed lines in figure 9.6 (a): for neat toluene and  $x_{\text{tol}}=0.7$  the experimental  $R(t_p)$  values are interpolated well, the  $x_{\text{tol}}=0.4$  sample was studied at a higher temperature and consequently the agreement is worse. The finding that the  $R(t_p)$  decay in  $x_{\text{tol}}=0.7$  is well described by the parameters found for neat toluene (except for the plateau  $f_\beta$ ), is a further indication for an unaltered  $\tau_\beta$  also at this (relatively low) toluene concentration. Consequently the conclusions drawn from the superposition of dielectric spectra in figure 9.4 appear valid.

The resulting concentration dependence of the plateau value  $f_\beta$  is represented by the full symbols in figure 9.7:  $f_\beta$  obtained in the mixtures of toluene with picoline and PCB54 coincide within the experimental error. The line shape changes observed at  $T \approx 107$  K in mixtures of toluene with compounds as diverse as picoline and PCB are hence virtually identical and only dependent on the mole fraction of toluene in

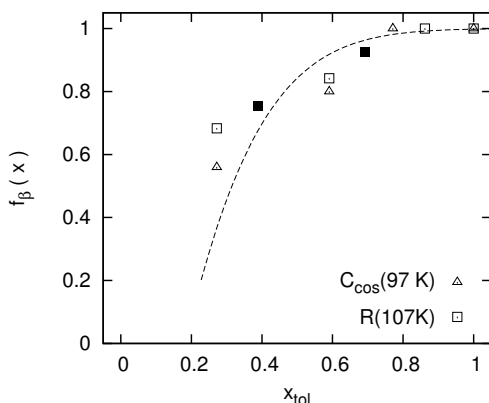


**Figure 9.7:** Plateau value  $f_\beta$  in toluene / picoline from the fits via equation 8.5 to the  $R(t_p)$  values in figure 9.6 (a) (full symbols). For comparison the fraction  $f_\beta$  determined in toluene / PCB from  $R(t_p)$  decays at the same temperature and cosine-cosine correlation functions at lower temperatures are given (open symbols). The line serves as guide for the eye.

the mixtures.

$R(t_p)$  of neat picoline-d<sub>7</sub> and obtained in a mixture with  $x_{\text{tol}}=0.7$  toluene-d<sub>0</sub> is displayed in fig. 9.6 (b). In neat picoline almost no dependence of the line shape on the inter pulse delay  $t_p$  is found at 115 K, as expected for a system without a (pronounced)  $\beta$ -process. The  $t_p$ -dependence observed in the mixture with toluene is however comparable to the one found for toluene-d<sub>5</sub>. For a quantitative analysis we fitted the data of neat picoline at 115 K via a linear term  $R(t_p) = R_0 - R_l \cdot t_p$  (dotted line in figure 9.6 (b)), which was subsequently introduced into equation 8.5 to account for the decay in the picoline-d<sub>7</sub> / toluene-d<sub>0</sub> mixture:

$$R'(t_p, x) = R_0 \left[ f_\beta(x) \cdot \exp\left(-\left(\frac{t_p}{\tau}\right)^\beta\right) + (1 - f_\beta(x)) R_l t_p \right], \quad (9.1)$$

i.e. the fraction  $f_\beta$  contributes to the  $\beta$ -process and hence the stretched exponential decay in  $R(t_p)$ , whereas the remainder of picoline molecules exhibits the behaviour of the neat system. This approach models the  $R(t_p)$  decay of picoline-d<sub>7</sub> in the mixture with  $x_{\text{tol}}=0.7$  toluene by again employing the same parameters  $\tau, \beta$  as obtained for neat toluene-d<sub>5</sub> in the same temperature range ( $f_\beta=0.64$ , dashed line in figure 9.6 (b)).

The  $R(t_p)$  dependence in picoline-d<sub>7</sub> affirms the contribution of the latter to the  $\beta$ -process of toluene, as speculated from the relaxation strength in dielectric. Hence we can interpret  $f_\beta$  again as the fraction of molecules with an active  $\beta$ -process. From the excess strength observed in figure 9.5 (a) for  $x_{\text{tol}}=0.7$  (i.e. the difference between the experimental value and the interpolation for toluene) we can then calculate the relaxation strength  $1-S$  for the fraction  $f_\beta=0.64$  of picoline molecules contributing to the  $\beta$ -process, which yields  $1-S \approx 0.09$  at 122 K. This value is comparable to  $1-S$  found in neat toluene below  $T_g$ , as  $T_g$  of the present concentration is  $124.4 \text{ K}^2$ .

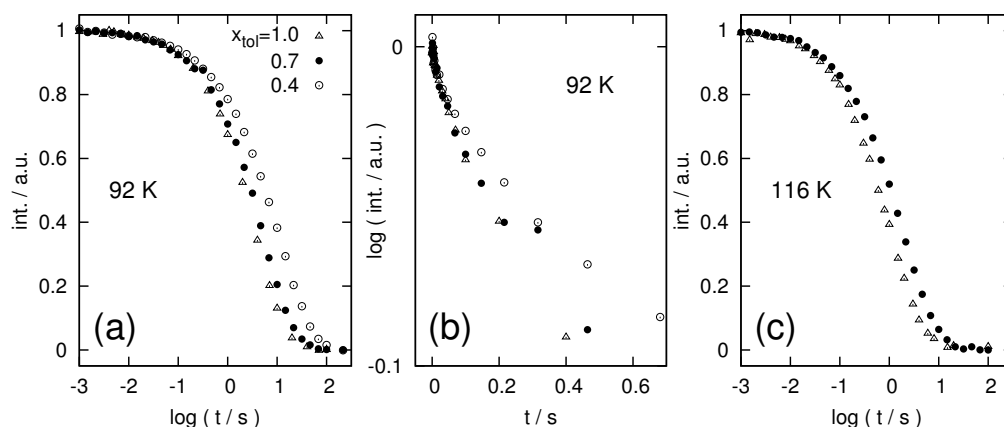


**Figure 9.8 (a):** Magnetization curves for samples with different concentrations of toluene-d<sub>5</sub> in picoline recorded at  $T=92$  K [Tschirwitz 2001], neat toluene from [Vogel 2000a]. **(b):** Same data in linear/log representation. **(c):** Magnetization curve for  $x_{\text{tol}}=0.7$  toluene-d<sub>5</sub> in picoline [Tschirwitz 2001] and neat toluene [Vogel 2000a] recorded at  $T=116$  K.

### Spin-lattice relaxation

$T_1$  of toluene-d<sub>5</sub> in mixtures with picoline was only measured at few temperatures below  $T_g=117$  K of neat toluene, nevertheless the magnetization curves in figure 9.8 allow us to recover the effects observed in mixtures of toluene-d<sub>5</sub> with PCB: the initial decay is similar to the one observed in the neat system for all concentrations. The magnetization curves in the mixtures with picoline exhibit again a pronounced, concentration dependent, stretching at longer times. As in case of the solid echo spectra, the respective temperatures of the individual experiments vary by about 2 K, hence  $G(\log \tau_\beta)$  varies for the different concentrations which alters the initial decay slightly.

As the available data is too sparse, a bi-modal fit as conducted for toluene / PCB is not in order for the present mixture<sup>3</sup>. Consequently the curves were fitted via a single stretched exponential function (cf. figure 9.9 (a)): the obtained  $\langle T_1 \rangle$  values exhibit the same concentration dependence as for the PCB containing mixtures:  $\langle T_1 \rangle$  of the  $x_{\text{tol}}=0.7$  mixture roughly coincides with the data of neat toluene below 117 K, although  $\langle T_1 \rangle$  in the mixtures is slightly longer. In the  $x_{\text{tol}}=0.4$  mixture  $\langle T_1 \rangle$  exhibits the same temperature dependence, the absolute values are however significantly larger. In a phenomenological approach we fitted  $\langle T_1 \rangle$  below 117 K in the mixtures via an Arrhenius function: the obtained  $\tau_0$  serves to quantify the change with concentration, cf. figure 9.9 (b). The observed concentration dependence of  $\tau_0$  is even quantitatively identical to the mixtures with PCB when plotted vs. the toluene mole fraction and hence represents a measure analogous to  $f_\beta$ .

So far all results obtained in the mixtures of toluene with picoline support the conclusions drawn in the previous chapter: again a fraction  $f_\beta$  of toluene molecules is observed that does not exhibit a  $\beta$ -process. The concentration dependence of  $f_\beta$  is

<sup>2</sup>For the same reduced temperature  $T_g/T$ ,  $1-S=0.14$  is found in neat toluene [Kudlik 1997b], as the  $R(t_p)$  dependence of toluene-d<sub>5</sub> yields a fraction with an active  $\beta$ -process of  $f_\beta=0.92$  for the given

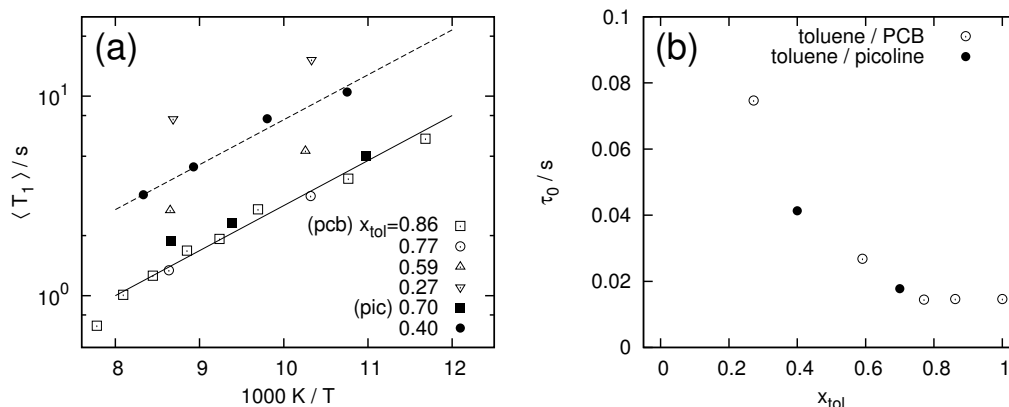


**Figure 9.9 (a):** Average spin lattice relaxation times  $\langle T_1 \rangle$  for mixtures of toluene- $d_5$  with PCB54 (open symbols) and picoline ([Tschirwitz 2001] full symbols) below  $T_g = 117$  K of neat toluene. The lines represent an Arrhenius fit to  $\langle T_1 \rangle$  in the low temperature regime. **(b):** Concentration dependence of  $\tau_0$  from the Arrhenius fits sketched in figure (a).

identical to one found in the system toluene / PCB. Furthermore we were able to demonstrate that a concentration dependent fraction of picoline molecules contribute to the  $\beta$ -process of toluene.

### 9.3 Toluene in polystyrene

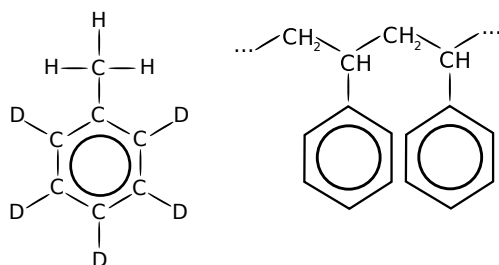


**Figure 9.10 left:** ring deuterated toluene- $d_5$ . **Right:** two monomeric units of polystyrene.

Already in 1975 Adachi et al. [Adachi 1975] reported three distinct processes in the dielectric susceptibility at fixed frequency of toluene / polystyrene mixtures (cf. figure 9.11 (a)): a virtually concentration independent process found in all samples except for neat polystyrene, that coincides with the time scale of the  $\beta$ -process in neat toluene. A second loss peak with a maximum steadily emerging from the  $\alpha$ -process of neat toluene (which we will denote  $\alpha'$ -process), relatively low concentration dependence<sup>4</sup> and a third process steadily emerging from the  $\alpha$ -process of neat polystyrene with a strong, non-linear concentration dependence absent in pure toluene. The

concentration, this is reduced to  $f_\beta \cdot (1-S) = 0.13$ .

<sup>3</sup>Due to the low number of data points the obtained parameters would appear artificial and not yield any further insight.

<sup>4</sup>Adachi et al. report a temperature for the maximum of this process also in the case of neat polystyrene (cf. figure 9.11 (a)), whereas the depicted relaxation strength has vanished, cf. figure

	polystyrene	toluene-d <sub>5</sub>
full name	atactic polystyrene	toluene-2,3,4,5-d <sub>5</sub>
$M_n$ [g/mole]	$\approx 1.6 \cdot 10^5$	97.17
$\rho$ [g/cm <sup>3</sup> ]	1.05	0.912
$T_g$ [K]	372	117

**Table 9.2:** Material characteristics of the components in the studied mixtures.

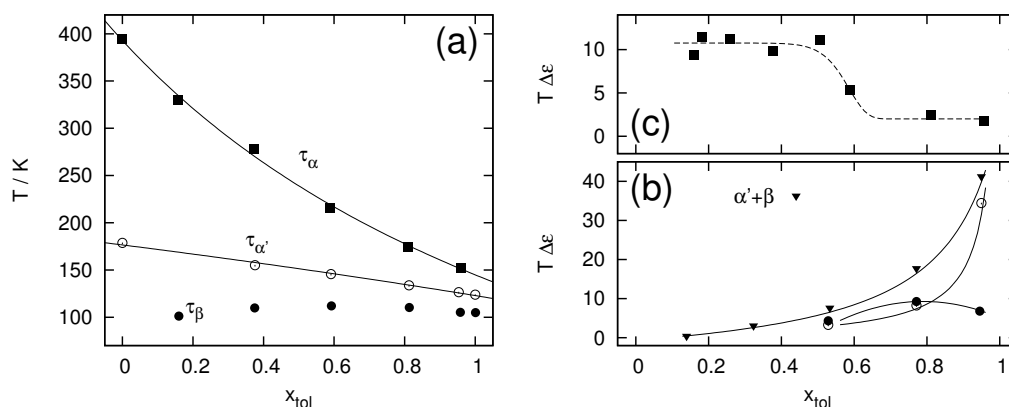


**Figure 9.11 (a):** Temperature at which the dielectric susceptibility  $\epsilon''$  exhibits a maximum at 1.6 kHz versus concentration. Figure adapted from [Adachi 1975]. The mole fraction is given in terms of the monomeric unit of polystyrene, i.e. the styrene molecular weight  $M_n=104.15$  g/mole. **(b):** Concentration dependence of the dielectric relaxation strength  $T \cdot \Delta\epsilon$ , the same symbols as in (a) are used [Adachi 1975]. **(c):**  $T \cdot \Delta\epsilon$  of the  $\alpha$ -process [Adachi 1975].

observation of two distinct relaxation peaks which mimic the dynamics of the pure components in the limits of high respectively low concentration is fostered in the present mixtures by the large  $T_g$  contrast of  $\Delta T_g=255$  K and the low dipole moment of polystyrene:  $\Delta\epsilon$  of the components is of comparable magnitude, rendering it unlikely that toluene contributions to the dielectric loss are submerged under the dominant loss of the high  $T_g$  component, as in the case of PCB and picoline.

On grounds of these findings and due to the fact that corresponding <sup>2</sup>H NMR results are available [Rössler 1985], but lack critical assessment in the light of the dielectric findings, we have chosen to reflect selected literature data of the system toluene/polystyrene here. Not only the arise and temperature dependence of the three distinct processes itself, also the concentration dependence of their dielectric relaxation strength  $\Delta\epsilon$  is compatible to our findings in the afore discussed mixtures, as seen in figure 9.11 (b) and (c). Due to the lack of isothermal spectra it is not possible to monitor the temperature dependence of e.g.  $\Delta\epsilon_\beta$ , but it is clearly seen that (accepting that the Curie law holds) the relaxation strength of the  $\beta$ -process

(b). Spectra of pure polystyrene are not included in [Adachi 1975] and the contradiction is not discussed by the authors.

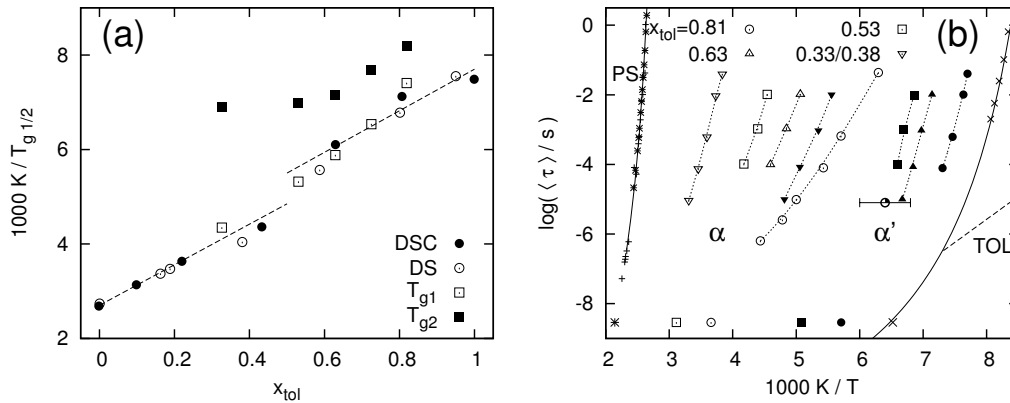


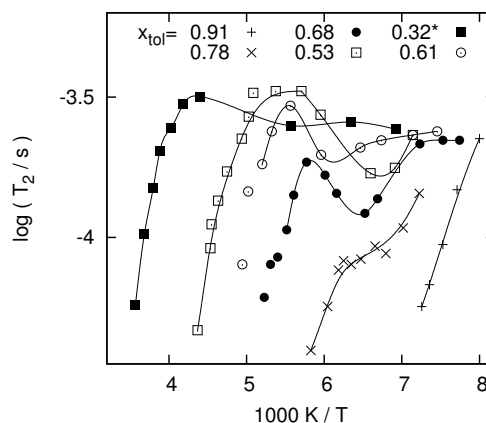
**Figure 9.12 (a):** Concentration dependence of the glass transition temperature in toluene / polystyrene mixtures. Dielectric and calorimetric  $T_g$ s ( $\circ$ ,  $\bullet$ ) from [Adachi 1975] and more recent calorimetric data ( $\square$ ,  $\blacksquare$ ) from [Taniguchi 2004]. Lines serve as guide for the eye. **(b):** Correlation times corresponding to the frequency of the loss maximum for  $\alpha$ - (open symbols) and  $\alpha'$ -process (full symbols) [Taniguchi 2004]. Correlation times of neat toluene ( $\times$ ) from [Kudlik 1997b], neat polystyrene data taken from [Pschorn 1991] (+, NMR) and [Hintermeyer 2008] (\*, DS). Secondary relaxation of neat toluene sketched as dashed line. Time constants in the ns-regime from  $T_1$  minima [Rössler 1985] with corresponding symbols, see text. Dotted lines serve as guide for the eye.

traverses a maximum at intermediate concentrations, which resembles the arise of a plateau or shoulder in  $1-S$  around the same concentrations for toluene in PCB and picoline (cf. figures 8.4 (b) and 9.5(a)).

As the relaxation strength of the  $\beta$ -process grows at intermediate concentrations,  $\Delta\epsilon$  of the  $\alpha'$ -process decreases in a manner that the total relaxation strength  $\Delta\epsilon_\beta + \Delta\epsilon_{\alpha'}$  depicts a steady, monotonic concentration dependence. The relaxation strength of the  $\alpha$ -process on the other hand is virtually constant for high polystyrene concentrations and exhibits a strong decrease for  $x_{\text{tol}} > 0.5$ .

In a more recent publication the same authors presented refined calorimetric measurements [Taniguchi 2004], in the course of which a second step in the heat capacity corresponding to the  $\alpha'$ -process at intermediate concentrations was found, cf. figure 9.12 (a). In the same publication isothermal dielectric spectra (yet with a rather narrow frequency window) are reported, the corresponding time constants are plotted in figure 9.12 (b): the depicted scenario is comparable to the one observed in toluene / PCB, i.e. for all concentrations two distinct loss peaks (in addition to the  $\beta$ -process of toluene) are observed that follow a VFT temperature dependence. The dynamics of polystyrene and (a fraction of) toluene are hence decoupled, whereas the constant relaxation strength  $\Delta\epsilon$  of the  $\alpha$ -process at low toluene concentrations in figure 9.11 (c) points towards a contribution of toluene molecules to the  $\alpha$ -process of PS. Consequently again a bi-modal scenario is observed for the toluene dynamics in the mixtures.

**Figure 9.13:** Spin-spin relaxation times  $T_2$  of polystyrene- $d_x$  for different concentrations of toluene in polystyrene [Rössler 1985].  $T_2$  in the concentration  $x_{\text{tol}}=0.32$  was recorded in PS- $d_3$ , the remainder in PS- $d_5$ .



### 9.3.1 NMR results

For the present system compatible  $^2\text{H}$  NMR measurements [Rössler 1985] exist, which, due to the selective nature of the technique can resolve some of the open questions regarding the dielectric results. From the multitude of  $^2\text{H}$  NMR data we will only discuss a few aspects which appear relevant in the current context, whereas the remainder of findings is qualitatively in agreement with the results presented for the system toluene / PCB in chapter 8.

Spin lattice relaxation measurements ( $\omega_L=55$  MHz) were conducted for polystyrene- $d_5$  and toluene- $d_3$  individually in the mixtures, hence the time constants extracted from the minimum condition, cf. equation 3.29, can be opposed to comparable concentrations<sup>5</sup> in dielectric spectroscopy (additional points in the ns regime in figure 9.12). The time constants from the  $T_1$  minima of PS are compatible with a VFT extrapolation of the dielectric  $\tau_\alpha$  for the respective concentrations, those of toluene correspond to  $\tau_{\alpha'}$  from DS. In mixtures of toluene and PCB the  $T_1$  minimum of toluene- $d_5$  was also dominated by the  $\alpha'$ -process, bi-modal behaviour, i.e. a contribution of toluene to the  $\alpha$ -process of PCB, was only observed at relatively lower temperatures (cf. figure 8.16).

At lower temperatures the spin-spin relaxation times  $T_2$  of polystyrene, cf. figure 9.13 (a), depict the arise of a shallow minimum around 150 K, very similar to the effects observed in chapter 6 and 8, where the minimum was attributed to the fast, anisotropic motion of the  $\beta$ -process in the respective systems. As however polystyrene is a type-A glass former, i.e. exhibits no  $\beta$ -process in the neat form, and the (again concentration independent)  $\tau_\beta$  of toluene would yield a minimum for  $\tau = 1/\delta$  at significantly lower temperatures<sup>6</sup>, a different process has to account for the observed minimum. The condition  $\tau = 1/\delta$  at the temperature of the  $T_2$  minimum yields correlation times comparable to the  $\alpha'$ -process for the given concentrations (sketched as horizontal bar in figure 9.13 (b)). A distinct  $T_2$  minimum in polystyrene is only observed in the range  $x_{\text{tol}}=0.53-0.68$  and the dielectric  $\alpha'$ -process of the  $x_{\text{tol}}=0.53$

<sup>5</sup>DS:  $x_{\text{tol}}=0.81$  and  $0.53$ , polystyrene- $d_5$   $T_1$ :  $x_{\text{tol}}=0.80$  and  $0.53$ , toluene- $d_3$   $T_1$ :  $x_{\text{tol}}=0.72$  and  $0.55$ .

<sup>6</sup>At about 110 K, cf. figure 8.22 (b). The  $T_2$  data reported by Rössler [Rössler 1985] do however not extend to temperatures lower than 125 K.

and 0.63 samples lies right in the respective time window. Consequently the spin-spin relaxation times of polystyrene give strong hints towards a (concentration dependent) contribution of PS to the  $\alpha'$ -process of toluene via an anisotropic, small angular reorientation – much like the  $\beta$ -process.

## 9.4 A model for the concentration dependence of the $\beta$ -process

In the previous sections we established a scenario of dynamically distinct toluene fractions arising in binary mixtures of the compound: depending on concentration and temperature a fraction of toluene molecules exhibits a fast  $\alpha'$ -process ( $\tau_{\alpha'} \ll \tau_{\alpha}$ ) and the  $\beta$ -process of neat toluene, whereas the remainder of molecules contributes to the  $\alpha$ -process of the high  $T_g$  component and no longer to the  $\beta$ -process. Such a model has proven very versatile in the description of the results from the multitude of conducted experiments, it is however due to the fast exchange mechanism observed between the processes not possible to strictly quantify the concentration dependence of the individual fractions above  $T_g$ . Below the glass transition temperature such an effective exchange is however no longer present, consequently we will focus on a quantitative assessment of the observed concentration dependence of the  $\beta$ -process in this temperature regime.

In the following we introduce a model in the attempt to rationalise the concentration dependent relaxation strength of the  $\beta$ -process by means of the self-concentration of toluene, i.e. via the changes imposed on the energy landscape for varying local concentrations. It became evident in the course of this work that the  $\beta$ -process of toluene exhibits rather universal characteristics in mixtures with substances as diverse as picoline and PCB54. The relaxation strength of the  $\beta$ -process in the mixtures is subject to a distinct concentration dependence: the changes in  $f_{\beta}$  observed at intermediate and low toluene contents were explained with the emergence of a fraction of molecules with suppressed (or no)  $\beta$ -process and a contribution of the high  $T_g$  component to the  $\beta$ -process.

As all these observations were made below the glass transition temperature of neat toluene, we can safely regard the matrices as rigid on our experimental time scale. Hence the simplest approach to model the energy landscape probed by a certain toluene molecule is to describe it via nearest neighbour contacts. Jones et al. [Jones 1991] proposed a simple lattice model to describe the line shape and  $T_1$  results in a polymer diluent mixture, which provides a good starting point for the considerations in this section.

We hence assume a simple cubic lattice with six neighbours per site, where each site is occupied according to random statistics and the probability  $p$  to find a molecule of species A on a site is equal to the mole fraction of the species  $p = x_A$ . The fraction of sites which are completely surrounded by molecules of type A is then given via

$$F_0 = p^6. \quad (9.2)$$

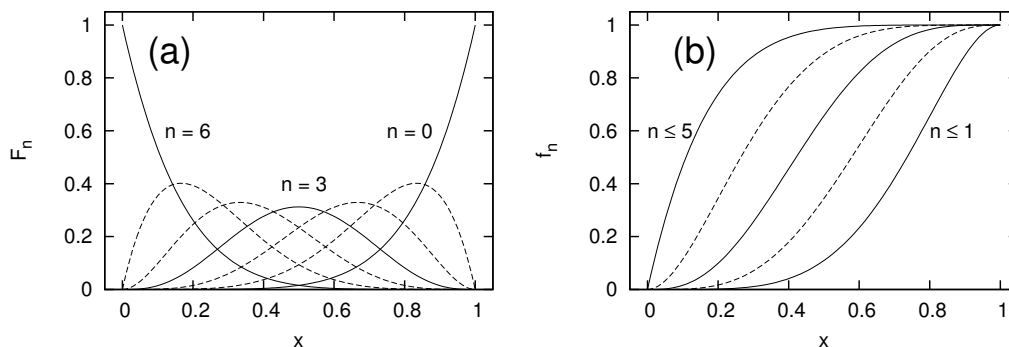


**Figure 9.14 (a):** Concentration dependent populations  $F_n$  for type A molecules with  $n$  neighbours of species B in the simple lattice model. **(b):** Cumulative concentration dependent populations  $f_n$ .

The fraction  $F_n$  of species A adjacent to  $n = 1, \dots, 6$  neighbours of type B reads:

$$F_n = \binom{6}{6-n} p^{6-n} (1-p)^n. \quad (9.3)$$

The resulting population densities are plotted in figure 9.14 (a). The relaxation behaviour of a toluene molecule in this simple approach is however not expected to change continuously with its local environment, as we observed a threshold concentration of about  $x_{\text{tol}}=0.75$  in  $f_\beta$ . Therefore we introduce the cumulative populations  $f_n$ , denoting the probability to find at least  $n$  toluene molecules in the first coordination shell of the molecule under consideration:

$$f_n = \sum_{i=0}^n F_i, \quad (9.4)$$

which already qualitatively resemble the experimentally found concentration dependence of  $f_\beta$ , cf. figure 9.14 (b).

### 9.4.1 Application

Figure 9.15 displays the agreement between the experimentally obtained fraction of toluene molecules with an active  $\beta$ -process ( $f_\beta$ ) and the findings in the lattice model for  $f_3$  and  $f_4$  (equation 9.4). According to the proposed geometry the model predicts that a toluene molecule in mixtures with PCB54 or picoline contributes to the  $\beta$ -process of the neat system when surrounded by at least two to three other toluene molecules, i.e. adjacent to a maximum of three to four molecules of a different species<sup>7</sup>.

In dielectric spectroscopy we observed the opposite effect in 1-*S*: an excess strength arises for intermediate concentrations. As all molecules under consideration in this work exhibit non-vanishing dipole moments, dielectric spectroscopy – opposed

<sup>7</sup>The given numbers are an artificial result of the geometrical constraints of the model, i.e. the construction of the lattice. The qualitative argument however holds for all geometries.

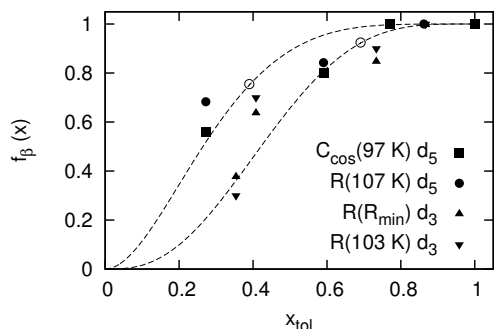


**Figure 9.15:** Concentration dependent fraction  $f_\beta$  of toluene molecules exhibiting a  $\beta$ -process in mixtures with PCB54 (full symbols) and picoline (open symbols [Tschirwitz 2001]), the lines represent  $f_4$  and  $f_3$  (left to right) calculated in the lattice model.

to  $^2\text{H}$  NMR – always measures a bulk quantity: the response of both species in the binary mixtures. Figure 9.16 displays  $1-S \approx \Delta\epsilon_\beta/\Delta\epsilon$ , i.e. the fraction of the total relaxation strength that is attributed to the  $\beta$ -process of toluene in mixtures with PCB. For a discussion within the present model, we have to account for the concentration dependent contribution of toluene to the total relaxation strength of the sample. Concentration dependencies of  $1-S$  and  $\Delta\epsilon$  have been discussed in chapter 7: the relaxation strength  $1-S^{\text{tol}}$  resulting from a linear interpolation via equation 7.4 is given as dotted line in figure 9.16. As the dipole moment of PCB54 and picoline is substantially larger than the one of toluene,  $1-S^{\text{tol}}$  strongly decreases already at relatively high toluene concentrations. For concentrations  $x_{\text{tol}} \geq 0.8-0.9$  the result of equation 7.4 coincides with the experimental data of toluene / PCB and toluene / picoline, at lower concentrations however significant deviations are observed. To account for the fraction of toluene molecules without a  $\beta$ -process, equation 7.4 was multiplied with  $f_4$  (for which best agreement with  $^2\text{H}$  NMR data in figure 9.15 was found):

$$1 - S^{\text{tol}}(x_{\text{tol}}) = f_4(x_{\text{tol}}) \cdot \frac{x_{\text{tol}} \cdot (1 - S_0^{\text{tol}})}{x_{\text{tol}} + (1 - x_{\text{tol}}) \cdot \Delta\epsilon_0^{\text{B}}/\Delta\epsilon_0^{\text{tol}}} \quad (9.5)$$

The result is represented by the dash-dotted line in figure 9.16 (a): the changes in  $1-S$  predicted within the lattice model are restricted to low concentrations, where the relaxation strength of toluene has almost vanished. Consequently the differences introduced by  $f_\beta$  are very subtle in the case of toluene / PCB, for toluene in picoline the results of equation 9.5 have been omitted in figure 9.16 (b), as they coincide with those of equation 7.4. It hence becomes obvious that the changes imposed by the fraction  $1-f_\beta$  are of very subtle nature for the quantities measured by dielectric spectroscopy and are easily overlooked or even below the experimental error margins – whereas in  $^2\text{H}$  NMR due to the selectivity of the method, distinct effects are observed. The dominant deviations in  $1-S$  at intermediate concentrations arise from a contribution of the high  $T_g$  component to the  $\beta$ -process of toluene, as demonstrated in section 9.2.3 for the case of toluene in picoline. In this respect it is counter-intuitive that the decay in  $1-S$  at high toluene concentrations is in agreement with equation 7.4: assuming that all PCB54 or picoline molecules contribute to the  $\beta$ -process, a constant  $1-S$  would be observed. Even if the respective  $1-S^{\text{B}}$  of the latter molecules is smaller than found in toluene at the respective temperature, a distinct deviation

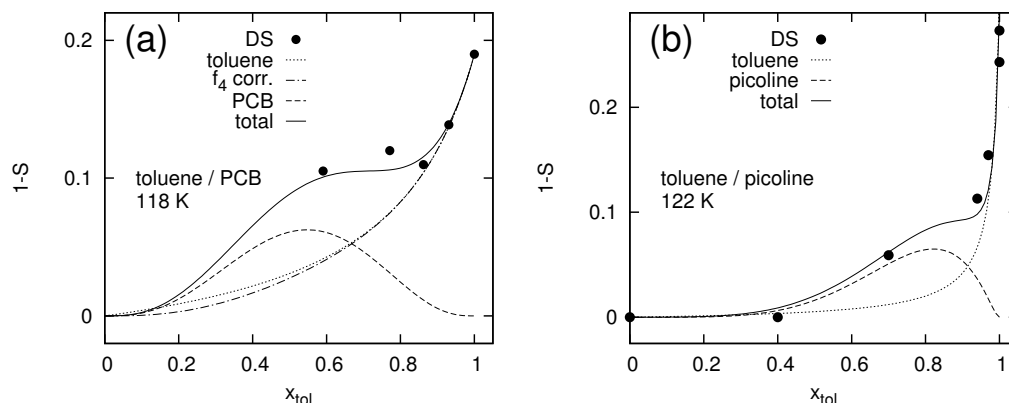


**Figure 9.16 (a):** Relative dielectric relaxation strength of the  $\beta$ -process  $1-S$  in the toluene / PCB54 mixtures ( $\bullet$ , [Cangialosi 2009]) at 118 K. The dotted line represent a linear extrapolation for the concentration dependent relaxation strength of toluene (equation 7.4), the dash dotted line is the toluene contribution corrected for  $f_4$  in the lattice model. The dashed line denotes the contribution of PCB54 to the  $\beta$ -process calculated from  $F_2 + F_3$ , the full line is the sum of toluene and PCB contributions to the  $\beta$ -process (again corrected via  $f_4$ ). **(b):** Same representation for mixtures of toluene with picoline at 122 K [Tschirwitz 2001], here the picoline contribution is modelled via  $F_1$ .

would appear already in the high concentration limit. If we assume a cooperative nature also for the contribution of species B to the  $\beta$ -process, we can model the excess strength in  $1-S$  via

$$1 - S_n^B(x_{tol}) = s^B \left(1 - S_0^{tol}\right) F_n(x_{tol}) \Delta\epsilon^B(x_{tol}), \quad (9.6)$$

which is plotted as dashed line in figure 9.16. Here  $s^B$  accounts for a reduced relaxation strength of the contributing high- $T_g$  component molecules and  $F_n$  from equation 9.3 models the cooperative nature of the dynamics. The sum of the toluene and PCB54 / picoline contributions is in agreement with the experimental  $1-S$  in both cases for  $s^B = 0.6$ , albeit with  $F_n = F_2 + F_3$  for the mixtures with PCB54 and  $F_n = F_1$  in the system toluene / picoline. As the quality of data in the toluene / PCB54 mixtures is rather poor and concentrations below  $x_{tol}=0.6$  are missing, we will not further stress the differences. For the mixtures of toluene and polystyrene only isochronal dielectric measurements are available (cf. section 9.3) and hence a quantitative modelling of the experimental  $1-S$  is not possible in this system. The reported relaxation strength  $T\Delta\epsilon_\beta$  in figure 9.11 (b) however exhibits a peak at about  $x_{tol}=0.8$  – as does  $1-S_1^B$  (dashed line figure 9.16), i.e. the results are comparable to the mixtures of toluene and picoline.

According to the present model the dielectric measurements consequently depict a scenario in which a molecule of species B contributes to the  $\beta$ -process (of toluene) if it is found in an environment with five toluene neighbours and one of the same species – for higher and lower local concentrations a contribution is not observed. Explicit conclusions from this counter-intuitive behaviour are not appropriate at this point, as certainly further experimental proof is required.

# Discussion and outlook

---

In the previous chapters we have selectively studied the primary and secondary relaxation of toluene in mixtures with PCB54. All  $^2\text{H}$  NMR techniques –  $T_1$ , line shape analysis, stimulated echo, 2D NMR spectra – concertedly demonstrate that a fraction of toluene molecules exhibits dynamics significantly faster than the PCB54 component at all concentrations, i.e. the motion is decoupled. Then again, at typically slightly higher temperatures, a slower toluene fraction enters the  $^2\text{H}$  NMR time window and the same experiments reveal sub-ensembles with reorientation on the time scale of PCB. The fact alone that this behaviour can not be comprehensively explained via a single distribution  $G(\log \tau_\alpha)$  – regardless of how broad and asymmetric it may become – yields strong arguments for a bimodal relaxation behaviour of toluene in the present mixtures. The observation of “islands of mobility” with regard to the  $\beta$ -process at low temperatures is clearly in favour of such a scenario and the model based on the latter findings has proven to sufficiently reproduce all obtained  $^2\text{H}$  NMR results. The interdependence of the fast  $\alpha'$ -process on the  $\beta$ -process of toluene – which were assumed to be coupled in the model – demonstrates the significance of the  $\beta$ -process for glassy dynamics: the behaviour of the structural relaxation of a certain sub-ensemble, observed by  $^2\text{H}$  NMR at temperatures well above the (lower)  $T_g$ , is already imprinted in its  $\beta$ -process in the glassy state.

With regard to future studies of binary mixtures, the present results suggest that the application of a single experimental technique is unlikely to allow for definite conclusions. The pronounced dynamic heterogeneities in such systems represent a challenge for any technique with a rather narrow time window, such as NMR. Broadband techniques like dielectric spectroscopy on the other hand often lack the required selectivity: even for mixtures of compounds with vastly different dipole moments, it may become difficult to de-convolute the contributions in either concentration limit. A systematic combination of methods, by means of a mixture of components with comparable dipole moments and different NMR active nuclei like  $^{31}\text{P}$  and  $^2\text{H}$  for example, could yet serve to further clarify the nature of dynamics in binary systems. We will now conclude this discussion with a few remarks on the observed “islands of mobility”. The proposed lattice model provides arguments for an explanation of the observed concentration dependence for  $\beta$ -process via a certain degree of cooperativeness. The model was applied in the low temperature regime,  $T < T_g$ , where no effective exchange mechanisms are present and the local concentration does not change with time in first approximation. Under these conditions one may speculate that, as long as the environment of a toluene molecule is dominated by other molecules of the same species, the energy landscape is comparable to the one in the neat system and the molecule exhibits a  $\beta$ -process. If – upon lowering the toluene concentration – a local  $\beta$ -process would probe the steadily changing energy landscape

of its surroundings, one would expect to find a distinct concentration dependence in all of its properties: time scale, distribution  $G(\log \tau_\beta)$  thereof and mechanism, i.e. angular amplitude and consequently relaxation strength. In contrast our  $^2\text{H}$  NMR findings in mixtures of toluene and PCB indicate an unmodified  $\beta$ -process of virtually all toluene molecules at high concentrations and a threshold concentration of  $x_{\text{tol}} \approx 0.7$  below which the  $\beta$ -process vanishes in certain sub-ensembles, while others still exhibit the relaxation pattern of the neat system. In the lattice model this decrease of  $f_\beta$  was attributed to the absence of a  $\beta$ -process for molecules with less than two to three neighbouring toluene molecules, indicating a cooperative reorientation of the latter size as mechanism for the  $\beta$ -process in toluene.

Interestingly, and against common perception in terms of single molecules as dynamic probes for the respective environment, the model predicts a certain cooperativeness also for the molecules of the high  $T_g$  component contributing to the  $\beta$ -process of toluene: a single probe molecule – whether it be PCB, picoline or polystyrene – does apparently not participate in the  $\beta$ -process. A contribution of the high- $T_g$  component is only observed for intermediate local concentrations of the latter, before the  $\beta$ -process vanishes in the limit of low toluene concentration.

The arguments for a cooperativeness of the  $\beta$ -process in case of toluene are strong in the present mixtures. A certain degree of cooperativeness would furthermore explain the – for a local process – rather high activation enthalpy and is in agreement with the random first-order transition theory, which predicts reorientation of string-like or percolation-like clusters as origin for the secondary relaxation [Stevenson 2010]. The concentration dependence of the contribution from the high- $T_g$  component on the other hand has to be further analysed and conclusions should be drawn only with great care. The counter-intuitive behaviour in the limit  $x_{\text{tol}} \rightarrow 1$  demands for further affirmative experiments:  $^2\text{H}$  NMR studies on high ( $x_{\text{tol}} > 0.95$ ) and low ( $x_{\text{tol}} < 0.4$ ) concentrations of toluene- $\text{d}_0$  in picoline- $\text{d}_7$  for example.

With regard to the simple geometry assumed in the lattice model, one might propose to examine binary mixtures composed of plastic crystals. Singh et al. [Singh 2009] have studied mixtures of cyanocyclohexane and cyclohexylchloride by means of differential scanning calorimetry and dielectric spectroscopy: although the amount of data and extensiveness of interpretation is rather sparse, the obtained relaxation times  $\tau_\alpha$  give strong hints towards the formation of a plastically crystalline phase in the mixtures. Neat cyclohexylchloride forms a plastic crystal with a *fcc* lattice and a lattice constant of  $a = 9.05 \text{ \AA}$  at 244 K [Diky 1994], the phase can be supercooled and exhibits a calorimetric  $T_g$  at 116 K [Murthy 2000] – hence structure and dynamics in the plastic crystalline phase are very similar to the case of cyanocyclohexane. Although the nature of the  $\beta$ -process in cyclohexylchloride remains unclear,  $^2\text{H}$  NMR studies of binary mixtures composed of cyanocyclohexane and a cognate compound are promising not only with regard to the simple geometrical structure and the lack of translational motion, but especially as the  $\beta$ -process of cyanocyclohexane is now well studied and yields pronounced effects in  $^2\text{H}$  NMR measurements above  $T_g$  due to its fast and non-merging nature.

## Part III

# Summary, Appendix & Bibliography



## CHAPTER 11

# Summary

---

The present study employs various solid state  $^2\text{H}$  NMR techniques to elucidate glassy dynamics in plastic crystals and binary mixtures of glass forming substances. The focus hereby lies on the Johari-Goldstein  $\beta$ -process, which – as it turns out – not only plays a key role for the understanding of glassy dynamics in neat systems, but also in binary mixtures thereof.

The first part is devoted to the plastic crystalline (PC) phase of cyanocyclohexane, the previously unknown structure of which was suggested to be face-centred cubic via X-ray diffraction measurements. A 2D  $^2\text{H}$  NMR assessment of the molecular motion of the  $\alpha$ -process demonstrated that dynamics is not governed by the symmetry of the lattice, rather molecular reorientation in cyanocyclohexane can be modelled via the same distribution of small and large angular jumps as reported for many structural glass formers. Although the stimulated echo technique yields a strong temperature dependence of the latter fractions, it was shown that this effect can be rationalized by means of the time-window of the experiment and the inherent decoupling of jump-times within the distribution of angles. This analysis also holds in case of previously studied structural glass formers and questions the arise of a dynamical crossover at temperatures somewhat above  $T_g$ .

The  $\beta$ -process of cyanocyclohexane is below  $T_g$  well described by models developed for the structural glass former toluene, where the C- $^2\text{H}$  bond is confined to the base circle of a cone, i.e. also the secondary relaxation is not significantly affected by the translational symmetry of the PC phase. As  $\alpha$ - and  $\beta$ -process do not merge in cyanocyclohexane, pronounced effects were observed at high temperatures: for the first time a separate minimum in the spin-lattice relaxation  $T_1$  was found for the  $\beta$ -process; furthermore the solid echo spectra at  $T > T_g$  exhibit an articulate and characteristic deviation from a Pake pattern over a broad temperature range.

The latter fast motion limit line shape effects ( $\tau_\beta \ll 1/\delta$ ) allow for a direct determination of the degree of restriction: a model based on a Gaussian distribution of cone opening angles  $\chi$  proved adequate for a detailed modelling of the spectral evolution in this temperature regime.  $\langle 1/T_1 \rangle$  was modelled in the whole temperature range (70 K to 285 K) by means of the spectral density from dielectric spectroscopy, the results in terms of the relaxation strength  $1-S$  are in agreement with the line shape analysis.

Hence the attribution of the prominent  $^2\text{H}$  NMR features above  $T_g$  to the  $\beta$ -process has proven valid: fast motion limit line shape effects and the second minimum in  $T_1$  naturally arise due to the time scale separation of  $\alpha$ - and  $\beta$ -process in cyanocyclohexane and are in full agreement with an extension of previous models for the  $\beta$ -process in structural glass formers at  $T < T_g$ . Furthermore the present study emphasizes the important role of the  $\beta$ -process for glassy dynamics, as it demonstrates that a

substantial fraction of correlation is lost via the  $\beta$ -process at high temperatures if the processes do not merge – which again stimulates discussion about the nature of dynamics at temperatures above the merging in other glass forming systems.

The second part addresses the dynamics of the glass former toluene in binary mixtures. Below  $T_g$  of neat toluene – in absence of effective exchange mechanisms – a pronounced concentration dependence of the  $\beta$ -process was observed in mixtures of toluene and a polychlorinated biphenyl (PCB54), which exhibits a significantly higher  $T_g$ : whereas the distribution of correlation times  $G(\log \tau_\beta)$  remains unaltered, the relaxation strength of the process significantly decreases below a threshold concentration of  $x_{\text{tol}} \simeq 0.7$ . Stimulated echo experiments demonstrated that the attenuation in relaxation strength arises from a concentration dependent fraction of toluene molecules,  $1-f_\beta$ , which do no longer exhibit a  $\beta$ -process. This finding is in accordance with bi-exponential magnetization curves observed in a (concentration dependent) temperature regime around  $T_g$  of the mixture. Hence the “islands of mobility” concept for the  $\beta$ -process, refuted in the case of neat glass formers, was introduced in binary mixtures thereof.

Based on these findings a model was developed that links the fraction  $1-f_\beta$  to toluene molecules in a local PCB54 rich environment, which only exhibit the  $\alpha$ -process of the latter, whereas the remainder of molecules  $f_\beta$  reorient on a faster time scale ( $\alpha'$ -process) and show a  $\beta$ -process. This bimodal approach with two distinct toluene sub-ensembles was shown to explain the observed behaviour in virtually all NMR experiments, whereas an adaptation via a single broad distribution  $G(\log \tau_\alpha)$  for the toluene motion was infeasible. The relative weight of the fractions is a function of concentration and temperature, which results naturally as 2D NMR spectra demonstrated that exchange between the respective sub-ensembles exists. At high temperatures the majority of toluene molecules exhibit the fast  $\alpha'$ -process, whereas below (the upper)  $T_g$  more and more toluene molecules appear “frozen” on the PCB54 component and hence only exhibit the  $\alpha$ -process of the latter. The proposed scenario predicts the arise of two glass transition temperatures, which was confirmed via the emergence of a small second step in DSC measurements.

To elucidate the mechanism of  $\alpha$ - and  $\alpha'$ -process, 2D NMR methods were employed: although the processes are not clearly separated within the  $^2\text{H}$  NMR time window and presumably both contribute to the results, no change in the mechanism of motion was detected. Toluene molecules in binary mixtures with PCB54 proceed via the same mechanism as in the neat system –  $\alpha$ - and  $\alpha'$ -process both appear to be isotropic processes governed by typical glassy dynamics.

To widen the validity of the present study, previous results from other binary mixtures containing toluene were reassessed in the light of our findings: all features regarding the  $\beta$ -process were recovered in the system toluene/picoline, i.e. again “islands of mobility” were detected. Furthermore a contribution of the high- $T_g$  component picoline to the  $\beta$ -process of toluene was affirmed by  $^2\text{H}$  NMR measurements, as anticipated in the case of toluene/PCB54 from dielectric results. The concentration dependence of  $f_\beta$  below  $T_g$  in diverse mixtures of toluene was successfully described within a simple lattice model, i.e. via static nearest neighbour contacts. This dependence of the  $\beta$ -process on the local toluene concentration provides strong arguments for a cooperativeness of the process, in contrast to the general perception.

# Zusammenfassung

---

Die vorliegende Arbeit verwendet verschiedene Methoden der  $^2\text{H}$  Festkörper-NMR, um die Dynamik in plastischen Kristallen und binären Mischungen von Glasbildnern aufzuklären. Ein Schwerpunkt liegt hierbei auf dem Johari-Golstein  $\beta$ -Prozess, welcher für das Verständnis der Dynamik sowohl in reinen Systemen als auch binären Mischungen von Glasbildnern eine Schlüsselrolle einnimmt.

Teil I ist der plastisch-kristallinen (PC) Phase von Cyanocyclohexan gewidmet, welche (wie mittels Röntgenstreuung gezeigt wurde) vermutlich eine kubisch flächenzentrierte Struktur aufweist. 2D  $^2\text{H}$  NMR-Untersuchungen legten dar, dass der Reorientierungsmechanismus des  $\alpha$ -Prozesses nicht von der Gittersymmetrie geprägt ist. Vielmehr kann die Bewegung mittels der gleichen Verteilung von Groß- und Kleinwinkelsprüngen beschrieben werden, die bereits in vielen strukturellen Glasbildnern gefunden wurde. Obwohl der relative Anteil an Großwinkelsprüngen im Experiment eine starke Temperaturabhängigkeit aufweist, konnte gezeigt werden, dass sich dieser Befund mittels Zeitfenstereffekten der verwendeten Methode erklären lässt und eine direkte Konsequenz der inhärenten Entkopplung der Zeitskalen des Elementarsprungs für große und kleine Sprungwinkel darstellt. Da diese Analyse von allgemeiner Gültigkeit ist, stellt sie das Auftreten eines dynamischen Übergangs in Gläsern oberhalb von  $T_g$  infrage.

Der  $\beta$ -Prozess von Cyanocyclohexan unterhalb von  $T_g$  lässt sich mittels Modellen beschreiben, die anhand von  $^2\text{H}$  NMR-Experimenten in Toluol entwickelt wurden, d.h. auch die Sekundärrelaxation zeigt in diesem Temperaturbereich keine Besonderheiten, welche sich auf die Translationssymmetrie der PC-Phase zurückführen lassen. Da die Zeitskalen von  $\alpha$ - und  $\beta$ -Prozess in Cyanocyclohexan auch bei hohen Temperaturen getrennt sind, wurden in diesem Bereich ausgeprägte Effekte beobachtet: Erstmals wurde ein Minimum in der Spin-Gitter-Relaxation  $T_1$  aufgrund des  $\beta$ -Prozesses gefunden. Desweiteren zeigen die Festkörperspektren deutliche und charakteristische Abweichungen von einem Pake-Spektrum über einen breiten Temperaturbereich oberhalb von  $T_g$ . Diese Spektren im schnellen Grenzfall ( $\tau_\beta \ll 1/\delta$ ) erlauben es direkt die einschränkende Geometrie des  $\beta$ -Prozesses zu bestimmen: Basierend auf einer Bewegung innerhalb eines Konus und mittels einer Gaußverteilung an Öffnungswinkeln konnte die Linienform der Spektren bei allen Temperaturen reproduziert werden.  $\langle 1/T_1 \rangle$  konnte ebenfalls über den zugänglichen Temperaturbereich (70 K to 285 K) mittels der Spektraldichte aus der dielektrischen Spektroskopie modelliert werden, wobei die erhaltene Relaxationsstärke  $1-S$  die Ergebnisse der Linienformanalyse bestätigte. Die prominenten Effekte in der  $^2\text{H}$  NMR-Linienform und Spin-Gitter-Relaxation oberhalb von  $T_g$  sind somit eindeutig dem  $\beta$ -Prozess zuzuordnen und ergeben sich direkt aus einer Erweiterung bestehender Modelle zum  $\beta$ -Prozess unterhalb von  $T_g$  aufgrund der Zeitskalenseparation von  $\alpha$ - und  $\beta$ -Prozess

in Cyanocyclohexan.

Zudem verweist die vorliegende Studie auf die bedeutende Rolle des  $\beta$ -Prozesses für die Dynamik in unterkühlten Flüssigkeiten, da der  $\beta$ -Prozess in Cyanocyclohexan bei hohen Temperaturen zu einem signifikanten Verlust an Orientierungskorrelation führt und somit Anlass zu weiteren Diskussionen über die Dynamik in strukturellen Gläsern bei Temperaturen oberhalb des Zusammenlaufens von  $\alpha$ - und  $\beta$ -Prozess liefert.

Der zweite Teil dieser Arbeit befasst sich mit der Dynamik des Glasbildners Toluol in binären Mischungen. In Mischungen mit einem polychlorierten Biphenyl (PCB54) wurde bei Temperaturen unterhalb der Glasübergangstemperatur reinen Toluols, d.h. in Abwesenheit eines schnellen Austauschprozesses, eine ausgeprägte Konzentrationsabhängigkeit des  $\beta$ -Prozesses gefunden. Während die Verteilung von Korrelationszeiten  $G(\log \tau_\beta)$  konstant bleibt, nimmt die Relaxationsstärke des Prozesses unterhalb einer Konzentration von  $x_{\text{tol}} \simeq 0.7$  stark ab. Mithilfe der Technik des Stimulierten Echos wurde dieses Absinken der Relaxationsstärke einem konzentrationsabhängigen Anteil  $1-f_\beta$  von Toluolmolekülen zugeordnet, die keinen  $\beta$ -Prozess mehr aufweisen. Dieser Befund ist im Einklang mit bimodalen Magnetisierungskurven, die in einem (konzentrationsabhängigen) Temperaturbereich um  $T_g$  gefunden wurden. Folglich stellt die "islands of mobility"-Hypothese, welche für den Fall reiner Systeme widerlegt wurde, eine gültige Beschreibung binärer Mischungen dar.

Anhand dieser Beobachtungen wurde ein Modell entwickelt, welches den Anteil  $1-f_\beta$  mit Toluolmolekülen verknüpft, die sich in einer Umgebung mit lokal hoher PCB54-Konzentration befinden und nur den  $\alpha$ -Prozess jener Substanz aufweisen, wohingegen die restlichen Moleküle schnellere Dynamik (den  $\alpha'$ -Prozess) und einen  $\beta$ -Prozess zeigen. Dieser bimodale Ansatz mit zwei dynamisch unterscheidbaren Toluol-Anteilen ermöglicht es nahezu alle NMR-Resultate im Detail zu erklären, wohingegen eine Anpassung mittels einer einzelnen Korrelationszeitenverteilung  $G(\log \tau_\alpha)$  nicht möglich war. Die relative Gewichtung der Anteile ist eine Funktion der Temperatur und Konzentration; weiterhin wurde mittels 2D NMR-Spektren Austausch zwischen den Fraktionen nachgewiesen. Bei hohen Temperaturen nimmt ein Großteil der Toluolmoleküle am schnellen  $\alpha'$ -Prozess teil, unterhalb von  $T_g$  "frieren" jedoch mehr und mehr Moleküle an der PCB54-Komponente aus und zeigen nur noch deren  $\alpha$ -Prozess. Das vorgeschlagene Szenario prognostiziert das Auftauchen zweier Glasübergangstemperaturen, was mittels einer zweiten (schwachen) Stufe in DSC Messungen nachgewiesen wurde.

Um den Mechanismus des  $\alpha$ - und  $\alpha'$ -Prozesses zu untersuchen, wurden weitere 2D NMR-Methoden eingesetzt: Obwohl die Prozesse innerhalb des NMR-Zeitfensters nicht deutlich getrennt sind und somit beide zu den Resultaten beitragen, wurde keine Änderung des Bewegungsmechanismus gegenüber reinem Toluol festgestellt. Toluolmoleküle in Mischungen mit PCB54 reorientieren mittels derselben Sprungwinkelverteilung wie im reinen System – es scheint sich sowohl bei  $\alpha$ - als auch beim  $\alpha'$ -Prozess um eine isotrope Bewegung mit typischer Glasdynamik zu handeln.

Um die Aussagekraft der Studie zu untermauern, wurden Literaturdaten weiterer binärer Mischungen von Toluol im Lichte der vorliegenden Ergebnisse neu ausgewertet: Alle Beobachtungen bezüglich des  $\beta$ -Prozesses wurden in Mischungen von Toluol und Picolin bestätigt, auch hier wurden "islands of mobility" gefunden. Weiterhin

wurde eine Beteiligung der Picolinmoleküle am  $\beta$ -Prozess von Toluol mittels  $^2\text{H}$  NMR nachgewiesen. In Mischungen mit PCB54 zeichnete sich dieses Verhalten anhand dielektrischer Daten ab. Die Konzentrationsabhängigkeit von  $f_\beta$  unterhalb von  $T_g$  in verschiedenen Mischungen von Toluol wurde anhand eines einfachen Gittermodells erklärt. Diese Abhängigkeit des  $\beta$ -Prozesses von der lokalen Toluolkonzentration liefert entgegen der gemeinhin akzeptierten Sichtweise Hinweise auf eine (schwache) Kooperativität.



# Additional results: cyanocyclohexane

---

## Contents

---

<b>A.1 Dielectric spectroscopy</b> . . . . .	<b>199</b>
<b>A.2 Spin-lattice relaxation</b> . . . . .	<b>200</b>
<b>A.3 Spin-spin relaxation times</b> . . . . .	<b>202</b>
<b>A.4 Correlation of time scale and geometry for the <math>\beta</math>-process</b> .	<b>202</b>

---

In the following we briefly discuss additional data obtained from  $^2\text{H}$  NMR measurements on cyanocyclohexane, as well as further dielectric data and interpolations thereof employed in the analysis and simulations in part I.

## A.1 Dielectric spectroscopy

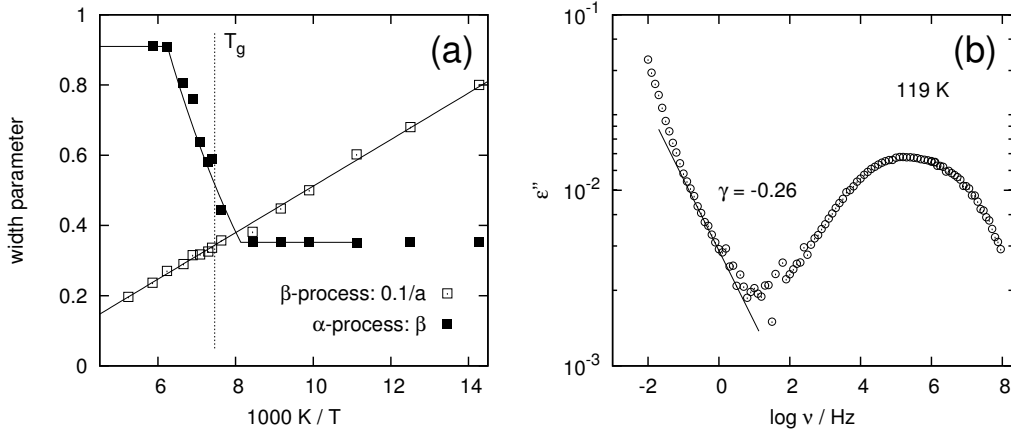
### Distribution parameters

Figure A.1 (a) presents the width parameters  $\alpha, \beta$  of the generalized gamma (GG) and  $G_\beta$  distributions as obtained from fits to dielectric data [Tschirwitz 2002a]. The interpolation of the shape parameter  $\beta$  of the GG distribution for the  $\alpha$ -process (full line) is employed in the random walk simulations of the solid echo line shape in figure 6.24 and of the stimulated echo presented in section 6.4.4. The parameter  $\alpha$  in equation C.12 was thereby kept constant ( $\alpha=20$ ).

The distribution  $G_\beta$  for the  $\beta$ -process was used in section 6.4.2 for means of comparison with the log-Gaussian distribution, which was employed in the majority of simulations. The shape parameter  $a$  is given with according interpolation in figure A.1 (a). The parameter  $b$  in equation C.17 was set to one, i.e. a symmetric distribution was chosen (as found by dielectric spectroscopy). The width parameter  $W$  of the log-Gaussian distribution with according interpolation for simulation purposes is presented in figure 6.4 (b), we found no significant differences between line shape simulations employing either distribution.

### Excess wing

Figure A.1 (b) presents the dielectric spectrum of cyanocyclohexane at  $T=119\text{ K}$ . In section 6.4.4 it was speculated that the observed temperature dependence of the  $t_e$ -dependent stimulated echo is (partially) linked to the dynamics of an excess wing. The given spectrum demonstrates the presence of a small wing on the high frequency



**Figure A.1 (a):** Width parameters  $\beta, a$  of the generalized gamma and  $G_\beta$  distributions as obtained from dielectric spectroscopy [Tschirwitz 2002a]. The full lines represent interpolations employed for random walk simulations in part I. **(b):** Low temperature dielectric spectrum ( $T=119$  K, [Tschirwitz 2002a]) that indicates the existence of an excess wing in cyanocyclohexane. A crossover from the high frequency flank of the  $\alpha$ -peak to a power law with an lower exponent is observed.

flank of the  $\alpha$ -process at the given temperature. Although the feature is quite subtle in contrast to type-A systems, i.e. glass formers without a  $\beta$ -peak in the dielectric spectrum, an excess wing appears to be present also in the plastic crystalline phase of cyanocyclohexane.

## A.2 Spin-lattice relaxation

### Extreme narrowing regime

Above  $T_m=285$  K, in the simple liquid, dynamics in cyanocyclohexane is fast relative to the NMR frequency ( $\tau \approx 10^{-12} s \ll 1/\omega_L$ ). Correlation times obtained from the extreme narrowing condition

$$\frac{1}{T_1} = \frac{4}{3} \delta^2 \tau \quad (\text{A.1})$$

are plotted in figure A.2 (a) (full circles), which are approximately in agreement with results from dynamic light scattering [Surovtsev 2003] in the liquid phase.

Below the melting point, for temperatures  $250 \text{ K} < T < T_m = 285 \text{ K}$ , we observed the same behaviour as described by Surovtsev et al. [Surovtsev 2003]: depending on the cooling rate, thermal hysteresis of the sample and ageing the transition to phase I (the plastic crystalline phase) was incomplete, i.e. it always existed to some extent coevally to the liquid or another unknown (possibly also plastic crystalline) phase with a different  $\alpha$ -relaxation time  $\tau_\alpha$ , reflected in somewhat arbitrary spin lattice relaxation times. Since no systematic dependence of the phase transition on the control parameters was found, the temperature range under discussion was neglected in this work. In dielectric and light scattering studies all measurements below 250 K were reproduced on several cooling runs and displayed no dependence on the thermal

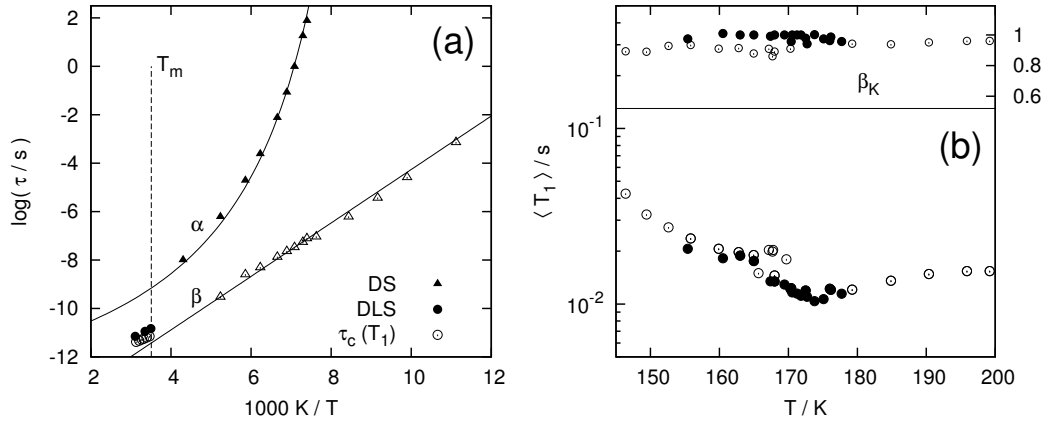


**Figure A.2 (a):** Time constants for the liquid phase of cyanocyclohexane: dynamic light scattering [Surovtsev 2003] and  $^2\text{H}$  NMR spin lattice relaxation. For comparison time constants for the plastic crystalline phase from dielectric spectroscopy are given [Tschirwitz 2002a]. **(b):** Detail around the lower minimum in  $T_1$ . Full and open points originate from several different cooling runs, the corresponding  $\beta_K$  values are marked accordingly.

history of the sample. We found the same behaviour in our measurements and therefore state that at this temperature the transition to phase I is complete and that the phase is stable on all experimental time scales<sup>1</sup>, since a transition to phase II (the ordered crystalline phase) below  $T_t=217$  K was not observed within this work.

### Discontinuity around 170 K

Another peculiarity regarding the magnetization curves of cyanocyclohexane is the behaviour at temperatures around 170 K. As seen in figure A.2 (b) there appears a discontinuity in the  $\langle T_1 \rangle$  values originating from a slightly different stretching parameter  $\beta_K$  observed in different measurements at the same temperature. In an approximately 25 K wide temperature region around 170 K the value of  $\beta_K$  was found to be either close to one (full symbols in fig. A.2 (b)) or around 0.85. Yet no systematic dependence on the cooling rate or ageing of the sample could be found and this particularity is not reflected in any other  $^2\text{H}$  NMR experiment.

In the same temperature region a subtle step in the DSC measurements of Pinvidic et al. [Pinvidic 1988] was observed that was identified by the authors with the free chair-chair transformation of cyanocyclohexane. Whereas a possible correlation of the effects can not be waived, it appears however unlikely that the conformational change of cyanocyclohexane imposes the observed effects on the spin-lattice relaxation of the sample.

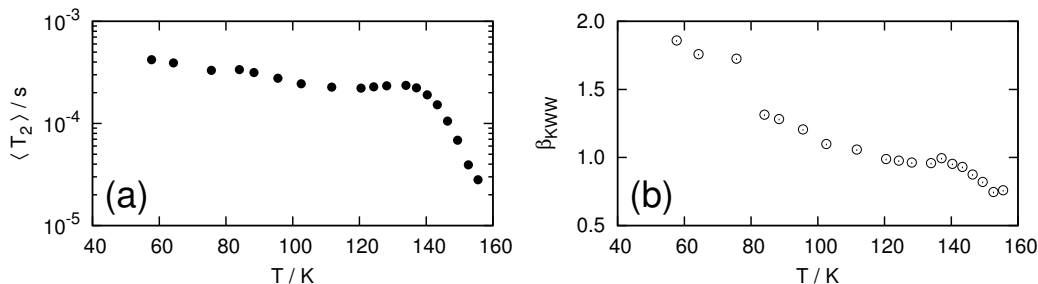


**Figure A.3 (a):** Average spin-spin relaxation times  $\langle T_2 \rangle$  of cyanocyclohexane. **(b):** Corresponding stretching parameter  $\beta_K$ .

### A.3 Spin-spin relaxation times

Figure A.3 (a) displays the spin-spin relaxation times  $\langle T_2 \rangle$  of cyanocyclohexane in the low temperature regime, which represents a repetition of figure 6.11 (b) on linear temperature scale for the sake of clarity. Figure A.3 (b) displays the corresponding stretching parameter  $\beta_K$ , which was omitted in figure 6.11 (b).

### A.4 Correlation of time scale and geometry for the $\beta$ -process

Whereas solid echo line shape changes below  $T_g$  are unambiguously connected to secondary processes in all glass forming systems, a possible influence of the  $\alpha$ -process has to be discussed at temperatures above  $T_g$  – i.e. where the pronounced fast motion limit effects in cyanocyclohexane are observed. The spin lattice relaxation time  $T_1$  on the other hand is clearly governed by the  $\beta$ -process in the temperature regime under discussion (almost 100 K below the temperature of the  $T_1$  minimum of the  $\alpha$ -process).

As the heterogeneous nature of glassy dynamics is reflected in a non-exponential spin-lattice relaxation in the respective temperature range, partially relaxed NMR experiments can provide insight into possible correlations between  $\alpha$ - and  $\beta$ -process [Böhmer 2006] or between time scale and geometry of a single process.

We recorded partially relaxed solid echo spectra in cyanocyclohexane at 146.8 K, i.e. the build-up time  $t_0$  between the saturation pulses and the solid echo sequence was varied. At this temperature the stretching parameter  $\beta_K$  of the magnetization curve in cyanocyclohexane is roughly 0.85 and this heterogeneity is reflected in the spectra recorded at different build-up times (figure A.4): the spectrum recorded with the shortest magnetization recovery time (corresponding to 10% of  $M_{\infty,z}$ ) displays the largest deviation from a rigid limit Pake spectrum and the smallest apparent spectral width  $C_x$ . For longer times  $t_0$  the spectra become broader and the pronounced contraction around the singularities is reduced. In figure A.4 (c) the corresponding  $C_x$  values are given:  $C_{50}$  exhibits an almost linear dependence on

<sup>1</sup>The X-ray diffraction experiments in section 6.2 conducted at 230 K are also in favour of a neat phase existing in this regime.

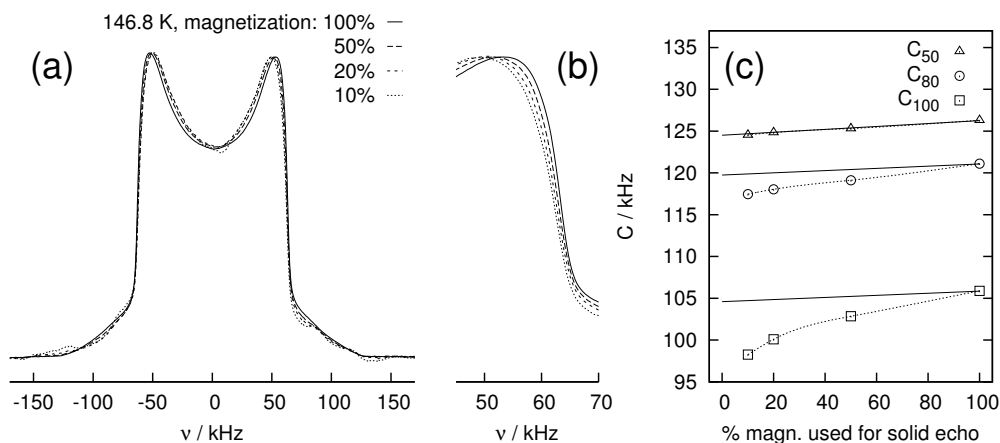


**Figure A.4 (a):** Solid echo spectra for  $t_p = 20 \mu\text{s}$  recorded after different magnetization build-up times, demonstrating a correlation between  $T_1$  and the fast motion limit effects on the solid echo line shape. **(b):** Detail around the upper, inner singularity. **(c):** Corresponding apparent spectral widths  $C_x$ , lines serve as guide for the eye.

the employed magnetization. In  $C_{80}$  and  $C_{100}$  the changes observed for short  $t_0$  are more pronounced.

The results provide evidence for a positive correlation between sub ensembles with a short spin-lattice relaxation  $T_1$  on the one hand and strong effects on the solid echo line shape on the other hand, which gives further evidence for the attribution of the fast motion limit line shape to the  $\beta$ -process in cyanocyclohexane.



# Additional results: binary glass forming systems

## Contents

<b>B.1 Dielectric spectroscopy</b> . . . . .	<b>205</b>
<b>B.2 Methyl group dynamics</b> . . . . .	<b>207</b>
<b>B.3 Spin-spin relaxation times</b> . . . . .	<b>208</b>
<b>B.4 <math>T_1</math> weighted stimulated echo experiments</b> . . . . .	<b>208</b>

In the following sections we briefly review additional experimental results that have been omitted in part II of this work.

## B.1 Dielectric spectroscopy

### VFT interpolation

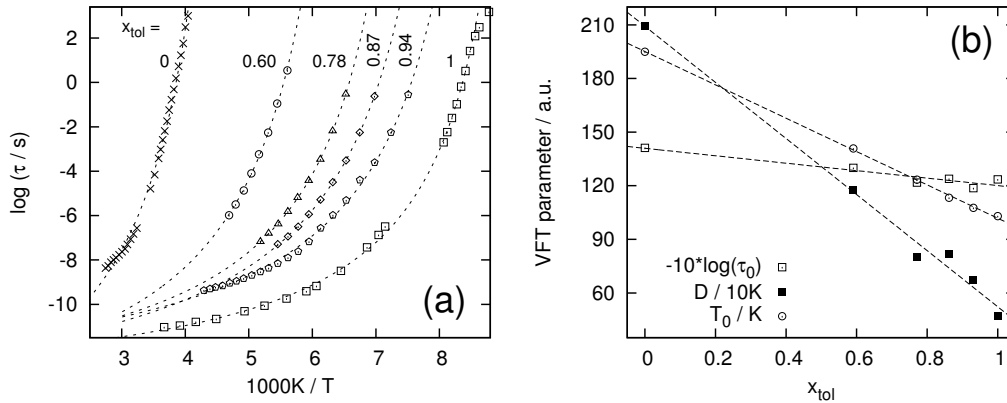


**Figure B.1 (a):** VFT fits to the time constants from dielectric spectroscopy of toluene in PCB54 [Cangialosi 2008]. **(b):** Concentration dependence of the corresponding VFT parameters. The dashed lines represent an interpolation employed for intermediate concentrations.

To overcome the lack of dielectric results for some of the studied concentrations of toluene in PCB54, we attempt to interpolate the concentration dependence of the time constants for the  $\alpha$ -process. The VFT fits to the time constants of toluene in PCB54 [Cangialosi 2008], neat toluene [Kudlik 1999] and neat PCB54 [Casalini 2002] presented in figure B.1 (a) yield approximately linear dependence of

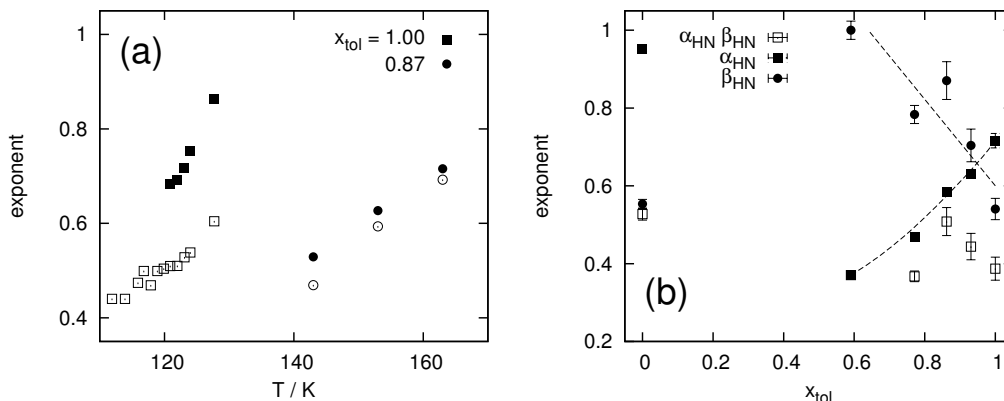


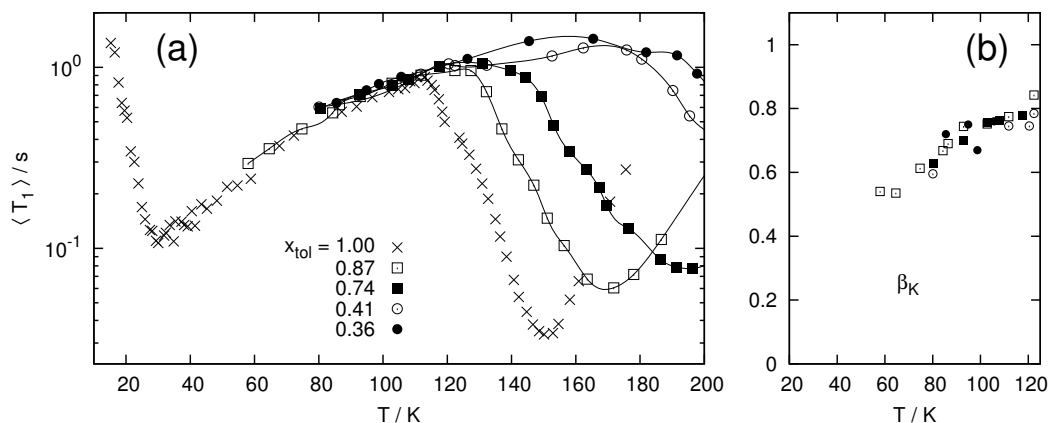
**Figure B.2 (a):** Havriliak-Negami exponents of the low frequency side ( $\alpha_{HN}$ , full symbols) and the high frequency flank ( $\alpha_{HN} \cdot \beta_{HN}$ , open symbols) of the low frequency peak in figure 8.2 (a) and the  $\alpha$ -process in neat toluene [Kudlik 1997b]. **(b):** Shape parameters from a Havriliak-Negami fit to the spectra presented in figure 8.3. A distinct discontinuity between neat PCB54 and the lowest toluene concentration in the mixtures is observed.

all parameters ( $D, T_0$  and  $\log \tau_0$ ) on  $x_{tol}$ , as demonstrated in figure B.1 (b). Hence parameter interpolations obtained from the dashed lines serve for a rough comparison of  $\tau_\alpha$  from dielectric spectroscopy with the  $^2\text{H}$  NMR results of toluene- $d_3$  in PCB in chapter 8. The observed concentration dependence of the VFT parameters is in agreement with  $T_g(x_{tol})$  obtained from DSC measurements, which also exhibits linear temperature dependence in the present system.

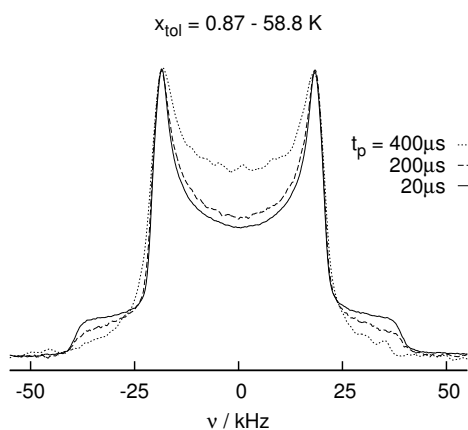
### Havriliak-Negami shape parameters

Figure B.2 (a) displays Havriliak-Negami exponents (cf. section C.3.1) from a fit to the dielectric spectra of  $x_{tol}=0.87$  toluene in PCB54 (cf. figure 8.2 (a)) in comparison with data of neat toluene [Kudlik 1997b]. In contrast to neat toluene the dielectric loss peak in mixtures with PCB54 is approximately symmetric.

The concentration dependence of the Havriliak-Negami exponents in figure B.2 (b) (from fits to the dielectric spectra presented in figure 8.2 (a)) demonstrate that the shape of the  $\alpha$ -peak steadily emerges from the one observed in neat toluene at high toluene contents. The overall width of the loss peak broadens with increasing PCB54 concentration (decrease in  $\alpha_{HN}$ ) and the shape is rendered more symmetric as  $\beta_{HN} \rightarrow 1$ . At  $x_{tol}=0.60$  the loss peak is hence rather broad and well described by a Cole-Cole equation. The peak of neat PCB54 on the other hand is well interpolated by a Cole-Davidson with  $\alpha_{HN} \rightarrow 1$ . As dielectric data for  $x_{tol}<0.60$  is not available, it remains unclear if the peak shape steadily emerges for  $x_{tol} \rightarrow 0$  or if a discontinuity arises for vanishing toluene concentrations.



**Figure B.3 (a):** Average spin lattice relaxation times  $\langle T_1 \rangle$  of toluene- $\text{d}_3$  in PCB54 at  $\omega_L = 46.07 \text{ MHz}$  and neat toluene- $\text{d}_3$  ( $\times$ ) [Qi 2000] recorded at  $\omega_L = 34.4 \text{ MHz}$  in the low temperature regime. The full lines serve as guide for the eye. **(b):** Corresponding stretching parameter  $\beta_K$ .



**Figure B.4:**  $t_p$ -dependence in the solid echo spectrum of  $x_{\text{tol}}=0.87$  toluene- $\text{d}_3$  in PCB54 at lowest temperatures. The time scale of the methyl group rotation approaches  $\tau = 1/\delta$  and hence imposes line shape changes for longer inter pulse delays. In contrast to the small angular reorientations of the  $\beta$ -process, the tetrahedral jumps of the methyl group impose a rise in  $R(t_p)$  for prolonged  $t_p$  values.

## B.2 Methyl group dynamics

In figure 8.7 we omitted the low temperature regime in the discussion of  $T_1$  for mixtures of toluene- $\text{d}_3$  and PCB54. Figure B.3 presents  $\langle T_1 \rangle$  at low temperatures in comparison with data of neat toluene- $\text{d}_3$  [Qi 2000] recorded at  $\omega_L=34.4 \text{ MHz}$ . It becomes obvious, that the low temperature behaviour of  $\langle T_1 \rangle$  is not significantly altered in the mixtures with PCB54, i.e. the energy landscape probed by the tunnelling methyl group of toluene- $\text{d}_3$  is not subject to strong changes in the binary mixtures.

The effect of the methyl group rotation on the solid echo line shape at lowest temperatures is demonstrated in figure B.4: if the correlation time approaches  $\tau = 1/\delta$ , the tetrahedral jumps impose a rise in the central intensity of the spectra for prolonged  $t_p$ -values – as opposed to the small angular displacements of the  $\beta$ -process, which yield a decrease in  $R(t_p)$ . Consequently line shape studies of the  $\beta$ -process are restricted to a narrower temperature range in toluene- $\text{d}_3$  with respect to

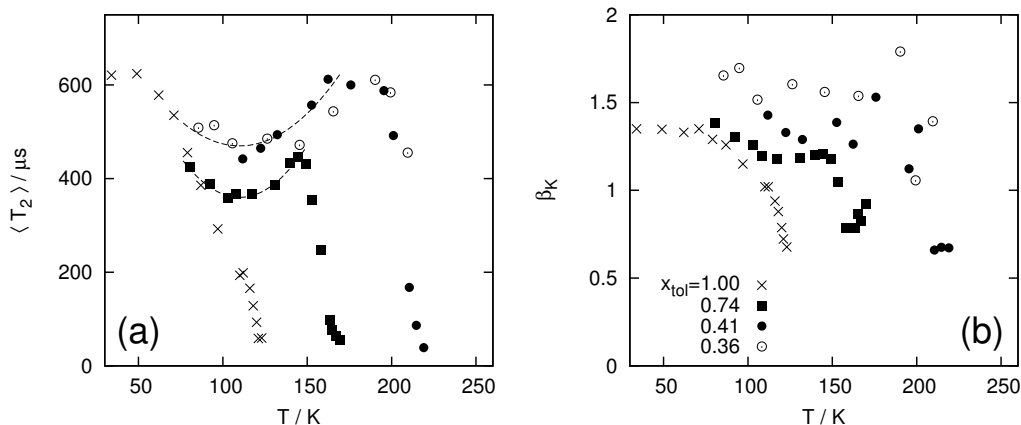
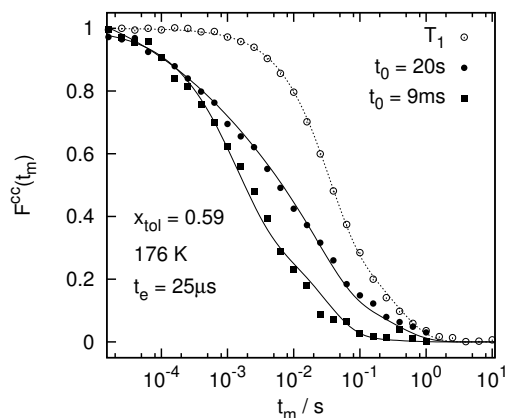


**Figure B.5 (a):** Average spin spin relaxation times  $\langle T_2 \rangle$  of toluene- $d_3$  in PCB54. Repetition of figure 8.22 (b). Dashed lines serve as guide for the eye. **(b):** Corresponding stretching parameter  $\beta_K$ .

**Figure B.6:** Stimulated echo decays ( $F^{\text{cc}}, t_e=25 \mu\text{s}$ ) recorded for different magnetization build-up times  $t_0$ . For comparison the magnetization curve recorded at the same temperature is plotted (open symbols). A distinct difference in the 'long-time tail' of the stimulated echo curves is observed. The full lines are fits according to the procedure described in the text.



toluene- $d_5$ , where  $R(t_p)$  is dominated by the  $\beta$ -process even at lowest temperatures as the  $^2\text{H}$  NMR observables reflect the reorientation of the molecule as a whole.

### B.3 Spin-spin relaxation times

Figure B.5 (b) displays the stretching parameter  $\beta_K$  from Kohlrausch fits to the spin-spin relaxation measurements at low temperatures, which were omitted in figure 8.22. For the sake of clarity the corresponding spin-spin relaxation times  $\langle T_2 \rangle$  are repeated in figure (a).

### B.4 Spin-lattice relaxation weighted stimulated echo experiments

We attempted to (further) justify the bi-exponential description of  $T_1$  in section 8.5.7 by means of spin-lattice relaxation weighted stimulated echo experiments. In the

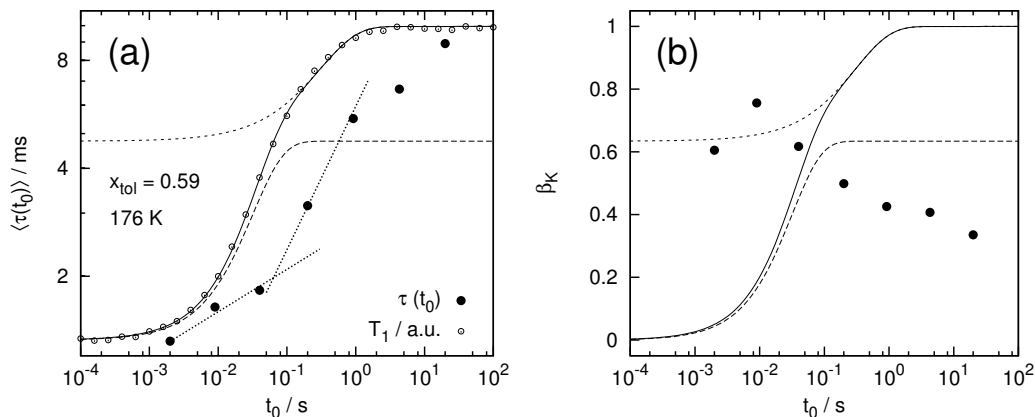


**Figure B.7 (a):** Time constants (●) for the stimulated echo decay (cosine-cosine correlation,  $t_e=25 \mu\text{s}$ ) for different magnetization build-up times  $t_B$  recorded in  $x_{\text{tol}}=0.59$  toluene- $d_5$  in PCB. For comparison the magnetization curve and corresponding stretched exponential fits are displayed in the same figure (y-scale a.u.). The dotted lines serve as guide for the eye. **(b):** Corresponding stretching parameters  $\beta_K$  to the time constants displayed in figure (a). Again the bi-exponential fit to  $T_1$  is given for reasons of comparison.

style of Böhmer et al. [Böhmer 2006] the dependence of the time constants extracted from the stimulated echo experiment on the magnetization build-up time was probed. For a concentration of  $x_{\text{tol}}=0.59$  the magnetization curve at 176 K is non-exponential and well described by bi-exponential fit, as demonstrated in figure B.7 (a). As the selected temperature is only slightly above  $T_g=173 \text{ K}$  for the given concentration, the spin-lattice relaxation is presumably governed by the  $\beta$ -process in this regime. In section 8.6 we introduced a bimodal scenario of toluene dynamics with a fraction of molecules exhibiting a fast  $\alpha'$ -process and the  $\beta$ -process of neat toluene, whereas the remainder participates in the slower  $\alpha$ -process and does no longer exhibit a (resolved) secondary relaxation. Given that this scenario holds and the correlation of  $\alpha$ - and  $\beta$ -process found by Böhmer et al. for neat systems prevails in binary mixtures, a correlation of either  $T_1$  fraction on the time constants of partially relaxed stimulated echo experiments is expected.

We measured the cosine-cosine correlation function  $F_{t_e}^{\text{cc}}$  for an evolution time of  $t_e=25 \mu\text{s}$ . Figure B.6 displays two  $F_{t_e}^{\text{cc}}$  decays for relatively short and long build-up times  $t_0$ : whereas the initial decay is akin in both curves, the one recorded for long  $t_0$  exhibits a more pronounced stretching.

As the effective  $T_1$  relaxation during the mixing time  $t_m$  of a partially relaxed stimulated echo experiment depends on the build-up time  $t_0$ , the fitting routine has to be adapted. The magnetization in this sequence is given via [Geil 2006]:

$$M^*(t_0, t_m) = M(t_m) - M(t_0 + t_m), \quad (\text{B.1})$$

where  $M(t_m)$  is obtained from the bi-exponential fit displayed in figure B.7 (a). Consequently the fitting procedure via equation 3.53 was modified to account for the  $t_0$ -dependent  $T_1$  decay. Correlation times  $\langle \tau(t_0) \rangle$  obtained in this manner are displayed in figure B.7 (a):  $\langle \tau(t_0 = 20\text{s}) \rangle$  is almost an order of magnitude longer

than  $\langle \tau(t_0 = 2ms) \rangle$ , i.e. a positive correlation between the  $\beta$ -process (governing  $T_1$ ) and the  $\alpha$ -process observed in the stimulated echo sequence is found in the present mixtures of toluene and PCB54.

Interestingly one notes a slight correlation between  $\langle \tau(t_0) \rangle$  and the bi-exponential magnetization build-up: during the fast  $T_1$  build-up the  $t_0$  dependence of  $\langle \tau \rangle$  is less pronounced than for longer times  $t_0$ , where the slow  $T_1$  fraction is probed – even though the fast portion accounts for more than 60% of magnetization at the given temperature. A similar behaviour is observed in the stretching parameter  $\beta_K$  plotted in figure B.7 (b): for short  $t_0$  (i.e. during  $T_1^f$ )  $\beta_K$  is approximately 0.6<sup>1</sup>, whereas the stretching becomes more pronounced for longer build-up times with  $\beta_K=0.34$  for  $t_0=20$ s. This finding is in contrast to the behaviour in neat glass forming systems, where Nowaczyk et al. [Nowaczyk 2006] found no dependence of  $\beta_K$  on  $t_0$ .

In summary the experiment is in agreement with the bi-modal scenario proposed in section 8.6, although the results are somewhat ambiguous and hence further experimental validation is needed.

---

<sup>1</sup>For short  $t_0$  the signal amplitude is lowest and hence more scatter is observed in the fit parameters.

# Details on the random walk simulations

---

In the following chapter we provide a brief discussion of the random walk simulation method employed throughout this work. The NMR observables were calculated in the style of Hinze et al. [Hinze 1998], a review of the technique with applications to super-cooled liquids and glasses can be found in [Böhmer 2001, Vogel 2000b, Vogel 2005]. The employed calculation routines are based on prior work in our group [Vogel 2000a, Lusceac 2005a, Medick 2002b, Baldus 2005], the explicit computer programs were however written as part of this work. Random walk simulations of  $^2\text{H}$  NMR experiments are typically forked into two subsequent tasks: the creation of a large number of single molecule trajectories and the calculation of the NMR signal from the latter.

## C.1 Creation of trajectories

The trajectory of a single C- $^2\text{H}$  bond is obtained by means of three simple steps:

- i. Choose an initial C- $^2\text{H}$  orientation  $\theta, \psi$  (again the external field  $\vec{B}_0$  is w.l.o.g. aligned along the  $z$ -axis).
- ii. Draw a waiting time  $\tau_w$  between two subsequent jump events.
- iii. Execute a jump, i.e. calculation of a new orientation  $\theta, \psi$  according to the employed model. If the overall time of the trajectory is sufficient for the calculation of the desired NMR signal, proceed with the next C- $^2\text{H}$  bond (step i), else go to ii.

The initial orientations of the C- $^2\text{H}$  bonds are randomly distributed on the unit sphere due to the disordered nature of studied systems (“powder”). To obtain better statistics, the initial orientations were generated via the *ZCW* method [Cheng 1973], which assures equally distributed sets of  $\theta, \psi$ .

For Poisson distributed jump events (cf. chapter 4) the waiting time between two successive events is obtained from an exponential distribution [Kampen 2007]:

$$\tau_w = -\tau_j \log(1 - z) \quad (\text{C.1})$$

where  $z$  is a random number from the interval  $[0; 1[$ . For a random jump type motion  $\tau_c = \tau_j$  holds, whereas for smaller jump angles  $\gamma$ ,  $\tau_j$  is obtained from equation 4.5. Due to the uncorrelated nature of jump events, furthermore no special care has to be taken in obtaining the first waiting time at the begin of the trajectory. In the presence of a distribution of correlation times  $G(\log \tau)$ ,  $\tau_j^i$  of each molecule

was drawn from this distribution at the beginning of the trajectory, the subsequent waiting times were obtained again from equation C.1. Exchange within  $G(\log \tau)$  was not considered, i.e.  $\tau_j^i$  remains fixed for molecule  $i$ .

In step three the new orientation is calculated according to the selected model. For a simple random jump process the new orientation is obtained via<sup>1</sup>:

$$\theta_{i+1} = \arccos(1 - 2z), \quad (\text{C.2})$$

with the random variable  $z \in [0; 1[$ . For a  $\gamma$ -jump type motion the new orientation resides on the base circle of a cone around  $\theta_i$ :

$$\theta_{i+1} = \arccos[\sin \theta_i \sin \gamma \cos \psi + \cos \theta_i \cos \gamma], \quad (\text{C.3})$$

with  $\psi$  randomly drawn from  $[0; 2\pi[$ . For the anisotropic reorientation of the  $\beta$ -process, the orientation of the cone axis in equation C.3 remains fixed during the calculation of a trajectory:  $\theta_i = \theta_0$ .

## C.2 Calculation of the NMR signal

After the individual trajectories have been created, the NMR signal for different pulse sequences can be obtained from the phases  $\phi$ . For the solid echo sequence equation 3.37 yields:

$$s(t) \propto \cos[\phi(t_p, t) - \phi(0, t_p)], \quad (\text{C.4})$$

wherein the phases

$$\phi(t_1, t_2) = \int_{t_1}^{t_2} \omega_Q(t') dt', \quad (\text{C.5})$$

are obtained from the individual trajectories  $\theta_i, \tau_w^i$ . The sum over all trajectories yields the NMR signal  $S(t)$  from which – as in the experiment – the spectrum is obtained by Fourier transformation after  $t = 2t_p$ . For a direct comparison with experimental spectra  $S(t)$  was damped with a Gaussian before Fourier transformation to account for dipolar broadening. Furthermore the calculated spectra were modified to account for pulse excitation effects in the experiment, arising from finite pulse lengths [Schmidt-Rohr 1994]:

$$A(\omega) = \omega_P t_P \frac{\sin\left(t_P \sqrt{\omega_P^2 + \frac{1}{2}\omega^2}\right)}{t_P \sqrt{\omega_P^2 + \frac{1}{4}\omega^2}}, \quad (\text{C.6})$$

where  $t_P$  is the experimentally employed 90° pulse length and  $\omega_P = \gamma B_1 = \pi / (2t_P)$  holds.

The NMR signal for the stimulated echo four pulse sequence is obtained in analogous manner. When considering short jump times  $\tau_j$ , it is hereby convenient to calculate the signal  $s(t)$  directly during each trajectory, as the individual phase increments during the mixing time  $t_m$  are not relevant.

<sup>1</sup>As in chapter 4 we will only consider EFG tensors with  $\eta = 0$  for the sake of simplicity here.

## C.3 Phenomenological model functions

The following section briefly introduces a number of phenomenological model functions that have been employed throughout this work in the description of dielectric (literature) data and as a starting point for random walk simulations. The presentation follows [Blochowicz 2003], where a refined discussion can be found.

### C.3.1 Distribution functions for the $\alpha$ -process

The following functions are commonly used to model the dielectric loss of the  $\alpha$ -process and were applied throughout this work.

#### Kohlrausch equation

The Kohlrausch [Kohlrausch 1854] or Kohlrausch-William-Watts equation [Williams 1970]

$$\Phi(t) = e^{-\left(\frac{t}{\tau_K}\right)^{\beta_K}}, \quad 0 < \beta_{CD} \leq 1, \quad (\text{C.7})$$

with the average relaxation time

$$\langle \tau \rangle = \frac{\tau_K}{\beta_K} \Gamma\left(\frac{1}{\beta_K}\right) \quad (\text{C.8})$$

yields after Fourier transformation an asymmetrically broadened peak with power laws  $\propto \omega$  at the low and  $\propto \omega^{-\beta_K}$  at the high frequency flank. The corresponding distribution of correlation times can only be obtained for certain values of  $\beta_K$  analytically.

#### Cole-Davidson equation

The Cole-Davidson equation [Davidson 1950] is often used to model the (asymmetrically) broadened  $\alpha$ -peak in dielectric spectra of supercooled liquids:

$$\hat{\epsilon} - \epsilon_\infty = \frac{\Delta\epsilon}{(1 + i\omega\tau_{CD})^{\beta_{CD}}}, \quad 0 < \beta_{CD} < 1. \quad (\text{C.9})$$

The resulting peak yields power laws  $\propto \omega$  at the low and  $\propto \omega^{-\beta_{CD}}$  at the high frequency flank. The average relaxation time reads:

$$\langle \tau \rangle = \tau_{CD} \beta_{CD}. \quad (\text{C.10})$$

Equation C.9 was applied for the modelling of  $T_1$  in cyanocyclohexane, cf. section 6.4.1. The corresponding distribution of correlation times is analytical, cf. [Blochowicz 2003], was however not used for the simulations in this work.

### Havriliak-Negami equation

The Havriliak-Negami equation [Havriliak 1966] represents a simple generalization of the Cole-Davidson equation with an adjustable power law on the low frequency side:

$$\hat{\epsilon} - \epsilon_{\infty} = \frac{\Delta\epsilon}{(1 + (i\omega\tau_{HN})^{\alpha_{HN}})^{\beta_{HN}}}, \quad 0 < \alpha_{HN}, \beta_{HN} \leq 1. \quad (\text{C.11})$$

This yields however the drawback, that for  $\alpha_{HN} < 1$  a mean correlation time is no longer defined.

### The generalized gamma distribution

For the majority of random walk simulations regarding the  $\alpha$ -process we employed the so-called generalized gamma (GG) distribution [Nicolai 1996, Blochowicz 2003]:

$$G_{GG}(\ln \tau) = N_{GG}(\alpha, \beta) e^{-\frac{\beta}{\alpha} \left(\frac{\tau}{\tau_0}\right)^{\alpha}} \left(\frac{\tau}{\tau_0}\right)^{\beta} \quad (\text{C.12})$$

with  $\alpha, \beta > 0$  and the normalization factor

$$N_{GG}(\alpha, \beta) = \left(\frac{\beta}{\alpha}\right)^{\frac{\beta}{\alpha}} \frac{\alpha}{\Gamma\left(\frac{\beta}{\alpha}\right)}. \quad (\text{C.13})$$

The corresponding average relaxation time reads:

$$\langle \tau \rangle = \tau_0 \left(\frac{\alpha}{\beta}\right)^{\frac{1}{\alpha}} \frac{\Gamma\left(\frac{\beta+1}{\alpha}\right)}{\Gamma\left(\frac{\beta}{\alpha}\right)}. \quad (\text{C.14})$$

The GG distribution was used to model the distribution of correlation times for the  $\alpha$ -process of cyanocyclohexane, cf. figure 6.35 (a) for example.

### C.3.2 Distribution functions for the $\beta$ -process

The following distributions of correlation times were employed in random walk simulations of the  $\beta$ -process in cyanocyclohexane and toluene.

#### The log-Gaussian distribution

Dielectric spectroscopy yields a Gaussian distribution of activation energies for the  $\beta$ -process [Kudlik 1997b]:

$$g(E) = \frac{1}{\sqrt{\pi}\sigma} \exp\left(-\left(\frac{E - E_{\beta}}{\sigma}\right)^2\right), \quad (\text{C.15})$$

which leads to a log-normal or log-Gaussian distribution of correlation times [Kudlik 1997b]:

$$G(\log \tau_{\beta}) = \frac{1}{\sqrt{\pi}\bar{\sigma}} \exp\left(-\left(\frac{\log(\tau_{\beta}/\tau_0) - E_{\beta}/(T \ln 10)}{\bar{\sigma}}\right)^2\right). \quad (\text{C.16})$$

This symmetric distribution was used to model the  $\beta$ -process of cyanocyclohexane and toluene in random walk simulations, with the distribution parameters obtained from dielectric spectroscopy, cf. figure C.1.

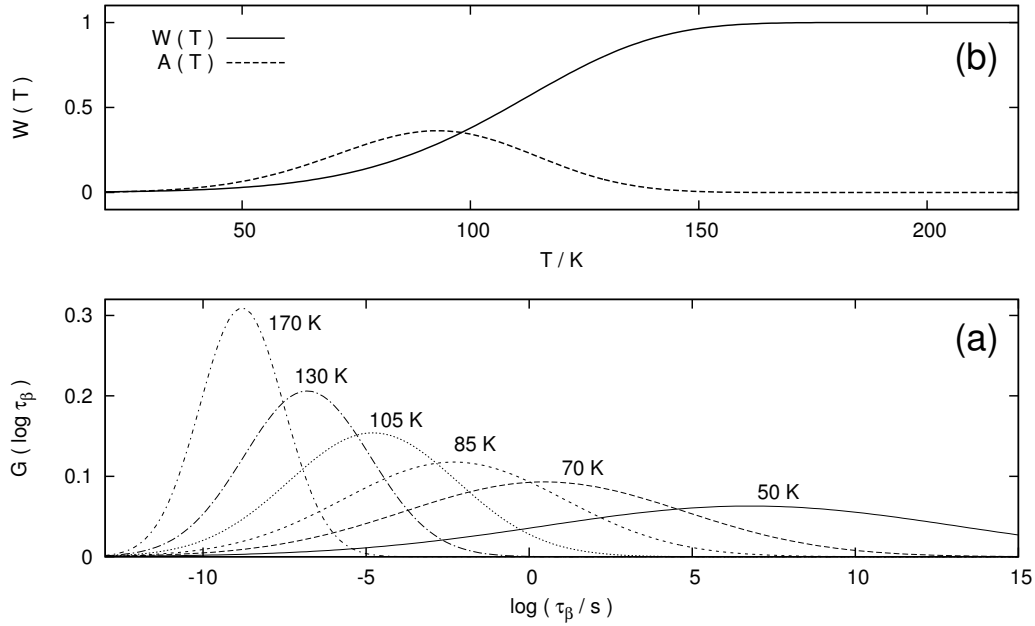


**Figure C.1 (a):** Log-normal distributions (equation C.16) of correlation times for the  $\beta$ -process in cyanocyclohexane. Parameters from [Kudlik 1997b]. **(b):** Corresponding weighting factor in the solid echo line shape ( $W$ , equation 6.3) and the cosine-cosine decay of the stimulated echo ( $A$ , equation 6.5).

### The $G_\beta$ distribution

In section 6.4.2 we also applied another distribution of correlation times for simulations of the  $\beta$ -process in cyanocyclohexane, the  $G_\beta$  distribution [Blochowicz 2003]:

$$G_\beta(\ln \tau) = N_\beta(a, b) \frac{1}{b \left(\frac{\tau}{\tau_m}\right)^a + \left(\frac{\tau}{\tau_m}\right)^b}, \quad (\text{C.17})$$

with the normalization factor

$$N_\beta(a, b) = \frac{a(1+b)}{\pi} b^{\frac{b}{1+b}} \sin\left(\frac{\pi b}{1+b}\right). \quad (\text{C.18})$$

For  $b = 1$  equation C.17 yields a symmetric peak with power laws  $\propto \omega^a$  and  $\propto \omega^{-a}$  in frequency domain.



# Bibliography

- [Abragam 1973] D. Abragam. Principles of nuclear magnetism. Oxford University Press, Oxford, 1973. [13](#), [18](#)
- [Adachi 1975] K. Adachi, I. Fujihara and Y. Ishida. *Diluent effects on molecular motions and glass transition in polymers. I. Polystyrene-Toluene*. J. Polymer Sci.: Polym. Phys. Ed., vol. 13, pages 2155–2171, 1975. [173](#), [181](#), [182](#), [183](#)
- [Affouard 2000] F. Affouard, E. Chochin, R. Decressain and M. Descamps. *Experimental and numerical signatures of dynamical crossover in orientationally disordered crystals*. Europhysics Letters, vol. 53, no. 5, page 035501, 2000. [63](#)
- [Affouard 2003] F. Affouard and M. Descamps. *Molecular dynamics simulation of norbornene plastic crystal*. Journal of Molecular Structure, vol. 651, pages 217–221, 2003. [63](#), [64](#)
- [Alegria 1994] A. Alegria, J. Colmenero, K.L. Ngai and C.M. Roland. *Observation of the Component Dynamics in a Miscible Polymer Blend by Dielectric and Mechanical Spectroscopies*. Macromolecules, vol. 27, no. 16, pages 4486–4492, AUG 1 1994. [118](#)
- [Amoureux 1983] J.P. Amoureux, M. Castelain, M.D. Benadda, M. Bee and J.L. Sauvajol. *Dielectric properties of 1-cyanoadamantane C<sub>10</sub>H<sub>15</sub>CN in its plastic phase*. Journal de Physique, vol. 44, no. 4, pages 513–520, 1983. [70](#)
- [Anderson 1972] J. E. Anderson. *Environmental Fluctuations and Rotational Processes in Liquids*. Faraday Symp. Chem. Soc., vol. 6, page 82, 1972. [38](#)
- [Angell 1988] C.A. Angell. *Structural instability and relaxation in liquid and glassy phases near the fragile liquid limit*. Journal of Non-Crystalline Solids, vol. 102, no. 1-3, pages 205–221, 1988. [7](#)
- [Angell 2000] C. A. Angell, K. L. Ngai, G. B. McKenna, P. F. McMillan and S. W. Martin. *Relaxation in glassforming liquids and amorphous solids*. J. Appl. Phys., vol. 88, no. 6, pages 3113–3157, 2000. [5](#)
- [Baldus 2005] Oliver Baldus. *NMR-Untersuchungen von m-Tricresylphosphat und seinen Mischungen mit Polystyrol*. PhD thesis, Univ. Bayreuth, 2005. [9](#), [91](#), [108](#), [110](#), [211](#)
- [Batchelder 1983] Lynne S. Batchelder, C. H. Niu and D. A. Torchia. *Methyl Reorientation in Polycrystalline Amino Acids and Peptides: A <sup>2</sup>H NMR Spin-Lattice Relaxation Study*. J. Am. Chem. Soc., vol. 105, pages 2228–2231, 1983. [49](#)
- [Bee 1983] M. Bee and J.P. Amoureux. *Molecular reorientations of 1-chloroadamantane in its plastic solid phase - Correlation times from incoherent quasielastic neutron scattering study*. Molecular Physics, vol. 48, no. 1, pages 63–79, 1983. [63](#)

- [Benkhof 1999] Stefan Benkhof. *Dielektrische Relaxation zur Untersuchung der molekularen Dynamik in unterkühlten Flüssigkeiten und plastischen Kristallen*. PhD thesis, Univ. Bayreuth, 1999. 10, 75, 101, 105, 121, 175
- [Bingemann 2007] D. Bingemann, N. Wirth, J. Gmeiner and E. A. Rössler. *Decoupled Dynamics and Quasi-Logarithmic Relaxation in the Polymer-Plasticizer System Poly(methyl methacrylate)/Tri-m-cresyl Phosphate Studied with 2D NMR*. *Macromolecules*, vol. 40, no. 15, pages 5379–5388, 2007. 117, 118, 119, 120
- [Blochowicz 1999a] T. Blochowicz, A. Kudlik, S. Benkhof, J. Senker, E. Rössler and G. Hinze. *The spectral density in simple organic glassformers: Comparison of dielectric and spin-lattice relaxation*. *J. Chem. Phys.*, vol. 110, no. 24, pages 12011–12022, 1999. 93, 101
- [Blochowicz 1999b] Th. Blochowicz, C. Karle, A. Kudlik, P. Medick, I. Roggatz, M. Vogel, Ch. Tschirwitz, J. Wolber, J. Senker and E. Rössler. *Molecular Dynamics in Binary Organic Glass Formers*. *J. Phys. Chem. B*, vol. 103, no. 20, pages 4032–4044, 1999. 118, 119
- [Blochowicz 2003] T. Blochowicz. *Broadband Dielectric Spectroscopy in Simple Organic Glass Formers and Binary Liquids: Frequency and Time Domain Spectroscopy, Non-Resonant Spectral Hole Burning*. PhD thesis, University of Bayreuth, 2003. 124, 161, 213, 214, 215
- [Blochowicz 2004] T. Blochowicz and E. Rössler. *Beta Relaxation versus High Frequency Wing in the Dielectric Spectra of a Binary Molecular Glass Former*. *Phys. Rev. Lett.*, vol. 92, no. 22, page 225701, 2004. 10, 11, 120, 125
- [Blochowicz 2006] T. Blochowicz, A. Brodin and E.A. Rössler. *Evolution of the Dynamic Susceptibility in Supercooled Liquids and Glasses*. In WT Coffey and YP Kalmykov, editors, *Fractals, Diffusion and Relaxation in Disordered Complex Systems, Part A*, volume 133 of *Advances in Chemical Physics*, pages 127–256. 2006. 5
- [Blochowicz 2010] T. Blochowicz. *Molecular Dynamics in Binary Glass-Formers: Concentration Fluctuations and Intrinsic Confinement Effects*. Talk, 2010. 119
- [Blochowicz 2011] T. Blochowicz, S. A. Lusceac, P. Gutfreund, S. Schramm and B. Stühn. *Two Glass Transitions and Secondary Relaxations of Methyltetrahydrofuran in a Binary Mixture*. *The Journal of Physical Chemistry B*, vol. 115, no. 7, pages 1623–1637, 2011. 118, 119, 120, 129, 145, 172, 174
- [Bloembergen 1948] N. Bloembergen, E. M. Purcell and R. v. Pound. *Phys. Rev.*, vol. 73, pages 679+, 1948. 19
- [Bock 2011] Daniel Bock. Unpublished, 2011. 34

- [Böhmer 1996] R. Böhmer, G. Hinze, G. Diezemann, B. Geil and H. Sillescu. *Dynamic heterogeneity in supercooled ortho-terphenyl studied by multi-dimensional deuteron NMR*. Europhys. Lett., vol. 36, page 55, 1996. [9](#)
- [Böhmer 1998a] R. Böhmer, R. V. Chamberlin, G. Diezemann, B. Geil, A. Heuer, G. Hinze, S. C. Kuebler, R. Richert, B. Schiener, H. Sillescu, H. W. Spiess, U. Tracht and M. Wilhelm. *Nature of the non-exponential primary relaxation in structural glass-formers probed by dynamically selective experiments*. J. Non-Cryst. Solids, vol. 235, pages 1–9, 1998. [9](#)
- [Böhmer 1998b] R. Böhmer and G. Hinze. *Reorientations in supercooled glycerol studied by two-dimensional time-domain*. J. Chem. Phys., vol. 108, no. 1, pages 241–248, 1998. [36](#)
- [Böhmer 2001] R. Böhmer, G. Diezemann, G. Hinze and E. Rössler. *Dynamics of supercooled liquids and glassy solids*. Prog. NMR Spectr., vol. 39, pages 191–267, 2001. [5](#), [9](#), [36](#), [62](#), [112](#), [211](#)
- [Böhmer 2006] R. Böhmer, G. Diezemann, B. Geil, G. Hinze, A. Nowaczyk and M. Winterlich. *Correlation of primary and secondary relaxations in a supercooled liquid*. Physical Review Letters, vol. 97, no. 13, SEP 29 2006. [9](#), [12](#), [147](#), [202](#), [209](#)
- [Bonjour 1981] E. Bonjour, R. Calemczuk, R. Lagnier and B. Salce. J. de Physique, vol. C6, page 63, 1981. [61](#)
- [Böttcher 1978a] Carl J. F. Böttcher and Paul Bordewijk. *Theory of electric polarization I: Dielectrics in static fields*. Elsevier Publishing Company, Amsterdam, 1978. [6](#), [92](#)
- [Böttcher 1978b] Carl J. F. Böttcher and Paul Bordewijk. *Theory of electric polarization II: Dielectrics in time-dependent fields*. Elsevier, Amsterdam, London, New York, 1978. [6](#)
- [Brand 2002] R. Brand, P. Lunkenheimer and A. Loidl. *Relaxation Dynamics in Plastic Crystals*. J. Chem. Phys., vol. 116, no. 23, page 10386, 2002. [61](#)
- [Cangialosi 2008] Daniele Cangialosi, Angel Alegriia and Juan Colmenero. *Dielectric relaxation of polychlorinated biphenyl/toluene mixtures: Component dynamics*. The Journal of Chemical Physics, vol. 128, no. 22, page 224508, 2008. [124](#), [125](#), [126](#), [127](#), [129](#), [130](#), [132](#), [165](#), [168](#), [170](#), [205](#)
- [Cangialosi 2009] Daniele Cangialosi. Private communication, 2009. [127](#), [188](#)
- [Casalini 2002] Riccardo Casalini and C. Roland.  *$\alpha$ -relaxation and the excess wing in polychlorinated biphenyls*. Physical Review B, vol. 66, no. 18, 2002. [125](#), [126](#), [130](#), [133](#), [137](#), [205](#)
- [Ceccorulli 1987] G. Ceccorulli, M. Pizzoli and M. Scandola. *Composition dependence of the glass transition temperature of polymer-diluent systems: 1. Experimental*

- evidence of a dual behaviour in plasticized PVC.* Polymer, vol. 28, pages 2077–2080, 1987. 118
- [Cheng 1973] Vera B. Cheng, Henry H. Suzukawa and Max Wolfsberg. *Investigation of a nonrandom numerical method for multlidimensional integration.* J. Chem. Phys., vol. 59, no. 8, pages 3992–3999, 1973. 37, 211
- [Colmenero 2007] J. Colmenero and A. Arbe. *Segmental dynamics in miscible polymer blends: recent results and open questions.* Soft Matter, vol. 3, page 1474, 2007. 120
- [Corfield 1964] G. Corfield and M. Davies. *Dielectric relaxation studies of rotator phase solids. Part 3. Cyclohexane derivatives.* Trans. Faraday Soc., vol. 60, pages 10–24, 1964. 66
- [Cuikermann 1973] M. Cuikermann, J.W. Lane and D.R. Uhlmann. *The role of ionic diffusion in vitreous ionic conductors.* J. Chem. Phys., vol. 59, page 3639, 1973. 5
- [Davidson 1950] D. W. Davidson and R. H. Cole. *Dielectric Relaxation in Glycerine.* J. Chem. Phys., vol. 18, page 1417, 1950. 213
- [Diky 1994] V.V. Diky, G.J. Kabo, A.A. Kozyro, A.P. Krasulin and V.M. Sevruc. *Thermodynamic properties of crystalline and liquid chlorocyclohexane and inversion of ring.* The Journal of Chemical Thermodynamics, vol. 26, no. 9, pages 1001 – 1013, 1994. 190
- [Dixon 1990] Paul K. Dixon, Lei Wu, Sidney R. Nagel, Bruce D. Williams and John P. Carini. *Scaling in the relaxation of supercooled liquids.* Phys. Rev. Lett., vol. 65, page 1108, 1990. 11
- [Donth 2001] E. Donth. *The glass transition: Relaxation dynamics in liquids and disordered materials.* Springer-Verlag, Berlin, Heidelberg, New York, 2001. 5
- [Ediger 2000] M. D. Ediger. *Spatially Heterogeneous Dynamics in Supercooled Liquids.* Ann. Rev. Phys. Chem., vol. 51, page 99, 2000. 5
- [Fox 1956] T.G. Fox. Bull. Am. Phys. Soc., vol. 1, page 123, 1956. 130
- [Fujara 1986] F. Fujara, W. Wefing and H. W. Spiess. *Dynamics of molecular reorientations: Analogies between quasielastic neutron scattering and deutron NMR spin alignment.* J. Chem. Phys., vol. 84, no. 8, pages 4579–4584, 1986. 26, 36
- [Gaikwad 2008] Ashish N. Gaikwad, Elizabeth R. Wood, To Ngai and Timothy P. Lodge. *Two Calorimetric Glass Transitions in Miscible Blends Containing Poly(ethylene oxide).* Macromolecules, vol. 41, no. 7, pages 2502–2508, 2008. 119
- [Gainaru 2007a] Catalin Gainaru. Unpublished, 2007. 110

- [Gainaru 2007b] Catalin Gainaru. *Dielectric Properties of Molecular Glass Formers; from the Liquid State to the Tunneling Regime*. PhD thesis, Universität Bayreuth, 2007. 110
- [Gainaru 2008] C. Gainaru, O. Lips, A. Troshagina, R. Kahlau, A. Brodin, F. Fujara and E. A. Roessler. *On the nature of the high-frequency relaxation in a molecular glass former: A joint study of glycerol by field cycling NMR, dielectric spectroscopy, and light scattering*. Journal of Chemical Physics, vol. 128, no. 17, 2008. 11, 111
- [Garwe 1996] F. Garwe, A. Schönhals, H. Lockwenz, M. Beiner, K. Schröter and E. Donth. *Influence of Cooperative  $\alpha$  Dynamics on Local  $\beta$  Relaxation during the Development of the Dynamic Glass Transition in Poly(*n*-alkyl-methacrylate)s*. Macromolecules, vol. 29, no. 1, pages 247–253, 1996. 12
- [Geil 1993] Burkhard Geil. *NMR-Untersuchungen zur Dynamik von ortho-Terphenyl in der unterkühlten Schmelze*. PhD thesis, Johannes Gutenberg-Universität Mainz, 1993. 36
- [Geil 1998] B. Geil, F. Fujara and H. Sillescu.  *$^2\text{H}$  NMR Time Domain Analysis of Ultraslow Reorientations in Supercooled Liquids*. J. Magn. Res., vol. 130, no. 1, pages 18–26, 1998. 90
- [Geil 2006] B. Geil, G. Diezemann and R. Boehmer. *Correlation of primary relaxations and high-frequency modes in supercooled liquids. I. Theoretical background of a nuclear magnetic resonance experiment*. Physical Review E, vol. 74, no. 4, Part 1, OCT 2006. 209
- [Gonthier-Vassal 1986] A Gonthier-Vassal and H Szwarc. *Glassy Crystals - Glass Transition in Crystalline Fluoro-Cyclohexane, Cyano-Cyclohexane and Isocyano-Cyclohexane*. Chemical Physics Letters, vol. 129, no. 1, pages 5–8, Aug. 1986. 66
- [Hansen 1997] C. Hansen, F. Stickel, T. Berger, R. Richert and E. W. Fischer. *Dynamics of glass-forming liquids .3. Comparing the dielectric alpha- and beta-relaxation of 1-propanol and o-terphenyl*. J. Chem. Phys., vol. 107, no. 4, pages 1086–1093, 1997. 10
- [Havriliak 1966] S. Havriliak and S. Negami. *A complex plain analysis of  $\alpha$ -dispersions in some polymer systems*. J. Polymer Sci. C, vol. 14, page 99, 1966. 214
- [Hensel-Bielowka 2002] S. Hensel-Bielowka and M. Paluch. *Origin of the High-Frequency Contributions to the Dielectric Loss in Supercooled Liquids*. Phys. Rev. Lett., vol. 89, no. 2, page 025704, 2002. 11
- [Heuer 1996] A. Heuer, J. Leisen, S. C. Kuebler and H. W. Spiess. *Geometry and time scale of the complex rotational dynamics of amorphous polymers at the glass transition by multidimensional nuclear magnetic resonance*. J. Chem. Phys., vol. 105, no. 16, pages 7088–7096, 1996. 9

- [Hintermeyer 2008] Julia Hintermeyer. *Dielektrische Spektroskopie an verschiedenen linearen Polymeren in Abhängigkeit vom Molekulargewicht*. Master's thesis, Universität Bayreuth, 2008. 183
- [Hinze 1996] G. Hinze, G. Diezemann and H. Sillescu. *Deuteron spin diffusion and spin lattice relaxation in amorphous solids*. The Journal of Chemical Physics, vol. 104, no. 2, page 430, 1996. 156
- [Hinze 1998] G. Hinze. *Geometry and time scale of the rotational dynamics in supercooled toluene*. Physical Review E, vol. 57, no. 2, page 2010, February 1998. 9, 36, 108, 143, 145, 146, 211
- [Hirose 2003] Y. Hirose, O. Urakawa and K. Adachi. *Dielectric study on the heterogeneous dynamics of miscible polyisoprene/poly(vinyl ethylene) blends: Estimation of the relevant length scales for the segmental relaxation dynamics*. Macromolecules, vol. 36, no. 10, pages 3699–3708, 2003. 118
- [Hoff 2010] Matthias Hoff. *<sup>31</sup>P-NMR Untersuchungen an Glasbildnern im Nanoconfinement*. Master's thesis, Universität Bayreuth, 2010. 34
- [Ivanov 1964] E. N. Ivanov. *NN*. Soviet Physics JETP, vol. 18, page 1041, 1964. 36
- [Johari 1970] G.P. Johari and M. Goldstein. *Viscous Liquids and the Glass Transition. II. Secondary Relaxations in Glasses of Rigid Molecules*. J. Chem. Phys., vol. 53, page 2372, 1970. 9
- [Johari 1973] Gyan P. Johari. *Intrinsic Mobility of Molecular Glasses*. J. Chem. Phys., vol. 58, no. 4, page 1766, 1973. 9
- [Johari 1976] Gyan P. Johari. *Glass Transition and Secondary Relaxations in Molecular Liquids and Crystals*. Annals of the N. Y. Acad. Sci., vol. 279, pages 117–140, 1976. 9, 10, 12
- [Jones 1991] A. A. Jones, P. T. Inglefield, Y. Liu, A. K. Roy and B. J. Cauley. *A Lattice Model for Dynamics in a Mixed Polymer Diluent Glass*. J. Non-Cryst. Solids, vol. 11, pages 556–562, 1991. 185
- [Jörg 2000] T. Jörg, R. Böhmer, H. Sillescu and H. Zimmermann. *Isotope effects on the dynamics of a supercooled van der Waals liquid*. Europhys. Lett., vol. 49, no. 6, pages 748–753, 2000. 9, 90, 108, 110
- [Kampen 2007] N.G. Kampen. *Stochastic processes in physics and chemistry*. North-Holland personal library. Elsevier, 2007. 211
- [Kant 2003] Rama Kant, Sanat K. Kumar and Ralph H. Colby. *What Length Scales Control the Dynamics of Miscible Polymer Blends?* Macromolecules, vol. 36, no. 26, pages 10087–10094, 2003. 118
- [Kohlrausch 1854] R. Kohlrausch. *Theorie des elektrischen Rückstandes in der Leidener Flasche*. Annalen der Physik, vol. 91, page 56, 1854. 8, 213

- [Krakoviack 2007] V. Krakoviack. *Mode-coupling theory for the slow collective dynamics of fluids adsorbed in disordered porous media*. Phys. Rev. E, vol. 75, page 031503, Mar 2007. 120
- [Kudlik 1997a] A. Kudlik, C. Tschirwitz, S. Benkhof, T. Blochowicz and E. Rössler. *Slow Secondary Relaxation Processes in Supercooled Liquids*. Europhys. Lett., vol. 40, no. 6, pages 649–654, 1997. 10
- [Kudlik 1997b] Andreas Kudlik. *Dielektrische Spektroskopie an organischen Glasbildnern*. PhD thesis, Universität Bayreuth, 1997. 5, 6, 7, 8, 75, 105, 124, 125, 126, 165, 168, 180, 183, 206, 214, 215
- [Kudlik 1998] A. Kudlik, C. Tschirwitz, T. Blochowicz, S. Benkhof and E. Rössler. *Slow secondary relaxation in simple glass formers*. J. Non-Cryst. Solids, vol. 235-237, pages 406–411, 1998. 10
- [Kudlik 1999] Andreas Kudlik, Stefan Benkhof, Thomas Blochowicz, Christian Tschirwitz and Ernst Rössler. *The dielectric response of simple organic glass formers*. J. Mol. Struct., vol. 479, pages 201–218, 1999. 6, 10, 68, 124, 125, 127, 130, 135, 137, 205
- [Kumar 1996] Sanat K. Kumar, Ralph H. Colby, Spiros H. Anastasiadis and George Fytas. *Concentration fluctuation induced dynamic heterogeneities in polymer blends*. The Journal of Chemical Physics, vol. 105, no. 9, pages 3777–3788, 1996. 118
- [Leheny 1997] R. L. Leheny and S. R. Nagel. *High-frequency asymptotic shape of the primary relaxation in supercooled liquids*. Eur. Phys. Lett., vol. 39, pages 447–452, 1997. 11
- [Levy 1983] Claire Levy and Giovanni D'Arrigo. *Relaxation processes in liquid and supercooled toluene by light scattering experiments*. Molecular Physics, vol. 50, no. 5, pages 917–934, 1983. 124
- [Lipari 1982] G. Lipari and A. Szabo. *Model-free Approach to the Interpretation of Nuclear Magnetic Resonance Relaxation in Macromolecules. 1. Theory and Range of Validity*. Journal of the American Chemical Society, vol. 104, no. 17, pages 4546–4559, 1982. 94, 101
- [Lubchenko 2007] Vassiliy Lubchenko and Peter G. Wolynes. *Theory of structural glasses and supercooled liquids*. Annual Review of Physical Chemistry, vol. 58, pages 235–266, 2007. 12
- [Lusceac 2004] S.A. Lusceac, I. Roggatz, P. Medick, J. Gmeiner and E.A. Rössler.  *$2H$  nuclear magnetic resonance study of the molecular motion in cyanoadamantane. I. Supercooled plastically crystalline phase*. Journal of Chemical Physics, vol. 121, pages 4770–80, 2004. 112
- [Lusceac 2005a] Sorin Lusceac. *Study of relaxation processes in simple glass formers by means of  $2H$  NMR spectroscopy*. PhD thesis, Univ. Bayreuth, 2005. 42, 46, 62, 63, 107, 211

- [Lusceac 2005b] Sorin Lusceac. Unpublished results. 2005. [72](#)
- [McCrum 1967] N.G. McCrum, B.E. Read and G. Williams. Anelastic and dielectric effects in polymeric solids. John Wiley & Sons, London, 1967. [9](#)
- [Medick 2002a] P. Medick, T. Blochowicz, M. Vogel and E. Rössler. *Comparing the dynamical heterogeneities in binary glass formers and in a glass former embedded in a zeolite - a  $^2\text{H}$  NMR study*. J. Non-Cryst. Sol., vol. 307-310, pages 565–572, 2002. [118](#)
- [Medick 2002b] Peter Medick, Michael Vogel and Ernst Rößler. *Large angle jumps of small molecules in amorphous matrices analyzed by 2D exchange NMR*. J. Magn. Res., vol. 159, no. 2, pages 126–136, 2002. [118](#), [119](#), [211](#)
- [Mehring 1983] M. Mehring. Principles of high resolution NMR in solids. Springer-Verlag, Berlin, 1983. [13](#)
- [Micko 2007] Björn Micko. *2D  $^2\text{H}$ -NMR Untersuchungen zur Sekundärrelaxation in Glasbildnern*. Master's thesis, Universität Bayreuth, 2007. [36](#), [46](#)
- [Moreno 2006] Angel J. Moreno and Juan Colmenero. *Relaxation scenarios in a mixture of large and small spheres: Dependence on the size disparity*. The Journal of Chemical Physics, vol. 125, no. 16, page 164507, 2006. [120](#)
- [Murthy 2000] S.S.N. Murthy. *Experimental study of multiple glass transitions within a material*. Thermochemica Acta, vol. 359, no. 2, pages 143 – 159, 2000. [190](#)
- [Ngai 1979] K. L. Ngai. Comments Solid State Phys., vol. 9, page 127, 1979. [12](#)
- [Ngai 2000] K. L. Ngai. *Dynamic and thermodynamic properties of glass-forming substances*. J. Non-Cryst. Solids, vol. 275, pages 7–51, 2000. [5](#)
- [Ngai 2004a] K. L. Ngai and S. Capaccioli. *Relation between the activation energy of the Johari-Goldstein  $\beta$ -relaxation and  $T_g$  of glass formers*. Phys. Rev., vol. E69, pages 031501–5, 2004. [10](#)
- [Ngai 2004b] K. L. Ngai and M. Paluch. *Classification of secondary relaxation in glass-formers based on dynamic properties*. J. Chem. Phys., vol. 120, no. 2, pages 857–873, 2004. [11](#)
- [Ngai 2010] K. L. Ngai, S. Capaccioli, M. Shahin Thayyil and N. Shinyashiki. *Resolution of problems in soft matter dynamics by combining calorimetry and other spectroscopies*. Journal of Thermal Analysis and Calorimetry, vol. 99, no. 1, pages 123–138, 2010. [120](#)
- [Ngai 2011] K.L. Ngai. Relaxation and diffusion in complex systems. Partially Ordered Systems. Springer, New York Dordrecht Heidelberg London, 2011. [5](#)
- [Nicolai 1996] Taco Nicolai, Jean Christophe Gimel and Robert Johnsen. *Analysis of Relaxation Functions Characterized by a Broad Monomodal Relaxation Time Distribution*. J. Phys. II France, vol. 6, no. 5, pages 697–711, 1996. [214](#)

- [Nowaczyk 2006] A. Nowaczyk, B. Geil, G. Hinze and R. Boehmer. *Correlation of primary relaxations and high-frequency modes in supercooled liquids. II. Evidence from spin-lattice relaxation weighted stimulated-echo spectroscopy*. Physical Review E, vol. 74, no. 4, Part 1, OCT 2006. 210
- [Pake 1948] F. E. Pake. *Nuclear Resonance Absorption in Hydrated Crystals: Fine Structure of the Proton Line*. J. Chem. Phys., vol. 16, no. 4, pages 327–336, 1948. 21
- [Petzold 2008] Nikolaus Petzold. *Depolarisierte Lichtstreuung an niedermolekularen Glasbildnern und plastischen Kristallen*. Master's thesis, Universität Bayreuth, 2008. 61
- [Pinvidic 1988] J.-J. Pinvidic. PhD thesis, Universite de Paris Sud, 1988. 67, 201
- [Pötzschner 2011] Björn Pötzschner. *<sup>31</sup>P-NMR Untersuchungen an molekularen und ionischen Glasbildnern*. Master's thesis, Universität Bayreuth, 2011. 34
- [Powles 1963] J. G. Powles and J. H. Strange. Proc. Phys. Soc., vol. 82, pages 6+, 1963. 20
- [Prevosto 2009] D. Prevosto, S. Capaccioli, M. Lucchesi, P. A. Rolla and K. L. Ngai. *Does the entropy and volume dependence of the structural alpha-relaxation originate from the Johari-Goldstein beta-relaxation?* Journal of Non-Crystalline Solids, vol. 355, no. 10-12, pages 705–711, 2009. 12
- [Pschorn 1991] U. Pschorn, E. Rössler, H. Sillescu, S. Kaufmann, D. Schaefer and H. W. Spiess. *Local and Cooperative Motions at the Glass Transition of Polystyrene: Information from One- and Two-Dimensional NMR as compared with other Techniques*. Macromolecules, vol. 24, pages 398–402, 1991. 35, 183
- [Qi 2000] F. Qi, G. Hinze, R. Böhmer, H. Sillescu and H. Zimmermann. *Slow and fast methyl group rotations in fragile glass-formers studied by NMR*. Chemical Physics Letters, vol. 328, no. 3, pages 257–262, September 2000. 207
- [Raber 1977] D.J. Raber, M.D Johnston and M.A. Schwalke. *Structure Elucidation with Lanthanide-induced Shifts. 2. Conformational-analysis of Cyclohexanecarbonitrile*. Journal of the American Chemical Society, vol. 99, no. 23, pages 7671–7673, 1977. 66
- [Ramos 1996] M. A. Ramos, Q.-W. Zou, S. Vieira and F. J. Bermejo. Czech. J. Phys., vol. 46, pages 2235+, 1996. 61
- [Resing 1965] H. A. Resing. *Apparent Phase—Transition Effect in the NMR Spin—Spin Relaxation Time Caused by a Distribution of Correlation Times*. The Journal of Chemical Physics, vol. 43, no. 2, pages 669–678, 1965. 19, 161
- [Reuter 1993] J. Reuter, T. Bruckert and A. Würflinger. *Differential thermal analysis under pressure on cyanocyclohexane, 1,2,3,4-tetrahydro-5,6-dimethyl-1,4-methanonaphthalene and 2-methyl-2-propanol*. Zeitschrift für Naturforschung

- Section A-A Journal of Physical Sciences, vol. 48, pages 705–708, MAY-JUN 1993. [66](#)
- [Roggatz 2000] Ingmar Roggatz. *NMR-Untersuchung zur Sondenbeweglichkeit in ungeordneten Festkörpern*. PhD thesis, Univ. Bayreuth, 2000. [31](#), [62](#)
- [Rössler 1984] E. Rössler and H. Sillescu.  *$^2\text{H}$  NMR study of supercooled toluene*. Chem. Phys. Lett., vol. 112, no. 1, pages 94–98, 1984. [8](#), [75](#), [125](#), [130](#), [131](#), [132](#), [162](#)
- [Rössler 1985] E. Rössler.  *$^2\text{H}$  NMR Untersuchungen am System Polystyrol-Toluol*. PhD thesis, Universität Mainz, 1985. [173](#), [182](#), [183](#), [184](#)
- [Schaefer 1995] D. Schaefer, J. Leisen and H. W. Spiess. *Experimental Aspects of Multidimensional Exchange Solid-State NMR*. J. Magn. Reson. A, vol. 115, page 60, 1995. [20](#)
- [Schmidt-Rohr 1991] K. Schmidt-Rohr and H. W. Spiess. *Nature of nonexponential loss of correlation above the glass transition investigated by multidimensional NMR*. Phys. Rev. Lett., vol. 66, no. 23, pages 3020–3023, 1991. [9](#)
- [Schmidt-Rohr 1994] Klaus Schmidt-Rohr and Hans Wolfgang Spiess. *Multidimensional solid-state NMR and polymers*. Academic Press, London, 1994. [13](#), [18](#), [23](#), [36](#), [37](#), [101](#), [212](#)
- [Schneider 1978] Hans Joerg Schneider and Volker Hoppen. *Carbon-13 nuclear magnetic resonance substituent-induced shieldings and conformational equilibria in cyclohexanes*. The Journal of Organic Chemistry, vol. 43, no. 20, pages 3866–3873, 09 1978. [66](#)
- [Schneider 2000] U. Schneider, R. Brand, P. Lunkenheimer and A. Loidl. *Excess Wing in the Dielectric Loss of Glass Formers: A Johari-Goldstein  $\beta$ -Relaxation?* Phys. Rev. Lett., vol. 84, no. 24, pages 5560–5563, 2000. [11](#)
- [Schneider 2001] Gerald Schneider.  *$^2\text{H}$  NMR-Untersuchungen der Sekundärrelaxation in den ungeordneten Phasen von Ethanol*. Master's thesis, Universität Bayreuth, 2001. [46](#), [73](#), [75](#), [79](#), [80](#), [85](#), [105](#)
- [Schramm 2010] Sebastian Schramm, Thomas Blochowicz, Emmanuel Gouirand, Robert Wipf, Bernd Stuhn and Yuriy Chushkin. *Concentration fluctuations in a binary glass former investigated by x-ray photon correlation spectroscopy*. The Journal of Chemical Physics, vol. 132, no. 22, page 224505, 2010. [119](#)
- [Schramm 2011] Sebastian Schramm. *Concentration Fluctuations and Molecular Dynamics in Binary Glass Formers*. PhD thesis, Technische Universität Darmstadt, 2011. [171](#), [172](#)
- [Shahin Thayyilab 2008] M. Shahin Thayyilab, S. Capacciola, D. Prevostoa and K.L. Ngai. *Is the Johari-Goldstein  $\beta$ -relaxation universal?* Philosophical Magazine, vol. 88, pages 4007–4013, 2008. [11](#)

- [Sherwood 1979] John N. Sherwood. *The plastically crystalline state*. John Wiley & Sons, Chichester, 1979. 61, 72
- [Sillescu 1992] W. Schnauss; F. Fujara; H. Sillescu. *The molecular dynamics around the glass transition and in the glassy state of molecular organic systems: A  $^2\text{H}$  nuclear magnetic resonance study*. *J. Chem. Phys.*, vol. 97, no. 2, pages 1378–1389, 1992. 73
- [Singh 1982] G. P. Singh, R. Vacher and R. Calemczuk. *J. de Physique*, vol. C9, pages 525+, 1982. 61
- [Singh 2008] L.P. Singh and S.S.N. Murthy. *Study of secondary relaxation in disordered plastic crystals of isocyanocyclohexane, cyanocyclohexane, and 1-cyanoadamantane*. *Journal of Chemical Physics*, vol. 129, no. 9, pages –, 2008. 70
- [Singh 2009] L.P. Singh, S.S.N. Murthy and G. Singh. *Study of supercooled orientationally disordered binary solid solutions II: cyclohexyl derivatives, neopentanol and neopentylglycol*. *Physical Chemistry Chemical Physics*, vol. 11, no. 40, pages 9278–9292, 2009. 70, 190
- [Slichter 1990] Charles P. Slichter. *Principles of magnetic resonance*. Springer, New York, 1990. 13
- [Stevenson 2010] Jacob D. Stevenson and Peter G. Wolynes. *A universal origin for secondary relaxations in supercooled liquids and structural glasses*. *Nature Physics*, vol. 6, no. 1, pages 62–68, JAN 2010. 12, 114, 190
- [Surovtsev 2003] N.V. Surovtsev, S.V. Adichtchev, J. Wiedersich, V.N. Novikov and E.A. Rossler. *Fast relaxation in the structural glass and glassy crystal of ethanol and cyano cyclohexane: a quasielastic light scattering study*. *Journal of Chemical Physics*, vol. 119, no. 23, pages 12399–12408, 2003. 67, 68, 71, 200, 201
- [Taniguchi 2004] N. Taniguchi, O. Urakawa and K. Adachi. *Calorimetric study of dynamical heterogeneity in toluene solutions of polystyrene*. *Macromolecules*, vol. 37, no. 20, pages 7832–7838, 2004. 118, 119, 129, 183
- [Timmermans 1961] J. Timmermans. *Plastic crystals: A historical review*. *Journal of Physics and Chemistry of Solids*, vol. 18, no. 1, pages 1 – 8, 1961. 61, 66
- [Torchia 1982] D. A. Torchia and Attila Szabo. *Spin-lattice relaxation in solids*. *J. Magn. Reson.*, vol. 49, no. 1, pages 107–121, 1982. 93
- [Tracht 1988] U. Tracht, M. Wilhelm, A. Heuer, H. Feng, K. Schmidt-Rohr and H.W. Spiess. *Phys. Rev. Lett.*, vol. 81, page 2727, 1988. 8
- [Tschirwitz 2001] C. Tschirwitz. Unpublished, 2001. 151, 173, 174, 175, 176, 177, 178, 180, 181, 187, 188

- [Tschirwitz 2002a] C. Tschirwitz, S. Benkhof, T. Blochowicz and E. Rössler. *Dielectric spectroscopy on the plastically crystalline phase of cyanocyclohexane*. J. Chem. Phys., vol. 117, no. 13, pages 6281–6288, 2002. 10, 61, 66, 67, 68, 69, 73, 74, 75, 77, 90, 91, 92, 96, 99, 104, 105, 109, 199, 200, 201
- [Tschirwitz 2002b] Christian Tschirwitz. Unpublished results. 2002. 67
- [Utracki 1990] L. A. Utracki. Polymer alloys and blends: Thermodynamics and rheology. Carl Hanser Verlag, Munich, 1990. 119
- [van Dusschoten 1999] Dagmar van Dusschoten, Ursula Tracht, Andreas Heuer and Hans W. Spiess. *Site Specific Rotational Mobility of Anhydrous Glucose near the Glass Transition As Studied by 2D Echo Decay 13C NMR*. J. Phys. Chem. A, vol. 103, no. 42, pages 8359 – 8364, 1999. 120
- [Vogel 1921] H. Vogel. *Das Temperaturabhängigkeitsgesetz der Viskosität von Flüssigkeiten*. Phys. Z., vol. 22, page 645, 1921. 7, 68
- [Vogel 1998] M. Vogel and E. Rössler. *Exchange Processes in Disordered Systems Studied by Solid-State 2D NMR*. J. Phys. Chem. A, vol. 102, no. 12, pages 2102–2108, 1998. 118
- [Vogel 2000a] M. Vogel. *<sup>2</sup>H NMR-Untersuchung der Sekundärrelaxation in organischen Glasbildnern*. PhD thesis, Univ. Bayreuth, 2000. 11, 36, 46, 73, 75, 79, 80, 83, 84, 85, 96, 98, 100, 105, 131, 136, 147, 150, 152, 153, 154, 155, 161, 162, 180, 211
- [Vogel 2000b] M. Vogel and E. Rössler. *Effects of Various Types of Molecular Dynamics on 1D and 2D <sup>2</sup>H NMR Studied by Random Walk Simulations*. J. Mag. Res., vol. 147, no. 1, pages 43–58, 2000. 46, 211
- [Vogel 2001a] M. Vogel and E. Rössler. *Slow  $\beta$ -process in simple organic glass formers studied by one- and two-dimensional <sup>2</sup>H nuclear magnetic resonance I*. J. Chem. Phys., vol. 114, no. 13, pages 5802–5815, 2001. 10, 124
- [Vogel 2001b] M. Vogel and E. Rössler. *Slow  $\beta$ -process in simple organic glass formers studied by one and two-dimensional <sup>2</sup>H nuclear magnetic resonance. II. Discussion of motional models*. J. Chem. Phys., vol. 115, no. 23, pages 10883–10891, 2001. 10
- [Vogel 2002] M. Vogel, C. Tschirwitz, G. Schneider, C. Koplin, P. Medick and E. Rössler. *A <sup>2</sup>H NMR and dielectric spectroscopy study on the slow  $\beta$ -process in organic glass formers*. J. Non-Cryst. Solids, vol. 307-310, pages 326–335, 2002. 10, 121
- [Vogel 2005] M. Vogel, P. Medick and E.A. Rössler. *Secondary Relaxation Processes in Molecular Glasses Studied by Nuclear Magnetic Resonance Spectroscopy*. Annual Reports on NMR Spectroscopy, vol. 56, pages 231–308, 2005. 5, 10, 11, 36, 46, 155, 211

- [Wachner 1999] Andrew M. Wachner and Kenneth R. Jeffrey. *A two-dimensional deuterium nuclear magnetic resonance study of molecular reorientation in sugar/water glasses*. The Journal of Chemical Physics, vol. 111, no. 23, pages 10611–10616, 1999. 120
- [Wagner 1998] Hermann Wagner and Ranko Richert. *Spatial Uniformity of the  $\beta$ -Relaxation in D-Sorbitol*. J. Non-Cryst. Solids, vol. 242, no. 1, pages 19–24, 1998. 10
- [Wefing 1988] S. Wefing, S. Kaufmann and H. W. Spiess. *Two-dimensional exchange NMR of powder samples. II. The dynamic evolution of two-time distribution functions*. J. Chem. Phys., vol. 89, page 1234, 1988. 36
- [Williams 1970] Graham Williams and David C. Watts. *Non-Symmetrical Dielectric Relaxation Behaviour Arising from a Simple Empirical Decay Function*. Trans. Farad. Soc., vol. 66, pages 80–85, 1970. 8, 213
- [Williams 1971] Graham Williams and David C. Watts. *Analysis of Molecular Motion In the Glassy State*. Trans. Farad. Soc., vol. 67, pages 1971–1989, 1971. 10, 92
- [Winterlich 2003] M. Winterlich, G. Diezemann, H. Zimmermann and R. Böhmer. *Microscopic origin of the nonexponential dynamics in a glassy crystal*. Physical Review Letters, vol. 91, no. 23, pages –, 2003. 62
- [Woessner 1962] D.E. Woessner. *Spin Relaxation Processes in a 2-Proton System Undergoing Anisotropic Reorientation*. Journal of Chemical Physics, vol. 36, no. 1, pages 1–8, 1962. 94
- [Woldbaek 1982] T. Woldbaek, A. Berkessel, A. Horn A and P. Klæboe. *The Conformation and Vibrational Spectra of Cyano- and Isocyanocyclohexane*. Acta Chemica Scandinavica A, vol. 36, pages 719–733, 1982. 67
- [Zetsche 1994] A. Zetsche and E.W. Fischer. *Dielectric studies of the  $\alpha$ -relaxation in miscible polymer blends and its relation to concentration fluctuations*. Acta Polymerica, vol. 45, no. 3, pages 168–175, 1994. 118



# List of Figures

2.1	Viscosity $\eta$ of salol . . . . .	5
2.2	Schematic sketch of the dielectric loss in a supercooled liquid . . . . .	6
2.3	Dielectric spectra of glycerol and toluene . . . . .	7
2.4	Dielectric time constants of glycerol and toluene . . . . .	8
2.5	Simulated model for the rotational motion of the $\alpha$ -process . . . . .	9
2.6	Relative relaxation strength of the $\beta$ -process in different glass formers . . . . .	10
2.7	2D spectra for limiting cases . . . . .	11
3.1	Energy splitting for an $I=1$ spin . . . . .	16
3.2	Solid echo pulse sequence . . . . .	20
3.3	Numerically calculated Pake spectra . . . . .	21
3.4	Two phase spectra resulting from a broad distribution of correlation times . . . . .	22
3.5	Stimulated echo pulse sequence . . . . .	24
3.6	Initial and remaining correlation of the stimulated echo experiment . . . . .	25
3.7	Distribution of reorientation angles for the isotropic models of random jump, rotational diffusion and a $20^\circ$ jump . . . . .	28
3.8	2D spectra for limiting cases . . . . .	30
3.9	2D spectra of exchange processes . . . . .	31
3.10	Circuit diagram of the $^{31}\text{P}/^1\text{H}$ double resonance probe . . . . .	32
3.11	Sketch of the $^{31}\text{P}/^1\text{H}$ double resonance probe . . . . .	33
4.1	Sketch of a random jump motion on a cone . . . . .	36
4.2	Random walk simulation of the sin-sin correlation function for a random jump . . . . .	38
4.3	Random walk simulations: $\langle \tau_c \rangle$ from stretched exponential fits to $F_{t_e}^{\text{SS}}$ . . . . .	39
4.4	Random walk simulations: stretching parameters and mean square error . . . . .	40
4.5	Simulated reduction factor $R_f$ of $F_{t_e}^{\text{SS}}$ and $F_{t_e}^{\text{CC}}$ . . . . .	41
4.6	Random walk simulations of the solid echo line shape according to different models of motion . . . . .	42
4.7	Reduction factor $R_{SE}$ and $R(t_p)$ of solid echo spectra calculated for different models of motion and definition of the line shape parameters $R(t_p)$ and $C_x$ . . . . .	43
4.8	Line shape parameters $R(t_p)$ and $C_x$ of simulated solid echo spectra . . . . .	43
4.9	Random walk simulations of the solid echo line shape for an underlying log-Gaussian distribution of correlation times . . . . .	44
4.10	Reduction factor $R_{SE}$ and weighting factor of the Lorentzian line from simulated two phase spectra . . . . .	45
4.11	Sketch of a random jump motion on a cone . . . . .	46
4.12	Simulated spectra for a random jump motion on a cone . . . . .	47
4.13	$R(t_p)$ and $C_x$ line shape parameters for a random jump motion on a cone . . . . .	48

4.14	Sketch of a random jump motion within a cone . . . . .	49
4.15	$R(t_p)$ and $C_x$ line shape parameters for a random jump motion within a cone . . . . .	50
4.16	$R(t_p)$ and $C_x$ line shape parameters for different cone opening angles	51
4.17	Reduction factors for random jump motions within/on a cone . . . . .	51
4.18	Simulated spectra for short $t_p$ and large cone opening angles $\chi$ . . . . .	52
4.19	Sketch of a multi step motion within a cone . . . . .	52
4.20	Correlation functions for a multi step process within a cone . . . . .	53
4.21	Correlation functions of a multi step motion within different cone sizes	54
4.22	$R(t_p)$ and $C_x$ line shape parameters for a random jump motion within a cone . . . . .	55
4.23	R and C line shape parameters for a random jump motion within a cone	55
4.24	Sketch of a multi step motion with a distribution of cone angles . . . . .	56
4.25	$R(t_p)$ and $C_x$ line shape parameters for a random jump motion within a cone . . . . .	56
4.26	Simulated spectra for a multi step motion within a distribution of cone opening angles . . . . .	57
5.1	Sketch of a plastic crystalline system . . . . .	61
5.2	2D exchange spectrum of cyanoadamantane . . . . .	62
5.3	Residual amplitude $F_\infty$ from $F_{t_e}^{SS}$ in cyanoadamantane . . . . .	63
5.4	Molecular dynamics simulation of plastically crystalline norbornene.	64
6.1	Molecular structure and phase diagram of cyanocyclohexane . . . . .	66
6.2	DSC curves and conformers of cyanocyclohexane . . . . .	67
6.3	Time constants of cyanocyclohexane from dielectric spectroscopy . . . . .	68
6.4	Relaxation strength and width of the $\beta$ -process in cyanocyclohexane	69
6.5	X-ray diffraction pattern of cyanocyclohexane at 230 K . . . . .	70
6.6	Sketch regarding the intermolecular distances in the plastic crystalline phase . . . . .	71
6.7	Average spin-lattice relaxation times of cyanocyclohexane . . . . .	73
6.8	Average spin-lattice relaxation times of type-B glass forming systems vs. $T_g/T$ . . . . .	75
6.9	Solid echo spectra of cyanocyclohexane for different temperatures . . . . .	77
6.10	Solid echo spectra of glass forming substances at $T_g/T \approx 1.2$ . . . . .	79
6.11	Relative spectral intensity at zero frequency . . . . .	80
6.12	Fit of solid echo spectrum and line shape changes in cyanocyclohexane	81
6.13	Apparent spectral width in cyanocyclohexane . . . . .	82
6.14	Stimulated echo decays of the cosine-cosine correlation in cyanocyclohexane . . . . .	83
6.15	Amplitude of the $F^{cc}$ decay in different glass formers . . . . .	85
6.16	2D exchange spectra of cyanocyclohexane. . . . .	86
6.17	Stimulated echo decays of cyanocyclohexane (sine-sine correlation) . . . . .	88
6.18	Residual amplitude $F_\infty$ in stimulated echo decays of cyanocyclohexane	89
6.19	Comparison of correlation times from stimulated echoes and dielectric spectroscopy . . . . .	90

6.20	Evolution time dependence of $\langle\tau\rangle$ . . . . .	91
6.21	Experimental and calculated spin-lattice relaxation times for cyanocyclohexane . . . . .	93
6.22	Order parameter S of the $\beta$ -process from $T_1$ model . . . . .	95
6.23	Random walk simulations for the $\beta$ -process below $T_g$ assuming random jump . . . . .	96
6.24	Random walk simulations concerning the influence of the $\alpha$ -process on the line shape above $T_g$ . . . . .	97
6.25	Cone model for high temperature solid echo line shape . . . . .	98
6.26	Model spectra for different temperatures . . . . .	99
6.27	Parameters for the Gaussian distribution of opening angles $G(\chi)$ . . . . .	100
6.28	Order parameters $S^{(l)}$ for the “motion on a cone” model . . . . .	102
6.29	Order parameters $S^{(l)}$ for the “motion on a cone” model cont. . . . .	103
6.30	Comparison of model with experimental apparent width $C_{80}$ . . . . .	104
6.31	Normalized apparent spectral width $C_{80}$ for different glass formers . . . . .	105
6.32	Solid echo spectra for different echo delays $t_p$ . . . . .	106
6.33	Solid echo spectra for different echo delays $t_p$ in m-FAN . . . . .	107
6.34	Bi-modal jump angle distribution to model stimulated echo decay time constants for the $\alpha$ -process . . . . .	108
6.35	Distributions of correlation times vs. geometry of motion . . . . .	109
6.36	Distributions of correlation times vs. geometry of motion for several glass forming systems . . . . .	110
6.37	Initial amplitude of $F_{t_e}^{ss}$ for different models of motion . . . . .	111
6.38	Sketch of single particle correlation functions $F_2$ in cyanocyclohexane . . . . .	113
7.1	Sketch of possible scenarios of time scale separation upon mixing . . . . .	118
7.2	Sketch of possible scenarios of time scale separation upon mixing . . . . .	119
8.1	Sketch of toluene-d <sub>x</sub> and PCB molecules . . . . .	123
8.2	Loss part of the dielectric permittivity of toluene / PCB54 mixtures . . . . .	125
8.3	Dielectric relaxation strengths in toluene / PCB mixtures . . . . .	126
8.4	Loss part of the dielectric permittivity of several concentrations at 118 K . . . . .	127
8.5	DSC curves of toluene / PCB54 mixtures . . . . .	128
8.6	Time constants extracted from the DSC curves and concentration dependence of $T_g$ . . . . .	129
8.7	Average spin lattice relaxation times of toluene-d <sub>5</sub> in PCB54 . . . . .	131
8.8	Time constants extracted from the $\langle T_1 \rangle$ minimum condition . . . . .	132
8.9	Concentration dependence of the high temperature $\langle T_1 \rangle$ minimum . . . . .	133
8.10	Solid echo spectra of toluene-d <sub>3</sub> and toluene-d <sub>5</sub> in PCB54 in the high temperature regime . . . . .	136
8.11	Weighting factor of the liquid line in solid echo spectra of the mixtures . . . . .	137
8.12	Concentration dependence of W(T) . . . . .	138
8.13	Apparent spectral width $C_x$ of solid echo spectra of toluene-d <sub>3</sub> in PCB54 . . . . .	139
8.14	2D exchange spectra of $x_{tol}=0.74$ toluene-d <sub>3</sub> in PCB . . . . .	140
8.15	Stimulated echo decay curves for three toluene-d <sub>3</sub> / PCB mixtures . . . . .	142

8.16	Average correlation times from stimulated echo decays . . . . .	143
8.17	Stretching parameters $\beta_K$ from stimulated echo decays . . . . .	143
8.18	Time constants from various stimulated echo measurements . . . . .	144
8.19	Stimulated echo decay curves (Zeeman) for different evolution times . . . . .	146
8.20	Solid echo spectra of toluene-d <sub>3</sub> in PCB54 and neat toluene-d <sub>5</sub> at similar absolute temperatures . . . . .	147
8.21	Solid echo spectra of toluene-d <sub>3</sub> in PCB54 for different concentrations at similar absolute temperatures . . . . .	149
8.22	Relative spectral intensity at zero frequency $R(t_p)$ and $T_2$ values of toluene-d <sub>3</sub> in PCB54 . . . . .	150
8.23	Relative spectral intensity at zero frequency $R(t_p)$ of toluene-d <sub>5</sub> in PCB54 and concentration dependence of the $\beta$ -process . . . . .	151
8.24	Detail around the lower singularity in solid echo spectra of toluene-d <sub>3</sub> in PCB54 . . . . .	152
8.25	Stimulated echo decay curves of toluene-d <sub>5</sub> in PCB54 for different evolution times below $T_g$ . . . . .	153
8.26	Amplitude of the $F^{cc}$ decay in different mixtures of toluene-d <sub>5</sub> in PCB54 . . . . .	154
8.27	Concentration dependence of the $\beta$ -process: additional results . . . . .	154
8.28	Magnetization curves for samples with different concentrations of toluene-d <sub>5</sub> in PCB54 . . . . .	155
8.29	Magnetization curves corresponding to figure 8.28 (a) . . . . .	156
8.30	Bi-exponential fits to magnetization curves of samples with different concentrations of toluene-d <sub>5</sub> in PCB54 . . . . .	157
8.31	Average spin lattice relaxation times from a bi-exponential fit . . . . .	159
8.32	Relative weighting of the fast $T_1$ component in the different toluene-d <sub>5</sub> /PCB mixture . . . . .	160
8.33	Model calculation in a non-decoupled scenario in comparison with <sup>2</sup> H NMR results . . . . .	162
8.34	Model calculation in a scenario of dynamic decoupling in comparison with <sup>2</sup> H NMR results . . . . .	164
8.35	Time constants and dielectric spectra of $x_{tol}=0.59$ toluene in PCB in comparison with results from a scenario of dynamic decoupling . . . . .	165
8.36	Sketch for a proposed bi-modal scenario . . . . .	165
8.37	Model calculation in a scenario of $\alpha$ - and $\alpha'$ -process in comparison with <sup>2</sup> H NMR results – $x_{tol}=0.59$ concentration . . . . .	167
8.38	Time constants and dielectric spectra of $x_{tol}=0.59$ toluene in PCB in comparison with results from an assumed bi-modal scenario . . . . .	168
8.39	Model calculation in a scenario of $\alpha$ - and $\alpha'$ -process in comparison with <sup>2</sup> H NMR results – $x_{tol}=0.77$ concentration . . . . .	169
8.40	Model calculation in a scenario of $\alpha$ - and $\alpha'$ -process in comparison with <sup>2</sup> H NMR results – $x_{tol}=0.86$ concentration . . . . .	169
8.41	Time constants and dielectric spectra of $x_{tol}=0.86-0.87$ toluene in PCB in comparison with results from an assumed bi-modal scenario . . . . .	170
8.42	Weighting factor $W_{T_1}$ from a bi-modal calculation vs. $\tau_\alpha$ . . . . .	171
9.1	Sketch of toluene-d <sub>5</sub> and 2-picoline-d <sub>7</sub> molecules . . . . .	174

9.2	Calorimetric measurements on different toluene / picoline mixtures .	175
9.3	Loss part of the dielectric modulus and time constants for different concentrations of toluene in picoline . . . . .	176
9.4	Loss part of the dielectric modulus for different concentrations of toluene in picoline at 100 K . . . . .	176
9.5	Total dielectric relaxation strength $\Delta\epsilon (T_g+1\text{ K})$ and relaxation strength of the $\beta$ -process 1- $S$ in picoline / toluene mixtures . . . . .	177
9.6	Interpulse dependence of the $R(t_p)$ value for different concentrations of toluene-d <sub>5</sub> in picoline . . . . .	178
9.7	Fraction $f_\beta$ in mixtures of toluene/picoline in comparison with the system toluene/PCB54 . . . . .	179
9.8	Magnetization curves for samples with different concentrations of toluene-d <sub>5</sub> in picoline . . . . .	180
9.9	Average spin lattice relaxation times $\langle T_1 \rangle$ for mixtures of toluene with PCB54 and picoline . . . . .	181
9.10	Sketch of toluene-d <sub>5</sub> and polystyrene molecules . . . . .	181
9.11	Temperature at which the dielectric susceptibility $\epsilon''$ exhibits a maximum at 1.6 kHz versus concentration . . . . .	182
9.12	Concentration dependence of the glass transition temperature in toluene / polystyrene mixtures . . . . .	183
9.13	Spin-spin relaxation times $T_2$ of polystyrene for different concentrations of toluene in PS . . . . .	184
9.14	Concentration dependent populations $F_n$ for type A molecules with $n$ neighbours of species B in the simple lattice model . . . . .	186
9.15	Concentration dependent fraction $f_\beta$ of toluene molecules exhibiting the $\beta$ -process of the neat system . . . . .	187
9.16	Relative dielectric relaxation strength of the $\beta$ -process 1- $S$ in mixtures of toluene with PCB54 and picoline in comparison with results of the lattice model . . . . .	188
A.1	Width parameters of the GG and $G_\beta$ distributions as obtained from dielectric spectroscopy and excess wing in dielectric spectra of cyanocyclohexane . . . . .	200
A.2	Time constants for the liquid phase of cyanocyclohexane and detail around the low temperature minimum in $T_1$ . . . . .	201
A.3	Average spin-spin relaxation times of cyanocyclohexane . . . . .	202
A.4	Solid echo spectra recorded after different magnetization build-up times	203
B.1	Interpolation of VFT parameters in toluene/PCB54 . . . . .	205
B.2	Shape parameters from a Havriliak-Negami fit to the spectra presented in figure 8.3 . . . . .	206
B.3	Average spin lattice relaxation times $\langle T_1 \rangle$ of toluene-d <sub>3</sub> in PCB54 at $\omega_L = 46.07\text{ Mhz}$ and neat toluene-d <sub>3</sub> in the low temperature regime .	207
B.4	$t_p$ -dependence in the solid echo spectrum of toluene-d <sub>3</sub> /PCB54 at lowest temperatures . . . . .	207

---

B.5	Average spin spin relaxation times $\langle T_2 \rangle$ of toluene-d <sub>3</sub> in PCB54 with corresponding stretching parameter $\beta_K$ . . . . .	208
B.6	Stimulated echo decays ( $F^{cc}, t_e=25 \mu\text{s}$ ) recorded for different magnetization build-up times $t_0$ . . . . .	208
B.7	Time constants from the stimulated echo decay for different magnetization build-up times $t_0$ recorded in $x_{\text{tol}}=0.59$ toluene-d <sub>5</sub> in PCB . . .	209
C.1	Distributions for the $\beta$ -process employed in random walk simulations of cyanocyclohexane . . . . .	215

# Acknowledgements

It would not have been possible to write this thesis without the help and support of the kind people around me, to only some of whom it is possible to give particular mention here.

First and foremost I would like to thank my supervisor Prof. Dr. Ernst Rössler for the open working environment he established in our group. I very much enjoyed working on my own ideas most of the time, yet he was always at hand with profound advice and ideas when needed. Furthermore I am indebted to his patience during the preparation of this thesis.

I would like to express my gratitude to Sorin Lusceac, who was a great source of advice during the first days of my diploma work and remained so ever since. He started the project on cyanocyclohexane and the long discussions we had together with Catalin Gainaru and Alexander Brodin made the lab work really worthwhile. The  $^2\text{H}$  NMR measurements on cyanocyclohexane would have been impossible without the help of H. Zimmermann, who synthesized the perdeuterated samples.

Furthermore I would like to thank Dunja Hirsemann for her help with the X-ray diffraction measurement, Daniele Cangialosi for the first ampoules of PCB54 and the  $\Delta\epsilon_\beta$  data on toluene/PCB54 mixtures as well as Ernst Naumann for his collaboration in the development of the double-resonance probe head – I very much enjoyed the time in Rheinstetten. The great work of the mechanics shop at NWII in building the parts for this probe is highly appreciated. Thanks are also due to Daniel Bock for proofreading one of the many versions of this thesis and Robert Kahlau for his help with everything “dielectric”.

In my daily work I have been blessed with friendly colleagues at Experimental Physics II and Inorganic Chemistry III, who made it a pleasure to work such long hours.

Last but not the least I would like to thank my parents for their support and Yvonne, whose loving care and understanding kept me going during the past chaotic years.